GENESIS AND DISTRIBUTION OF CA-AL SILICATES IN AEGEAN BLUESCHISTS AND IMPLICATIONS FOR FLUID FLOW IN SUBDUCTION ZONES

by

Philip Martin Bloor

This thesis is submitted for the degree of

Doctor of Philosophy

University of Edinburgh

1998

ABSTRACT

High grade blueschist metamorphism on the Aegean island of Syros involves the widespread growth of the calc-silicate minerals lawsonite, zoisite and epidote / clinozoisite in a wide range of lithologies. In calcareous metasediments the only realistic lawsonite-generating reaction appeared to be one involving calcite-breakdown and thus for significant reaction progress CO_2 would have to have been flushed from the rock by the infiltration of a water-rich fluid. Previous studies had noted local concentrations of lawsonite notably at the margins of meta-igneous bodies which apparently supported this hypothesis (Ridley 1982, Barr 1989). However, stable isotope and T-XCO_2 modelling studies by Barr (1989) suggested that local buffering of fluid composition on a cm to m scale occurred, apparently ruling out widespread pervasive fluid flow. This apparent paradox between abundance of lawsonite in the metasediments and the syn-metamorphic fluid regime prompted a comprehensive study of possible controls on the growth of lawsonite.

The distribution of lawsonite was mapped in the metasediments. Structural mapping was used to elucidate the strain history of the syn-blueschist deformation. Detailed petrographic and microfabric analysis of relevant samples was undertaken to document their petrologic and microstructural development and to identify lawsonite forming reactions. Changes in bulk rock composition accompanying the growth of lawsonite were assessed using XRF analysis coupled with the Isocon method of Grant (1986). Finally oxygen isotope analysis of quartz separates was used in an attempt to assess the extent of syn-metamorphic fluid flow.

The results show that in the greyschist units of northern Syros, lawsonite growth is controlled by a syn-deformational, fracture-controlled fluid infiltration event, traces of which are visible as quartz veins. Ca-bearing, water-rich fluid pervasively infiltrated the schists adjacent to the fractures resulting in the growth of large amounts of lawsonite by metasomatic reactions involving the breakdown of

mica. The scale of fluid transport and therefore the extent of metasomatic alteration is controlled by the deformation and compositional variation.

These observations confirm the suggestion in the previous studies that lawsonite growth is at least partially controlled by the infiltration of an externally-derived fluid. The preservation of small scale variation in fluid composition within significant parts of the metasediments is explained by the channelized nature of the event.

The timing of the infiltration event relative to the strain history suggests that it is synchronous with the transfer of the metasediments to the hanging wall of the subduction zone by the successive underplating required to generate uplift and so promote un-roofing. Thus, the results of the study shed light on important aspects of the fluid regime in subducted rocks during a critical phase of their tectonic history. Indeed, it is suggested that the process of underplating, which will inevitably perturb the local thermal structure, may be responsible for initiating the infiltration event by causing the generation of the fluid, or increasing the permeability of the infiltrated schists or both. Consideration of the inferred petrogenetic development of subducted material suggests that the fluid is produced by the dewatering of the slab during the transition from blueschist to eclogite assemblages. The similarity of the alteration to rodingitisation suggests that it may have interacted with ultramafic material prior to entering the greyschists.

ACKNOWLEDGEMENTS

Firstly I would like to thank my supervisors for their help in completing this thesis. John Dixon for his insights into the geology of Syros and his company on field work but most of all for unwavering support particularly when my own resolve was slipping, and Colin Graham for guiding me through some of the intricacies of metamorphic fluid flow.

There are a number of people in the department who I would like to thank for their help and technical expertise. I would like to give very big thanks to Shane Voss for helping me out on numerous occasions with a variety of computing problems. I would also like to thank Diana Baty and Yvonne Cooper for help with photography and drafting, Mike Hall for producing literally thin sections, Dodie James for help with XRF and Peder Aspen and Geoff Angel for help with XRD.

Extra big thanks to Paul and Allison, Ian, Coleen and Sally, and JT for putting me up and perhaps more importantly putting up with me at various points over the last year. Also thanks to all the other friends that I shared the Edinburgh experience with, Jo Valentine, Nearchos 'theo' Theodorou, Babs Page, Kev Fielding, Harriet Randle, Jon Kirby, Jo Flemming, Claire Glover, Stuart Craig, and James Ibbertson.

I also owe a huge debt of gratitude to my parents who have supported me both financially and emotionally throughout my education.

However, the greatest thanks of all go to Sandra not least for her photocopying, formatting and errand running over the last few days. Throughout the last three years she has provided an escape from the horrors of thesisdom and always managed to put a smile back on my face. Without her patience, understanding and support this thesis never would have been completed.

CONTENTS

CHAPTER 1

INTRODUCTION

1.1 Rationale and Aims

On the island of Syros in the Greek Cyclades, a well exposed sequence of mafic, pelitic, psammitic, and calcareous lithologies crop out. This suite of continental margin rocks has been metamorphosed under high grade blueschist facies conditions at depths of about 50 km during a subduction-related Eocene regional metamorphic event. This blueschist metamorphism has involved the abundant development of the Ca-Al-Silicate lawsonite in meta-igneous, meta-carbonate, and meta-sedimentary lithologies.

Preliminary field and petrographic observations on the distribution of lawsonite in the blueschists lead the authors of earlier studies to suggest that its development may be fluid controlled. In particular, they suggested that the growth of significant amount of lawsonite requires the infiltration of large volumes of externally-derived, water-rich fluid since no obvious calcium-bearing precursor phase could be inferred other than calcite. Lawsonite-forming reactions would thus generate CO_2 and be self-limiting unless water was abundantly available.

However, previous mineral equilibria, stable isotopic and fluid inclusion studies (Barr 1989) have suggested that during the blueschist metamorphism the majority of the rocks in the Syros section behaved as closed systems with little input of external fluid. Individual beds in those outcrops examined display local equilibrium on a cm to m scale. Thus arose an apparent paradox between the inferred locally buffered fluid regime in the blueschists during peak metamorphism and the simplest model for widespread lawsonite formation which implied high integrated fluid fluxes.

The principal aim of this project is to explain the development and distribution of the lawsonite in the blueschists of Syros and reconcile its occurrence with the apparent lack of pervasive external fluid control. As will be seen this study yields more information about the nature of the fluid regime in the Syros

metasediments during the blueschist metamorphism. Comparison of results from Syros with other lawsonite- and carbonate-bearing blueschist terrains allows more general conclusions to be drawn about fluid flow in subduction zones and overall processes of fluid recycling. This is useful as relatively little work has been carried out on modelling fluid flow regimes during specifically blueschist metamorphism.

1.2 Relevant Previous Work

3 major studies have previously been conducted into the geology of Syros each concentrating on different aspects of the geological history of the island. The first of these, by Dixon (1969) , includes a lithological map of northern Syros, the area of interest in this study, as well as a detailed study of the mineralogy, petrology and metamorphism of the meta-igneous rocks there.

Secondly, Ridley (1982) produced a detailed 1 : 10000 geological map of the whole of the island and examined the minor structures in the blueschists to determine the nature of the deformation. A brief analysis was undertaken of some of metamorphic features pertinent to theoretical heat-flow modelling. This modelling attempts to predict the P-T-t conditions associated with the tectonothermal evolution of the island.

Most recently, Barr (1989) studied the fluid-rock interaction during the blueschist and later greenschist facies metamorphism. She used an internally consistent data set in conjunction with Schreinemakers analysis and equilibrium thermodynamic calculations to construct T-X(CO_2) sections. By comparison of these grids with petrographic data she determined the composition of fluid in equilibrium with the blueschist assemblages. In addition, she carried out stable isotope and fluid inclusion studies to further constrain both the composition of the blueschist fluid and the extent of equilibrium between fluids throughout the blueschists.

Information from all three of these sources was used in the planning and execution of this project. The relevant information is summarised in the following sections.

1.2.1 General Geology of Syros

Description of geological succession and lithologies present

The majority of the island of Syros is composed of a coherent lithological succession which can be traced from the southern coast to the northern coast. This is a sequence of interbedded marble and meta-sedimentary units with occasional metabasic layers (Figure 1.1). In the south of the island, at the base of the sequence, the meta-sedimentary units consist of pelitic schists, quartzites, and quartzose schists. In general, passing up the sequence the quartz-rich units become scarcer and the metasedimentary units are dominantly pelitic in composition. In the north of the island the meta-sedimentary units are represented by thick sequences of pelitic Mg-glaucophane-white mica-chlorite-graphite schist, named 'greyschist' by Dixon (1968). Throughout the sequence the marble units are predominantly calcitic with occasional lenses and layers of yellowish or pink-brown dolomite-rich assemblages. This succession is thought to represent a continental margin sequence, with the southern lithologies representing a more proximal depositional environment than those in the north. Ridley (1982) noted rhythmic alternation of schist and marble in part of the sequence and interpreted this as a thrust stack. He suggested that parts of the sequence have been tectonically duplicated by thrusting in a north or north-westerly direction before the peak of metamorphism.

In the north of the island is an east-west trending belt composed of a large number of meta-igneous blocks held in an intervening matrix of serpentinite and pelitic derivatives. Dixon (1968) names this the 'northern gneiss-serpentinite belt' (see figure 1.1). The included igneous blocks are extremely variable in character ranging from finely striped glaucophane-epidote gneisses, to large and relatively

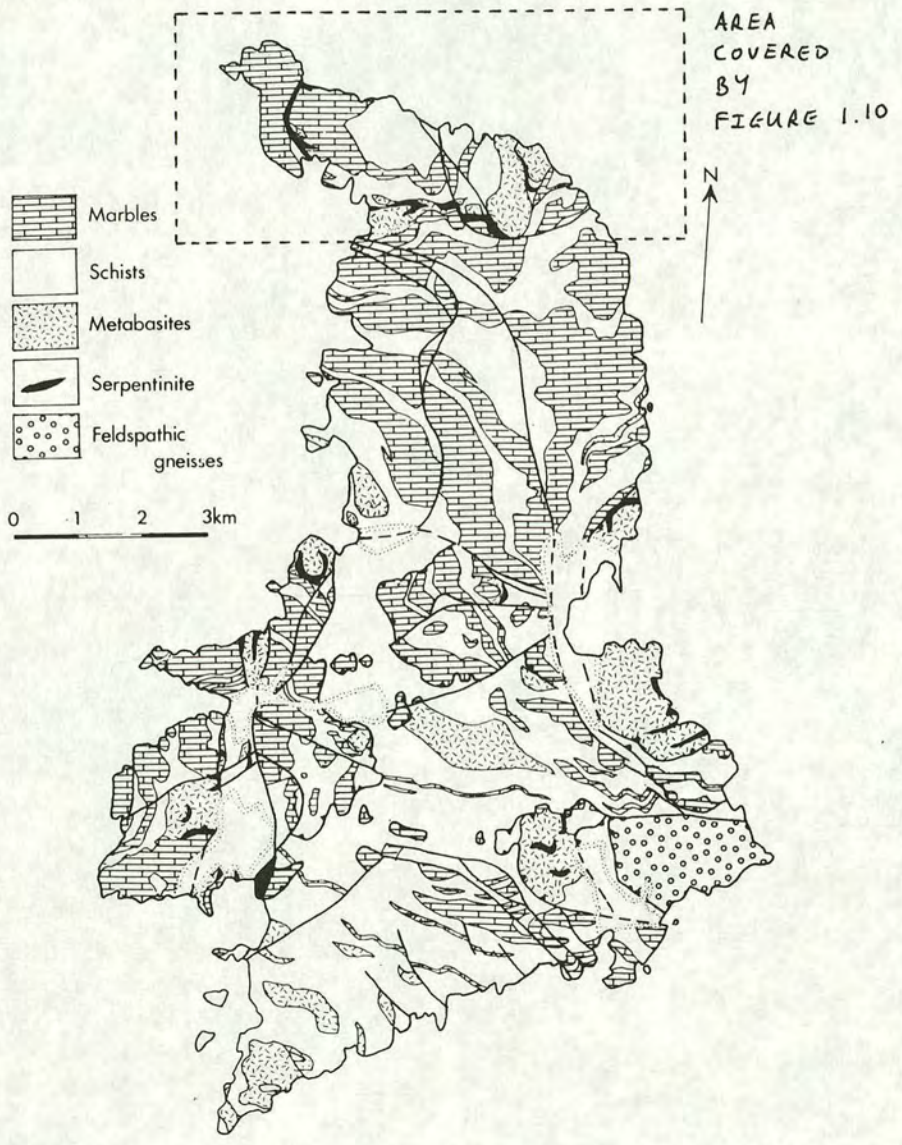

Figure 1.1 Simplified geological map of Syros taken from Ridley (1982).

undeformed, metagabbroic bodies which preserve their former igneous textures. Where the blocks are in contact with serpentinite they often exhibit spectacular metasomatic rims of concentric mono- and bi-mineralic assemblages. In such cases the serpentinite is completely replaced by talc-chlorite assemblages. On the east coast a large block of metagabbro is surrounded by concentric zones of metamorphosed conglomerate and breccia of igneous origin. Dixon (1968) interpreted this breccia as a sedimentary deposit, or debris flow of plutonic and volcanic material which was deposited on top and around the metagabbroic block, and subsequently concurred with the view of Blake et al that the whole northern belt is essentially an ophiolitic olistostrome subsequently deformed during blueschist metamorphism. Dixon and Ridley (1987) contains a concise summary of the main features of this belt.

South of the breccias on the east coast, and structurally below the gneiss-serpentinite belt a small melange unit occurs interbedded with a sequence of alternating thin marbles and schists. It consists of rounded metabasic blocks in a talc-chlorite matrix which often exhibit metasomatic rims. The position of this unit, in a meta-sedimentary sequence, suggests that it too is of sedimentary origin. Colourful blue-green schists underlying the melange unit suggest that its deposition was preceded by input of detrital serpentinite into the schists.

In a zone running across the centre of the island to the west coast the gneiss serpentinite belt is characterised by a continuous serpentinite body with included meta-igneous blocks ranging composition from glaucophane-epidote metabasites to jadeite-rich meta-acidites. Once again, the blocks show metasomatic rims and the vast majority of the serpentinite is reacted out to chlorite-talc assemblages. However, in small areas, where the concentration of included blocks is low, unaltered blue-green serpentinite occurs.

On the west coast there are two distinct locations which, while separated from the gneiss serpentinite belt, are clearly related to it. The first of these is a unit of metasomatic schists at Aspro. These are pale blue and green in colour, strongly

sheared, and contain included glaucophanitic meta-igneous blocks and discontinuous layers of white calcitic marble. This zone is also noted for its abundance of layer parallel lenses of ankerite, fuchsite and quartz. It is thought to represent a zone of schists rich in detrital serpentinite material which has been extensively metasomatised and sheared.

The second location of note is the Gria Spilia Gneiss Body. This a large relatively undeformed meta-igneous block surrounded by grey schist on the coast north of Aspro. It varies in composition from basic through intermediate to acid and still preserves many of its primary igneous textures. Small-scale concentric metasomatic zones have formed locally along its contact with the grey schists. It is inferred to be large olistolith some 500 m across.

It is within the lithologies of the Gneiss Serpentinite belt described above and the grey schists that surround it that the majority of the lawsonite observed in the Syros blueschists occurs. Thus this is the area that this study will be based on. More detailed accounts of lawsonite distribution within the belt are documented below.

Metamorphism and Deformation

The majority of the rocks on Syros were metamorphosed at depths about 50 km during a subduction-related high grade blueschist event which gives Eocene cooling ages (Altherr et al 1979). Observations on assemblages show that this took place at pressures of 14 to 19 Kbars and a temperature of 470$\pm$30°C (see figure 1.2). The only units on Syros not affected by this blueschist metamorphism are the Azolimnos gneisses and the Vari chloritic schists on the south-east coast. These have undergone an early epidote-amphibolite metamorphism and Ridley (1982) suggests that these allochthonous units may be down-faulted from higher levels of the syn-metamorphic pile.

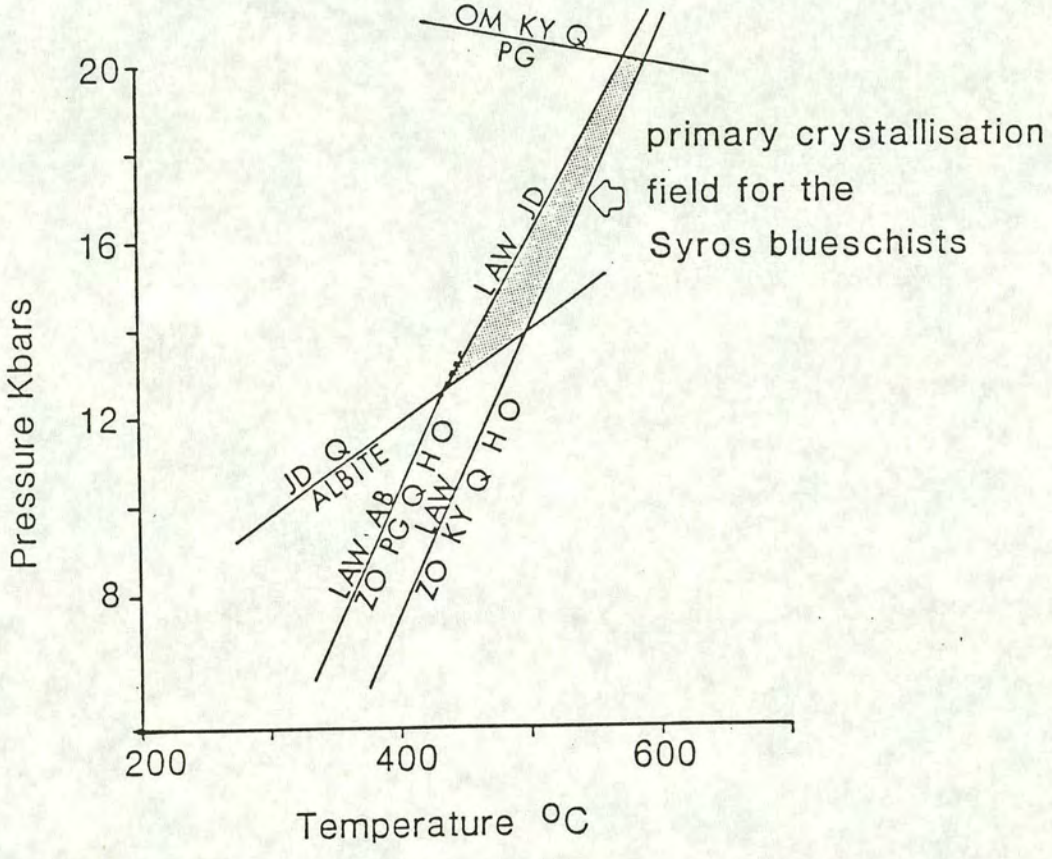

Figure 1.2 Calculated equilibria defining the peak PT conditions for the Syros blueschists. All equilibria calculated using thermocalc (Holland & Powell, 1988) and the extended data-set (Powell & Holland, 1988). Taken from Barr (1989).

During uplift the blueschists were sporadically overprinted by greenschist assemblages. This retrogressive event involved considerable externally derived fluid flow (Barr 1989). However, the greenschist overprint is largely restricted to southern Syros, and the rocks in and around the northern gneiss-serpentinite belt are virtually completely unaltered blueschists. Barr (1989) suggests that this may be the result of the thick marble sequences in the centre of the island impeding fluid flow up the pile.

The blueschist metamorphism is accompanied by intense ductile deformation described in detail by Ridley (1982). This is essentially a single continuous event although it can be divided into two broad phases. The first results in the formation of a pervasive layer parallel foliation. The second involves the folding of this foliation and compositional layering on a variety of scales during an episode of ductile thrusting. No evidence of any previous deformational event is preserved in the blueschists, though on stratigraphic grounds an early imbrication event duplicating the major marbles may have occurred (Ridley, 1982).

1.2.2 Fluid Regime during the Blueschist metamorphism

Only one previous study has considered the syn-metamorphic fluid regime in the Syros blueschists in any detail, that of Barr (1989). She used a number of independent techniques to assess both the composition of the synmetamorphic fluids and the extent of fluid transport / equilibrium within the blueschist metasediments. Her methodology and results are summarised in the following sections.

Mineral Equilibria Study

Barr constructed T-X(CO2) grids for the Syros blueschists using the extended thermodynamic data set of Holland & Powell (1988) in conjunction with the T-X SYSTEM program of Perkin, Brown & Berman (1986) and compared the results with the assemblages found in the greyschists. Despite the limitations on the method

imposed by the fact that only a finite number of components and phases can be conveniently represented in two dimensions the predicted assemblages agree closely with those present in all but the most extreme bulk compositions. This agreement supports both the validity of the grids and the conclusion that, in general, chemical equilibrium has been achieved in the metasediments.

Barr draws two important conclusions from the mineral equilibria study:-

1/ The Syn-metamorphic fluids are extremely water-rich.

All but one of the assemblages that Barr identifies in the meta-sediments contain a glaucophane lawsonite or a glaucophane epidote tie line or both. The T-X(CO2) grids clearly show that fluids in equilibrium with such assemblages are restricted to very water-rich compositions (Figure 1.3). It should be noted on this plot the most CO2-rich fluid, on the right hand side, is only one mol% CO2. Thus syn-metamorphic fluids must be almost pure water.

Barr notes that this conclusion is independently supported by the presence of lawsonite and sphene in the vast majority of the samples. Nitsch (1972, 1974) shows that a critical factor in the control of lawsonite stability is the composition of the coexisting fluid. In a pressure range of 3 to 7 Kb lawsonite and quartz is unstable with respect to calcite and pyrophyllite at values of $X(CO_2)$ greater than 3 mol%. Furthermore, the stability field of lawsonite and quartz in $T\text{-}X(CO_2)$ space decreases with increasing pressure over this range. Thus, at the elevated pressures of the Syros blueschist deformation lawsonite will only be stable in the presence of extremely water-rich fluids. Similarly, studies by Schuiling and Vink (1967) and Hunt and Kerrick (1977) on the reaction :-

$$\text{sphene} + CO_2 = \text{rutile} + \text{calcite} + \text{quartz}$$

conclude that, under pressure and temperature conditions relevant for Syros, sphene can only be stable in the presence of a very water-rich fluid. Thus the abundance of sphene in Syros meta-sediments is further evidence for the water-rich nature of the

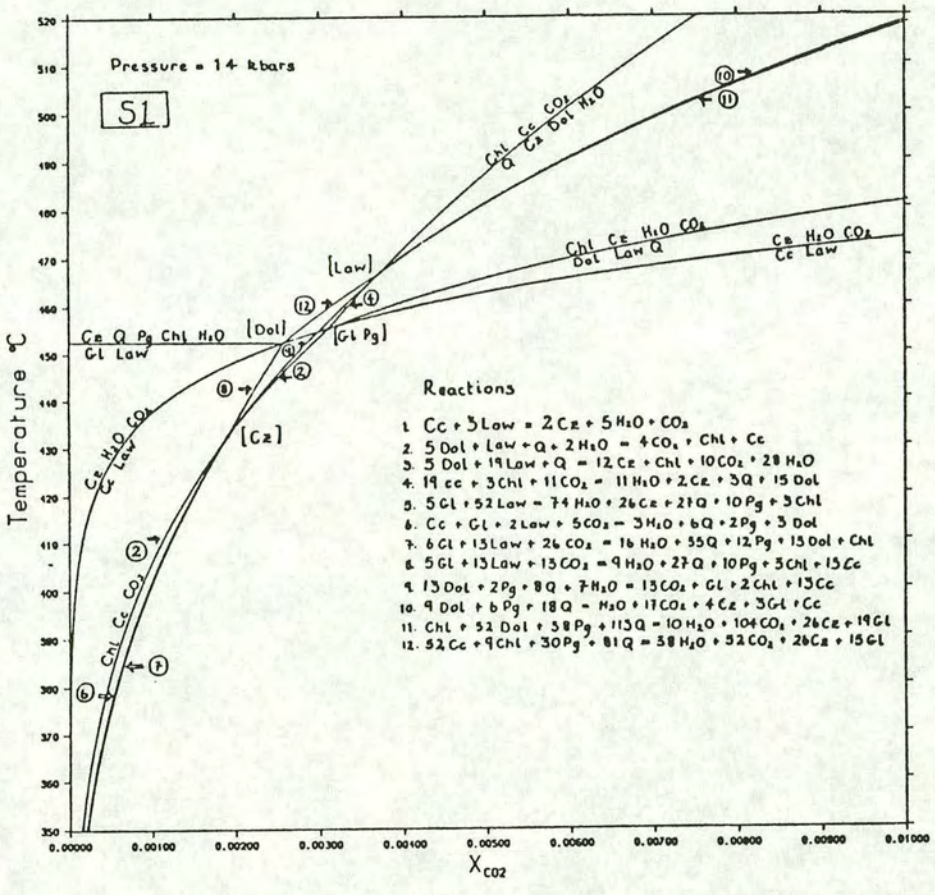

Figure 1.3 Calculated T-XCO_2 section for the Syros metasediments produced by Barr (1989).

fluid phase during the blueschist metamorphism. Barr superimposes the sphene/rutile equilibria on the T-X(CO_2) section (see figure 1.4) and concludes that, given the uncertainties in the thermodynamic data, the fit is very good.

2/ There is significant small scale variation in the composition of syn-metamorphic fluids

Barr placed observed assemblages into the T-X(CO_2) grids by comparing them with the compatibility tetrahedra for the 4 phase divariant fields. When assemblages from one outcrop are placed in the grid they fall in different divariant fields (Figure 1.5). This is vitally important as it implies that the assemblages are in equilibrium with fluid of different compositions. Barr deduced from this that each rock layer evolved as a closed, buffered system during the blueschist event and the input of external fluid was low or non-existent.

Stable isotopic analysis

Barr (1989) examined the variation of $\delta^{18}O$ and $\delta^{13}C$ in a range of lithologies in the blueschist rocks of Syros. Data was collected on each of the main lithological types; marble, schists and meta-basites.

Analysis of the carbonate from 17 pure marble samples showed that their $\delta^{18}O$ values were spread over a range of 23.8‰ to 29.1‰ (Figure. 1.6). All but two of the samples plotted in the normal range of Tertiary marine carbonates, 25 to 30‰ . There are often small drops in $\delta^{18}O$ values at the marble schist contact but this is not always the case. Other studies (e.g. Bickle and Baker 1990a) have shown that extensive infiltration of metamorphic fluid would be expected to cause a significant reduction in $\delta^{18}O$ values at the margin of marble layers. Thus, it appears that the marbles of northern Syros have experienced little fluid flow . Analysis of impure marbles showed some reduction of $\delta^{18}O$ but this depletion can be explained by $\delta^{18}O$

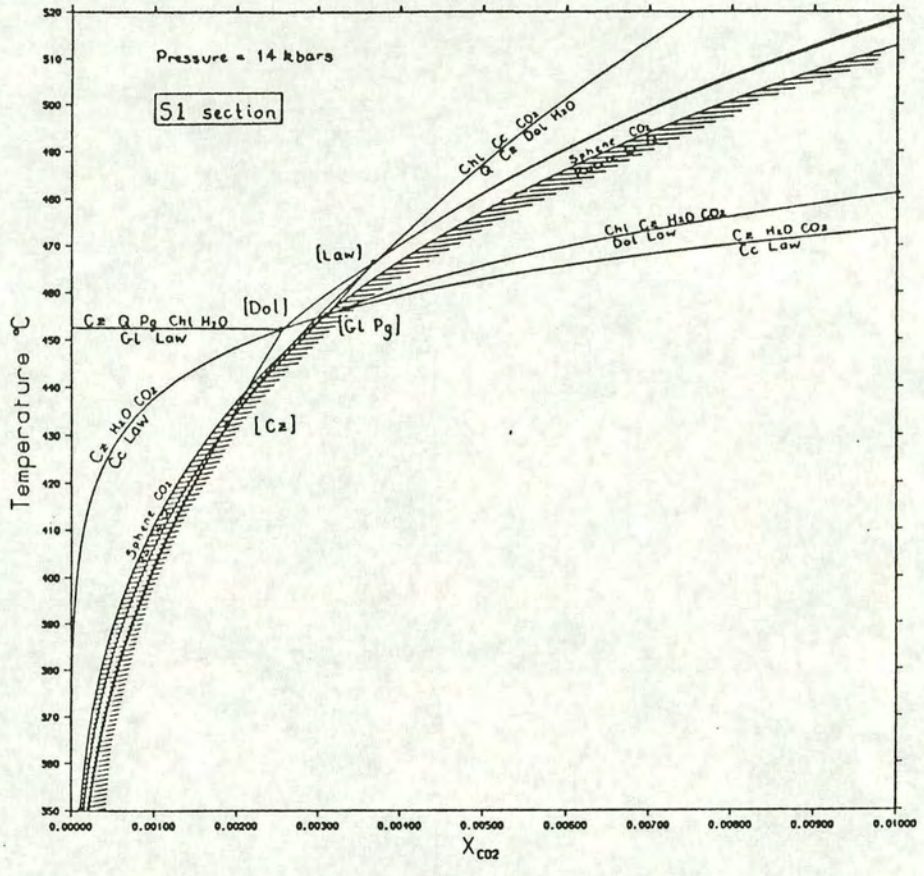

Figure 1.4 The equilibria sphene + CO2 = rutile + calcite + quartz superimposed on a T-CO2 section for the Syros metasediments. Taken from Barr (1989).

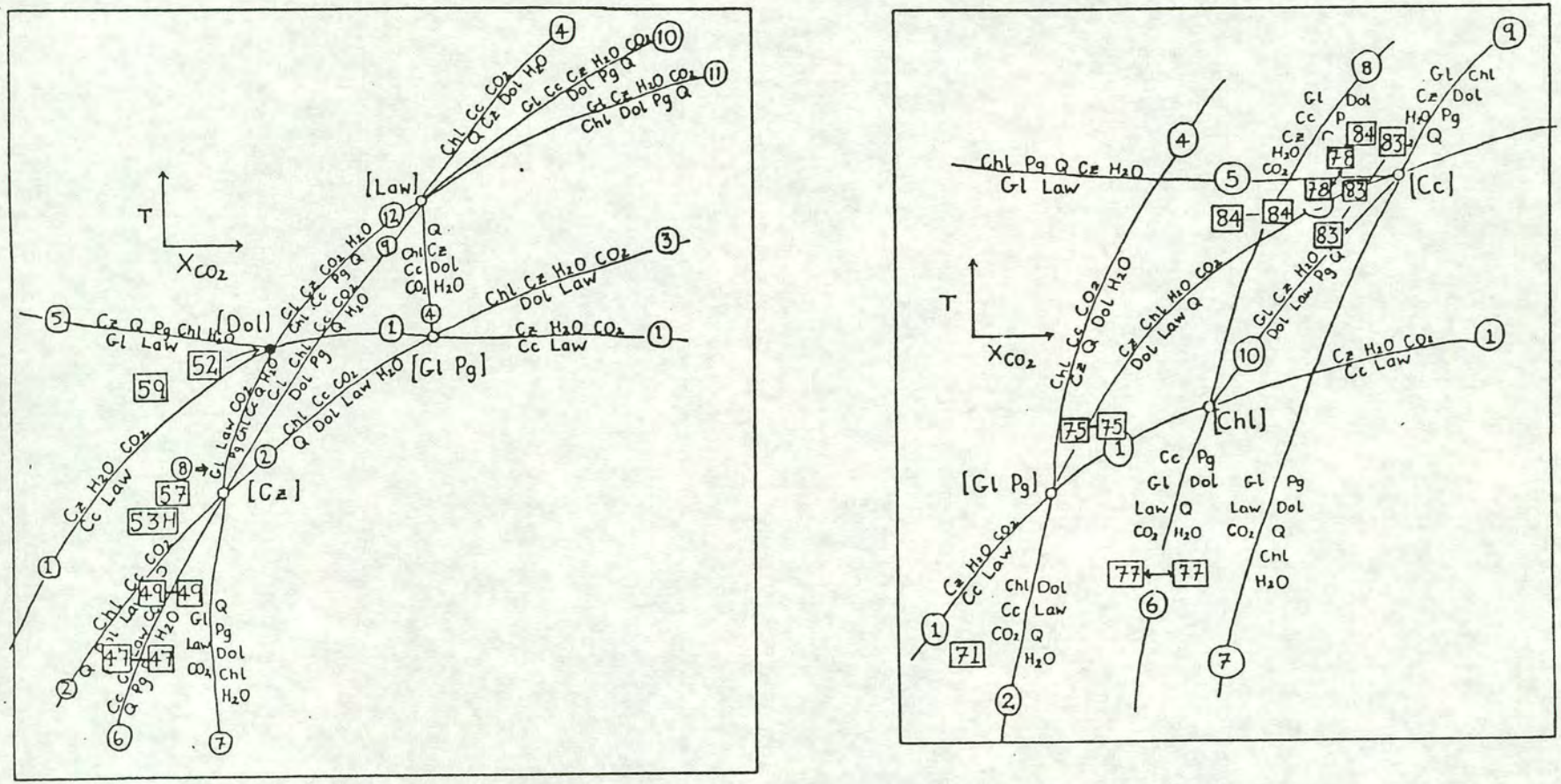

Figure 1.5 Schematic plots showing the distribution of assemblages from two outcrops in the metasediments when placed in the relevant T-CO2 sections.Boxed numbers refer to individual samples.Taken from Barr (1989).

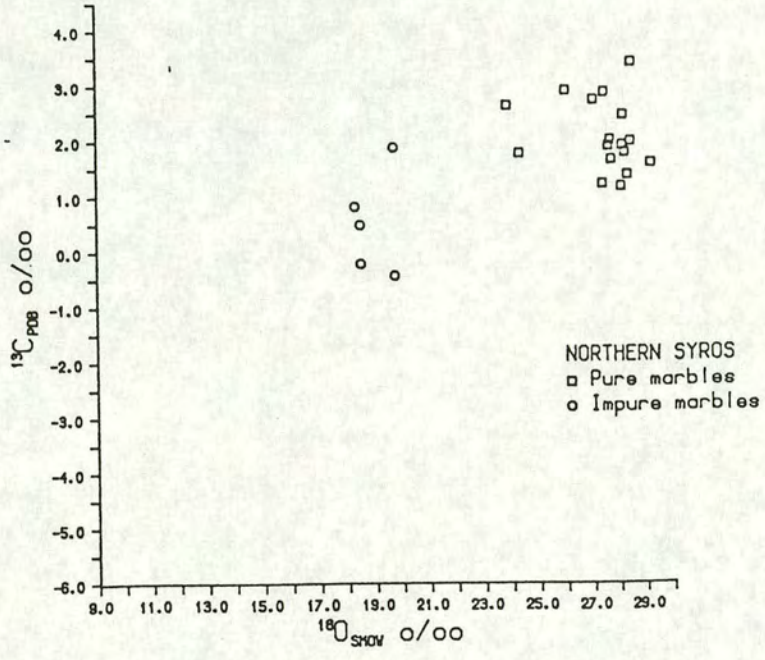

Figure 1.6. Plot of $\delta^{18}O$ versus $\delta^{13}C$ for calcite in marbles from northern Syros. (Barr 1989).

depletion associated with decarbonation reactions and the formation of calc-silicate minerals.

$\delta^{13}C$ values for the marbles vary between 1.2 and 3.4‰, within the range of -1 to 4‰ for $\delta^{13}C$ of marine limestones in Phanerozoic times. Barr suggests that very little modification of $\delta^{13}C$ values of the marbles has occurred and that the values essentially reflect original variation in pre-metamorphic carbon. However, she suggests that negative $\delta^{13}C$ values may indicate interaction with a fluid containing carbon derived locally from graphite-bearing schists.

Analysis of the carbonate from the schists (Figure 1.7) proved more problematic as it is difficult to assign a pre-metamorphic value for isotopic ratios. While the original values were probably close to that for unaltered limestones, the final value will depend on the amount and source of the silicate material present. Thus it is impossible to assess the effects of fluid flow. However, negative values for $\delta^{13}C$ lead Barr to suggest that a proportion of graphite-derived carbonate is present in the schists. She also suggests that this may be achieved by production of ^{13}C depleted methane in the schists.

In addition, stable isotope data were collected on silicates in both whole rock and mineral separate analyses from the schists and meta-basites. Interpretation of whole rock data for silicates is much more difficult than that for carbonates as the isotopic ratios are strongly dependent on the mineralogy of the samples. Thus, the mineralogical effects must be removed before the data can be compared directly. Barr achieves this by plotting $\delta^{18}O$ WR against chemical index, as defined by Garlick (1966) (Figure 1.8).

Examination of the plot produced shows that the meta-sediments tend to have higher whole rock ratios than the meta-basites , largely reflecting the higher modal abundance of ^{18}O-rich quartz in the schists. However, Barr notes that if the meta-sediments and meta-basites had equilibrated with a fluid of constant isotopic

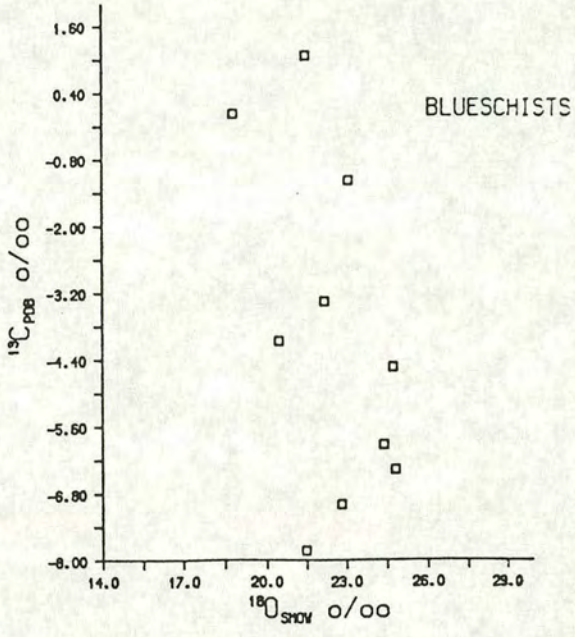

Figure 1.7 Plot of $\delta^{18}O$ versus $\delta^{13}C$ for carbonates in the blueschist metasediments. (Barr 1989).

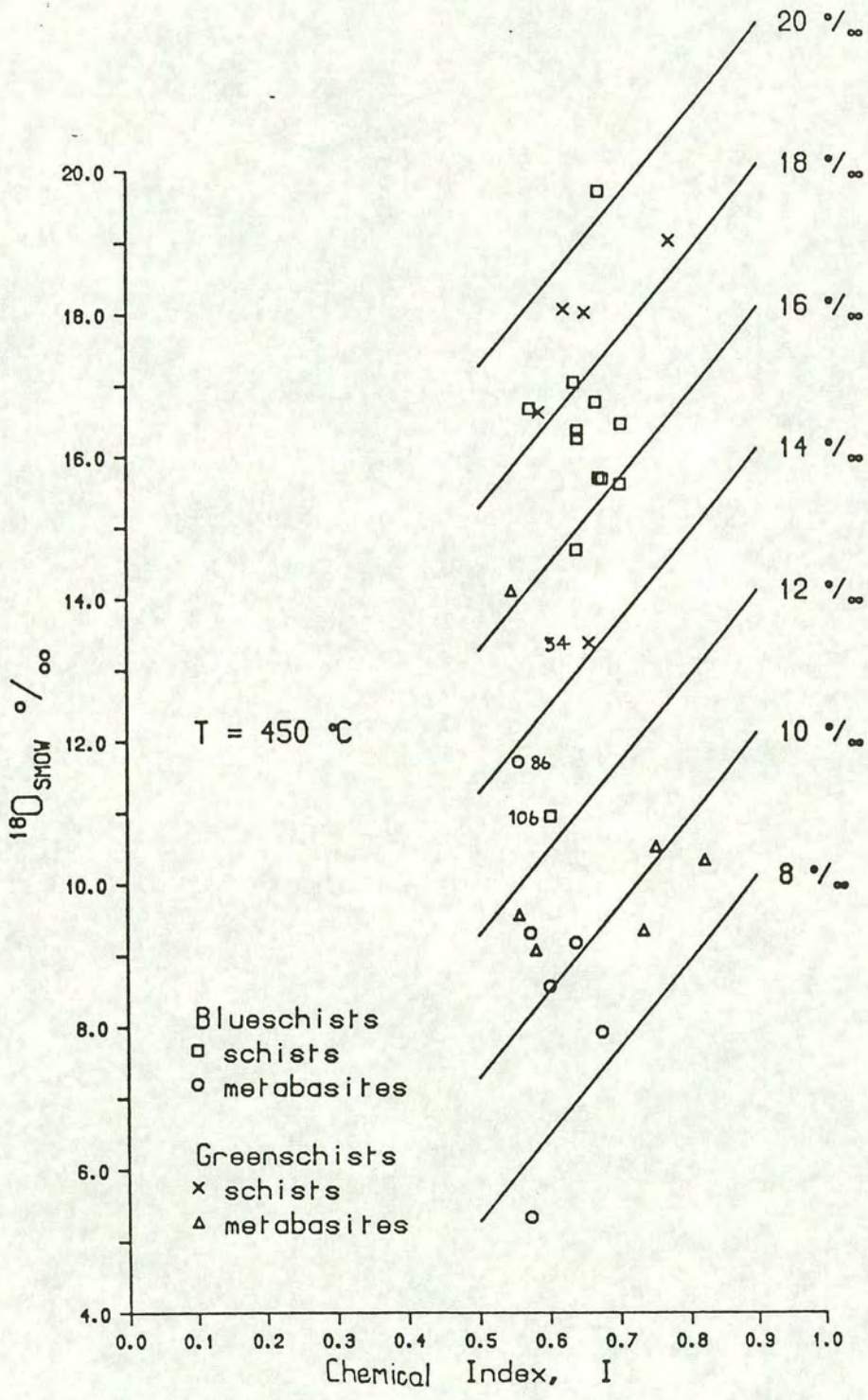

Figure 1.8 Plot of $\delta^{18}O$ against chemical index I for schist and metabasite whole rock samples. The isopleths refer to the isotopic composition of water in equilibrium with the whole rocks calculated for a temperature of 450 C. (Barr 1989).

composition, then on a Garlick plot the isotopic ratios of the rocks should reflect their chemistry i.e. there should be a straight line correlation between increasing $\delta^{18}O$ and increasing chemical index. The values should plot as a group dispersed along the appropriate fluid isopleth.

However, in the plot produced by Barr the whole rock values for the blueschist rocks are dispersed vertically. She concludes that this means that individual rocks equilibrated with fluid of different isotopic compositions, and therefore that the blueschist rocks have buffered the $^{18}O/^{16}O$ compositions of the coexisting fluids.

Finally, Barr analysed mineral separate data for blueschist rocks. The variation in isotopic fractionation between quartz-white mica and glaucophane-quartz from different samples may indicate that isotopic equilibrium was not established during the primary event, but Barr does not discount scatter during retrograde isotopic exchange. However, analysis of quartz from individual layers in a single outcrop showed 2.5‰ variation in $\delta^{18}O$ values. Barr takes this to indicate that there was little fluid communication across layers during the blueschist event.

Fluid inclusion data

Barr (1989) also analysed fluid inclusions with a view to identifying examples of early syn-metamorphic fluid and correlating it with fluid compositions predicted by mineral equilibria studies. Inclusions were studied from quartz occurring as segregations or within the rock matrix. The segregations can be constrained to the blueschist event as they are deformed and boudinaged, and the area suffered only one deformation, which was synchronous with the blueschist event (Ridley 1982). In addition, only small, texturally early quartz segregations were sampled in order to pinpoint syn-metamorphic fluids.

The fluid inclusions from the quartz in the blueschists appeared to represent several populations but all appear to be water-rich and no evidence was noted for CO_2-bearing two phase inclusions. However, virtually all of the inclusions were saline, with some actually salt saturated. Barr noted the presence of $NaCl_2$, $CaCl_2$ and MgCl in the saline solutions. She refers to the suggestion of Crawford et al (1979) that hydration reactions could cause increased salinity in the fluids. Barr also notes that the halite saturated inclusions were only noted in a sample containing 40% lawsonite by volume. While she acknowledges that this may just be a coincidence she suggests that there may be a link between halite-rich fluid and lawsonite development.

In addition to inclusions in quartz, Barr also analysed inclusions in garnets from a sample of blueschist meta-sediment. One can be certain that the garnet grew under blueschist conditions and therefore probably trapped inclusions of synmetamorphic fluid. Once again, the fluid was water-rich with no evidence of CO_2 but the salinity was much lower than for the quartz inclusions. Barr suggests it may represent an early fluid before hydration reactions concentrated the halides.

Finally, Barr notes that if the fluid inclusions in the blueschists preserve samples of fluid evolved during metamorphic reactions, a correlation between the compositions of the fluid and host rock should be expected. The Syros samples show no apparent difference in CO_2/H_2O ratio of the fluid from samples containing different mineral assemblages. However, Barr suggests this may merely reflect the fact that the equilibrium CO_2/H_2O ratio is so low that slight variation in the CO_2 content of the fluid between different samples are impossible to detect thermometrically.

Barr concludes that, while it is not possible to state unequivocally that the fluid inclusions present in the blueschists represent samples of synmetamorphic fluid, the absence of a CO_2 phase and the abundance of aqueous inclusions is compatible with the equilibrium phase assemblages.

1.2.3 Previous Investigations of fluid control of lawsonite growth

1.2.3.1 Lawsonite Growth on Syros

Barr (1989) considers the possible nature of fluid control of lawsonite in the Syros metasediments in some detail. She notes that while the degree of textural equilibrium in the blueschists makes it difficult, if not impossible, to identify the lawsonite-forming reactions the types of reaction that can be suggested are constrained by the possible precursor phases. The lawsonite must have formed from a carbonate precursor or a pre-existing Ca-silicate phase, such as epidote. On these grounds she suggests two possible reactions and assesses the consequences

1/ 2 calcite + pyrophyllite + H_2O = 2 lawsonite + 2 CO_2 + 4 quartz

Phengitic muscovite is actually the mica phase in the Syros rocks but as the precise reaction is unknown pyrophyllite is used as it simplifies the model and does not affect the overall conclusions.

The most important factor to note about this equation is that large volumes of CO_2 are produced at the same time as lawsonite. In low porosity rocks, this means that the build up of CO_2 will soon cause the fluid phase to buffer against the formation of lawsonite and little lawsonite will be produced. However, this is contrary to observations on Syros assemblages which can contain up to 40% by volume lawsonite. This apparent paradox can be explained in two ways:-

(a) Reaction at an invariant point

(b) Infiltration of an external fluid.

Barr discounts the first suggestion on the grounds that there is no mineralogical evidence to support it. She notes however, that the distribution of lawsonite in the field supports the second option. In particular, she cites the presence of lawsonite

bands at the margin of otherwise lawsonite free meta-basites as evidence of fluid infiltration as the driving mechanism behind lawsonite development.

However, Barr then estimates the volume of fluid required to produce the observed lawsonite concentrations. She estimates that at 14 Kb and 450°C, 28 cm^3 of pure water would be required to produce 1 cc of lawsonite per 100 cc of rock with 0.5% porosity. It should be noted that this is a minimum estimate as the fluid is assumed to be pure H_2O and each packet of fluid is assumed to mix perfectly with the 100 cc of rock ,generating 100% of the possible lawsonite. Nevertheless, it is a very large volume of water.

However, Barr recognises that this model for infiltration by external fluid is in direct contradiction to the internally buffered regime with little external input of fluid suggested by her mineral equilibria and stable isotope studies. She suggests that the contradiction may be accounted for by channelised flow along beds, but an attempt to identify this using $\delta^{18}O$ was inconclusive due to lack of data.

2/ 24 epidote + 6 C +3 SiO_2 = 11 grossular + 9 lawsonite + 9 almandine + 6 calcite + 3 H_2O

2 epidote + 5 H_2O + CO_2 = 3 lawsonite + 3 calcite

Barr notes the strong correlation between the occurrence of lawsonite and the presence of graphite in the schist. She also compares the lawsonite-bearing and lawsonite-free schists to see if there is any regular difference in assemblage between the two groups. She suggests that the assemblages fall into three main groups:-

(a) lawsonite + calcite + graphite

(b) lawsonite + calcite

(c) epidote + calcite (± a small amount of lawsonite).

From this data she suggests two distinct mechanisms for generating lawsonite. In the graphite-bearing schists she suggests a reaction such as 2(a).

involving in situ graphite burning. In order to liberate the oxygen required Fe^{3+} bearing epidote is reduced to Fe^{2+} bearing almandine garnet. This reaction would be coupled with an infiltration driven reaction in the graphite-free schists of the type quoted in 2(b). The CO_2 in the required H_2O-CO_2 fluid would be generated by the graphite burning in the adjacent rocks.

Overall the conclusion from Barr's study was that some form of channelised flow must have been involved to resolve the conflict between the implications of the lawsonite-forming reactions and the local equilibrium observed in general. Barr's T-X analysis had concentrated on lithologically variable calcareous schists and not on the relatively uniform but lawsonite-rich greyschists. Graphite burning could be an important mechanism but would not explain lawsonite growth in the calcite-free schists.

1.2.3.2 Lawsonite Growth in Alpine Blueschists

Pognante (1989a, 1991) has suggested that the growth of lawsonite during post eclogitic recrystallisation under blueschist facies conditions in the Eclogitic Micaschists of the southern Sesia Zone in the Italian Alps is controlled by the infiltration of water-rich fluids. As in the Syros metasediments the lawsonite is syntectonic and takes the form large euhedral porphyroblasts which were later pseudomorphed by clinozoisite and mica during uplift. Pognante notes that the distribution of lawsonite is very heterogeneous on sub-outcrop scale (Figure 1.9). Within the same protolith cm to m scale layers or irregular lawsonite-rich lenses grade into areas devoid of lawsonite. High concentrations of lawsonite also occur at the boundary between metabasites and micaschists. In addition, lawsonite is found in syn-deformational quartz veins along with omphacite ± phengite.

In the first of his papers, Pognante (1989) analyses the phase relations in the eclogitized metabasites. He notes that the lawsonite-bearing assemblages are stabilised by high μH_2O and therefore, that growth of lawsonite might be promoted

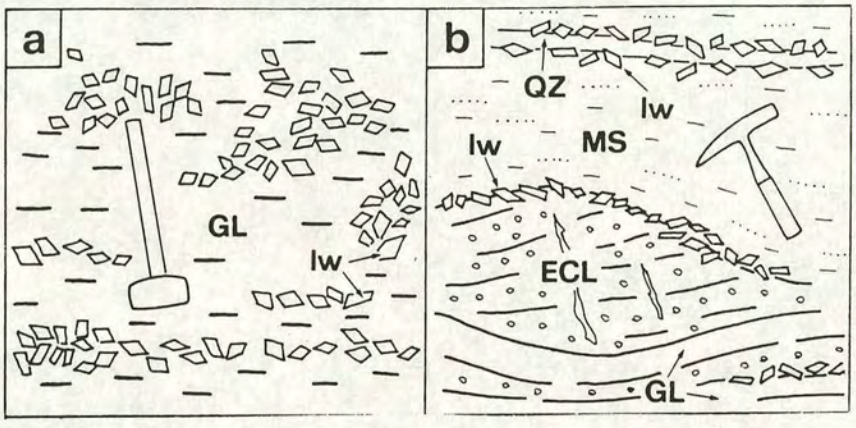

Figure 1.9 Sketches illustrating the distribution of lawsonite in the Eclogitic Micaschists of the southern Sesia zone.

a) Glaucophanite (GL) of the Eclogitic Micaschists (Malone valley, NW of Rocca Canavese). Porphyroblastic lawsonite pseudomorphed by zoisite overgrow a pre-existing foliation defined by glaucophane and garnet ; it has a very heterogeneous distribution and is concentrated either in discontinuous layers or in irregular lenses.

b) Eclogitic Micaschist (Malone Valley). Contact between micaschists (MS) and layered metabasics consisting of boudinaged glaucophane eclogites (ECL) and glaucophanites (GL). Porphyroblastic lawsonite pseudomorphed by zoisite occurs at the boundary between MS and ECL, between GL and ECL and at the selvages of a quartz-rich metamorphic vein (QZ) crosscutting MS. Taken from Pognante 1989.

by the infiltration of a water-rich fluid. In the second paper (Pognante 1991), he notes the evidence for the mobility of Ca in the synmetamorphic fluid phase provided by the presence of lawsonite bearing-veins and suggests that the growth of lawsonite might also involve metasomatic addition of Ca to the protolith.

1.3 Choice of Study Area

Lawsonite-bearing assemblages formed throughout the Syros meta-sediments during the blueschist facies metamorphism. However, for the purposes of this study it was decided to concentrate on two relatively extensive meta-pelitic units outcropping in the north of the island which were named the greyschists by Dixon (1969) (Figure 1.10). These units were chosen for a number of reasons.

1. Excellent preservation of peak blueschist assemblages.

As in the vast majority of the units in the northern parts of the island the greyschists exhibit little post peak blueschist alteration other than the pseudomorphic replacement of lawsonite by clinozoisite and micas. In the Lower Greyschist Unit there is no greenschist alteration. In the Upper Greyschist Unit retrogressive alteration is rare and limited to pseudomorphic replacement of garnet by chlorite and occasionally glaucophane by chlorite and albite.

2. Well developed syn-metamorphic structures.

The high sheet silicate content of the greyschists and the presence of clearly defined, fine-scale compositional layering means that they develop an array of structures on a variety scales during the syn-blueschist deformation. Interpretation of these structures provides a detailed record of the strain history. This is crucial in assessing the importance of variation in the state of strain and the relative timing of different events / processes.

3. Limited compositional variation.

The greyschists display only a limited amount of compositional variation and that present can be simply characterised. This limits the extent to which variation in lawsonite concentration can be due to primary compositional variation and makes it easier to distinguish variation in composition which results from major element metasomatism.

4. The greyschists contain large concentrations of lawsonite porphyroblasts which are easily identified in the field.

The schists contain some of the highest concentrations of lawsonite found within the meta-sediments. This lawsonite is present as striking large white rhombs which contrast strongly with the dark grey graphitic matrix. Thus it is possible to accurately map changes in concentration of lawsonite in the field.

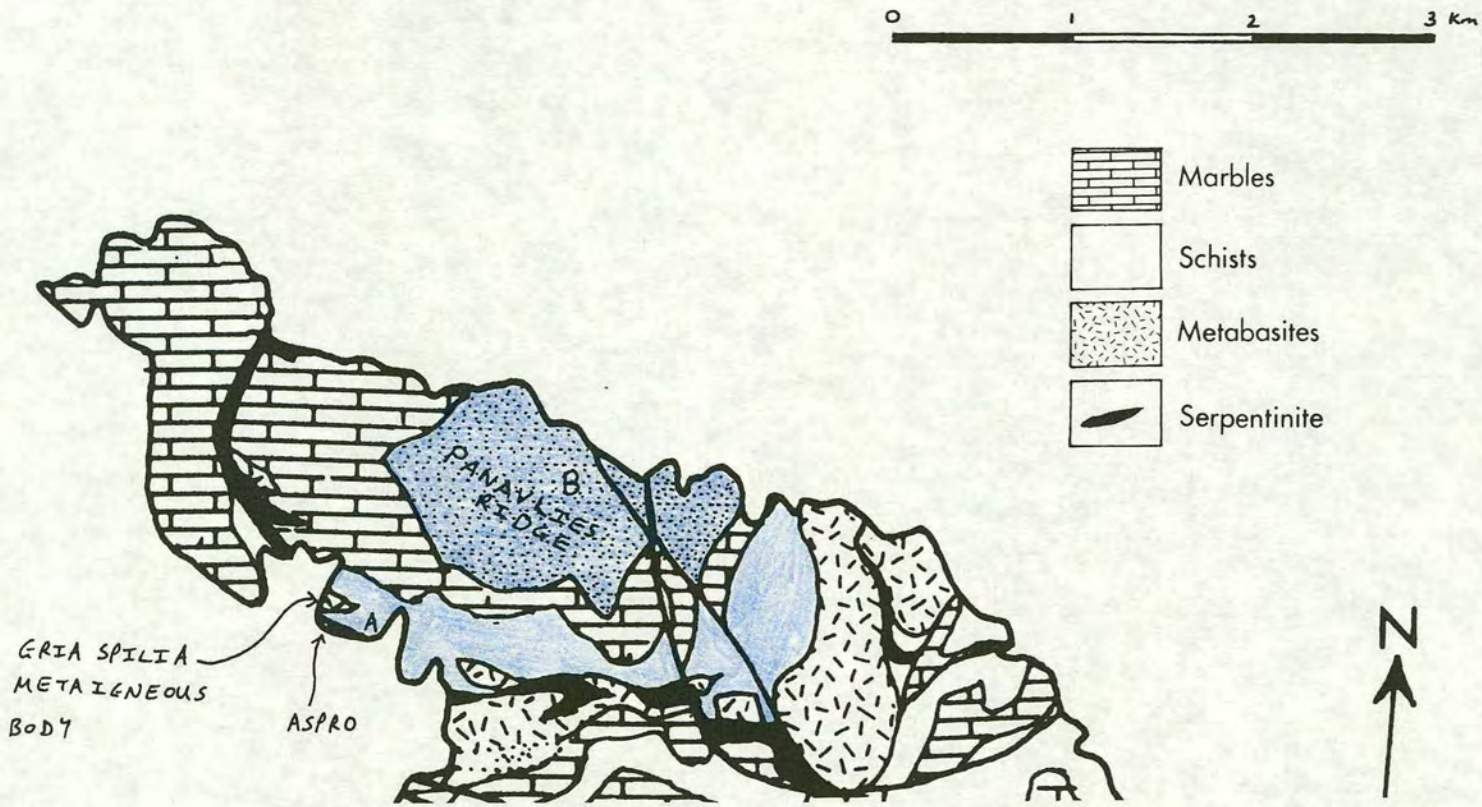

Figure 1.10 Geological map of part of northern Syros showing the position of the greyschist units (shaded in blue, UGSU stippled, LGSU plain). (A) marks the location of the Cedar Tree and Overhanging Outcrops. (B) Marks the position of the outcrops described in the UGSU.

CHAPTER 2

COMPOSITION, PETROLOGY AND MINERALOGY OF THE GREYSCHISTS

2.1 Introduction

The selection of the greyschists as the field area for the study is in part due to their composition and mineralogy. This chapter has two broad aims. Firstly to describe the characteristics of the primary sedimentary compositional variation so that this can be distinguished from compositional variation which results from metamorphic processes. Secondly, to describe the petrology of the schists and any light this sheds on the mechanisms associated with the growth of lawsonite.

2.2 Primary Compositional Variation in Greyschists

A group of 28 samples of graphitic schist collected from the Upper and Lower Greyschists Units were analysed to assess the extent and nature of pre-metasomatic compositional variation in the greyschists. Care was taken in selecting the samples to ensure that they fell outside that zones of alteration associated with quartz veins.

Overall, the samples display relatively minor variations in composition. Plotting the resulting data on the discrimination plot of Herron (1988) suggests that the proliths ranged in composition from shales to greywackes (Figure 2.1). This is consistent with their interpretation as relatively distal continental margin deposits.

Closer examination reveals a simple pattern of compositional variation within the data set. This is best illustrated by comparing the changes in concentration of individual components with changing Si content of samples (Figure 2.2). The concentration of Al, Fe, Mg, K, Ti, Mn and the majority of the minor elements decrease with increasing Si concentration as do the volatile contents of the samples (estimated by loss on ignition measured during preparation of samples for XRF). This is to be expected as the Si is the most abundant element and an increase in its concentration will cause a decrease in all components due to the closure effect. In addition, much of the Si is present as quartz which contains no trace elements or

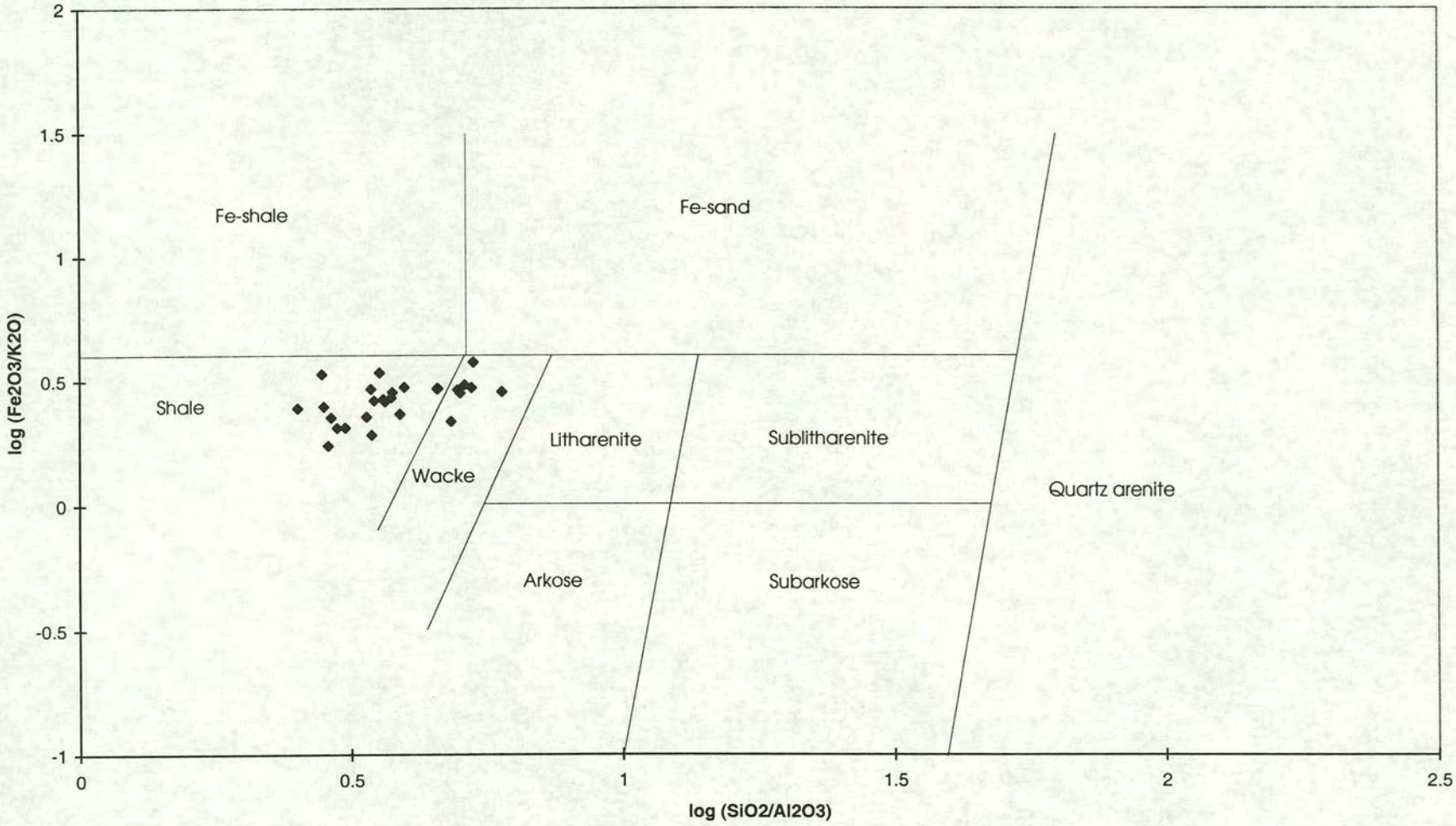

Figure 2.1 Discrimination using the method of Herron (1988) to identify the protolith of the greyschists.

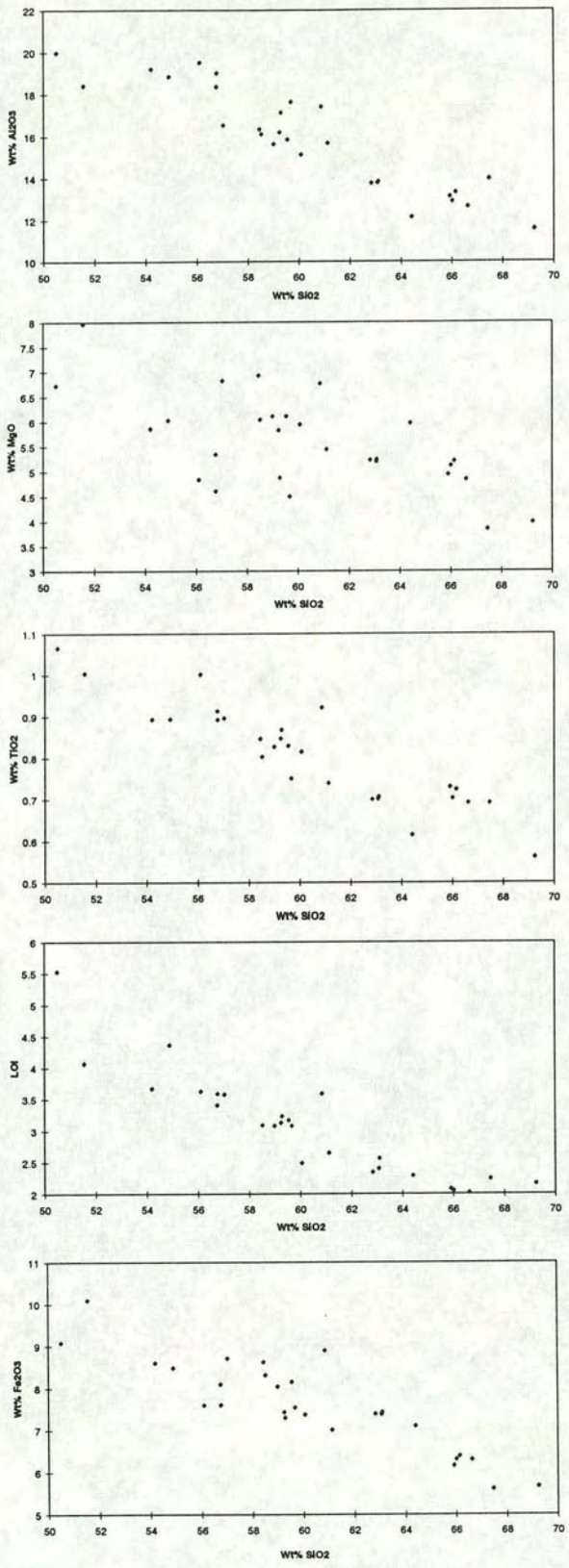

Figure 2.2a Series of plots showing the variation of other concentration other components with variation in silica content in unaltered samples of graphitic schist.

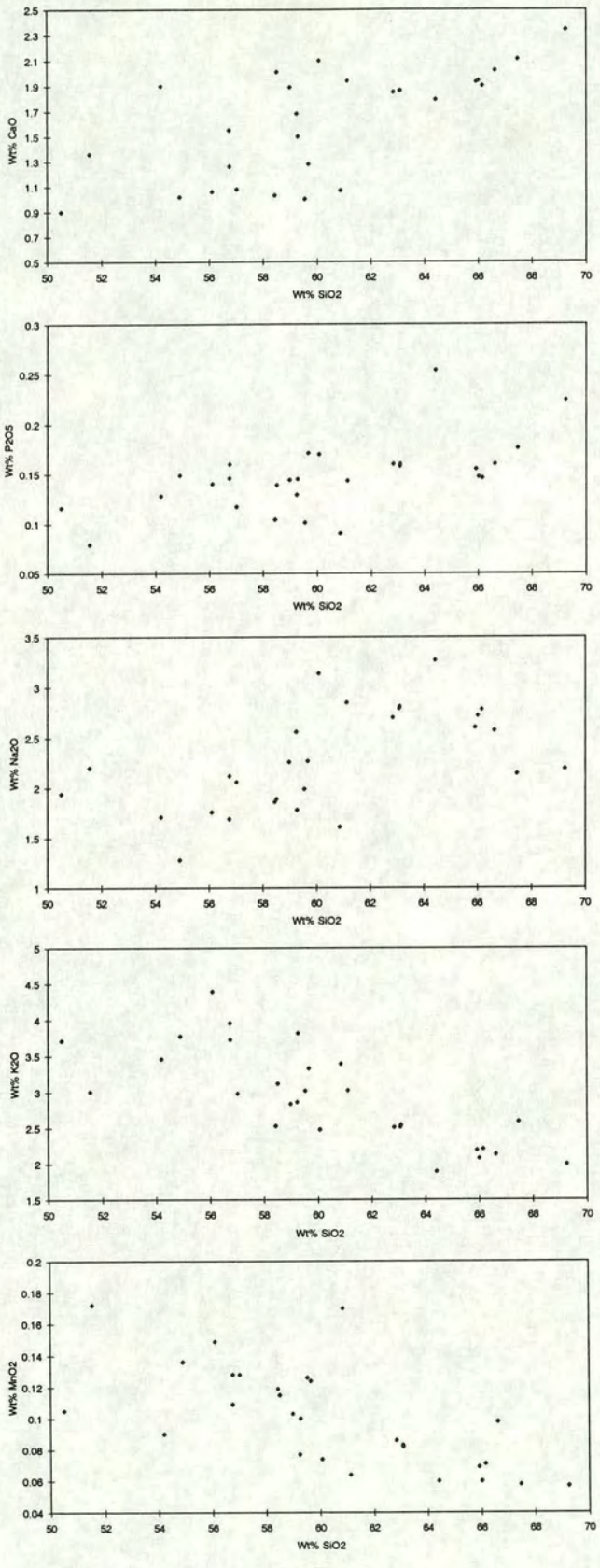

Figure 2.2b Series of plots showing the variation of other concentration other components with variation in silica content in unaltered samples of graphitic schist.

volatiles. However, in contrast, the concentrations of Ca, Na and P all increase with increasing Si content.

This pattern of compositional variation is attributed to primary sedimentary processes and can be modelled as resulting from the mixing in differing proportions of two detrital components. One a clay fraction rich in Al, Fe, Mg, K, Ti, Mn and trace elements and the other a quartz and feldspar fraction rich in Si, Ca, Na, and P. Such bi-modal compositional variation is often visible within the greyschists as alternating mica-rich and quartz-rich interlayers on a variety of scales.

2.3 Petrology of the Greyschists

Over 150 thin-sections were analysed using a combination of thin-section, XRD and electron probe analysis in order to characterise the peak blueschist mineral assemblage(s) in the greyschists and identify any possible reaction textures that might shed light on their petrogenesis and particularly the growth of lawsonite.

2.3.1 Identification of equilibrium mineralogy

Commonly accepted criteria were used to distinguish equilibrium assemblages. All minerals must occur in the same thin section. Each mineral must share contacts with all others with no evidence of reaction. However, three factors complicate the unequivocal identification of equilibrium assemblages in the grey schists.

(A) Identification of paragonite

All greyschist samples contain large quantities of white mica of which the vast majority is phengite. However, microprobe analysis reveals that they may also contain relatively small amounts of paragonite, typically intergrown with the phengite. Unfortunately, it proved impossible to distinguish the two micas optically.

Attempts to stain the phengite using the method of Laudron (1971) were also unsuccessful.

Paragonite can be identified by XRD. However, the low concentrations present in the greyschists may not be discernible. In addition, lawsonite pseudomorphs typically contain paragonite. Thus, the paragonite identified by XRD may not be part of the peak blueschist assemblage.

Overall, other than by undertaking time consuming, detailed microprobe analysis it is impossible to conclusively prove the presence of paragonite in the equilibrium assemblage of any particular sample. However, all samples that were analysed using the micro-probe did contain paragonite which appeared to be in equilibrium with the other phases present.

(B) Size of lawsonite pseudomorphs

The former presence of lawsonite in the schists is indicated by the presence of euhedral rhombic pseudomorphs typically 0.5 to 1.5 cm in size. The fact that it is pseudomorphed does not hinder the identification of peak blueschist equilibrium assemblages. The morphology of the pseudomorphs and the nature of the pseudomorphing phases leaves little doubt that the original phase was lawsonite. Furthermore, their structural status indicates that they were present during the deformation synchronous with the peak blueschist metamorphism while their preservation indicates that the pseudomorphing event itself post dated the deformation and hence the peak of the metamorphism.

However, the large size of the porphyroblasts means that establishing the presence of lawsonite in a thin section is dependent on where the sample is cut. This is especially true in comparatively lawsonite-poor samples where the porphyroblasts are widely spaced. Thus, it is possible that lawsonite forms part of the equilibrium assemblage even though it is not present in a particular thin section. Fortunately,

lawsonite is clearly visible in hand-specimen. In all thin sections in which it is visible it was clearly in equilibrium with the other blueschist phases. Thus, if it is visible in hand specimen it is assumed to form part of the equilibrium assemblage even though its textural status relative to the other phases could not be examined on a fine scale.

(C) Status of chlorite

In some thin sections two generations of chlorite are present: one resulting from the primary blueschist metamorphism and the other associated with patchy greenschist retrogression. Fortunately, they are generally easily distinguished. The primary chlorites are invariably colourless with low first order grey interference colours, display strongly undulose extinction and often oriented parallel to the S1 and folded during the S2 crenulation event. In contrast, the secondary chlorites are generally dark green and pleochroic with textures that suggest that they result from post-deformational replacement of primary blueschist minerals, typically garnet.

However, it is more difficult to assess the extent to which the primary chlorite is in equilibrium with other primary minerals. In many samples it is only present in very small quantities and thus it is difficult to find contacts between it and all other minerals present. In others it occurs in lens shaped segregations in mica welts or pressure shadows on garnets around which the S1 foliation defined by alignment of micas wraps. Within such bodies the chlorites typically display mosaic textures with no preferred orientation.

2.3.2 Results of analysis

Given the limitations documented in the previous section it proved difficult to rigorously determine the equilibrium assemblage present in the majority of samples. All samples were examined with a petrological microscope and the majority analysed by XRD but only a limited selection were analysed using an electron probe. The majority of phases are easily identified in thin section however, as noted above,

difficulty in identifying paragonite means that only in those samples analysed by electron micro-probe (EMP) can one be sure that the entire equilibrium assemblage has been identified. XRD added comparatively little useful information to that obtained by the other techniques.

In all the thin sections examined quartz, phengite, glaucophane, and garnet were all present and clearly in equilibrium. In addition, all those sections analysed by EMP contained paragonite which appears to be in equilibrium with these phases. Thus, it is assumed to be a constituent of the equilibrium assemblage in the vast majority if not all of the graphitic schists. Other than these minerals the only other major phases present are lawsonite and chlorite. A combination of thin-section and hand specimen analysis provides evidence for the presence of lawsonite in virtually all of the samples. As noted above it may be present in small quantities even in those samples in which it could not be identified. Primary chlorite was also identified in the vast majority of samples although its concentration varied considerably and in many cases it is only present in very small quantities. At least 5 samples analysed by EMP were found to contain all 7 major phases in equilibrium. Thus, the equilibrium assemblage in the grey schists can be summarised as

$$Qtz + Ph + Gl + Gar + Pg \pm Law \pm Chl.$$

These are typically accompanied by a number of accessory phases including sphene, graphite, rutile, tourmaline, apatite, zircon and allanite in decreasing order of abundance.

By far the most abundant phases are quartz, glaucophane and white mica each constituting 15 to 30% of individual slides. It is impossible to accurately quantify the relative proportions of paragonite and phengite in the white mica. However, in those slides probed there is much more phengite than paragonite. Garnet typically constitutes 5-10%. Proportions of lawsonite and chlorite are highly variable.

The relatively uniform mineralogy of the greyschists is consistent with the limited extent of bulk rock compositional variation. The equilibrium coexistence of

the phases is also consistent with the Gibbs phase rule. Disregarding accessory phases (sphene, rutile, apatite tourmaline and graphite) and regarding H_2O as a 'perfectly mobile' component (Korzhinskii 1959) the schists can be modelled as a 7 component system SiO_2-Al_2O_3-FeO-MgO-CaO-Na_2O-K_2O. Thus, Qtz + Ph + Gl + Gar + Law + Chl + Pg represents a divariant assemblage. Fe_2O_3 can be ignored as a component as the schists are strongly reduced and no phases contain significant amounts of Fe^{3+}.

2.3.3 Possible reaction textures

In general the Syros blueschists display little or no evidence of the prograde reactions responsible for their development (Barr 1989). The greyschists are no exception. The inclusion fabrics of some glaucophane grains clearly indicate that they overgrow pre-existing mica fabrics, a relationship first noted by Ridley (1982). In addition, he suggests that the distribution of chlorite is consistent with its breakdown to form garnet although the evidence is largely circumstantial. No other reaction textures have been documented.

Considerable effort was taken in this study to identify possible reaction textures with a view to gathering evidence for possible lawsonite generating reactions, but with little success. In general all the phases present in individual slides appear to be in textural equilibrium.

However, the presence of chloritoid in some of the greyschist samples suggests that they passed through the Gl-Ctd stability field. Chloritoid is present as very small corroded grains which were only identified during microprobe analysis of the sections and it is clearly not in equilibrium with the other phases present.

Guiraud et al (1990) modelled mineral equilibria in pelitic blueschists in the system Na_2O-FeO-MgO-Al_2O_3-SiO_2-H_2O. The resulting petrogenetic grid is applicable to the greyschists. As noted above, all the major phases in the greyschists

can be represented by the components SiO_2-Al_2O_3-FeO-MgO-CaO-Na_2O-K_2O-H_2O. thus the only components present in the greyschists but not accounted for in the model are K_2O and CaO. Guiraud et al suggest that the presence of K_2O in the form of phengite will not affect the topology of the grid but merely shift the reactions limiting paragonite-bearing assemblages slightly so as to stabilise these assemblages.

The grid indicates that the lower pressure boundary of the Gl-Ctd stability field is the reaction Gl + Ctd = Pg + Chl + Gar. If the greyschists had crossed this reaction it would account for the assemblages present. Above the reaction the they would contain the assemblages Gl-Ctd-Pg-Chl, Gl-Ctd-Pg-Gar or Gl-Ctd-Gar-Chl (Figure 2.3a). Below the reaction as the Gl-Ctd tie-line is removed, the assemblages Gl-Pg-Chl-Gar or Ctd-Pg-Chl-Gar become stable depending on the bulk composition of the schists (Figure 2.3b). The fact that the former assemblage is present in the greyschists suggests that they are relatively Na and Mg rich and Fe poor.

Elsewhere in the Syros meta-sediments, in more Fe^{3+}-rich assemblages, Gl-Ctd remains stable up to the end of the blueschist metamorphism (Barr 1989). This is consistent with the findings of Guiraud et al (1990) who suggest that the addition of ferric iron to the system will enlarge the PT range over which the two phases may co-exist.

2.3.4 Implications for lawsonite generation

Examination of the petrography and petrology of the greyschists provides no direct evidence for the processes involved in the generation. In all samples examined it is clearly in equilibrium with the other blueschist phases present. There is no obvious correlation between the presence of lawsonite and the presence or concentration of any of the other phases.

However, it is significant that the schists contain no other dominantly calcium bearing phases and in particular it is noteworthy that they are carbonate-free. Thus, if

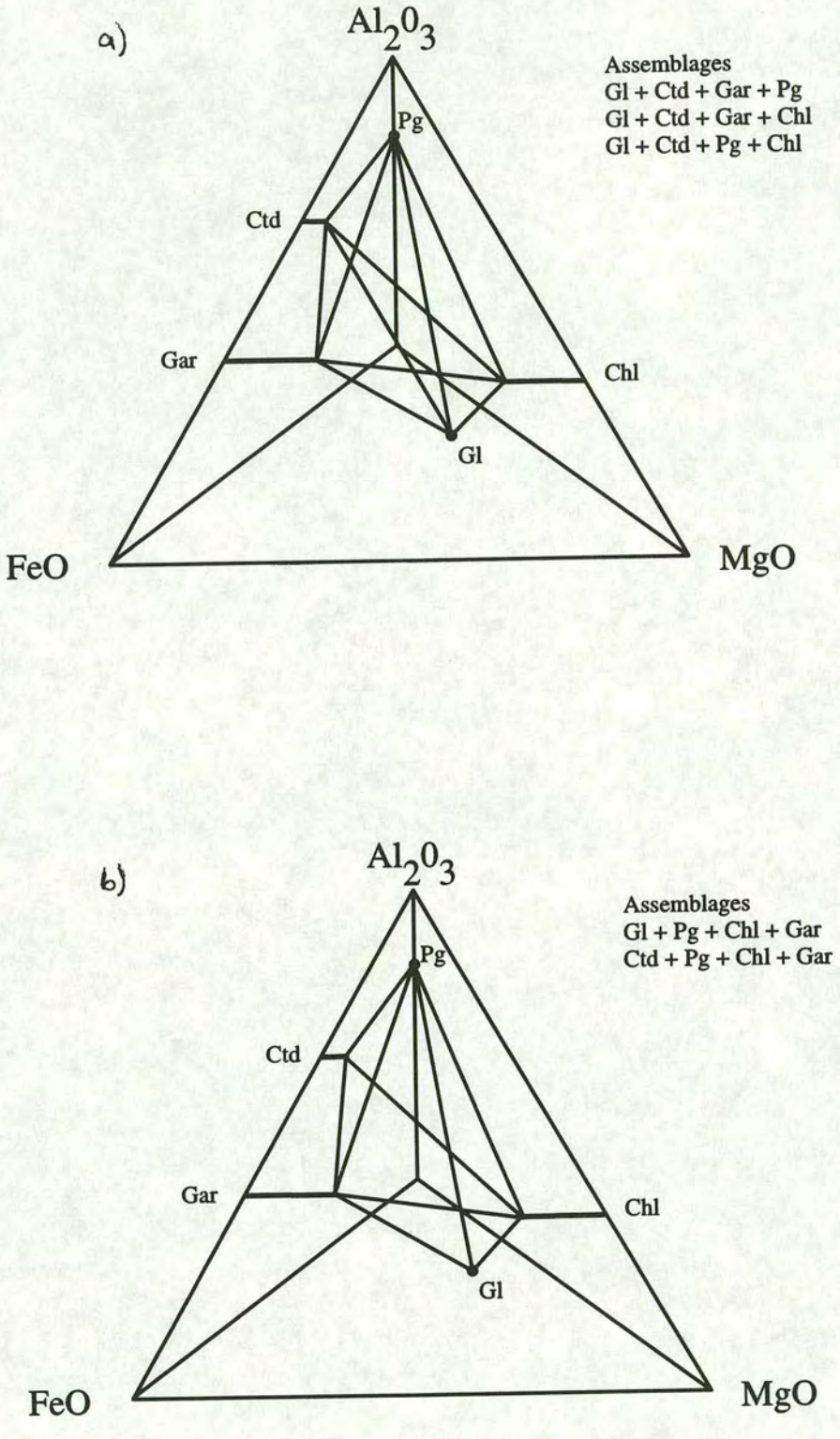

Figure 2.3 Phase compatibility tetrahedra showing stable assemblages in the system Na_2O-FeO-MgO-Al_2O_3-SiO_2-H_2O on either side of the reaction Gl + Ctd = Pg + Chl + Gar.

all lawsonite growth is the result of the breakdown of another calcium-bearing phase then this reaction must have gone to completion in all parts of the greyschists. This is clearly incompatible with the suggestion of Barr (1989) that the idiosyncratic distribution of lawsonite, and particularly changes in concentration parallel to compositional layering, is the result of varying degrees of progress of a fluid controlled reaction.

2.4 Mineral Descriptions and Chemistry

Garnet

Garnets occur as small euhedral to sub-hedral porphyroblasts up to 3 mm in size. They are often poikiloblastic containing inclusions of all the other constituent phases except lawsonite.

Some typical microprobe analyses are listed in Table 2.1. Normative molecules were calculated using the method documented in DHZ appendix X. The Fe^{3+} content calculated on the basis of 16 cations and 24 O was less than 0.1 for the vast majority of analyses so the andradite content was ignored. Results show that garnets are predominantly solid solutions between almandine and grossular (Figure 2.4). However, a regular pattern of zoning is evident within each porphyroblast. This involves a decrease in the spessartine and grossular content from core to rim and a parallel increase in almandine and pyrope.

Chlorite

Primary chlorite in the greyschists is colourless and displays normal first order grey birefringence colours. It is typically intergrown with white mica but may also occur as isolated laths in quartz-rich layers or as mono-mineralic pressure shadows on garnets.

	1 Rim	1 Core	2 Rim	2 Core	3 Rim	3 Core
SI	37.41	37.31	38.04	37.75	38.24	38.26
TI	0.09	0.13	0.08	0.08	0.1	0.17
AL	21.41	20.96	21.29	21.04	21.18	21.03
CR	0.02	0.03	0.09	0.04	0	0.04
FE	28.22	25.18	28.33	26.79	28.78	26.4
MN	0.31	4.48	0.24	3.24	0.62	4.82
MG	2.71	1.23	3.01	1.54	2.4	1.28
CA	9.32	10.01	9.49	10.24	9.55	9.71
TOTAL 1	99.49	99.33	100.57	100.72	100.87	101.71
Si4+	5.95	6.00	6.00	5.99	6.02	6.02
Ti4+	0.01	0.02	0.02	0.01	0.01	0.02
Al3+	4.01	3.97	3.92	3.94	3.93	3.90
Fe3+	0.07	0.00	0.06	0.06	0.01	0.01
Fe2+	3.69	3.39	2.89	2.84	3.77	3.46
Mn2+	0.04	0.61	0.88	0.60	0.08	0.64
Mg2+	0.64	0.30	0.30	0.39	0.56	0.30
Ca2+	1.59	1.72	1.95	2.17	1.61	1.64
TOTAL	5.96	6.01	6.01	6.00	6.03	6.04

Table 2.1 Representative analyses and structural formulae of garnets from the greyschists.

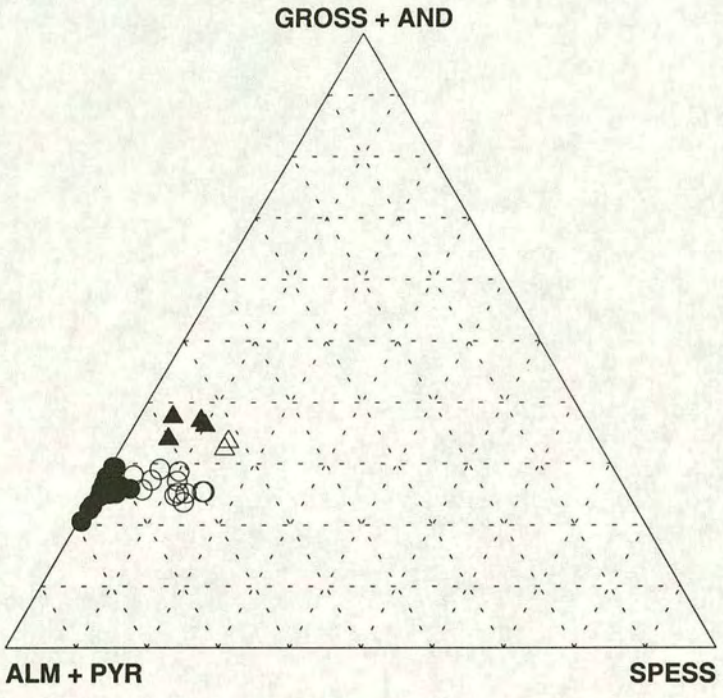

Figure 2.4 Plot showing composition of greyschist garnets in terms of mole percentage grossular + andradite-almandine+ pyrope-spessartine. Circles=pelitic schists, triangles= calc silicates, open symbols = cores, solid symbols = rims.

Some typical probe analyses for greyschist chlorites are given in Table 2.2. They were classified using the method of Hey (1954) as this does not require a knowledge of the Fe^{3+} content only the total iron. Results show that chlorite compositions fall in restricted range on the boundary between ripidolite and pycnochlorite (Figure 2.5). X_{Fe} ranges from 0.3 to 0.35 and silica content from 5.5 to 5.6 cations pfu.

Phengite

Phengite is the only K-bearing phase in the greyschists. It is generally present as fine grained aggregates oriented parallel to the foliation and often intergrown with chlorite and paragonite.

Table 2.3 gives some typical compositions for phengites from the greyschists. Compositions of those analysed range from 3.39 to 3.65 Si ions pfu with a concomitant increase in Fe and Mg content. Phengites may contain up 7% of a paragonite component. No zoning was identified within individual grains.

Paragonite

Paragonite is typically intergrown with phengite in mica and identical in appearance. Probe analyses show that their celadonite component is negligible however they may contain up to 7% of a muscovite component (Table 2.4).

Sodic amphibole

Sodic amphibole is present in schists as fine to medium grained, sub to euhedral crystals oriented parallel to the foliation. They are invariably colourless and only very weakly pleochroic.

	1	2	3	4	5	6
SiO2	26.9	26.83	26.35	26.96	26.71	26.95
TiO2	0.01	0.01	0.02	0.02	0.03	0.02
Al2O3	19.77	20.09	20.27	20.2	19.82	19.62
FeO	19.45	18.51	19.21	18.47	18.34	18.38
MnO	0.06	0.07	0.07	0.06	0.04	0.05
MgO	19.98	20.29	19.68	20.42	20.29	20.5
CaO	0.02	0.01	0.02	0	0.03	0.02
Na2O	0	0.01	0.01	0	0.01	0
K2O	0	0.01	0.03	0.01	0.03	0.03
TOTAL	86.19	85.83	85.66	86.14	85.3	85.57
Si	5.58	5.56	5.5	5.57	5.57	5.6
Ti	0	0	0	0	0	0
Al	4.84	4.91	4.99	4.92	4.88	4.81
Fe	3.38	3.21	3.35	3.19	3.2	3.2
Mn	0.01	0.01	0.01	0.01	0.01	0.01
Mg	6.18	6.27	6.12	6.28	6.31	6.35
Ca	0	0	0	0	0.01	0
Na	0	0	0	0	0	0
K	0	0	0.01	0	0.01	0.01
TOTAL	20	19.98	20	19.97	19.99	19.99

Table 2.2 Representative analyses and structural formulae of chlorites from the greyschists.

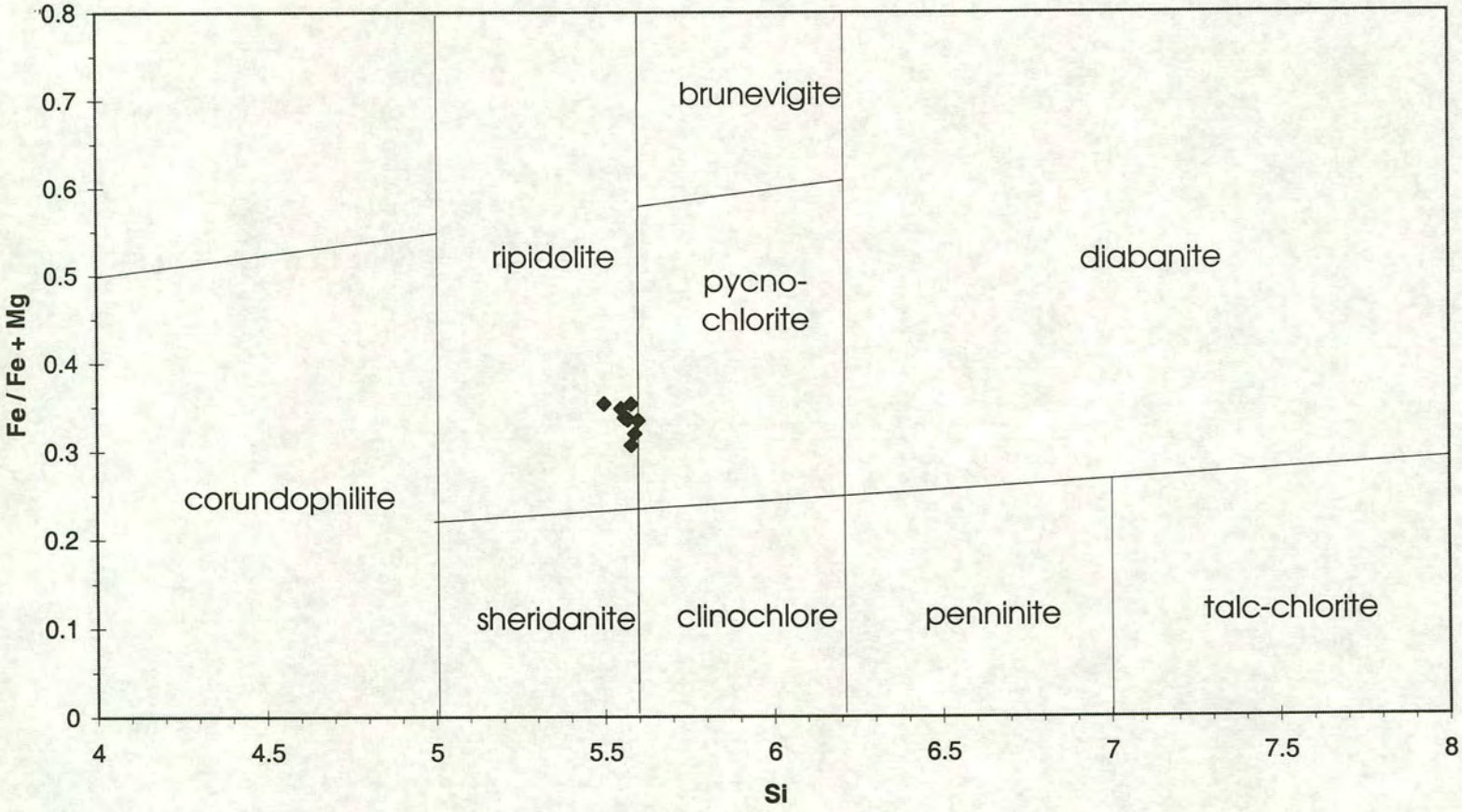

Figure 2.5 Classification of greyschist chlorites (after Hey 1954)

	1	2	3	4	5	6
SiO2	51.46	50.81	50.43	48.85	50.91	51.07
TiO2	0.27	0.19	0.17	0.19	0.22	0.23
Al2O3	27.48	27.58	27.63	27.01	27.9	27.8
FeO	2.01	1.67	2.03	1.85	1.76	1.75
MnO	0	0	0.02	0.03	0	0
MgO	3.61	3.57	3.47	3.46	3.33	3.47
CaO	0	0	0	0	0	0.01
Na2O	0.18	0.24	0.34	0.48	0.46	0.49
K2O	9.54	9.59	9.6	9.78	9.58	9.4
TOTAL	94.55	93.65	93.69	91.65	94.16	94.22
Si	6.85	6.83	6.79	6.75	6.81	6.82
Ti	0.03	0.02	0.02	0.02	0.02	0.02
Al	4.31	4.37	4.39	4.4	4.4	4.38
Fe	0.22	0.19	0.23	0.21	0.2	0.2
Mn	0	0	0	0	0	0
Mg	0.72	0.71	0.7	0.71	0.66	0.69
Ca	0	0	0	0	0	0
Na	0.05	0.06	0.09	0.13	0.12	0.13
K	1.62	1.64	1.65	1.72	1.63	1.6
TOTAL	13.8	13.82	13.86	13.95	13.85	13.83

Table 2.3 Representative analyses and structural formulae of phengites from the greyschists.

	1	2	3	4	5	6
SiO2	47.06	47.9	47	47.04	47.94	47.17
TiO2	0.03	0.04	0.05	0.04	0.03	0.03
Al2O3	39.35	39.66	39.66	39.73	39.14	39.29
FeO	0.27	0.28	0.3	0.18	0.45	0.27
MnO	0.02	0	0	0	0	0
MgO	0.26	0.23	0.22	0.15	0.26	0.2
CaO	0.07	0.06	0.06	0.15	0.07	0.07
Na2O	6.87	5.71	6.41	6.74	6.65	6.68
K2O	0.98	0.92	0.91	0.71	0.63	0.83
TOTAL	94.91	94.8	94.61	94.74	95.17	94.54
Si	6.03	6.1	6.02	6.02	6.1	6.05
Ti	0	0	0	0	0	0
Al	5.94	5.95	5.99	5.99	5.87	5.94
Fe	0.03	0.03	0.03	0.02	0.05	0.03
Mn	0	0	0	0	0	0
Mg	0.05	0.04	0.04	0.03	0.05	0.04
Ca	0.01	0.01	0.01	0.02	0.01	0.01
Na	1.71	1.41	1.59	1.67	1.64	1.66
K	0.16	0.15	0.15	0.12	0.1	0.14
TOTAL	13.93	13.7	13.85	13.87	13.83	13.87

Table 2.4 Representative analyses and structural formulae of paragonites from the greyschists.

Typical compositions are shown in Table 2.5. Calculation of the Fe^{2+} and Fe^{3+} contents reveals that they contain little or no ferric iron. On a Miyashiro diagram they plot as glaucophanes with an X_{Fe} of 0.2 to 0.34 (Figure 2.6). A regular zoning pattern is often evident in individual grains. This involves a decrease in Ca and Fe from core to rim and a concomitant increase in Mg, Si and Na. The behaviour of Al is variable.

Chloritoid

Chloritoid is present in the greyschists as rare, small corroded grains. Probe analyses show that they are iron-rich with $X_{Fe} = 0.77$ (Table 2.6). As with other ferro-magnesian phases they contain virtually no ferric iron.

Lawsonite

The former existence of lawsonite in the greyschists is indicated by the presence of rhombic pseudomorphs composed of clinozoisite and white mica. The mica component is typically composed of a fine scale intergrowth of paragonite and phengite. The individual phases are only visible on microprobe backscatter images. Probe analysis produces anomalous compositions which fall inside the muscovite-paragonite solvus (Table 2.7).

Three samples containing unaltered lawsonite were collected during the study. Two are from calc-silicate horizons while the other is from a lawsonite-bearing quartz vein. In the calc silicates the lawsonites are large poikiloblasts with well developed lamellar twinning. Probe analysis shows that their compositions are close to the ideal lawsonite formula although they do contain small amounts of Fe and Ti (Table 2.7)

	1	2	3	4	5	6
SiO2	56.05	57.53	56.29	57.64	57.27	58.06
TiO2	0.08	0.03	0.02	0.03	0.02	0.03
Al2O3	11.91	11.85	11.64	11.91	11.64	11.72
FeO	9.33	8.62	9.21	8.74	8.34	8.96
MnO	0.04	0.02	0.03	0.04	0.01	0.02
MgO	10.26	10.63	10.51	10.54	10.94	10.17
CaO	1.68	1.19	2.26	1.17	1.32	0.82
Na2O	6.73	7.08	6.45	6.99	6.95	7
K2O	0.03	0.03	0.04	0.01	0.01	0.03
TOTAL	96.11	96.98	96.45	97.07	96.5	96.81
Si	7.8	7.89	7.813	7.907	7.891	7.985
Ti	0.08	0.003	0.002	0.003	0.002	0.003
Al	1.955	1.916	1.905	1.926	1.891	1.9
Fe3+	0.131	0.104	0.117	0.067	0.108	0
Fe2+	0.955	0.885	0.952	0.936	0.853	1.031
Mn	0.005	0.002	0.004	0.005	0.001	0.002
Mg	2.129	2.173	2.174	2.147	2.238	2.084
Ca	0.251	0.175	0.336	0.172	0.195	0.121
Na	1.817	1.883	1.736	1.859	1.857	1.867
K	0.005	0.005	0.007	0.002	0.002	0.005
TOTAL	15.057	15.039	15.046	15.024	15.037	14.998

Table 2.5 Representative analyses and structural formulae of glaucophanes from the greyschists.

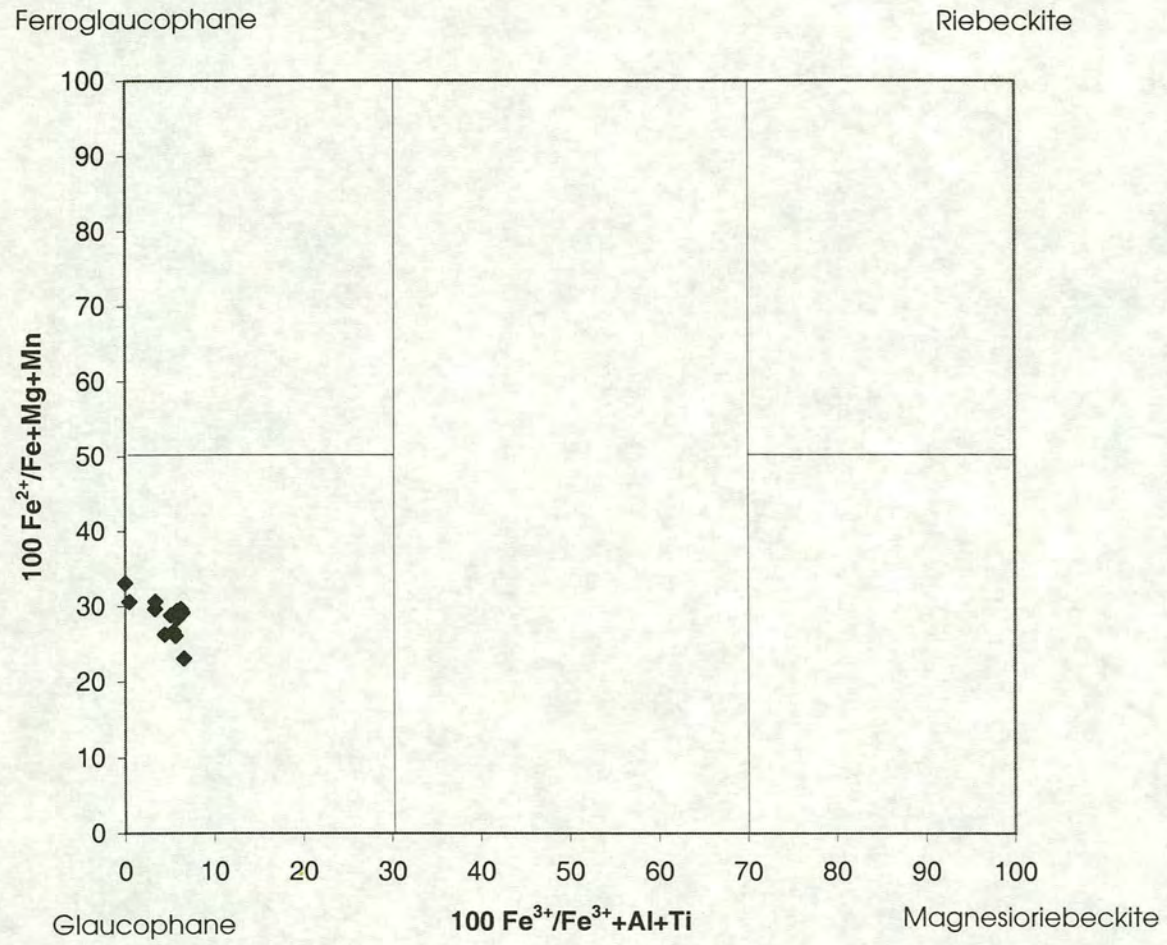

Figure 2.6 Classification of sodic amphiboles in a Miyashiro diagram (Miyashiro 1957).

	1	2	3
SiO2	23.89	23.51	23.58
TiO2	0	0	0
Al2O3	40.52	40.34	40.38
Cr2O3	0	0	0
FeO	22.75	22.58	22.78
MnO	0.19	0.15	0.21
MgO	3.51	3.34	3.36
TOTAL	90.88	89.92	90.31
Si	0.995	0.989	0.989
Ti	0	0	0
Al	1.989	2.001	1.995
Fe3+	0.022	0.02	0.028
Fe2+	0.77	0.775	0.771
Mn	0.007	0.005	0.008
Mg	0.218	0.21	0.21
TOTAL	4.001	4	4.001

Table 2.6 Representative analyses and structural formulae of chloritoids from the greyschists.

	1	2
SiO2	36.52	36.43
TiO2	0.41	0.07
Al2O3	30.07	30.11
FeO	0.52	0.38
MnO	0	0
MgO	0.07	0.02
CaO	17.32	17.13
Na2O	0	0.02
TOTAL	84.91	84.16
Si	2	2.009
Ti	0.017	0.003
Al	1.94	1.957
Fe	0.021	0.016
Mn	0	0
Mg	0.006	0.002
Ca	1.016	1.012
Na	0	0.002
TOTAL	5	5.001

	1	2	3	4	5
SiO2	47.87	47.26	47.48	48.49	47.2
TiO2	0.04	0.04	0.05	0.04	0.02
Al2O3	38.89	38.58	38.73	37.23	37.34
FeO	0.85	0.69	0.89	1.04	0.17
MnO	0	0.01	0.02	0.03	0
MgO	0.24	0.28	0.28	0.73	0.28
CaO	0.05	0.06	0.05	0.05	0.24
Na2O	3.62	3.58	3.53	2.87	2.23
K2O	1.29	1.12	1.28	2.43	3.73
TOTAL	92.85	91.62	92.31	92.91	91.21
Si	6.19	6.19	6.18	6.3	6.26
Ti	0	0	0	0	0
Al	5.93	5.95	5.94	5.71	5.84
Fe	0.09	0.08	0.1	0.11	0.02
Mn	0	0	0	0	0
Mg	0.05	0.05	0.05	0.14	0.06
Ca	0.01	0.01	0.01	0.01	0.03
Na	0.91	0.91	0.89	0.72	0.57
K	0.21	0.19	0.21	0.4	0.63
TOTAL	13.4	13.38	13.39	13.4	13.42

Table 2.7 Representative analyses and structural formulae of unpseudomorphed lawsonite from the greyschists and probe analyses of micaceous aggregates from lawsonite pseudomorphs.

2.5 Post Peak Blueschist Alteration

2.5.1 Lawsonite pseudomorphing event

All the lawsonite in the graphitic schists has been pseudomorphed and its former presence is now indicated by rhombic aggregates of clinozoisite and white mica. The textural status of the pseudomorphs and the morphology of their internal fabrics clearly indicate that lawsonite growth was synchronous with the later stages of the deformation accompanying the blueschist event (Chapter 6). However, lawsonite breakdown to its current pseudomorphing phases must have taken place after the deformation had ceased. In all samples examined in this study the lawsonite pseudomorphs preserve their euhedral shape. This would not be expected to be the case if the breakdown preceded the end of the deformation as the weaker pesudomorphing phases could not have preserved their shape during deformation.

Dixon (1969) and Ridley (1982) suggest that the breakdown is the result of reactions of the form:

lawsonite + K^+ = clinozoisite + muscovite + H_2O

lawsonite + Na^+ = clinozoisite + paragonite + H_2O

These are the equivalent of the high temperature breakdown of lawsonite to sillimanite or kyanite + zoisite + quartz + H_2O at higher activities of water and reactions involving Na and K will occur at lower temperatures than that for the isochemical breakdown of lawsonite (Dixon 1969). Thus, it is the availability of alkali ions to react with lawsonite that controls its breakdown.

This conclusion is supported by two other observations on the meta sediments:-

- The only examples of un-pseudomorphed lawsonite found within the grey schist units occur in very alkali-poor calc silicate horizons or lawsonite-bearing quartz veins or segregations.

- The pseudomorphing assemblage is controlled by the bulk rock chemistry of the lithology in which the pseudomorphs occur. In the K-rich metapelites such as the greyschists they are typically composed of clinozoisite + muscovite ± paragonite. In contrast, in the Na-rich meta-basites they are composed of clinozoisite + albite.

In other examples the alkalis reacting with the lawsonite are provided by the synchronous breakdown of other phases in the matrix such as albite (e.g. Gomez-Pugnaire et al 1985). However, this does not appear to be the case in the greyschists. All other phases remain unaltered during the lawsonite pseudomorphing event.

Alternatively, the alkalis might be provided by an externally derived infiltrating fluid (Yardley and Baltatzis 1985). The effects of this event on the greyschists might complicate the identification of geochemical and stable isotopic changes accompanying the original growth of lawsonite. However, such an infiltration event would have to be remarkably pervasive on a large scale in order to explain the extent of lawsonite pseudomorphing event. Virtually all lawsonite is pseudomorphed in the entire Syros blueschist terrain and not just in the greyschists. In addition, it is difficult to understand how an infiltration driven event can be reconciled with clear local control of the pseudomorphing assemblage.

Instead it seems likely that the K and Na involved in the pseudomorphing is more locally derived. The only K-bearing phase in the greyschist is phengite and this seems the only possible source of ionic K for the lawsonite pseudomorphing. It seems likely that a fluid phase would be present in the schist throughout the blueschist metamorphism. If this is in equilibrium with phengite then it would contain some K+ ions which could react with the lawsonite. Removal of K from the fluids immediately adjacent to the lawsonite porphyroblasts would generate an concentration gradient and cause localised diffusion of K in the pore fluid toward the reaction site. This in turn would cause more phengite to dissolve into the fluid. A similar process can be envisaged with the dissolution of paragonite in the matrix and its growth in the pseudomorphs. The reaction of six moles of lawsonite only requires

the dissolution of one mole of mica so that depletion may not be obvious in a thin section.

2.5.2 The greenschist retrogression

A considerable proportion of the blueschist rocks on Syros have been overprinted by a later, lower to medium pressure greenschist event. This is most strongly developed in the south of the island and largely absent in the northern most parts of the exposed section. However, some alteration is occasionally present. In the grey schists this is typically visible as the replacement of garnet by chlorite and the breakdown of glaucophane to albite + chlorite. While significant parts of the U.G.S.U. have been strongly affected by the overprint it is entirely absent in those parts of the L.G.S.U. examined in this study.

Barr (1989) suggests that the greenschist overprint is accompanied by fluid infiltration. Such infiltration by an externally derived fluid may significantly change the stable isotopic signature of rocks with which it interacts. Furthermore, Matthews and Schliestadt (1984) suggest that the blueschist to greenschist transformation on the nearby island of Sifnos is accompanied by changes in bulk rock composition. Barr (1989) questions their interpretation and identifies no such changes on Syros. However, no samples that showed any evidence of greenschist overprint were used for either stable isotopic or geochemical analysis.

CHAPTER 3

STRUCTURAL HISTORY OF THE GREYSCHIST UNITS

3.1 Introduction

The aim of this chapter is to describe as comprehensively as possible the macro and micro structural development of the greyschists and produce a detailed strain history for the syn-blueschist deformation.

Field and geochemical data show that a significant proportion of the Ca-Al silicates in the greyschists are genetically related to syn-deformational quartz veins. In order to fully understand the veining event it is vital to relate it to a coherent structural frame work. This allows the timing of formation of individual veins to be accurately determined relative to the finite strain and the timing of other events during the metamorphism.

Importantly, this will allow the relationship between the deformation and the formation of the veins to be assessed. Vein formation is controlled by the localised stress field and hence related to the incremental strain at the time of their growth. The strain in the greyschists is markedly inhomogeneous, most notably when comparing the L.G.S.U and U.G.S.U. It is possible that the formation of Ca-Al silicate generating veins in different parts of the greyschist is controlled by the state of strain rather than representing a single synchronous veining event.

Furthermore, variations in the strain regime during the metamorphism will reflect different stages in the subduction of the sedimentary packet. Thus, it may be possible to relate the veining to larger scale tectonic processes.

Ridley 1982 described the characteristics of the deformation for the whole of the succession. The work in this study concentrates on producing a more detailed structural history for the greyschist alone. As will be seen, while the deformation in the upper and lower units shares some characteristics, the overall style of deformation in the two units is markedly different in style and intensity. Thus the deformation within the two units will be described in separate sections. A further

section will then compare and contrast the deformational styles and consider how they may be related temporally and spatially.

3.2 Pre-Blueschist Structures

3.2.1 Sedimentary layering

Sedimentary layering is generally well preserved throughout the main sequence of the Syros metasediments. On a large scale it is visible as thick marbles interbedded with pelitic, psammitic and metabasic horizons in varying proportions. Ridley (1982) infers some tectonic repetition due to pre-metamorphic thrusting and suggests that the succession represents a stacked continental margin sequence. Several later tectonic breaks which are active during the blueschist metamorphism are also present (section 3.6). However, the units between these discontinuities appear to represent largely undisturbed sedimentary successions.

Within the greyschist units the primary layering is visible as alternating quartz-rich and mica-rich horizons with occasional calc-silicate interbeds. Preservation of the layering is variable but it is best where the syn-blueschist deformation is weakest such as in the strain shadow of the Gria Spilia Meta-igneous Block. There it is clearly visible as quartz rich horizons up to 5 cm thick alternating with thinner mica-rich horizons less than 1 cm thick (Figure 3.1). Sedimentary structures of uncertain origin are also preserved (Figure 3.2).

Within the rest of the greyschist the layering is typically preserved but the individual horizons are usually markedly thinned .It is often visible as alterations of quartz-rich and mica-rich layering on a 1 to 10 mm scale, commonly accentuated by parallel, fine scale graphite laminations (Figure 3.3). The graphite typically, but not exclusively, concentrates in the mica-rich layers. This presumably reflects an original higher proportion of organic material in the finer, more aluminous fractions of the sedimentary protolith.

Figure 3.1 Well preserved layering in the lee of the Gria Spilia Meta Igneous Block.

Figure 3.2 Possible sedimentary structure in the Grey Schist from the lee of the Gria Spilia Meta Igneous Block.

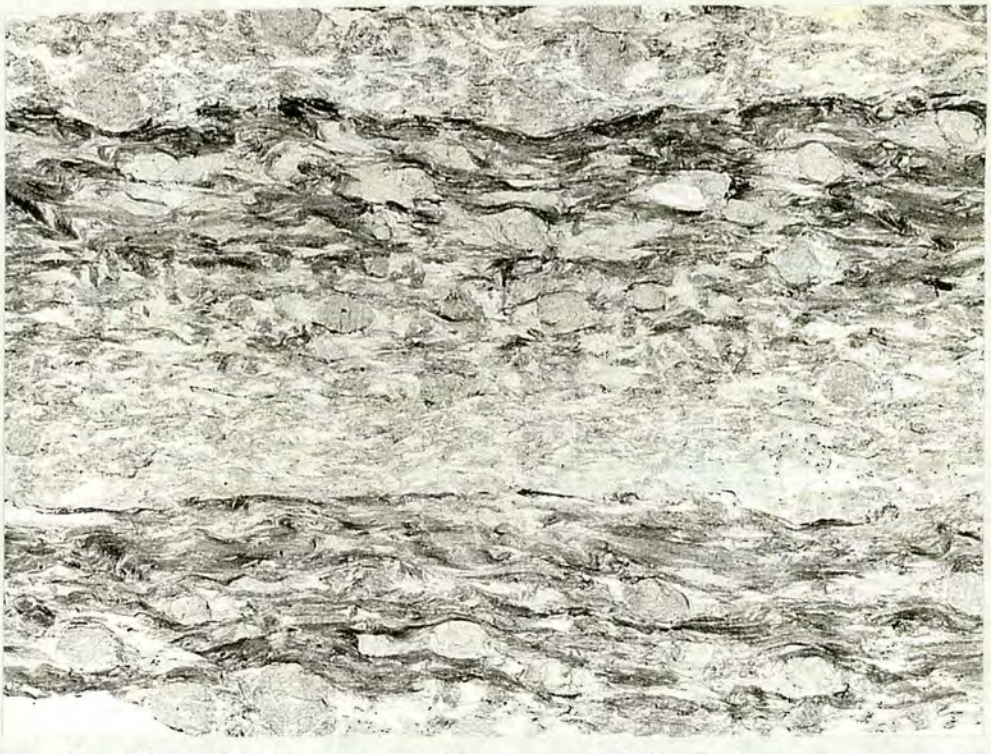

Figure 3.3 Bimodal Quartz and Mica compositional layering accentuated by concentration of graphite in micaceous interlayers (sample 94/4, x 6)

Such bimodal interlayering might be interpreted as resulting from metamorphic differentiation. It is likely that there has been some transfer of material between the quartz-rich and mica-rich horizons during the metamorphic recrystallization which may have accentuated the layering. However, variation of layer thickness perpendicular to strike, the rare preservation of sedimentary structures and parallelism of the layering with clearly primary compositional layers such as calc-silicates and marbles show that in this case that it is essentially a primary sedimentary feature.

3.2.2 Gria Spilia meta igneous block

Embedded within the western end of the study area in the Lower Grey Schist Unit (LGSU) is a 20m wide body of largely undeformed igneous material, the Gria Spilia Meta-igneous Block. It contains a semi-coherent stratigraphy ranging from basic gneisses at the base through more acidic compositions up section to a zone of authigenic breccias. Within the latter zone, completely undeformed examples of meta-basite net-veined by more acidic material are preserved (Figure 3.4). The uppermost part of the sequence is less easy to classify. Ridley (1982) interprets it as a composite breccia with at least three components, including clasts of various types of net-vein complex, and reciprocal intrusions and net veining.

The nature of the contact with the surrounding greyschists is different at opposite ends of the block. At the Upper margin it is clearly tectonic. The zone of gneiss adjacent to the margin is clearly deformed and the schists are phyllonitic in character (Figure 3.5). In contrast the contact at base is sedimentary. Layering in the schist is sub-parallel to the contact and in some cases appears to be truncated at a shallow angle (Figure 3.6). Along the intervening margin the exact nature of the contact is largely obscured by extensive zones of metasomatism and lack of outcrop. However, it appears to be sedimentary rather than tectonic.

Figure 3.4 Net veining in the Gria Spilia Meta Igneous Block.

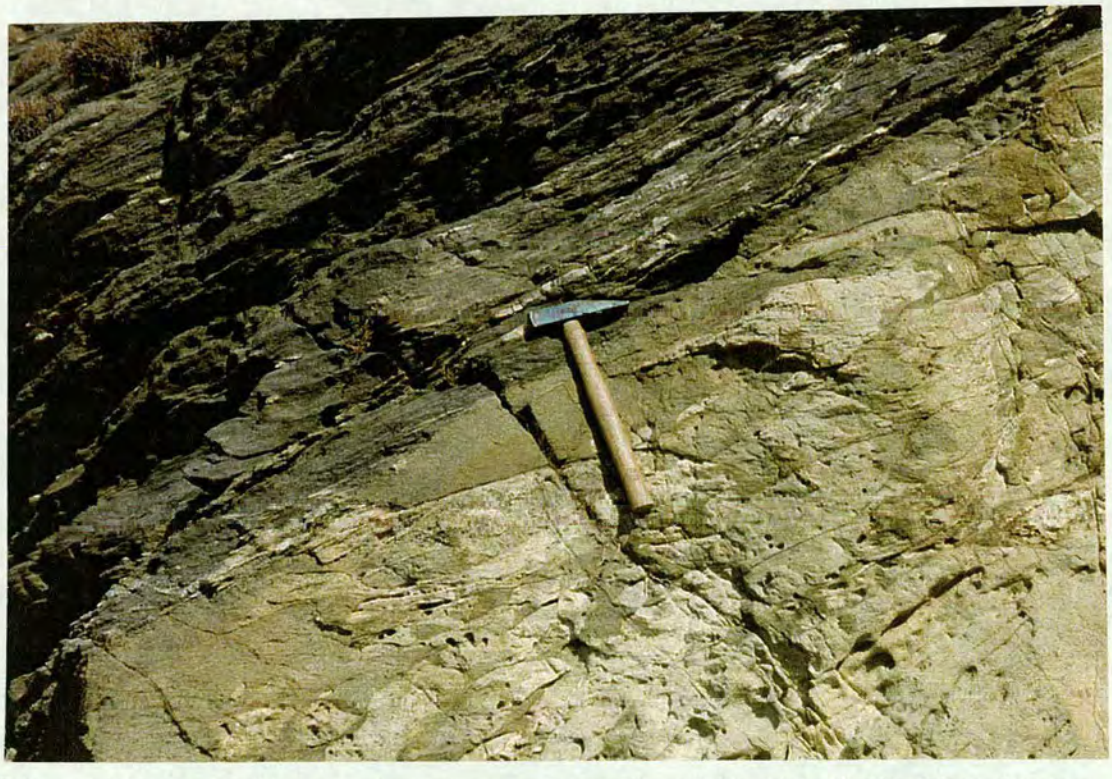

Figure 3.5 Tectonic contact at the upper margin of the Gria Spilia Meta Igneous Block.

Figure 3.6 Folded sedimentary contact at the base of the Gria Spilia Meta Igneous Block.

Figure 3.7 Typical asymmetric fold of finely layered grey schist in the LGSU.

3.3 Syn-blueschist Deformation in the LGSU

3.3.1 Macro structures in the LGSU

The dominant fabric element in the Syros metasediments is a flat lying foliation sub-parallel to lithological layering. In the LGSU, this fabric is present as a penetrative schistosity formed by the strong alignment of white mica, chlorite glaucophane and lenticular bodies of quartz. In his regional structural study, Ridley (1982) suggests that, over much of the island, this foliation is at least in part inherited and transposed from the original sedimentary fabric represented by the alternating quartz-rich and mica-rich layers. It is conceivable that it has a more complex developmental history and was derived from a pre-existing foliation. This possibility will be discussed in a later section. Nevertheless, it may be considered the final stage in the first recognisable fabric to form during the blueschist deformation and hence is designated S1.

The greyschists were then folded by upright to gently inclined, largely intrafolial folds on a variety of scales ranging from mm scale folds of mica lamellae to metre scale folds of the sedimentary layering (Figure 3.7). The folds are close to tight with a consistent north eastward vergence ('z' looking Northwest). Fold axes trend north-west and Axial planes are oriented at a high angle to bedding. The style of folding varies with lithology. In units with quartz-rich horizons they are typically well formed asymmetric folds with rounded hinges. In some cases the hinges are slightly bulbous but there is little significant thinning of the short limbs. In more uniform mica-rich horizons lacking prominent quartzose layers, chevron folds are more common.

The S1 foliation is folded with the bedding, and the minerals that define it are simply bent and fractured or annealed around the fold hinges. There is no evidence for any axial planar, syndeformational mineral growth but the S1 is commonly crenulated. The intensity and appearance of the crenulation varies considerably. It is

most strongly developed in the hinge regions and short limbs of asymmetric folds where it forms closely packed tight microfolds of the S1 foliation. In more quartz-rich lithologies, movement of quartz from fold limbs to fold cores by pressure solution accentuates the effect of the crenulation causing the formation of an effective second, spaced cleavage in an axial planar orientation to the folds. In contrast, in the more mica-rich units the second cleavage is absent and the crenulation often takes the form of small scale repeated crenulations of the mica lamellae similar to the perfect angular chevrons seen folding the bedding. Within unfolded regions the crenulation is typically confined to mm scale mica-rich domains or completely absent. Thin sections reveal weaker crenulations in the longer limbs of the folds but these are often invisible in the field. This second planar fabric axial planar to the folding and at a high angle to the S1 is referred to as the S2.

The folding event is also accompanied by the formation of a strong, composite lineation oriented parallel to the fold axes in the plane of the S1 foliation. The main component of this lineation is the folding of the S1 foliation by the asymmetric mica crenulations described above. However, this is accompanied by the alignment of glaucophane and lenticular bodies of quartz, often present as pressure shadows on garnets, parallel to the fold axes. Ridley (1982) suggests that the lineation is best visualised as an intersection between the original S1 foliation and the axial planar S2 foliation.

Elsewhere in the Syros meta-sediments, Ridley (1982) identifies a second, less well developed, lineation defined by aligned glaucophane needles which is at an angle to the fold axes and hence orthogonal to the dominant lineation. He suggests that this second lineation is parallel to the movement direction during ductile thrusting responsible for the syn-blueschist deformation. This second lineation is rarely discernible in the LGSU. This is largely due to the small angle between the two lineations in this region but also partly due to the relative rarity of horizons in exhibiting coarse prismatic glaucophane.

3.3.2 Micro structural fabric development in the LGSU

Macro-scale observations in the field indicate that the structures present in the LGSU can be divided into 2 main elements, an S1 layer parallel foliation and a later crenulation of this fabric referred to as the S2. This section documents the microstructural characteristics of the two fabrics and discusses the controls on and the mechanisms of their formation.

S1 cleavage in the lower unit

As noted above, the dominant fabric in the grey schist units is the layer parallel, penetrative S1 schistosity. Invariably, the main element of this foliation is a strong preferred orientation of mica plates, often intergrown with chlorite, and accompanied by less perfect alignment of glaucophane, sphene and lenticular quartz bodies. However the appearance and strength of the fabric is variable and largely controlled by the composition of particular horizons.

The cleavage is most perfectly developed in lithologies with high modal proportions of both quartz and mica, and in which the mica is evenly distributed (Figure 3.8). In such horizons the micas are present as perfectly aligned, clear, sub-rectangular laths set in a groundmass of approximately equant polygonal quartz grains. While they may possess undulose extinction, the quartz grains typically have straight grain boundaries, triple point interfacial boundaries approaching 120° and rare sub-grain formation but no evidence of neoblast growth. Prismatic glaucophanes are oriented parallel to the mica in the in the plane of the foliation. Where the crenulation is strongly developed they are aligned parallel to the lineation but otherwise their long axes appear to be randomly oriented. They generally lack undulose extinction but may have some sub-grain formation parallel to length.

Ridley (1982) suggests that the appearance of the quartz and the lack of undulose extinction in the micas and glaucophane show that dynamic recovery is dominant relative to dynamic recrystallization. He concludes that the fabric is in

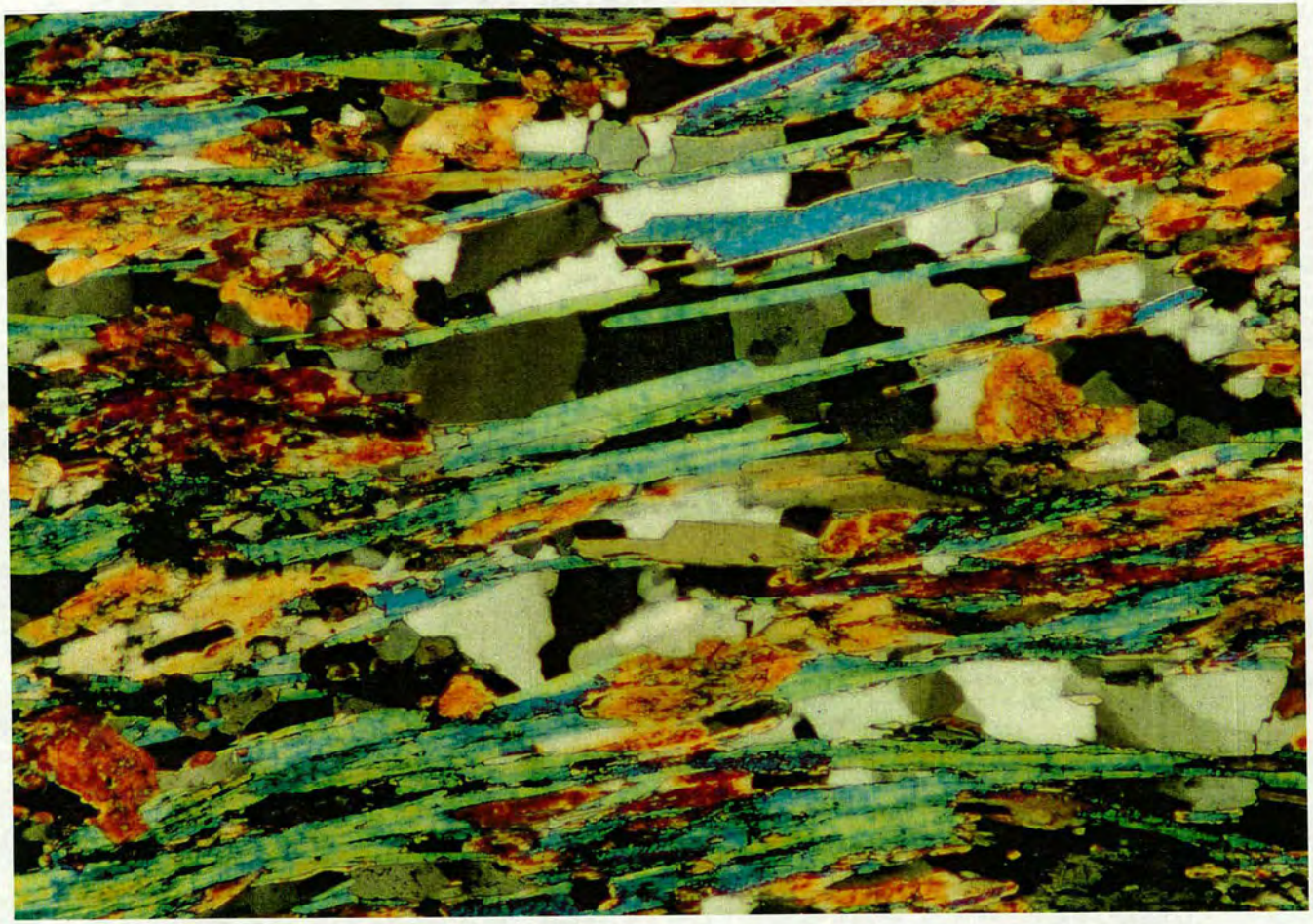

Figure 3.8 Classic S1 fabric from the LGSU (sample 92/30F, x32).

dynamic (steady state) equilibrium and is indicative of steady application of both stress and strain rate.

However, horizons with quartz and mica-rich compositions described above form only a subsidiary part of the LGSU. In most samples, the model fabric described above is only visible to the quartz pressure shadow formed on garnets and other isolated quartz-rich domains. The typical greyschist lithologies show a range of fabrics controlled by variation in modal composition and distribution of the fabric forming phases.

Compositional variation in the greyschists is controlled by primary sedimentary layering. The typical bimodal layering is often very well preserved on fine, sub-thin-section scales. In the clearest examples it is visible as mica rich layers alternating with quartz and glaucophane-rich layers on a scale of 1 to 10 mm (Figure 3.3). This layering is typically accentuated by the preservation of fine graphite -rich laminations parallel to the sedimentary layering. The graphite-rich horizons normally coincide with the mica-rich layers. This fine compositional layering may cause considerable variation in the appearance of the S1 on small scales.

Within the quartz and glaucophane rich layers the fabric may approach the model steady state fabric described above. However, with increasing glaucophane content the fabric becomes less well defined and more irregular. The sheet silicates which are the main fabric forming element are less numerous and often distorted and bent around the glaucophanes. The glaucophane grains themselves seen less able to rotate into parallelism with the foliation and may exhibit considerable variation in orientation. In general the fabric produced is less penetrative on a fine scale, often appearing chaotic in the most extreme samples. Within thicker glaucophane-rich horizons this leads to a massive appearance in hand specimen.

In contrast, within the mica-rich interbeds the S1 foliation is strongly developed and pervasive on a very fine scale. Within such layers the micas are

concentrated in almost monomineralic, irregular welts or thin, more laterally continuous horizons rather than being distributed among the other phases. The mica grain size is typically much smaller in these zones than in the model fabric. They are usually composed of minute, interlocking, mica laths aligned sub parallel to the schistosity. This variation in grain size appears to be controlled by the presence or absence of graphite.

In the fine-grained domains the mica cleavage planes are lined with concentrations of fine graphite grains and the mica exhibits strongly undulose extinction. In contrast, within graphite-free areas the mica is much coarser and individual grains have clear sharp extinction. These differences are due to the inhibition of recovery processes by graphite within the graphite-rich zones by grain boundary pinning. Experimental studies have clearly shown that the presence of small grains of a second phase effectively inhibits grain boundary migration. In this case this stops the annealing and coarsening within graphite-rich mica domains.

Origin of the S1 Foliation

Throughout the blueschist metasedimentary succession the S1 foliation is parallel to the primary compositional layering. This layering is typically excellently preserved on a variety of scales. As noted above, within the LGSU in many samples it is visible as mm scale quartz and mica-rich interbeds often accentuated by thin graphite-rich laminations. This layering is clearly a primary sedimentary effect rather than the result of a metamorphic differentiation process. It is possible that some differentiation has occurred during recrystallization but this must have been limited in extent.

Where lithologies preserve such fine scale features it seems impossible that they have experienced any pervasive heterogeneous deformation during their burial and metamorphism. However, they have clearly experienced considerable flattening perpendicular to sedimentary layering. Where bedding is situated in a strain shadow,

such as adjacent to the Gria Spilia Meta-igneous Block, it is markedly thicker than that in the normal grey schists. Significantly, these are the only schists in the area not containing a strong layer parallel fabric. These observations suggest that the pre-S2 strain in the greyschist units was dominated by flattening perpendicular to sedimentary layering and that it was this flattening that caused the formation of the S1 fabric.

The assumption of layer parallel flattening in the early part of the deformation is consistent with the appearance of the calc silicate interbeds in the lower grey schists. These are typically present as discontinuous tablets parallel to bedding and S1 and often contain quartz veinlets perpendicular to layering (Figure 3.9). The individual blocks may be folded into asymmetrical S2 folds but the break-up of the horizons clearly predates this folding. The disruption of the these layers can be attributed to symmetrical boudinage of the more competent calc-silicate horizons during the early flattening strain.

The S1 probably originated in a syn-sedimentary to diagenetic layer parallel phyllosilicate fabric. During burial and metamorphism this fabric became stronger and coarser due to a combination of recrystallization and the mechanical rotation of inequant grains into parallelism. This coarsening effect is best observed in the mica-rich horizons. Where they are graphite-free recrystallization and recovery has produced coarse aggregates of clear grains. However, as noted above, where they are graphite-rich and these processes are inhibited the micas form fine grained felts with undulose extinction. These fine grained fabrics probably preserve one of the earliest stages in the post-sedimentary development of the S1 fabric essentially frozen in time while the surrounding graphite-free areas continue to develop.

This interpretation is at least partially supported by the presence of graphite dust fabrics in the cores of glaucophanes. These fabrics are identical to those seen in the mica welts and appear to result when glaucophanes overgrow areas of graphite-rich mica. Occasionally, the glaucophane grain clearly straddles the boundary

Figure 3.9 Boudinaged calc-silicate layer in LGSU.

Figure 3.10 Glaucophane grains partially overgrowing a graphite-rich mica welt.(Sample 92/3, x32)

between a graphite-free, quartz-rich domain and an adjacent graphite-rich mica domain (Figure 3.10). When this occurs the glaucophane overlapping the mica domain contains a graphite dust fabric while that within the quartz domain is graphite-free. In many cases the glaucophane internal fabrics have remained continuous with the mica+graphite fabrics they overgrow and in the majority of cases they are sub-parallel to the S1 in the matrix (Figure 3.11). This shows that there has been little or no disruption of the S1 fabric since the growth of the glaucophane. Later strain is typically confined to continued flattening indicated by the bending of the S1 fabric around the tips of glaucophane grains. Any discordance in the internal and external fabrics is probably due to rotation of the glaucophane into parallelism with the S1 after growth.

Nevertheless, there is some evidence for at least localised heterogeneous deformation predating or synchronous with the development of the dominant foliation. Occasional samples contain microfolds discordant with the S2 crenulation and often with axial planes at a low angle to the S1 (Figure 3.12). Within others elongate domains of short mica laths are visible between the mica lamellae defining the foliation. In rare samples these are clearly the preserved hinge zones of microfolds with axial planes oriented parallel to the S1. Such structures are often interpreted as relics of a crenulation event.

However it seems impossible for the S1 fabric in the Syros meta-sediments to be formed generally by the crenulation of an earlier fabric. In order to form the S1 foliation any crenulation event would have to be regional in extent to account for the uniform occurrence of the fabric throughout the blueschist sequence, and pervasive on a sub thin-section scale to be consistent with its penetrative nature. As noted above, bedding is well preserved in the LGSU and in many samples textural evidence suggests that has been no heterogeneous deformation of layering during the formation of the S1. Any pervasive crenulation event would be expected to cause considerable disruption of primary layering, especially on the scale of fine graphite

Figure 3.11 Several glaucophanes overgrowing a fine grained mica and graphite fabric with little or no post growth fabric development. (Sample 92/4B, x32)

Figure 3.12 Sample containing 2 discordant crenulations. Open crenulation at high angle to S1 in upper left is S2. (Sample 92/166, x15)

laminations. Instead, the observed fabrics must be related to localised micro-folding occurring during the evolution of the S1.

Many of the anomalous crenulations appear to be spatially and genetically related to deformed quartz bodies. Figures 3.13 and 3.14 are taken from a sample containing an early quartz vein which may originally have been oblique to S1. This has now been microfolded and in the short limbs of asymmetric, cm scale folds is present as numerous en echelon lenses. In the longer limbs of the microfolds the quartz vein is parallel to the S1 and the matrix contains open crenulations with axial planes at a high angle to S1 and S0 (Figure 3.13). This may be interpreted as a weakly developed S2 fabric. In contrast, in the shorter limbs of the microfold where the vein is intensely deformed the matrix contains tightly packed crenulations with axial planes at a low angle to the S1 in the longer limbs (Figure 3.14). Realignment of micas in the limbs of these microfolds in combination with the en echelon quartz lenses produced by the dissection of the vein produce an incipient cleavage axial planar to the larger scale folding of the quartz vein and sub-parallel with S0/S1 in the longer limbs.

With continuing strain, the relation between the intensely crenulated fabric and the folding of a quartz vein will become less clear. Eventually it would result in a localised transposition fabric, possibly with relic microfolds, but indistinguishable in orientation from the regional S1. Such a fabric development would seem to account for the presence of apparently non-S2 crenulations adjacent to deformed quartz bodies parallel to the S1. In these cases the microfolding is caused, and its appearance controlled, by the buckling of the quartz veins rather than the larger scale folding of layering during the F2.

The classification of such fabrics in terms of S1 and S2 is problematic. They fold what appears to be an S1 foliation and hence in a chronological sense might be designated S2. In some cases they seem to be broadly synchronous with the regional S2 and the quartz veins merely seem to accentuate its development. However, in

Figure 3.13 Weakly developed S2 at high angle to S1 adjacent to long limb of deformed quartz vein. (Sample 92/48).

Figure 3.14 Strongly developed transposition fabric parallel to S1, adjacent to deformed quartz vein. Slide is in same orientation as Figure 3.13. (Sample 92/48).

many samples they appear to predate the regional S2 crenulation and are caused by local heterogeneities rather than larger scale folding of layering. This difficulty arises largely due to the essentially artificial division of the deformation into more than one event. While it is convenient to consider the fabric development in the meta-sediments in terms of S1 and S2, they are both the result of a continuous deformation (Ridley 1982). In general the first stage of the deformation does not involve folding. However, it is likely that localised microfolding of the S1 may occur where heterogeneities exist and result in the hybrid S1/S2 fabrics observed. Such locally controlled heterogeneous deformation probably occurred in an essentially spatially and temporally random manner throughout the development of the S1 and continues during the folding associated with the S2. Thus the apparently anomalous crenulations reflect the effect of local heterogeneities during the continuous evolution of the S1 rather than a coherent crenulation event.

In some samples the relic microfold hinges cannot be related to any obvious anisotropy . They occur as isolated lenses within fine grained mica welts. Once again they appear to result from micro folding of the S1 rather than any pre-existing fabric. They seem to form as crenulations/kink bands at low angles to the S1 which rotate into parallelism with it. The S1 then reforms around them to produce zones of short mica grains discordant with the external foliation. In some cases it is possible that this reorientation of crenulations is related to the proximity of porphyroblasts. In others a trigger mechanism cannot be identified. Occasional samples may exhibit microfolds with greatly differing orientation in a single field of view suggesting a complicated but largely indecipherable local structural history on a small scale (Figure 3.15).

Ridley (1982) also considers the possibility that the S1 forms relatively late in the metamorphism and that the onset of folding is genetically linked to the its formation. He notes that in similar sedimentary compositions from other lower grade blueschist terrains the early fabrics are dominated by lawsonite-albite or lawsonite-jadeite with only interstitial mica and chlorite and more granulose textures. Such

Figure 3.15 Slide containing multiple discordant crenulation of the S1 suggesting a complicated structural history possibly associated with the quartz vein. Glaucophane containing graphite fabric oblique to the S1 has clearly been pulled apart during the veining event.(Sample 92/11B, x14).

rocks may not contain a sufficiently strong anisotropy to initiate buckling. However, it seems likely that the mineralogy of the more aluminous interbeds in the greyschists has been dominated by sheet silicates throughout the recrystallization of the blueschist and unlikely that they ever possessed a granulose texture. In addition it seems unlikely that the formation of a strong anisotropy initiates the folding. The primary sedimentary layering and especially the presence of strong calc silicate horizons would seem to provide a strong enough anisotropy before the formation of the S1.

Is the S1 a Transposition Foliation?

The fine scale structures of the greyschist indicate that the S1 is not derived from an earlier fabric by crenulation. However, it is possible that the layer parallel fabric is the result of transposition of sedimentary layering on a larger scale.

Other studies of deformation during high pressure metamorphism have suggested that layer parallel foliations defined by alignment of inequant minerals similar to the S1 in the greyschists are the result of transposition of primary layering during the earliest stage of the deformation (Williams & Compagnoni, 1983; Helper, 1986; Patrick, 1988). In these cases, the foliation is shown to be axial planar to one or more episodes of intrafolial, isoclinal folding and may be associated with the formation of a lineation parallel to the fold axes. However, within the limbs of the folds sedimentary layering is preserved. Fabrics formed in this way may be designated transposition foliations, S_T.

Given the similarity in tectonic environment, lithologies and observed fabric in these studies with those for the Syros blueschists it seems possible that the S1 schistosity is a transposition fabric. If this were the case then relics of a pre-S1 folding event should be present within the blueschist metasediments. However, no early folds of sedimentary layering were identified in the LGSU. All folding of

bedding also folds the S1 foliation and is therefore assigned to the D2 folding event which is present throughout the blueschist succession.

Nevertheless, the recognition of such a transposition event may be difficult when the scale of folding is large and/or associated fold hinges have been partially or totally destroyed during the later stages of the deformation (Turner and Verhoogen, 1963). The scale on which observations are made is crucial in that an outcrop on a fold limb may appear to contain an undisrupted sedimentary succession while relic fold hinges in nearby outcrops may show that the sequence is intensely folded. Thus, the absence of meso- to macroscopic early folds in the relatively small area covered by the LGSU does not necessarily preclude the formation of the S1 during a transposition event. The amplitude of the early folding may be too large for it to be apparent when observed on a small scale.

However, Ridley (1982) mapped the whole of the Syros succession and concludes that there was no evidence for an earlier episode of folding. He notes that all the folds observed are consistent with formation under constant axes of strain and thus regards them as recording one deformation event. Even rare occurrences of fold interference are best attributed to diachronous nucleation of folds during the same deformation event. Hence, while he suggests that the fabric is transposed from an original sedimentary layering and phyllosilicate fabric he uses this term without any genetic connotation of formation during an episode of folding.

Given the absence of recognisable pre-S1 folding of layering the only remaining model consistent with the formation of the S1 by transposition is one in which the all evidence of the transposition is destroyed during later deformation. This deformation would have to be, at least locally, extremely intense in order to completely remove all traces of folding. In addition, the parallel compositional layering observed within the greyschists and throughout the main succession would have to be at least in part a differentiated metamorphic fabric. No evidence for the

destruction of sedimentary layering on this scale as identified in either this study or that of Ridley (1982).

Thus it does not appear that the S1 fabric is related to transposition on any scale. All observations are consistent with its formation parallel to compositional layering early in the burial and metamorphism.

Folding, Crenulation and Lineation

On a thin section scale, the folding of the greyschists is evident as an intermittently developed crenulation of the S1 foliation (Figure 3.16). The phases which form the S1 are strongly deformed during this episode but there is little evidence of new mineral growth. The mica fabric is bent around the small scale fold hinges often with a marked reduction of grain aspect ratio in the fold hinge zones. Any intragranular flexing and fracturing is generally annealed out within the more graphite free zones but recovery is less complete in graphite-rich mica welts.

Where the crenulation is strong glaucophane prisms are reorientated with the mica fabric. They occasionally exhibit extension fractures perpendicular to their prism axes which are healed by growth of new glaucophane. In samples in which the crenulation is just beginning to affect the S1 individual prisms may be bent with the surrounding mica fabric without fracturing (Figure 3.17). Other phases such as rutile occasionally display similar plastic behaviour.

The crenulation exhibits a range of strength and style within the LGSU. It is most strongly developed in the short limbs of decimetre scale asymmetric folds. In such situations the crenulation takes the form of numerous, isoclinal, tightly packed microfolds with parallel axial planes at a high angle to lithological layer (Figure 3.18). In more quartz-rich lithologies the crenulation may be accompanied by the transfer of quartz from fold limbs to fold cores which accentuates the folding and causes the formation of an effective spaced S2 cleavage. In particularly extreme

Figure 3.16 Asymmetric S2 crenulation in a fine grained mica welt.(Sample 92/4, x20)

Figure 3.18 Strongly developed S2 crenulation in the hinge zone of a decimetre scale fold. (Sample 92/2, x8)

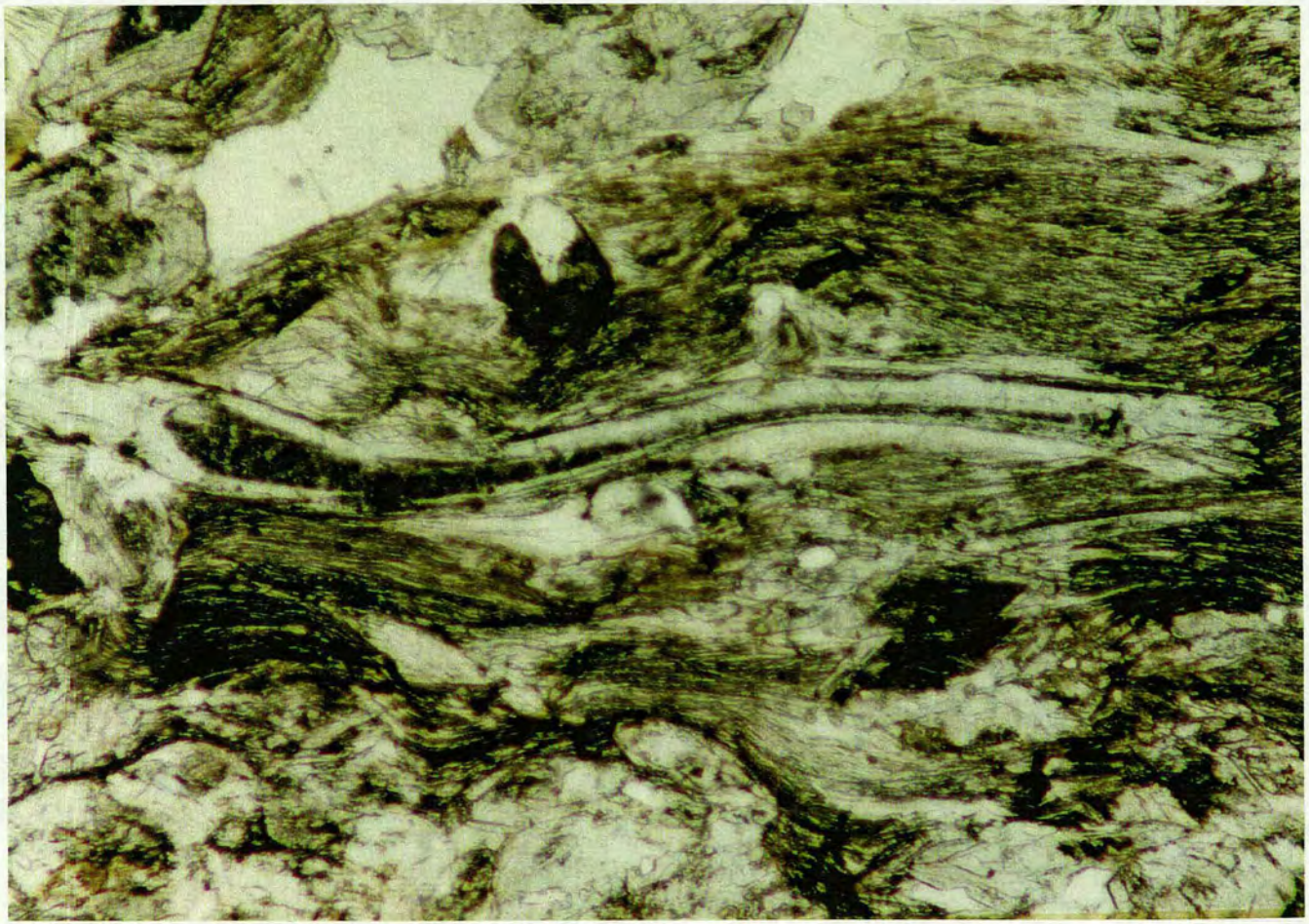

Figure 3.17 Prismatic glaucophane grain plastically deformed during the development of a weak S2 crenulation. (Sample 92/163 x25).

examples the cleavage becomes so pronounced the rock becomes divided into micro lithons and the majority of the later strain is taken up by the S2 foliation.

At the other extreme, within the long limbs of the folds, the S2 crenulation is commonly completely absent or it takes the form of rare microfolds confined to particularly mica rich patches. In such cases, the crenulation is often little more than a gentle undulation of the S1 fabric. In samples with a less strongly developed S2 crenulation the orientations of the micro-fold axial planes may be very irregular and in extreme examples the folding is markedly disharmonic (Figure 3.19).

In addition to positioning relative to macro-scale folds, the strength and nature of the crenulation is at least partially controlled by compositional variation in the grey schist samples on a variety of scales. As noted above, the S2 fabric reaches its most extreme expression in quartz-rich lithologies situated on the short limbs of macro-scale folds. Where very mica-rich schists are in a similar structural position the crenulation is still strongly developed but the micro-folds take the form of tightly spaced almost perfect chevron folds and there is no real development of an S2 cleavage (Figure 3.20). Perhaps more significantly, where the S2 is most weakly developed, the crenulation is only visible within mica -rich horizons. In such cases, while scattered microfolds with a regular orientation may be present in mica welts and discontinuous mica-rich horizons, adjacent quartz and/or glaucophane-rich domains show no evidence of the crenulation. This is due to the lesser propensity of glaucophane to reorientate relative to the sheet silicates and the fact that the S1 fabric is often itself irregular as the mica laths present bend and bow around the glaucophane grains.

Furthermore, as noted in the previous section, the relative proportions of graphite in different domains may also significantly affect the appearance of micro fabrics in the greyschists by inhibiting recovery in micas. Graphite-rich mica domains contain finely defined, unannealed microfolds. In contrast, in graphite free zones coarser, clear laths define more blocky, less obvious crenulation of the S1.

Figure 3.19 Irregular, disharmonic S2 crenulation at a high angle to S1. (Sample 92/31A, x12)

Figure 3.20 Well developed chevron crenulations from a fold core in a mica-rich schist. (Sample 92/12, x15)

3.4 Syn-Blueschist Deformation in the UGSU

3.4.1 Macro Structures in the UGSU

The dominant fabric in the Upper Grey Schist Unit (UGSU) is a flat lying foliation defined by the alignment of sheet silicates, glaucophane and quartz aggregates. However, unlike the S1 foliation in the lower unit, it is a transposition foliation axial planar to recumbent isoclinal folds. Thin-section observation confirm that it is the product of a pervasive crenulation of an earlier foliation.

The transposition event has extensively disrupted the sedimentary layering. Quartz-rich and mica-rich interbeds, apparently identical to those in the LGSU, are typically tightly folded on a 1 to 10 cm scale (Figure 3.21). The more competent quartzose horizons are markedly thinned relative to those in the LGSU and are often boudinaged on a small scale (Figure 3.22). Where the deformation is strongest, the schist is composed of en echelon micro-boudins and rootless fold hinges of quartzose composition surrounded by a mica-rich matrix with a penetrative crenulation cleavage. Quartz veins cross-cutting the original sedimentary layering are now present as isolated fold hinges and en echelon lenses parallel to the foliation (Figure 3.23). The combination of the boudinaging of the quartz-rich layering and quartz veins with the development of a pervasive S2 in the mica-rich layers produces an intense composite foliation (Figure 3.24).

Larger scale folds of layering are rare and generally only preserved in the more competent calc-silicate horizons and low strain zones (Figure 3.25). They are typically present as rootless fold pairs and single fold hinges often exhibiting strongly thinned limbs and bulbous and enlarged hinge regions (Figure 3.26). In contrast to the upright, close to tight folds in the LGSU the folds evident in the UGSU are invariably tight to isoclinal and their axial planes are at a low angle to layering, generally less than 25°. The orientation of the fold axes displays considerable variation, ranging from NW to NE.

Figure 3.21 Tightly folded fine scale quartz and mica interlayering from the UGSU.

Figure 3.22 Strongly boudinaged fine scale quartz and mica interlayering in the UGSU.

Figure 3.23 Strongly deformed quartz vein in the UGSU.

Figure 3.24 Outcrop in the UGSU counting an intense, composite transposition fabric accentuated by the presence of a dissected quartz vein.

Figure 3.25 Tight folding preserved in a calc-silicate layer in a low strain zone within the UGSU.

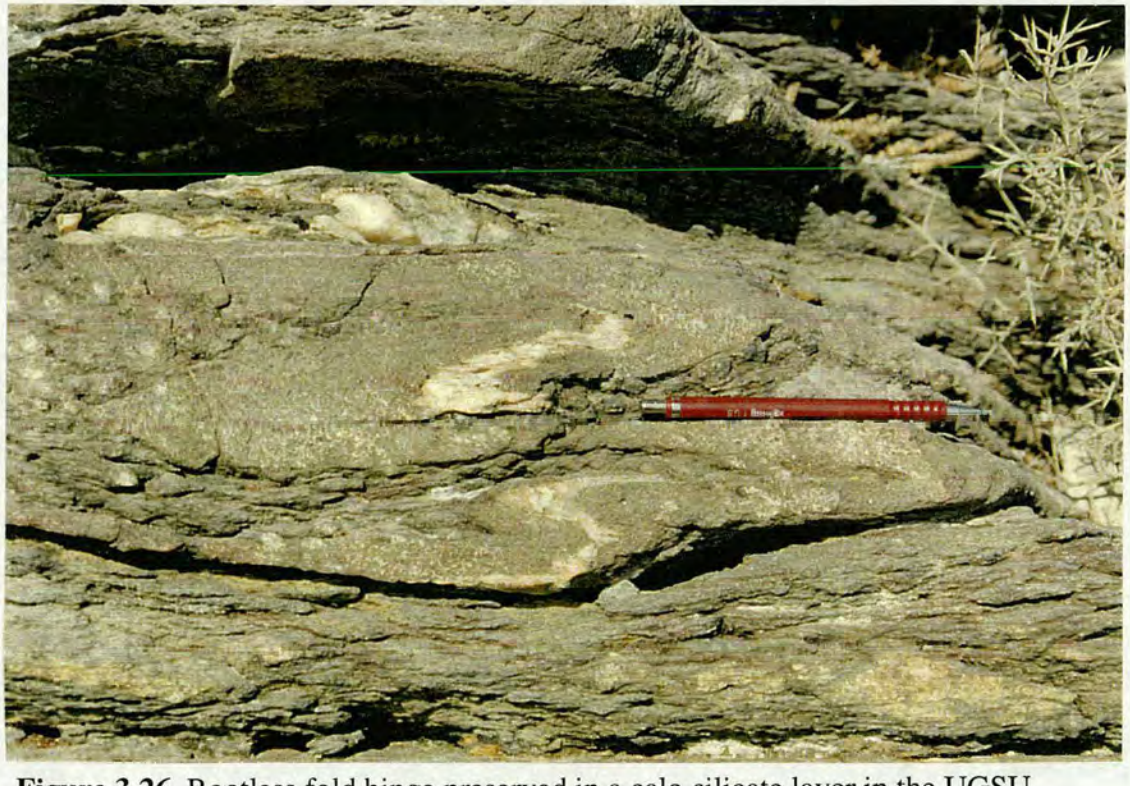

Figure 3.26 Rootless fold hinge preserved in a calc-silicate layer in the UGSU.

Within these low strain zones where folds are preserved a layer parallel foliation is visible folded with the layering. It is typically crenulated to some extent but no discrete axial planar fabric has formed. This foliation has an identical structural status to the S1 in the LGSU and there is no reason to assume that it is not a remnant of the same fabric.

Further relics of pre and early transposition structures are present adjacent to mega boudins of meta-carbonate material several metres long and up to a metre thick. These take the form of small pockets of apparently un-deformed S1 (Figure 3.27), areas with open microfolds of the S1 and occasional well preserved isoclinal fold pairs in the adjacent schists (Figure 3.28).

The boudins themselves are largely unaffected by the transposition of the schist fabrics. There may be limited interfolding of the pelites and the boudin material at the boundaries but there is no folding of the boudins on a larger scale. The matrix fabrics in the meta-carbonate material are poorly formed. In those boudins with a significant mica content a poorly developed S1 layer parallel fabric is apparent. However, in many cases, this appears to have been overprinted, probably by the post-folding extensional foliations, producing more complicated fabric patterns.

These observations suggest that the early stages of the deformation in the UGSU were identical to those in the LGSU. A pervasive layer parallel S1 foliation formed within a coherent sequence of finely bedded meta-sediments. This primary layering consisted of interlayered quartz-rich and mica-rich horizons with occasional calc-silicate horizons. The discontinuous nature of these more competent horizons suggests that they were boudinaged during this early layer parallel flattening.

This sequence was then intensely folded into recumbent isoclinal folds and the layer parallel S1 was crenulated. However, with increasing deformation the strain

Figure 3.27 Weak S1 fabric apparently preserved in a depression in the margin of a mega-boudin.

Figure 3.28 Isoclinal folding preserved adjacent to a large meta-carbonate boudin.

became strongly partitioned around more competent regions. Isolated folds of calc-silicate horizons and the strain shadows of thicker meta-carbonate boudins preserve the early stages of the fabric development. In contrast, within the less competent pelitic regions primary layering is transposed and the S2 crenulation fabric has become an almost penetrative foliation. The strain in the later stages of the deformation is taken up by the S2 cleavage which wraps around the low strain windows.

The strong lineation visible in the LGSU is largely absent in the UGSU. This is due to the destruction of the S2 micro-folds, which form the main component of the lineation, during the later stages of the differentiation of the crenulation cleavage.

In the final stages of the syn-blueschist deformation the S2 foliation is cut by later extensional structures. Over most of the area this takes the form of a steeply dipping, spaced, extensional crenulation (Figure 3.29). In one region a second extensional crenulation is present which dips in the opposite direction to the dominant fabric. this may be a conjugate feature possibly associated with late stage kink band. In other parts of the area the late extension takes the form of steeply dipping micro-shear zones (Figure 3.30). Where present these impart a distinct hummocky topography to the S2 cleavage planes.

3.4.2 Micro structural fabric development in the UGSU

The greyschists in the UGSU appear to have experienced the same early stages of development as the LGSU but have experienced much greater strain in the later stages of the deformation. Field observations suggest that relatively un-modified S1 is only preserved in exceptional circumstances while in the majority of the unit it is replaced by an almost penetrative S2 crenulation cleavage. Thus rather than discussing the S1 and the S2 related folding event separately, as for the Lower Unit, in relation to the Upper Unit it seems more sensible to discuss the S1 and S2 fabrics jointly while discussing the post S2 structures in a separate section. A later section

Figure 3.29 Spaced extensional crenulation visible due to preferential erosion of cleavage planes.

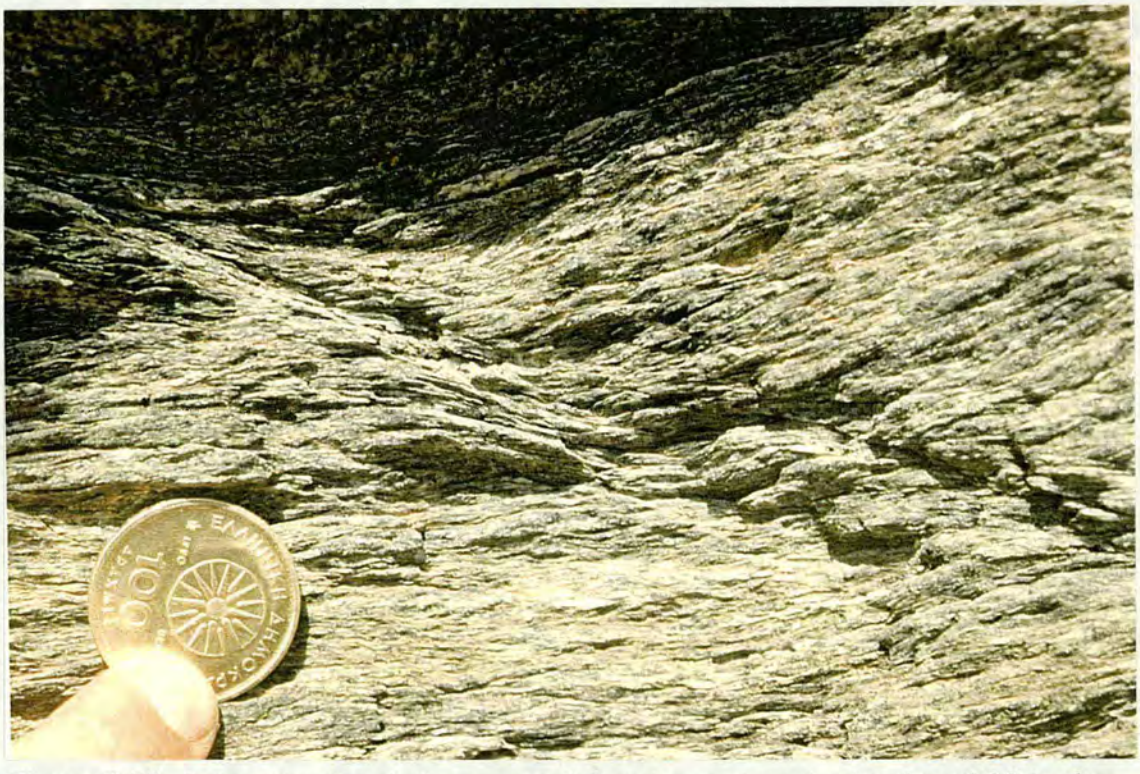

Figure 3.30 Late extensional shear zone deforming a strongly developed S2 in the UGSU.

will compare the relation between the deformations in the Lower and Upper Units in more depth.

S1 and S2 fabrics in the UGSU

As noted above the dominant fabric in the UGSU is a flat lying transposition fabric, the S2. It is defined by alignment of mica, glaucophane and quartz aggregates with subsidiary contributions from chlorite and sphene. The individual phases are identical in appearance and behaviour to those in the LGSU. As in the LGSU, the earlier fabrics are folded by the S2 crenulation with no evidence of new mineral growth. However, in the UGSU the crenulation is clearly much more intense and in the most extreme examples produces a penetrative, differentiated crenulation cleavage with little or no trace of earlier fabrics preserved. Due to considerable variation in the magnitude of the strain in different domains a complete record of the transposition of the S1 fabric is preserved.

In the least deformed samples, taken from low strain windows associated with rootless folds, continuous primary layering is still visible in the schist and is accompanied by a layer parallel S1 foliation. These fabrics are indistinguishable from those present in the LGSU. However, even in these cases the layering is folded and the S1 is strongly crenulated. As in the LGSU, the appearance of the S2 is controlled by the composition of individual domains. Mica-rich layers often exhibit tight, closely packed crenulations while the adjacent quartz and glaucophane-rich layers are apparently unaffected. Within fold cores crenulations in the mica-rich layers are often markedly disharmonic.

With increasing strain the schists become pervasively crenulated on a fine scale (Figure 3.31). Primary compositional layering is entirely destroyed on a thin-section scale. As the micas in the fold limbs become aligned to the new fabric the hinges of the folds become isolated in microlithons and a spaced S2 cleavage is formed. This stage of fabric development is approximately equivalent to the strongest

Figure 3.31 Strongly crenulated S1 in UGSU with formation of an incipient spaced S2 cleavage. (Sample 93/36, x12).

Figure 3.32 Fairly strongly developed S2 transposition cleavage with intermittent preservation of microfolds. (Sample 93/40, x12.5)

development of the S2 foliation in the LGSU. Within more quartz-rich lithologies this process is accentuated by the transfer of quartz from fold limbs to fold cores to produce a true differentiation cleavage.

As the strength of the S2 increases an increasing proportion of the mica aligns with the foliation and relic fold hinges become confined to isolated lenses between the cleavage lamellae (Figure 3.32). Within the most extreme examples virtually all trace of the crenulation event may be destroyed in the schist matrix. However, occasional fold hinges are typically still visible within the strain shadow of garnet porphyroblasts (Figure 3.33).

Where pre-and syn-tectonic quartz veinlets are present in the schists the transposition event transforms them into en echelon lens parallel to the S2. These, along with the remains of dissected sedimentary layering make a significant contribution to the transposition fabric in the most extreme samples.

Post Transposition Fabrics

As noted in section 3.4.1 parts of UGSU contain late extensional fabrics. The extensional crenulation shown in Figure 3.34 is typical of such structures. It deforms a penetrative S2 cleavage and thus clearly post-dates the transposition event. However, it merely folds the blueschist mineralogy without reaction and thus still occurs during the blueschist metamorphism.

Figure 3.33 S2 crenulation preserved adjacent to garnet porphyroblasts in a slide with an otherwise penetrative S2 cleavage. (Sample 93/25, x11)

Figure 3.34 S3 extensional crenulation deforming a well developed S2 cleavage. (Sample 93/31, x6).

3.5 Relationship Between Deformation in the LGSU and UGSU

The deformation history of the greyschists, as documented above, is broadly similar both the LGSU and UGSU. Both possess an early layer-parallel schistosity defined by peak blueschist minerals. This foliation is then folded into a series of asymmetric folds with the formation of a composite lineation parallel to the fold axes but with no new mineral growth. However, the style of this folding event is markedly different in the two units.

Within the LGSU folds are generally close to tight and the associated axial planar crenulation is only locally strongly developed. Fold axes plunge fairly steeply NW and axial planes are oriented at a high angle to bedding. the asymmetry of the folds is a constant Z facing NW.

In contrast, within the UGSU folds are tight to isoclinal. The crenulation is has developed into an almost penetrative, S2 transposition foliation which extensively disrupts primary layering. Fold axes are flat lying and trend approximately ENE with axial planes at a low angle to bedding. The asymmetry of the folds is a constant Z facing E.

At first glance it seems difficult to reconcile these contrasting characteristics with formation during a single deformation event. However, Ridley (1982a; 1982b) proposed a model which appears to elegantly account for the variation observed.

In mapping the blueschist structures over the whole island he noted that the dominant lineation, i.e. that parallel to the F2 fold axes, is distributed in arcs. Below the NGSB these are broad and span the width of the island. Above the NGSB, the area of the present study, there are a number of tighter arcs (Figure 3.35).

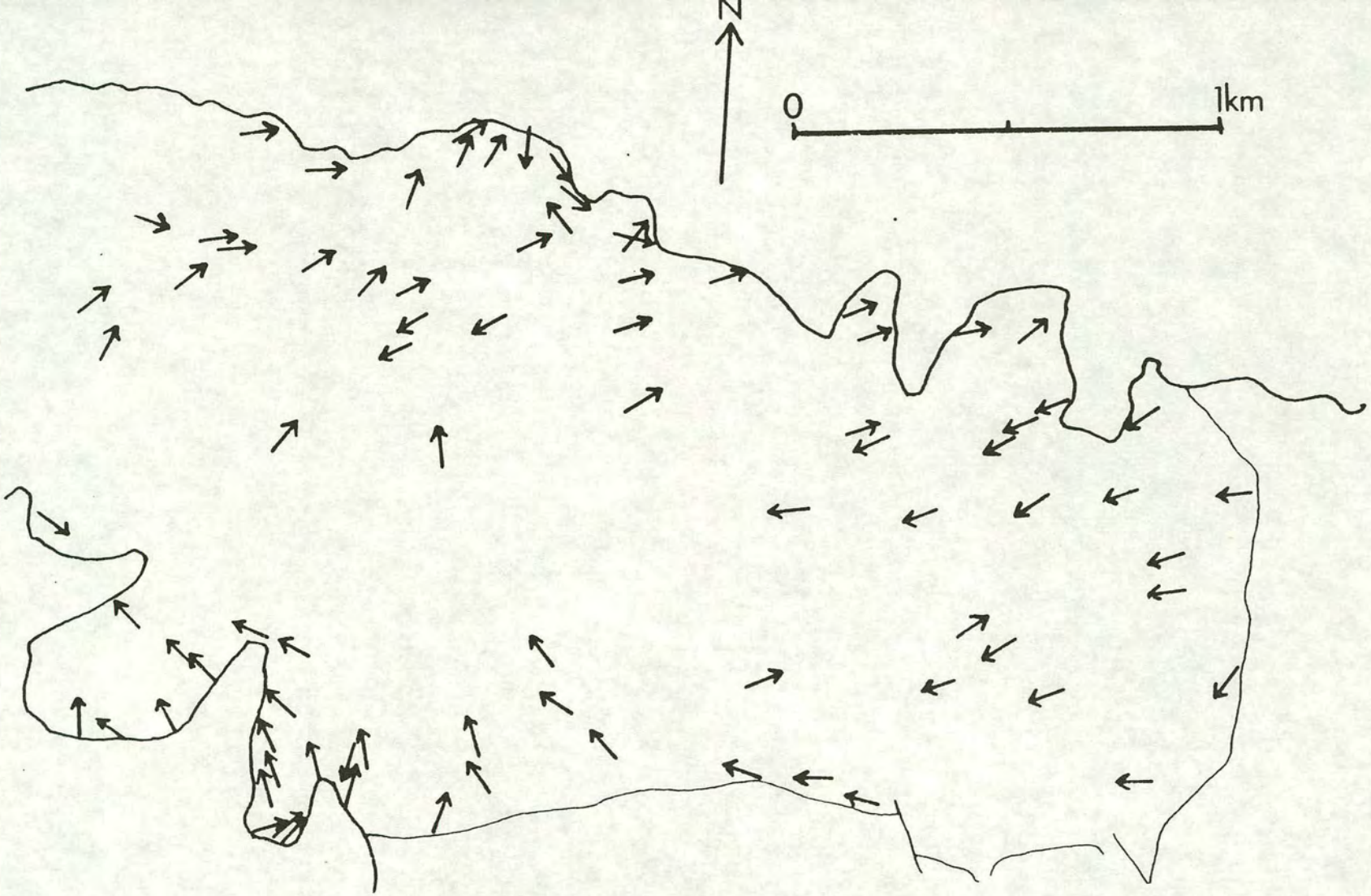

Figure 3.35 Lineation trend patterns for the sequence above the gneiss-serpentinite belt.

All recorded measurements shown. (Taken from Ridley, 1982)

Ridley also recognised a second lineation defined by the alignment of glaucophane needles. Other authors (Schwerdtner, 1970; Ramsay and Stuart, 1973) suggest that in foliated rocks amphiboles will tend to align to the major axis of the two dimensional strain ellipse in the plane of the foliation. Ridley (1982) proposes that if the strain approximates to simple shear this direction should be a close approximation of the displacement. He supports this conclusion by showing that the alignment of the lineation is indeed closely to the displacement vector derived from a Hansen (1971) plot.

Within those parts of the sequence in which the fold axes trend ENE the glaucophane lineation tends to orthogonality with the dominant lineation. However, as the dominant lineation curves toward the NW the angle decreases. The glaucophane lineation is no longer developed where the angle between it and the dominant lineation is less than 40° (Ridley 1982b). Thus the variation in the orientation of the dominant lineation can be viewed as zones of asymmetric folds with fold axes sensibly perpendicular to the movement direction which curve into zones oblique to parallel to the movement direction.

Rattey and Sanderson (1982) show that similar localised oblique structures are related to differential forward movement of thrust segments giving localised wrench tectonics. Noting this work and other studies considering the total strain fields produced by superimposing wrench and thrust shears (Coward, 1980; Coward and Kim, 1981; Sanderson, 1982) Ridley suggested that the oblique zones may be explained in a similar fashion. In order to test this model he rearranged the mathematical treatment of Sanderson (1982) to produce theoretical plots of lineation orientation against fold axial plane inclination and their coupled co-variation with changing strain parameters (Figure 3.36).

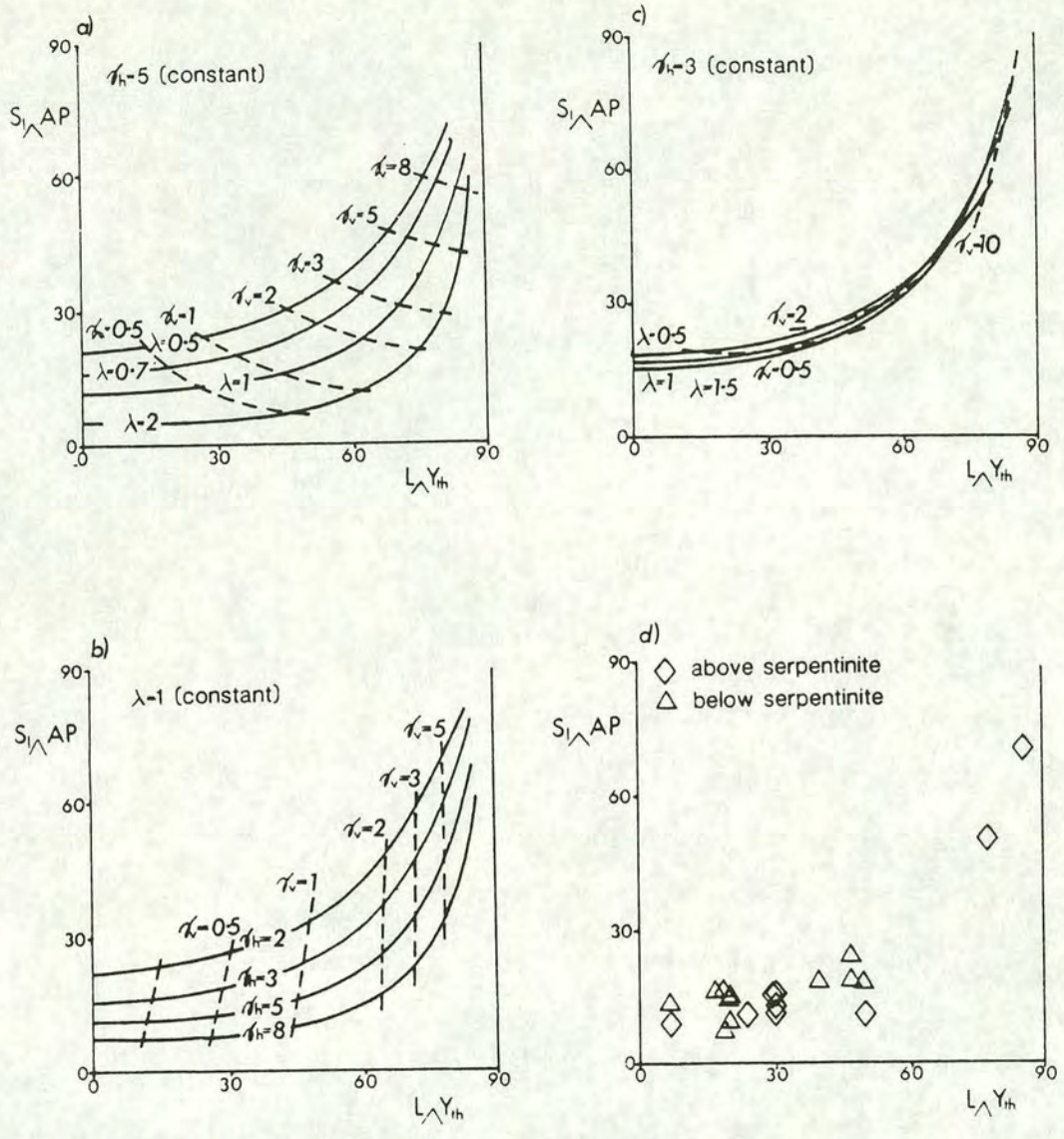

Figure 3.36 Theoretical and actual plots of the angle between the fold axial planes and lithological layering ($S_1 \wedge AP$) against the orientation of the dominant lineation with respect to the 'Y' axis of thrust shear ($L \wedge Y_{th}$). The variation is in each case with increasing wrench shear (γ_v). a) keeping thrust shear (γ_u) constant and varying the shear-parallel elongation (λ), taken up vertically. b) keeping the shear-parallel elongation constant with various thrust shears (γ_u). c) keeping thrust shear constant and with shear-parallel elongation taken up along the thrust strikes. d) data from Syros, discriminating between the sequences above and below the gneiss-serpentinite belt and plotting only the tightest folds from any one area. (Taken from Ridley, 1982)

The variation of the angular relations between fabric elements predicted by these plots agrees well with those observed on Syros and provide compelling evidence that they are caused by superimposed and synchronous thrust and wrench shear. As the component of wrench shear increases, measured by the decrease in the angle between the displacement direction and the dominant lineation, relative to the thrust shear, the angle between the fold axial planes and bedding also increases. However, if the thrust shear is large enough, no increase in dip will be apparent until the wrench shear exceeds 2. Thus, the angle between the dominant lineation and the displacement direction may be up to 60° before any difference in micro structures is visible. Ridley (1982) plots orientation data from Syros on an identical plot and shows that the distribution is indistinguishable from that obtained in the theoretical model. However, he notes that the fit does not define a unique set of parameters.

From the pattern of lineations and the style of the folding Ridley (1982) divides the sequence above the NGSB into a number of thrust lobes separated by wrench zones (Figure 3.37). He than uses this to produce a three dimensional schematic model (Figure 3.38). The positions of the 2 areas studied in the course of this project are marked on both diagrams. The UGSU area forms a section perpendicular to the front of a thrust lobe in which the strain is dominated by thrust shear, hence the small angle between layering and the fold axes. In contrast, the high angle between fold axial planes and layering and the NW trend of the folding indicates that the LGSU area is located within a zone of relatively high wrench shear. The sense of asymmetry in the folding indicates that it cannot be a continuation of the same lobe in which the UGSU lies. Instead it is placed in the adjacent thrust lobe on the opposite side of the wrench zone which forms the boundary between it and the lobe containing the UGSU area.

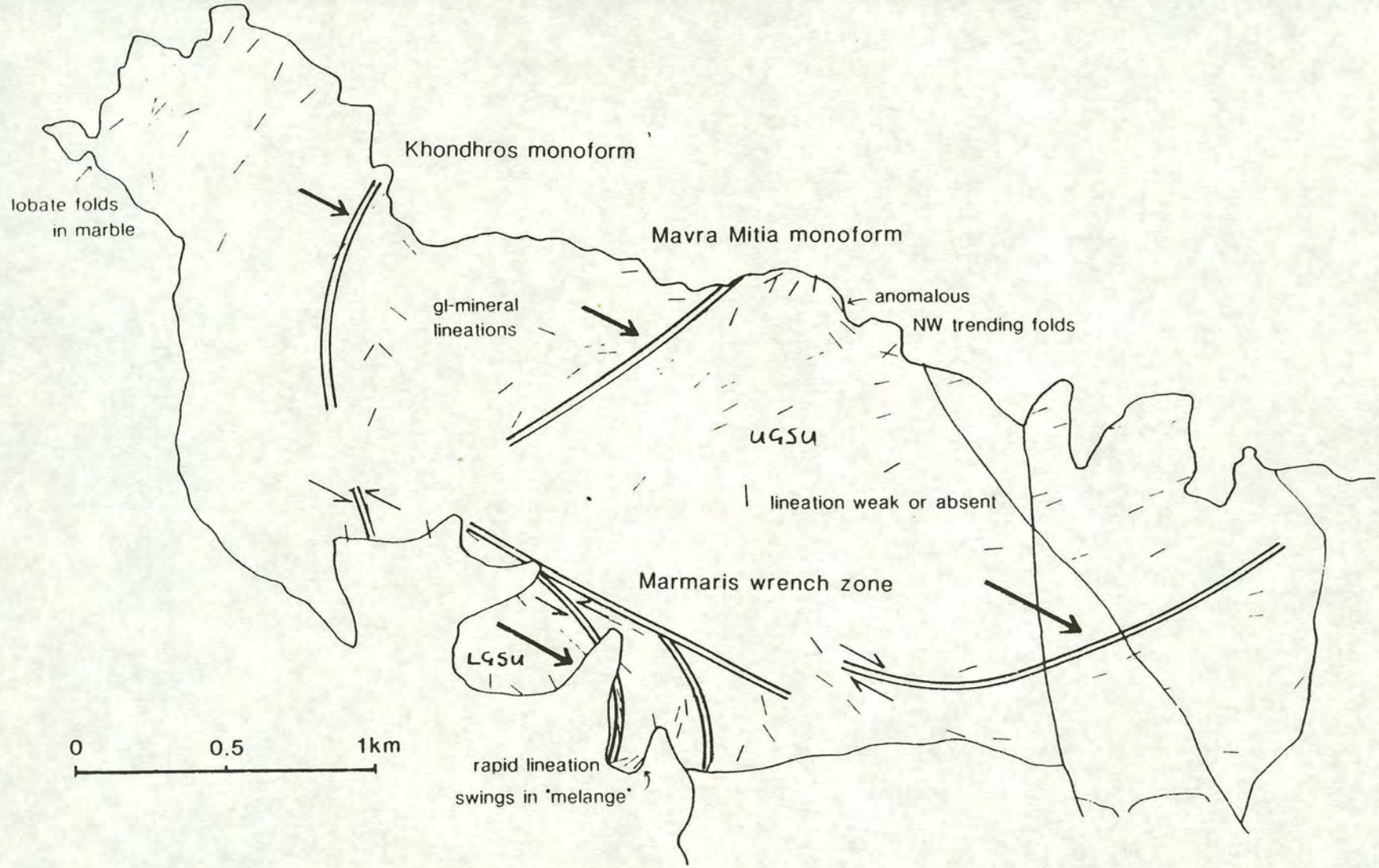

Figure 3.37 Interpretative summary of the 'lineation arcs' and truncation relationships in the upper sequence. The arrows give the sense of thrust and wrench displacements inferred. (Taken from Ridley, 1982)

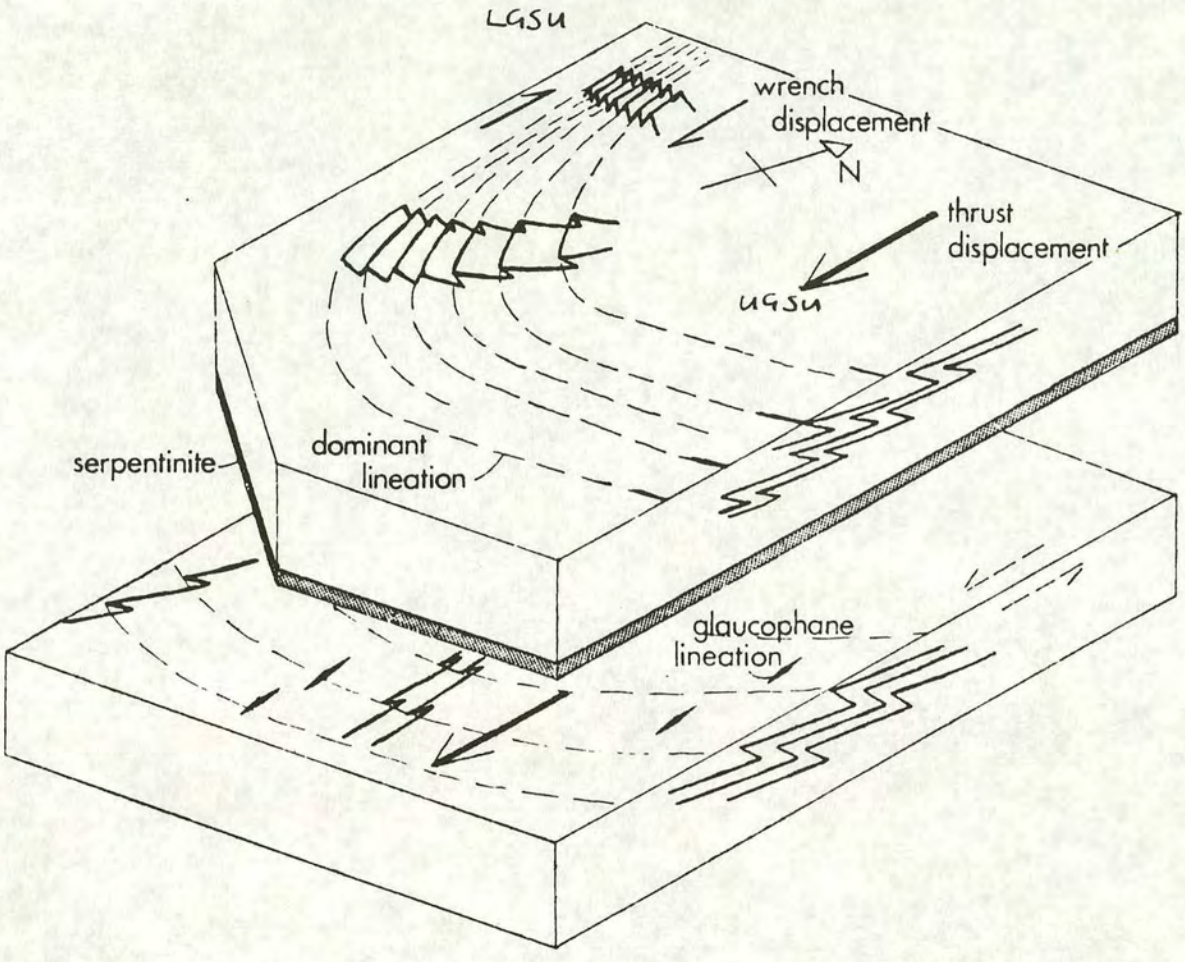

Figure 3.38 Schematic sketch of the spatial covariation of the lineation orientation and the microfold orientation, asymmetry and tightness as seen on Syros and their relationship to the inferred displacements and sense of shear strain. (Taken from Ridley, 1982)

3.6 Tectonic Breaks Above the NGSB

Ridley (1982) infers 2 tectonic breaks in the succession above the NGSB (Figure 3.39). The main break runs along the contact between the LGSU and the overlying marble unit from Ormos Grizas on the E coast to Ormos Gramata on the W before curving N to Kondros. The second can be traced from Trakilaki NW until it joins the main break N of Grammata.

Both are characterised by the presence of minerals associated with metasomatic reactions involving serpentinite. The greyschists at or near the contact are typically enriched in phases such as calcite, ankerite, fuchsite and omphacite. In many locations the boundary is marked by ankerite + omphacite, chloritic and glaucophanitic horizons. Locally derived, metasomatised clasts of schist and marble may be present in chlorite or glaucophane-rich assemblages forming 'micro melanges' (Ridley, 1982).

Ridley (1982) suggests that the presence of these rocks can be attributed, at least partially, to the former presence of serpentinite bodies. Chloritic units are interpreted as reacted out serpentinite bodies similar to those present in the NGSB described by Dixon (1969). Micro melanges are assumed to have formed by the fragmentation of the once continuous serpentinite bodies or the extreme deformation of ultramafic-rich debris horizons. The occurrence of Cr-rich fuchsitic micas also seems to attest to the presence of ultra-mafic material.

It seems likely that the position of these breaks is genetically linked to the presence of serpentinite. The metasomatic schists in the Aspro melange zone possess an extremely strong, fine grained foliation sub parallel to layering. Thin sections reveal that this is a reformed schistosity resulting from the crenulation of an earlier fabric (Figure 3.40). Thin marble layers inter bedded with the schists are folded into tight to isoclinal asymmetric folds with the same sense of asymmetry as the F2 folds in the adjacent greyschists (Figure 3.41). The intense layer-parallel foliation appears

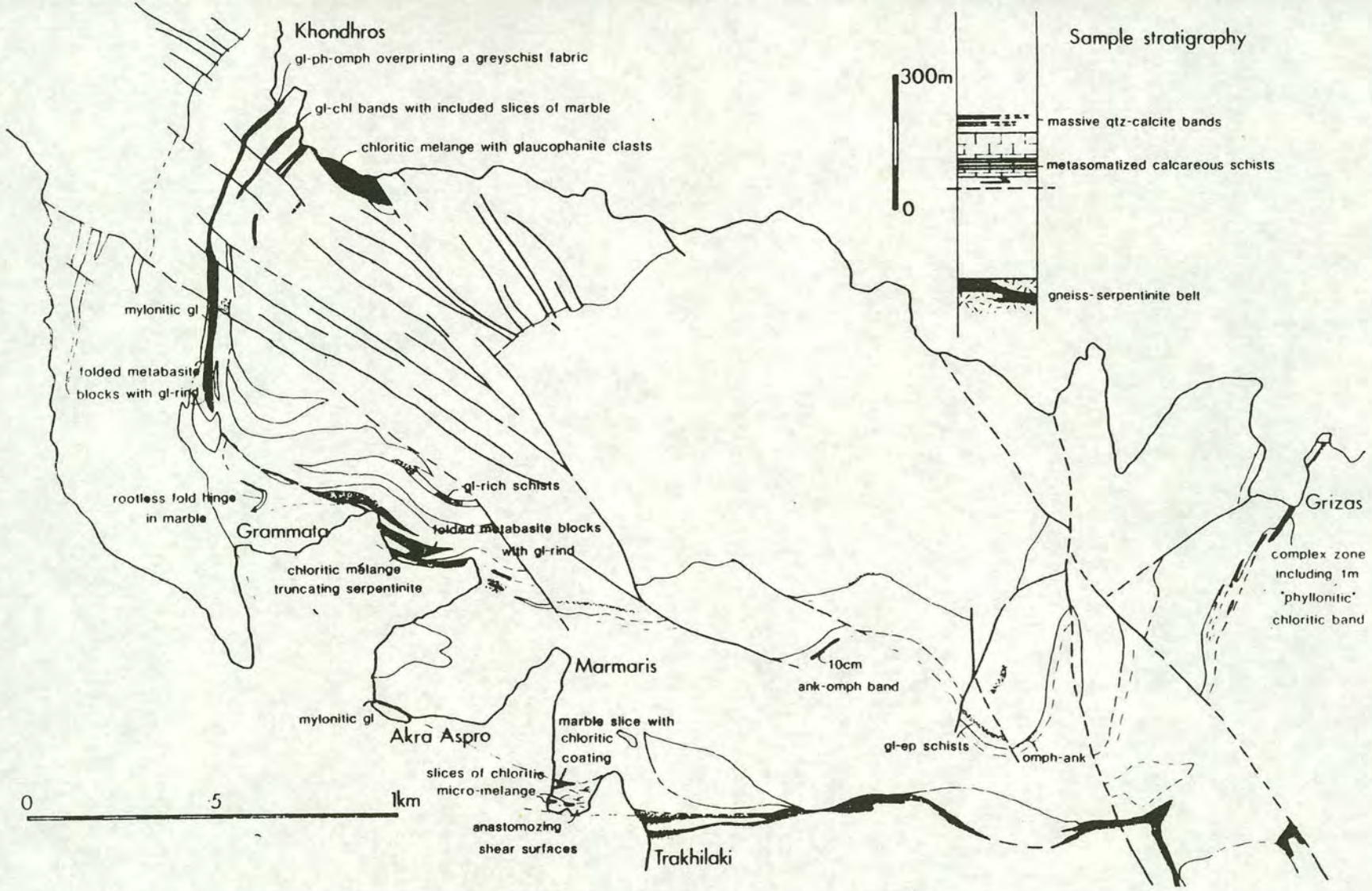

Figure 3.39 Summary of the critical outcrops giving the form and distribution of the syn-metamorphic tectonic breaks in the upper sequence. The inset gives the stratigraphy for the eastern half of the area covered, where less laterally variable. (Taken from Ridley, 1982)

Figure 3.40 Traces of the crenulation event responsible the formation of the foliation in Aspro melange zone preserved in the lee of a lawsonite porphyroblast. (Sample 91/ASP6, x6)

Figure 3.41 Tightly folded marble horizons interbedded with schists containing a penetrative foliation which is axial planar to the folds, from the Aspro melange zone.

to be axial planar to these folds. Thus, the Aspro zone seems to be the focus of intense localised strain during the F2 event, approaching the intensity of that seen in the UGSU. The boundary between highly strained metasomatites and the overlying greyschists is sharp and apparently conformable. The simplest model accounting for these features is the high proportion of serpentinite in the melange unit makes it mechanically weaker than the surrounding greyschists and thus it partitions the strain. The tectonic breaks are thus analogous to the NGSB which appears to act as a mechanical discontinuity throughout the bulk of the deformation but on much smaller scale. The eventual sealing of the 'faults' may be related to the reacting out of the serpentinite (Ridley 1982).

The geometry and timing of the movement on the breaks is difficult to assess. Ridley (1982) notes that the movement clearly predates the large scale syn-blueschist monoclinal folding at Mavro Mitia and Khondros. However, he concludes that it is impossible to constrain the timing of the initiation of movement.

All the metasomatic assemblages are compatible with formation at the peak of blueschist metamorphism. Within the Aspro melange zone the deformation clearly continues after the growth of lawsonite. The transposition fabric wraps around the porphyroblasts and microfolds of the earlier fabric are preserved in strain shadows. This suggests that movement on the lower break continued late in the blueschist metamorphism. Within the marbles at Aspro there is a zone of fault breccia which appear to be the result of late faulting. Ridley (1982) notes a similar Post metamorphic fault coincident with the lower tectonic break at Trakilaki. Thus the syn-metamorphic movement on the lower break may be accentuated by post metamorphic brittle deformation.

The timing of movement on the main tectonic break appears to be diachronous (Ridley 1982). East of Marmaris the contact is effectively annealed out suggesting the movement ceased relatively early in the metamorphism. This is consistent with the continuity across this boundary of the lineation arcs produced by

the relatively late ductile thrusting. In contrast in the west, intense strain and brecciation appears to have continued almost to the end of the blueschist event (Ridley 1982). Ridley suggests that this strain incompatibility may be accounted for by a transformation to more ductile strain and / or movement on the lower fault line.

In summary, it appears that the sequence above the NGSU contains 2 'faults' which were active during the blueschist deformation and were probably initiated by slip on relatively weak serpentinite-rich horizons. Movement occurred on the upper break at first but then transferred to the lower break later in the deformation, possibly due to the reacting out of the serpentinite. The presence of brittle deformation along the lower break suggests that some of the movement post-dates the metamorphism. The continuity of the lineation arcs across the upper break indicates that the LGSU, UGSU and intervening marble constituted a single tectonic block at least during the F2 folding.

3.7 Summary of the Structural Development of the Greyschists

The syn-blueschist deformation in the Syros greyschist can be divided into two distinct phases. The main product of the first phase is a strong layer-parallel foliation resulting from the alignment of various components including sheet silicates, amphiboles and mm-scale aggregates of quartz. This is the dominant syn-blueschist structural fabric and is present over the whole of the island except in the cores of more competent meta-igneous blocks. In the micaceous greyschists it takes the form of a penetrative schistosity. However, the development of the S1 does not involve any significant disruption of the primary sedimentary layering. In particular, there is no evidence that it involves the folding and transposition of an earlier fabric. No traces of pre-S1 metamorphic fabrics have been found on Syros during this or earlier studies. Any syn-S1 folding is very localised and is associated with specific ductility contrasts such as the presence of early quartz veins. The only systematic disruption accompanying the formation of the S1 is common chocolate block boudinage of more competent calc-silicate horizons.

The main feature of the second phase of the deformation is widespread asymmetric folding on a range of scales from mm size crenulations of the S1 to metre scale folds of compositional layering. This is typically accompanied by a lineation defined by the intersection of crenulation hinges with the S1 and the alignment of glaucophane prisms and quartz pressure shadows on garnets. In contrast to the relatively uniform character of the first phase of deformation, the style and intensity of the second phase varies considerably even within the relatively small area over which the greyschists are exposed. In the LGSU it is relatively weak. Folds of layering are comparatively open and widely spaced. Crenulations of the S1 are weakly developed and a true S2 axial planar fabric is only found in the hinge regions of the larger scale folds. The axial planes of the folds are at a high angle to compositional layering and the S1. In the UGSU the second phase is far more intense. In the vast majority of the unit it results in the complete transposition of the S1 and bedding to produce a penetrative flat lying S2 cleavage. Scattered rootless fold pairs are preserved in more competent calc-silicate horizons and, on a smaller scale in strain shadows adjacent to garnet and lawsonite porphyroblasts. the folds are tight to isoclinal with axial planes at a low angle to compositional layering.

The generation of the folds is attributed to an episode of ductile thrusting. Overall strain during this event approximates to simple shear with a component of shortening parallel to layering (Ridley 1982). The variation in strain and orientation of fold axial planes is attributed to variation in the ratio of wrench shear and thrust shear at different points within individual thrust lobes.

The strain regime responsible for the formation of the S1 foliation is more difficult to define. All the features of this stage of the deformation are consistent with pure shear flattening perpendicular to layering particularly the presence of very fine scale graphitic laminae preserved inside and outside glaucophane crystals. Such an interpretation would imply that the onset of the folding marks a major change in the strain regime in the meta-sediments from co-axial to non-coaxial deformation.

However, overall one would expect major shear zones such as subduction zones to be sites of intense non-coaxial deformation. If the S1 is the result of pure shear flattening such non-coaxial deformation would have to be partitioned outside the Syros section. However, the appearance of the S1 is also consistent with formation under bulk simple shear with the shear plane sub-parallel to primary layering. Such an interpretation would not require as significant a change in the strain regime at the onset of folding, merely the addition of a component of shortening to the on-going simple shear regime. This could be the result of minor changes in the boundary conditions of the Syros 'packet' such that fold instabilities develop. Such an interpretation also removes the need for complete strain partitioning during the early stage of the deformation. It will be proposed in chapter 8 that such a change could be consistent with the transfer of a subducting packet from the footwall to the hanging wall i.e. with the operation of underplating.

CHAPTER 4

TIMING OF LAWSONITE GROWTH

4.1 Introduction

In the previous chapter I described the syn-blueschist deformation in the greyschists. In chapter 5, I will show that much of the lawsonite growth in the greyschists is spatially related quartz veins which are the product of a syn-deformational fluid infiltration event. As noted in section 3.1 it is crucial to establish its timing relative to the strain history as precisely as possible.

Many of the lawsonite porphyroblasts in the greyschists contain well developed internal fabrics. Interpretation of these fabrics provides an insight into the timing of their growth relative to the development of the external fabrics and therefore to the wider strain history.

In this chapter I will discuss the internal fabrics observed in the lawsonites in the light of current models for the formation of such fabrics and consider the implications for the timing of lawsonite.

4.2 General description of Lawsonite Internal Fabrics

Pseudomorphs after lawsonite are present in a large proportion of the greyschist assemblages as euhedral, rhombic porphyroblasts up to 3 cm in size. In most cases they are poikiloblastic. The dominant included phase is quartz but all other phases present in the greyschists have been observed, including garnet.

The dominant S1 layer parallel fabric always wraps around the pseudomorphs and they occasionally develop symmetrical, quartz pressure shadows parallel to the foliation. Where a strong S2 crenulation is present in the matrix the pressure shadows are aligned parallel to the axial planes of the microfolds. Thus, in all cases the cessation of lawsonite growth predated the end of the blueschist deformation. However, the intensity of the post lawsonite deformation is variable.

The lawsonites commonly contain well defined internal fabrics (Figure 4.1). These suggest they overgrew a fabric similar to that present in the matrix. Unlike the garnets the grain size inclusions is the same as that in the external foliation. In some cases, the lawsonites clearly pseudomorph a strongly developed quartz and mica fabric identical to the model S1 (Figure 4.2). Where garnets are included these often exhibit well formed pressure shadows aligned parallel to the included foliation. These observations are consistent with the lawsonites growing considerably later than the garnets and thus including a more mature metamorphic fabric.

Directional fabrics preserved in lawsonites are typically straight in the core and curved in the rims producing sigmoidal geometries. The straight portions of the included fabrics range from sub-parallel to the external fabric to being strongly oblique to it. The maximum angle between Si and Se is typically 45 to 60° in the LGSU, but up to 90° in the UGSU. Within individual thin sections the internal fabrics are generally sub-parallel (Figure 4.3). There may be some variation in the angle between Si and Se in adjacent porphyroblasts but they dip in the same direction relative to the external foliation. The asymmetry of sigmoidal fabrics always records the same sense of relative rotation between Si and Se. In the LGSU where the external fabric is the S1 the internal fabric remains continuous with the external fabric irrespective of the magnitude of the angular discordance. In the UGSU where the external fabric is the S2 transposition foliation the external fabric truncates the internal fabric.

4.3 Interpretation of Porphyroblast Internal Fabrics

The lawsonite internal fabrics described above clearly contain a significant amount of information about the timing of their growth and the nature of the fabric that they overgrew. The interpretation of such syn-tectonic fabrics is reliant on the mechanisms by which they are assumed to have formed. The predominant distinction is between models in which the porphyroblasts remain static relative to geographical co-ordinates during development of the external fabric and those in which they

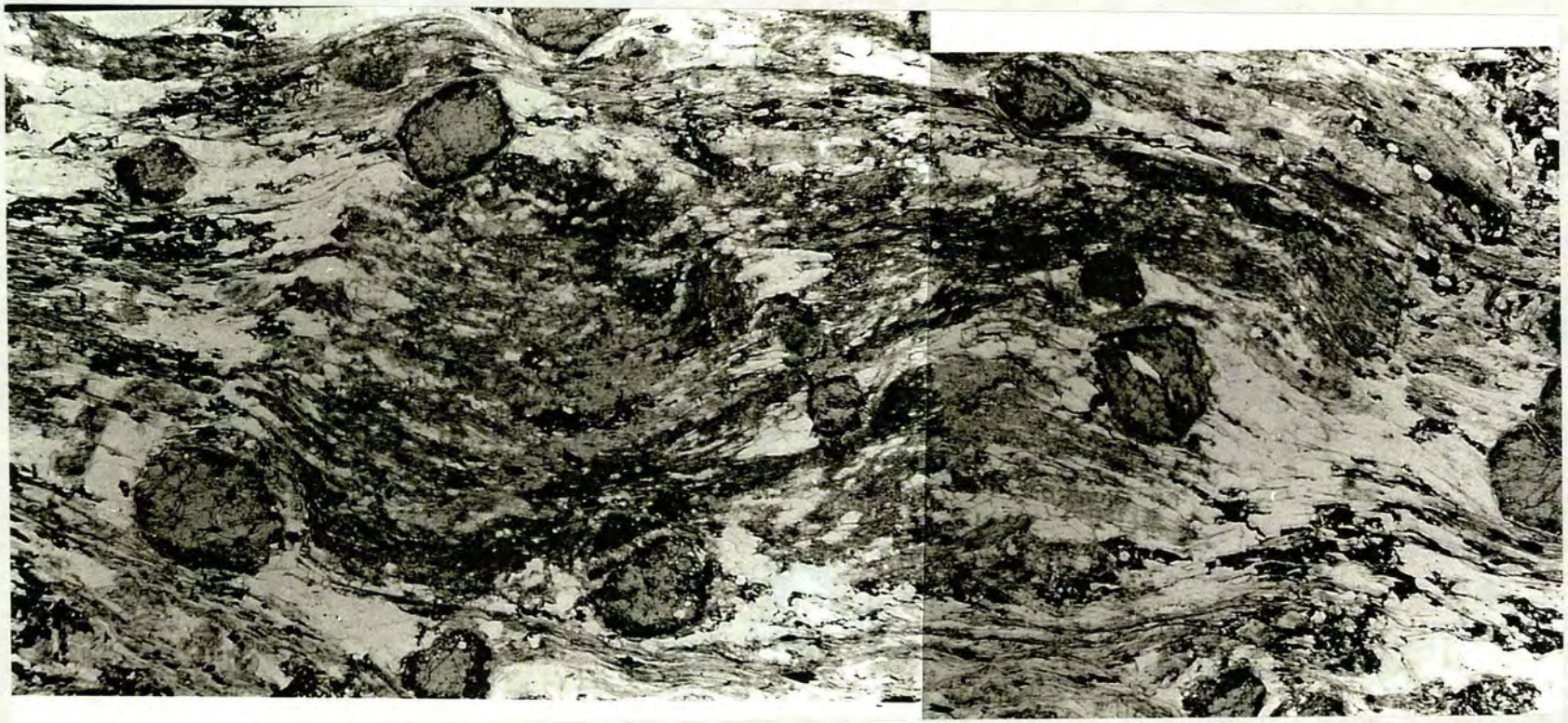

Figure 4.1 Large lawsonite porphyroblast containing a classic sigmoidal inclusion fabric. Straight portion of fabric is strongly oblique to the external S1 but curves into continuity with it at the margin of the porphyroblast. Overgrowth fabric appears identical to that in matrix including garnets with well developed pressure shadows. (Sample 92/74, x6)

Figure 4.2 Lawsonite pseudomorph with birds nest internal fabric apparently recording the overgrowth of a quartz and mica fabric similar to that in the matrix. (Sample 92/30C, x15).

Figure 4.3 Two lawsonites with parallel inclusion fabrics oblique to the external S1 foliation. (Sample 92/80, x9).

porphyroblast internal and external fabrics are described below. The applicability of such models to the Syros greyschists will then be discussed.

4.3.1 Rotational models

The simplest and perhaps most intuitive explanation for the occurrence of porphyroblasts containing oblique straight or sigmoidal internal fabrics continuous with the external fabric is that the porphyroblasts have rotated relative to the matrix and to geographical co-ordinates. Numerous studies have suggested that this process explains the formation of a range of oblique inclusion fabrics (e.g. Spry, 1963; Rosenfeld, 1970; Schoneveld, 1977, 1979; Oleson, 1982; Vissers & Mancktelow, 1992; Busa & Grey, 1992).

Porphyroblasts are interpreted as having overgrown a pre-existing or developing fabric and rotated relative to it so that Si becomes discordant to Se (Figure 4.4). The rotation is caused by non-coaxial strain in the matrix producing differential shear on the porphyroblast margins. The shape of the fabrics is controlled by the finite strain, the ratio of growth rate to strain rate, and the stage of the progressive deformation during which the porphyroblasts grew (Barker, 1994) (Figure 4.5). If the porphyroblast growth is inter-deformational or the growth rate is rapid relative to the strain rate then the result would be a straight Si oblique to Se. However, if the porphyroblast growth were entirely syndeformational, i.e. it rotated as it formed, then the resulting fabric would be curve. Similarly, porphyroblasts with straight cores and curved rims would indicate that rotation only occurred during the last stages of growth. However, the possibility that deformation involving typical regional metamorphic strain regimes can cause such porphyroblast rotation has been questioned in a number of recent papers (e.g. Bell, 1985; Bell et al. 1992). These studies have shown that it is perilous to assume that porphyroblasts have rotated relative to geographical co-ordinates without careful investigation.

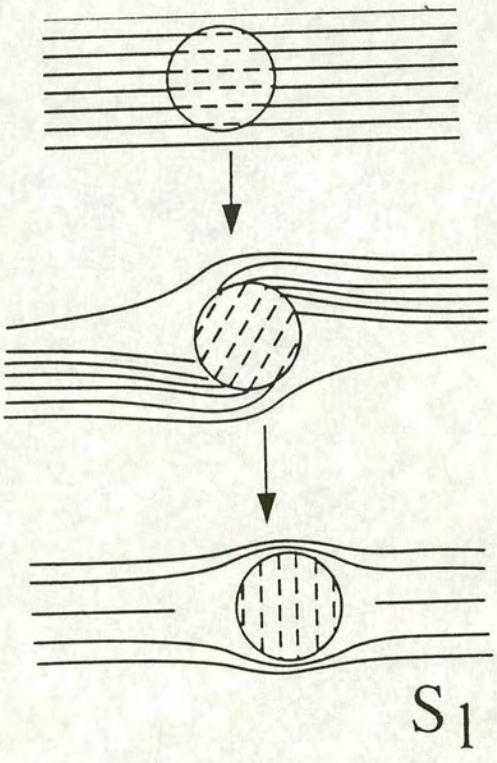

Figure 4.4 Formation of oblique inclusion fabric by overgrowth of a foliation followed by porphyroblast rotation relative to it.

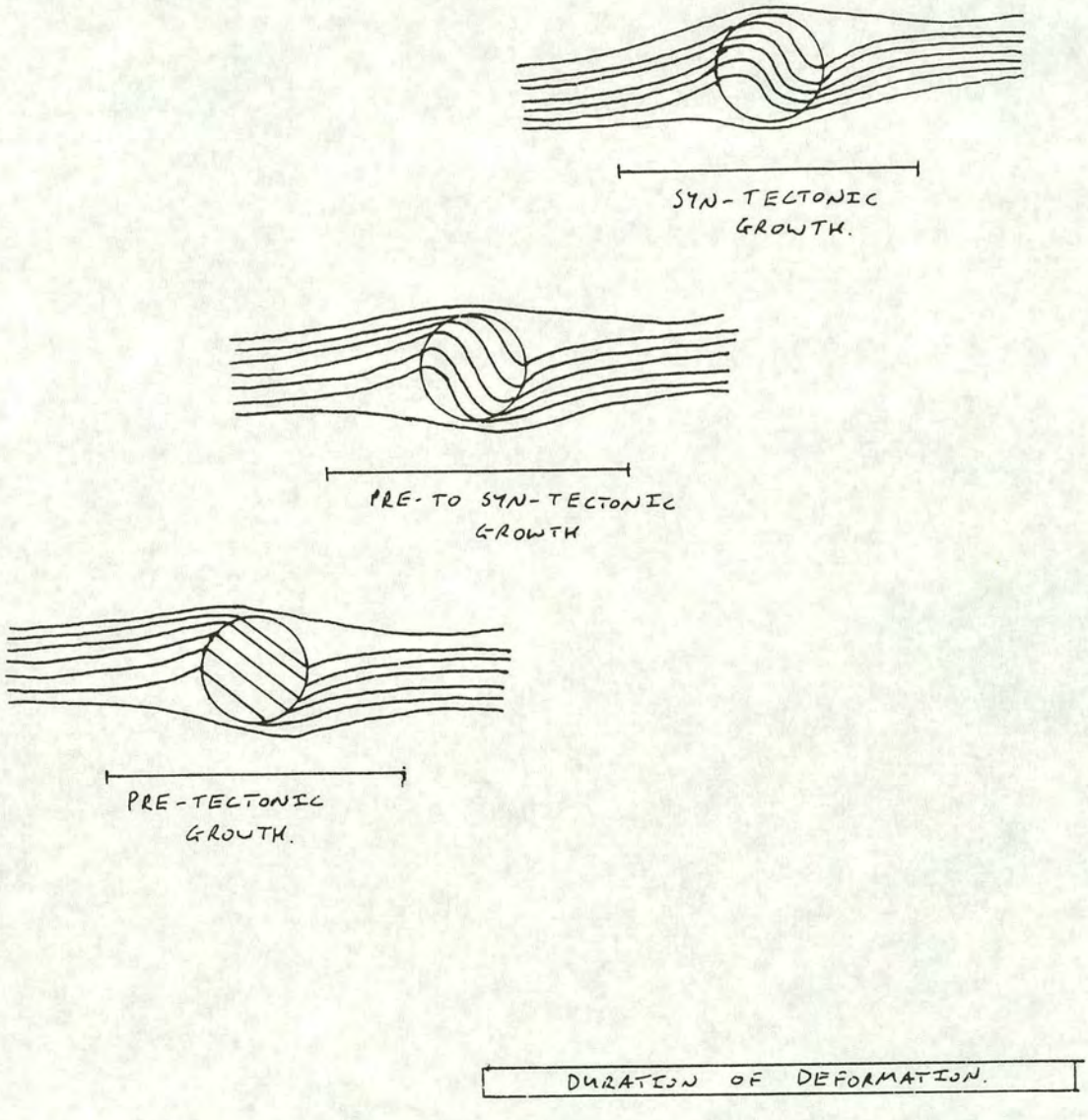

Figure 4.5 Illustration of the control of S1 morphology by timing of porphyroblast growth relative to deformation when applying the rotational model.

4.3.2 The 'Bell' model

Bell (1985) proposed a non-rotational model to explain the occurrence of straight to sigmoidal inclusion fabrics. While accepting that porphyroblasts must rotate under conditions of strong, non partitioned, non coaxial deformation he suggested that such conditions are rare during deformation (Bell et al. 1986). Instead the model proposes that localisation of progressive shearing in phyllosilicates and graphite will cause strain partitioning and lead to progressive inhomogeneous simple shear or even progressive bulk homogeneous shortening.

Using the Bell model oblique inclusion trails within porphyroblasts are typically interpreted as the result of the overgrowing of differing stages in the evolution of a crenulation cleavage (Bell & Rubenach, 1983) (Figure 4.6) The exact nature of the internal fabrics is dependent on the stage of the crenulation event they over grow. The crenulation cleavage may evolve to such an extent that no trace of it remains in the external fabric (stage 6 of Bell & Rubenach, 1983). Thus, the Bell model interprets porphyroblast internal fabrics as the relics of earlier foliations which often destroyed in the matrix by later deformation events.

4.3.3 The Ramsay model

Ramsay (1962) proposed another model in which porphyroblasts can develop straight or sigmoidal inclusion fabrics oblique to the external fabric while remaining fixed relative to geographical co-ordinates which in some ways was the precursor of the Bell model. He suggests that pure shear oblique to a pre-existing foliation will cause wholesale rotation of the fabric while porphyroblasts overgrowing the fabric remain static (Figure 4.7). If the porphyroblast growth were syn-deformational then it would be expected to develop a sigmoidal internal fabric oblique to the external fabric while if it were pre-deformational then the preserved fabric would be straight

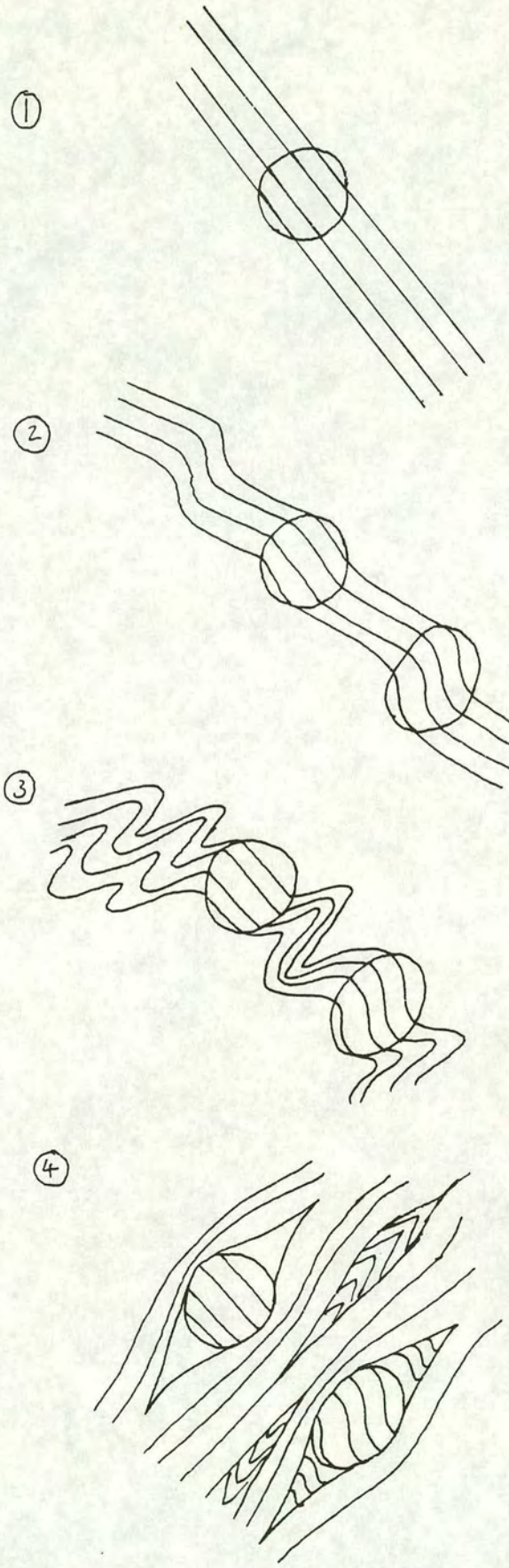

Figure 4.6 Formation of straight and sigmoidal oblique inclusion fabrics by overgrowth of various stages in the crenulation of an earlier fabric.

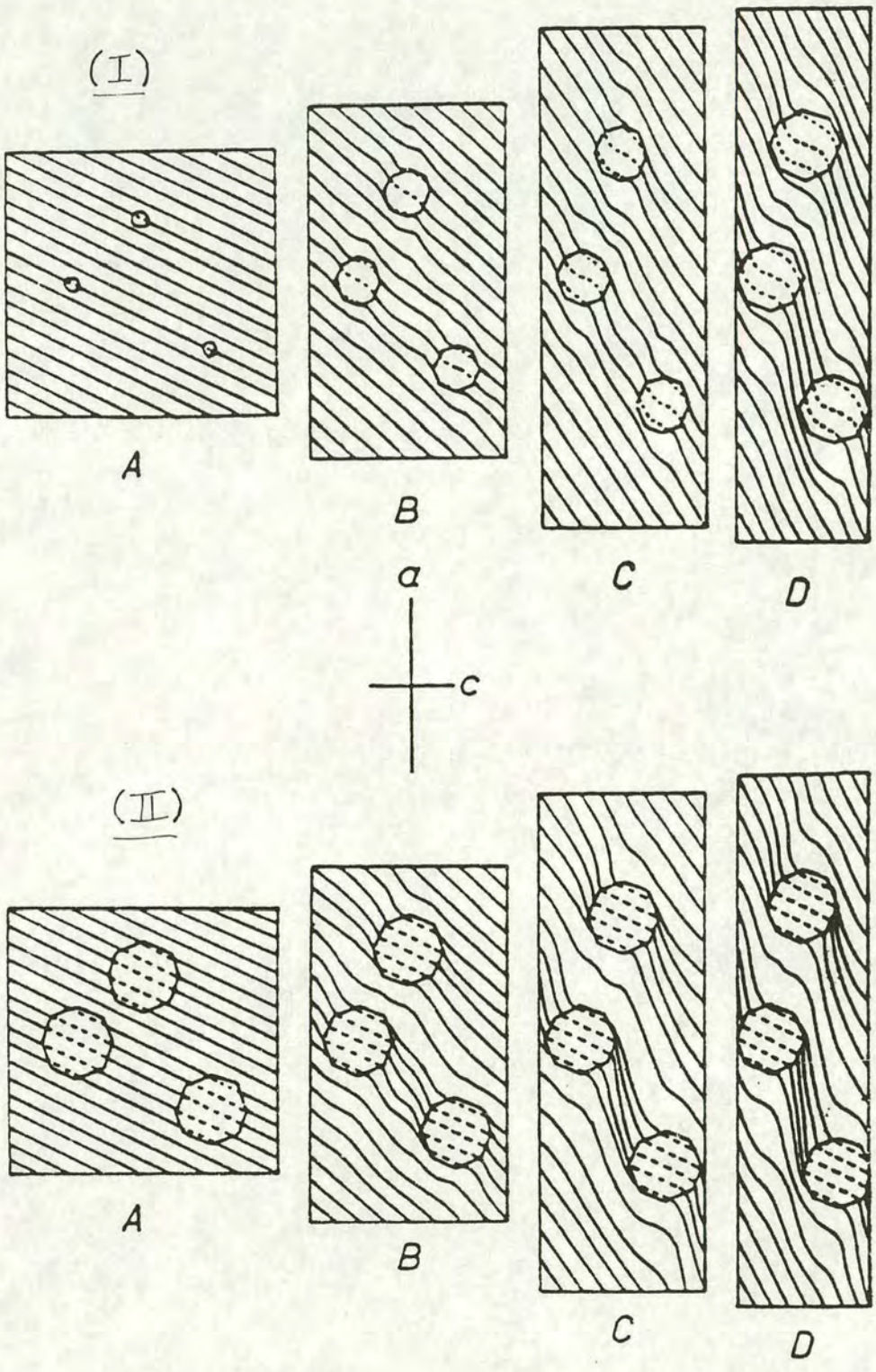

Figure 4.7 Formation of oblique inclusion fabric by rotation of an external foliation relative to porphyroblast due to pure shear flattening. Syn-tectonic growth results in sigmoidal fabrics (I). Pre-tectonic growth results in straight fabrics (II).

and oblique. Specifically, he proposed that such fabric evolution would occur due to flattening during the formation of similar style folds. Wilson (1971) further considered the implications of such a fabric evolution and Keenan (1971) applied it to model the development of a single similar fold.

4.4 Interpretation of Porphyroblast fabrics from the greyschists

Using the models described above, 3 possible mechanisms would seem to account for the formation oblique internal fabrics observed in the lawsonites.

a) Syn-tectonic overgrowth of a pre-S1 foliation followed by reformation / realignment of the external fabric while the porphyroblasts remain static.
b) Syn-tectonic overgrowth of the S2 crenulation with no porphyroblast rotation.
c) Syn-tectonic overgrowth of the S1 followed by rotation of the porphyroblasts.

The first of these options may be discounted immediately. It would require that either an early fabric existed at a high angle to layering which realigned/reformed parallel to layering or there was wholesale rotation of both layering and a parallel foliation around static porphyroblasts. Neither history seems plausible.

The formation of a foliation as well developed as that preserved in the lawsonites at a high angle to layering would require a significant component of shortening parallel to layering. This layering imparts a strong planar anisotropy, to the greyschists which readily buckles during later folding events and hence would be expected to do so under such a strain regime. However, no pre-S2 folds which might be associated with the formation of the pre-S1 fabric are present. It seems unlikely that such a strong fabric in this orientation could develop without some attendant disruption of layering. Furthermore, there appears to be no plausible mechanism by which such a high angle fabric could become realigned parallel to layering. As noted in the previous chapter, the excellent preservation of fine scale primary layering and the absence of any fold structures to which the S1 is axial planar rules out the

possibility of a pre-S1 crenulation event. The only other obvious mechanism which might account for the realignment is the rotation of the foliation during the formation of similar folds as suggested by Ramsay (1962). In order to account for the relative rotation of considerably greater than 45° between Si and Se the magnitude of the strain associated with the folding would have to be large (Wilson, 1971). There is no evidence for any episode of folding other than the F2. Within the LGSU this event is clearly not intense enough to cause the observed rotations. The F2 folding in the UGSU is probably of sufficient intensity to cause the required rotation. However, the S2 fabric is clearly the result of a pervasive crenulation event rather than the passive rotation of an earlier fabric. Evidence from low strain zones show that the fabric which is crenulated is a layer parallel S1 rather than a steeply dipping foliation which might account for the inclusion fabrics.

As noted above if the oblique internal fabrics do not result from the overgrowth of a pre-S1 fabric at a high angle to layering they may record the overgrowth of an earlier stage of the S1 which formed parallel to layering and then rotated with layering during a much larger scale reorientation of layering while porphyroblasts overgrowing it remained static. This would allow the application of the Ramsay model while accounting for the apparent lack of suitable folding. Furthermore, it would also remove the necessity for the early fabric to be orientated at a high angle to layering. It would require that the general dip of bedding in the meta-sediments was much steeper than that visible today during an earlier stage of the syn-blueschist deformation. This simplest way to account for this wholesale rotation of layering is if the entire sequence exposed on Syros represents one limb of a much larger, recumbent fold structure with an axial plane above or below the present erosion level. If this was the case then the constant sense of asymmetry of the F2 folds may be attributed to parasitic folding on the limb of the larger structure. Such a structural history is difficult to prove. By its very nature no evidence for its occurrence will be visible over the area covered. However, structures on a similar scale have been documented in the rest of the Cyclades. The geometry of the folding and variations in the trend of folds axes seem to be better explained by the ductile

thrusting models of Ridley (1982). On these grounds it seems difficult to support such an interpretation.

If the oblique internal fabrics do not record the overgrowth of a pre-S1 fabric they must result from the overgrowth of either the S2 crenulation or the overgrowth of an undeformed S1 followed by rotation of the porphyroblasts.

Many of the oblique fabrics appear consistent with the formation by overgrowth of the S2. Figure 4.8 shows a single lawsonite porphyroblast containing a straight inclusion fabric oblique to but continuous with the external S1. The preservation of mm scale graphitic layering within the sample indicates that it has experienced no pervasive heterogeneous deformation. Outside the porphyroblast the S1 is folded into a number of sub-parallel S2 crenulations with their axial planes at high angle to S0. A quartz pressure shadow parallel to the axial plane of the crenulation is present at one edge of the porphyroblast. Sheet silicates within the pressure shadow are also oriented parallel to the axial planes of the crenulation. This geometry is consistent with the lawsonite overgrowing the short limb of an asymmetric S2 microfold during an early open stage of its development. Meanwhile, outside the porphyroblast the crenulations have tightened considerably during post-lawsonite growth strain.

Other porphyroblasts clearly overgrow later stages of the development of the crenulation. Figure 4.9 shows two lawsonite porphyroblasts with sub parallel internal fabrics oblique to the S1. One contains an almost straight fabric which must represent an early stage in the folding of the S1 fabric. Within the second the inclusion fabric is clearly folded and appears to record the overgrowth of a tighter crenulation. The S2 crenulation in the matrix has then tightened considerably after the growth of the porphyroblasts. Figure 10 shows similar relations between the internal and external fabrics. A lawsonite contains a weakly crenulated fabric with axial planes parallel to those of the S2 crenulation in the matrix. This clearly results from the

Figure 4.8 Lawsonite containing a weakly sigmoidal fabric whose geometry is consistent with overgrowth of an earlier stage of the s2 crenulation visible in the matrix. Pressure shadows have formed on the porphyroblast parallel to the S2 axial planes. (Sample 92/4, x20).

Figure 4.9 Two lawsonites with sub-parallel inclusion fabrics oblique to the external foliation apparently resulting from the overgrowth of an early stage of crenulation visible in the matrix. (Sample 92/47, x16).

Figure 4.10 Lawsonite with an internal fabric preserving a weakly crenulated S2. The S1 has been rotated through 90°due to syn-S2 buckling of a quartz vein. The crenulation in the matrix has tightened considerably after the growth of the porphyroblast. (Sample 92/48, x12).

overgrowth of an earlier stage in the development of the external fabric. Significantly, no porphyroblasts are were found which contain a more highly developed S2 fabric which would indicate that they grew during the later stages of the folding event.

While the overgrowth of varying stages of S2 development seems to account for the fabrics described above fairly simply, the application of this mechanism to many other examples is not as straight forward. Figure 4.11 shows a lawsonite porphyroblast containing a sigmoidal internal fabric continuous with the external S1 similar to that noted above. However, in this case no S2 crenulation is present in the matrix. If we assume that the fabric results from the S2 we must assume that the porphyroblast has overgrown the only microfold present in the slide. As noted above, Bell 1986 proposes that the formation of crenulations will control the site of porphyroblast growth. This might account for the apparently fortuitous nature of its position. Alternatively, the lack of microfolds in the matrix might be due to localised decrenulation during the later stages of the folding event (Bell 1986, Phillips and Key 1992). However, it may be simpler to explain such fabrics in terms of porphyroblast rotation.

4.5 Porphyroblast Fabrics in the U.G.S.U

The fabrics discussed in the preceding section come from the L.G.S.U. The relatively simple structural history apparently preserved in these samples provide tighter constraints on possible mechanisms for the formation of the porphyroblast internal fabrics than those in the U.G.S.U.

Within the U.G.S.U the destruction of the pre-S2 fabrics in the majority of samples removes most traces of the earlier structural history. However, examination of structures in low strain zones indicate that the early stages of the syn-blueschist deformation was the same in both units. Thus it seems likely that the oblique

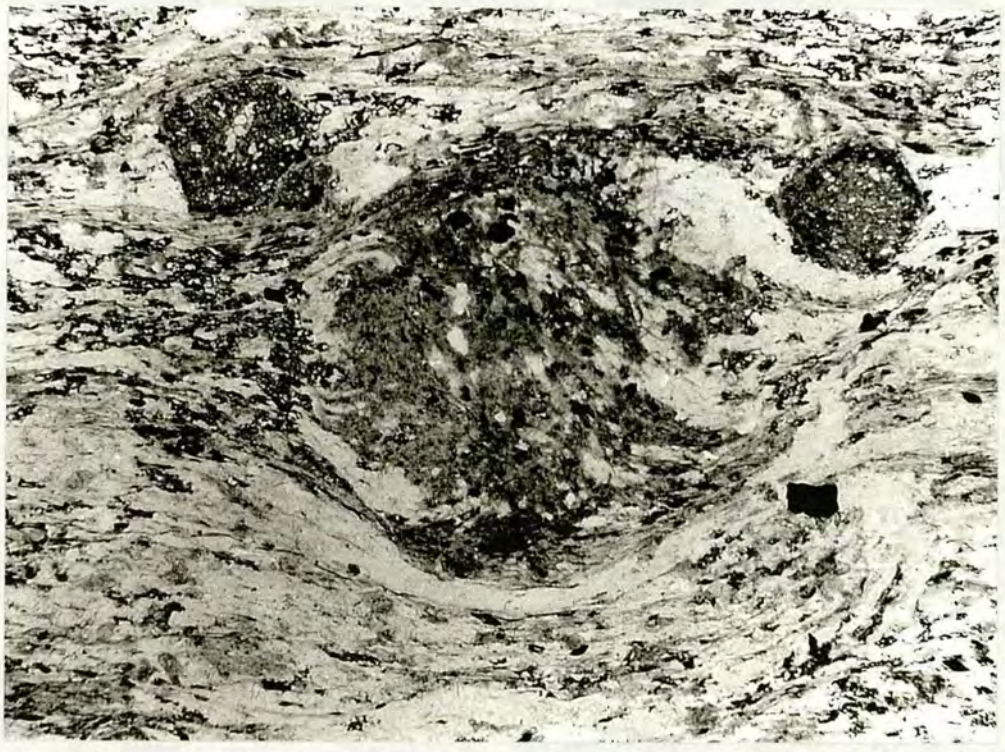

Figure 4.11 Lawsonite pseudomorph with sigmoidal fabric strongly oblique in core but continuous with S1 in rim. S1 wraps around porphyroblast with no sign of crenulation in the central fabric. (Sample 92/59A, x7).

Figure 4.12 Margin of a lawsonite porphyroblast from the U.G.S.U. with a well developed internal fabric oblique to the strongly developed S2 in the matrix. Includes preserved pre-S2 microfolds intrafolial to the included fabric. (Sample 93/34, x6).

inclusion fabrics evident in the U.G.S.U formed by the same processes as those in the L.G.S.U.

Those internal fabrics visible are identical in appearance to those in the L.G.S.U. Lawsonites overgrow a well developed foliation identical in appearance to the S1 fabric (Figures 4.12 and 4.13). However, internal fabrics invariably discordant to the external foliation. In general the angle between Si and Se is larger than that in the L.G.S.U., approaching 90° in many samples. This might be due either to the differing orientation of the S2 or a higher degree of porphyroblast rotation depending on the model applied to account for the formation of the fabrics. As in the L.G.S.U., all internal fabrics in a single section are sub-parallel. This strong preferred orientation is also visible on larger, outcrop scale (Figure 4.14). However, in some sections where Si is approximately perpendicular to Se internal fabrics may dip in opposite directions relative to the external fabric.

In many ways the micro-fabrics relationships visible in the U.G.S.U. are identical to those predicted by the 'Bell' Model for the formation of oblique internal fabrics by the realignment of the external foliation during a crenulation event. The S2 is clearly the result of intense crenulation event earlier stages of which may be preserved in low strain zones adjacent to porphyroblasts. The foliation often anastamoses around these low strain islands apparently recording partitioning of the strain during the its evolution. However, as the two units apparently share the same broad structural history there seem to be no grounds on which to propose that the internal fabrics record the existence of a pre-S1 foliation. Unlike the L.G.S.U. the intense S2 transposition event has largely destroyed the record of the early structural history which effectively rules out the existence of such a fabric in the L.G.S.U. However, it seems impossible that it could be present in the U.G.S.U. given the apparent close proximity of the two units throughout the syn-blueschist deformation.

Thus, as in the lower unit the oblique inclusion fabrics may be interpreted as an overgrowth of an early open stage of the S2 transposition event. The generally

Figure 4.13 Second lawsonite porphyroblast for same sample as Fig. 4.31. External S2 foliation clearly wraps around the grain. Internal fabric includes garnet with quartz pressure shadows. (Sample 93/34, x6).

Figure 4.14 Face of an outcrop in UGSU showing striking parallelism in the orientation of internal fabrics of lawsonites over a large area. Outlines and internal fabrics of individual porphyroblasts have been highlighted with black marker pen

steeper dip of Si relative to Se compared to the L.G.S.U. is consistent with the smaller angle between the axial planes of the S2 and the S1/S0 in the U.G.S.U. In all cases, the crenulation in the matrix has developed considerably since after growth of the porphyroblasts.

However, as in the LGSU, while all fabrics in the U.G.S.U. may be accounted for by the overgrowth of a crenulated S1 some could also be the result of over growth of an undeformed S1 followed rotation of porphyroblasts relative to the external fabric. It is possible that porphyroblasts displaying similar relationships between internal and external fabrics as those in Figure 4.11 existed before the folding event and the S2 fabric has merely reformed around them.

4.6 Implications of Internal Fabrics for the timing of lawsonite growth.

Many of the lawsonites in the LGSU clearly overgrow an early stage in the development of the S2 crenulation. It is clear that in these rocks the lawsonite growth is synchronous with an early stage of the folding event. Other lawsonite internal fabrics from the LGSU are more ambiguous. While they may result from the over growth of the S2 crenulation the relationships between the internal and external fabrics are just as consistent with formation by over growth of an undeformed S1 followed by rotation of the porphyroblast. If these fabrics are the result of porphyroblast rotation then the extent to which they constrain the timing of lawsonite growth is dependent on the strain regime in the greyschists during the formation of the S1.

As noted in the previous chapter (section 3.7), the syn S1 structures are consistent with formation during either pure shear flattening or simple shear. If the strain is pure shear then by definition it will be coaxial and there will be no rotational component to cause the rotation of the porphyroblasts. Thus, any porphyroblasts with sigmoidal fabrics formed by rotation must have grown after the onset of non coaxial deformation responsible for the folding and therefore be synchronous with this event. However, if the syn-S1 strain is simple shear then a component of rotational strain

will be present throughout the deformation and rotational porphyroblasts with sigmoidal internal fabrics may in principle have grown any stage during the development of the S1 and before the onset of folding. However, if this model is correct for some porphyroblasts the timing of their growth is at least partially constrained by the nature of the included fabric. As noted previously, it is well developed S1 identical to that in the matrix. Thus, the earliest that such porphyroblasts could have formed is during the final stages of the first phase of the deformation.

Overall, the porphyroblast internal fabrics suggest that the earliest that the lawsonite in the greyschists might have grown is during the latest stages of the first phase of the deformation during which the S1 forms. All porphyroblasts whose internal fabrics allow timing of growth to be established unequivocally grew during an early stage of the folding event. The more ambiguous lawsonite internal fabrics are consistent with growth at this time as well. No fabrics were found which indicate lawsonite growth during the later stages of the development of the S2. Thus, the interpretation of lawsonite internal fabrics suggests that the growth of lawsonite in the greyschists occurred over a period including the early stages of the folding event and possibly the final stage in the development of the S1.

It is important to note that this does not imply that the growth of lawsonite is exactly contemporaneous in all parts of the greyschists. It shows that lawsonite grew in different rocks at a similar point in their strain history. Given the heterogeneous nature of the folding event it seems highly unlikely that all the rocks of the greyschists reached a point in their strain history at the same time. So while the timing of lawsonite growth in each rock appears to occur at a similar stage in their deformation there may be some temporal variation the timing of its growth in different parts of the greyschists.

CHAPTER 5

DISTRIBUTION OF CA-AL SILICATES

5.1 Introduction

Previous studies on the Syros blueschists noted the uneven distribution of lawsonite and suggested that it is the result of some form of external control on lawsonite growth (Ridley 1982, Barr 1989). However, no specific controlling mechanism was identified.

In order to investigate this possibility and identify the nature of any controlling mechanism a detailed study of the distribution of lawsonite was undertaken. As noted previously, the two units of metapelites, the Upper and Lower Greyschist Units, were chosen as a study area largely due to their relatively uniform composition, lack of alteration and relatively simple structural history.

Field relations reveal that a significant proportion of the lawsonite, as well as epidote/clino-zoisite within the area is spatially related to syndeformational quartz veins. This chapter describes in detail a number of critical outcrops which illustrate the nature of the vein related Ca-Al silicate growth and relation to the syn-blueschist deformation.

5.2 Ca-Al Silicate Distribution in the L.G.S.U.

5.2.1 Cedar Tree Outcrop

The Cedar Tree Outcrop (C.T.O.) is actually a group of outcrops producing a 12 metre long semi-continuous exposure of grey schist approximately parallel to the strike of layering (Figure 5.1). They are composed of typical dark grey, graphitic schist with occasional calc-silicate interlayers. Bedding is well preserved on a 1 cm

to 5 cm scale and individual horizons can be traced for several metres across the outcrop. Composition of individual beds varies between strongly schistose, mica-rich layers , and more massive quartz and glaucophane -rich layers.

The schists contain a strongly developed, penetrative S1 foliation sub parallel to the compositional layering. No folding of the combined S0/S1 is visible in the field. However, thin sections reveal an irregularly developed S2 crenulation. This usually takes the form of asymmetric microfolds of the S1 with a Z to NW sense of asymmetry typically confined to mica-rich welts and interlayers. In quartz and mica - rich layers it is typically accompanied by the development of a lineation parallel to the fold hinges and defined by quartz pressure shadows on garnets. However, in some of the least deformed samples the S2 appears to be completely absent. In general, the crenulation event seems weaker in the C.T.O. than elsewhere in the L.G.S.U.

The schists are cut by two steeply dipping quartz veins which are at a high angle to both bedding and schistosity. The first of these is exposed along the entire front face of the outcrop as a quartz-coated face dipping approximately 40° to 140° (Figures 5.1 and 5.2). It is essentially planar with only small variations of dip along its length. The second vein is less extensive and runs sub-parallel to the first, for 3 m, 15 to 20 cm away from it, before thinning and eventually dying out (Figure 5.3). Where it is exposed at the southern end of the outcrop in a face perpendicular to both bedding and the plane of the vein it also thins out and disappears down section within 30 cm of the top of the exposure. The smaller vein pinches and swells along its length varying in thickness from 1 to 3 cm while the quartz coating the front face is up to 2 cm thick. At first sight both veins appear to be unaffected by the syn-blueschist deformation.

The schists contain numerous quartz bodies approximately perpendicular to the upright veins and sub-parallel to the layering and S1. In most cases these are

Figure 5.1 Long range photograph of the exposure which makes up the C.T.O. The remnants of the planar quartz vein are clearly visible.

Figure 5.2 Close up of the larger of the planar quartz veins. This clearly shows the high concentration of pale pink lawsonite present with the schists and intruding into the vein.

Figure 5.3 Top surface of the outcrop showing the two sub-parallel veins and associated lawsonite growth.

present as thin, discontinuous, en-echelon lenses or veinlets a few mm thick parallel to, and contained within, the foliation. Some of the more continuous veinlets clearly cross-cut the layering and foliation at a low angle. Occasionally, isolated fold hinges are preserved with the foliation in an axial planar orientation. The majority of these bodies appear to represent deformed pre- or syn-deformational quartz veins predating the formation of the upright veins. In one case a folded quartz vein is continuous across and clearly cross-cut by the smaller of the two upright veins. However, it is possible that some of the quartz bodies parallel to the S1 are off shoots of the later veins. In particular, where a transverse section of the smaller vein is visible at the S end of the C.T.O. the adjacent schists contain a high concentration of smaller quartz veinlets parallel to the S1 which may have grow from its margins. It is possible that this apparent dispersion of the fluid into the surrounding schists is related to the down section termination of the smaller vein.

Lawsonite Distribution

The most striking feature of the outcrop is the high concentration of lawsonite pseudomorphs next to the upright vein that forms the front face of the outcrop. The pseudomorphs are clearly visible as white, euhedral, rhombic prisms up to 3 cm in length and 3 cm across contrasting strongly with the dark grey matrix (Figure 5.4). Where a significant thickness of vein quartz is still present on the face the lawsonite pseudomorphs clearly extend into the vein itself. In the upper surface of the outcrop this high concentration of lawsonite next to the vein is visible in the schists for several cm away from the vein margin (Figure 5.3). The relationship between lawsonite growth and veining is also obvious next to the smaller vein where lawsonite pseudomorphs are concentrated in clumps along the vein margins (Figure 5.5). Measurement of the linear percentage of lawsonite along successive transects parallel to the two upright veins at increasing distances from them, show that the modal proportion of lawsonite decreases markedly away from the larger vein before increasing again in the schists adjacent to the smaller vein (Figure 5.6). This observation is also supported by point counting of thin sections taken from individual

Figure 5.4 High concentration of lawsonite in the schists immediately adjacent to the vein face revealed by the removal of the quartz vein itself.

Figure 5.5 Close up of the smaller of the two veins showing vein related lawsonite growth in the adjacent schists.

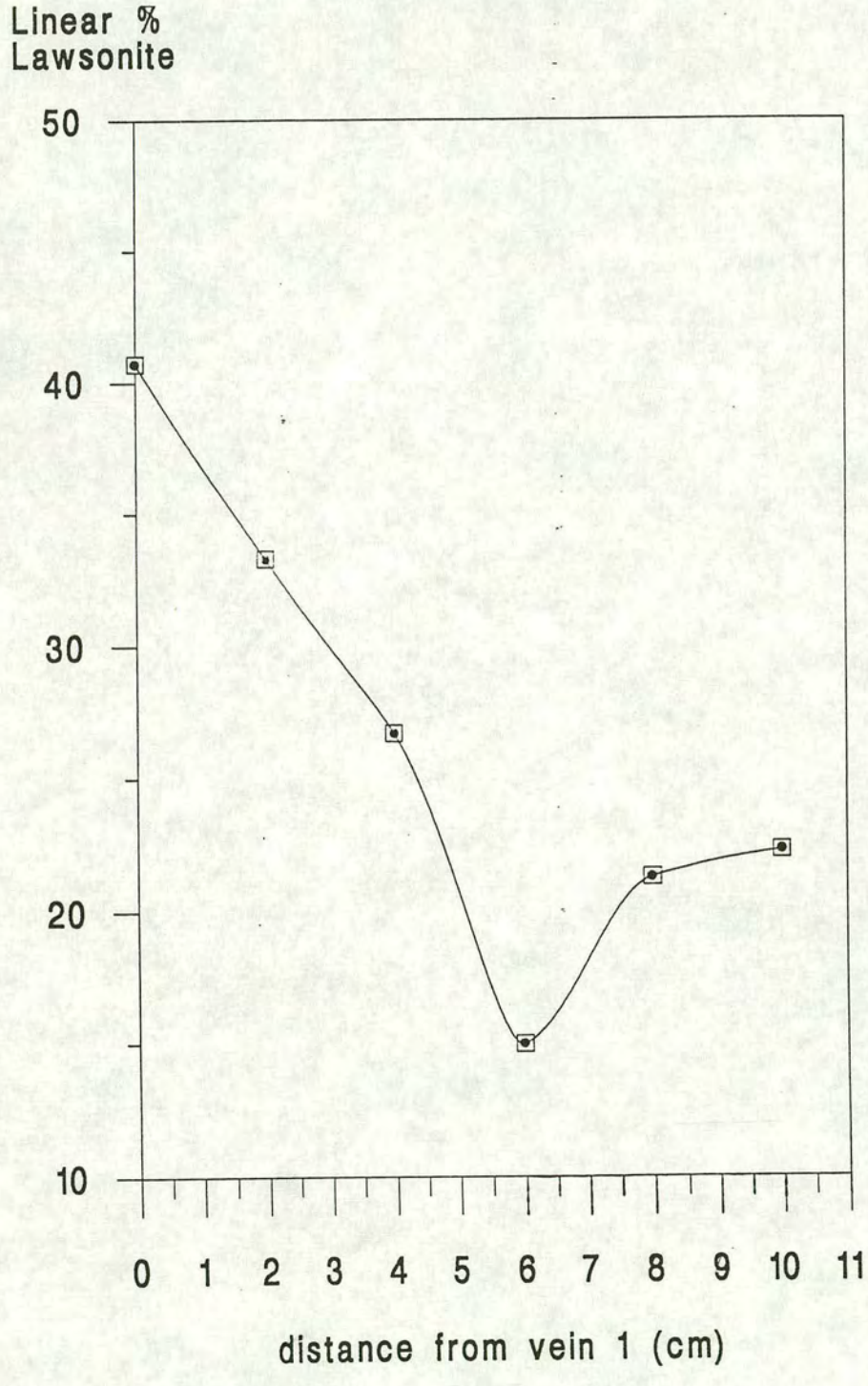

Figure 5.6 Graph showing the variation of lawsonite concentration along transects parallel to the two upright veins in the region between them shown in figure 5.3.

compositional layers and examination of polished sections cut parallel and perpendicular to the veins.

In sections perpendicular to both the upright veins and bedding the concentration and distribution of lawsonite varies considerably from layer to layer. Many layers have uniformly high concentrations of lawsonite with no apparent decrease in modal proportion within the cross-section exposed in the outcrop. In others the schists appear to be almost lawsonite free with only a few growing in the schist immediately adjacent to the veins. However, in many of the layers lawsonite concentration can be seen to decrease from a maximum in the vein margin to almost zero over a distance of a few tens of cm (Figures 5.7 and 5.8).

Overall it appears that the distance over which the vein affects the schists is highly variable with all lithologies growing lawsonite next to the vein but more susceptible layers growing it over considerably larger distances. The highest concentration of lawsonite appears to be in more micaceous layers with a well formed schistosity while the lawsonite-poor and lawsonite-free schists tend to be the more massive quartz- and glaucophane-rich layers.

These observations strongly suggest that much, if not all the lawsonite growth in the C.T.O. is related to the upright quartz veins. For horizons in which there is a clear decrease in lawsonite away from the veins there seems no other solution to adequately explain the distribution. Where lawsonite concentration in a particular horizon is uniform high over the length of the observed section it offers no positive evidence for the external control of lawsonite. Instead it may simply reflect greater isochemical growth due to primary compositional variation. However, such horizons may be interpreted as more permeable horizons in which a lawsonite generating infiltration front has travelled further than in those adjacent. Similarly, lawsonite-free horizons may represent impermeable lithologies or ones whose composition does not react with the fluid to produce lawsonite.

Figure 5.7 Section through a greyschist horizon at a high angle to the upright vein. Lawsonite concentration clearly decreases from right to left away from the vein.

Figure 5.8 Section through greyschist horizon perpendicular to the large upright vein in the C.T.O, showing a decrease in lawsonite concentration away from the vein. The vein is approximately coincident with the left margin of the photograph.

Timing of Veining and Lawsonite Growth

If the veining and lawsonite growth are genetically related as suggested by the spatial distribution of lawsonite in the C.T.O. the two phenomena must be contemporaneous. In the previous chapter it was shown that the lawsonites in the grey schists overgrow a well developed S1 foliation during the early stages of the F2 folding event. Within the C.T.O. all the lawsonite fabrics are consistent with such an interpretation. However, the amount of post-growth strain seems lower than that generally observed in many other areas of the L.G.S.U. Some porphyroblasts contain internal fabrics which are strongly discordant to the external foliation, however most internal fabrics show little or no angular discordance with the external foliation. This lower degree of discordance is probably largely due to the generally lower degree of finite strain in the C.T.O. but may also reflect a later timing of lawsonite growth relative to other parts of the grey schists. The latter conclusion is supported by the presence in some sections of garnets with strongly discordant internal fabrics alongside lawsonites whose fabrics are at a lower angle to the external foliation. Nevertheless, in all cases the external fabrics deflect around lawsonite porphyroblasts to some extent indicating that growth preceded the cessation of the syn-blueschist deformation.

Thus, if the veins and lawsonite growth are synchronous the veins must be syn-deformational despite their planar and apparently undeformed nature. Several lines of independent evidence suggest that this is the case. Most simply, thin-sections of the vein quartz reveal that it has experienced intense crystal plastic deformation. Large, presumably primary grains of quartz have strongly undulose extinction and often exhibit well developed deformation lamellae. They are often surrounded by discontinuous fringes of neoblasts producing an imperfect mortar texture.

In addition, the distribution of lawsonite within the schist immediately adjacent to the larger vein provides clear evidence for a significant component of flattening in the schists after the formation of the vein. The outlines of lawsonites visible on the partially quartz coated face on the front face of the outcrop were traced

onto acetate sheets. The method of Fry (1979) was then applied to examine variation in the distance between the centres of the porphyroblasts. The resulting plots produced markedly elliptical results. There is no apparent reason why the porphyroblasts should nucleate in anything other than a random pattern therefore the results suggest that the schists have experienced considerable component of flattening after lawsonite growth. The long axes of the strain ellipses are sub-parallel to the axial planes of the S2 crenulations and therefore they appear to record flattening during this stage of the deformation. There seems little doubt that the high concentration of lawsonite immediately adjacent to the vein is genetically related to it. Thus, the vein itself must be present for a significant proportion of F2 event.

This interpretation is supported by deformation of the lawsonite porphyroblasts themselves. Many elongate porphyroblasts with their prism axes parallel to the vein face and at a low angle to the long axes of the strain ellipses produced by the Fry plots contain clear evidence of post-growth extension (Figure 5.9). In contrast those with their prism axes parallel to the vein face but at a high angle to the long axis of the strain ellipse show no evidence of extension. This variation of strain controlled by orientation is clearly visible in stereographic projection. This variation in strain is broadly consistent with the extensional and compressional fields of the finite strain ellipse for the S2 event (Figure 5.10).

Thus, structural evidence clearly shows that despite their apparent lack of deformation the formation of the upright veins predated the end of the syn-blueschist deformation. Thus the age of the veins is compatible with that of lawsonite growth in the schists and hence with the suggestion that the two features are genetically related.

Several factors may be responsible for the lack of buckling in the planar veins either alone or in combination. The finite strain in the C.T.O. is relatively low. The veins may grow late in the deformation. The veins are orientated perpendicular to the fold axes of the S2 folds and may thus act as a free slip plane during the folding.

Figure 5.9 Prismatic lawsonites exposed in the plane of the larger of the upright veins, exhibiting well developed extensional fractures perpendicular to their long axes.

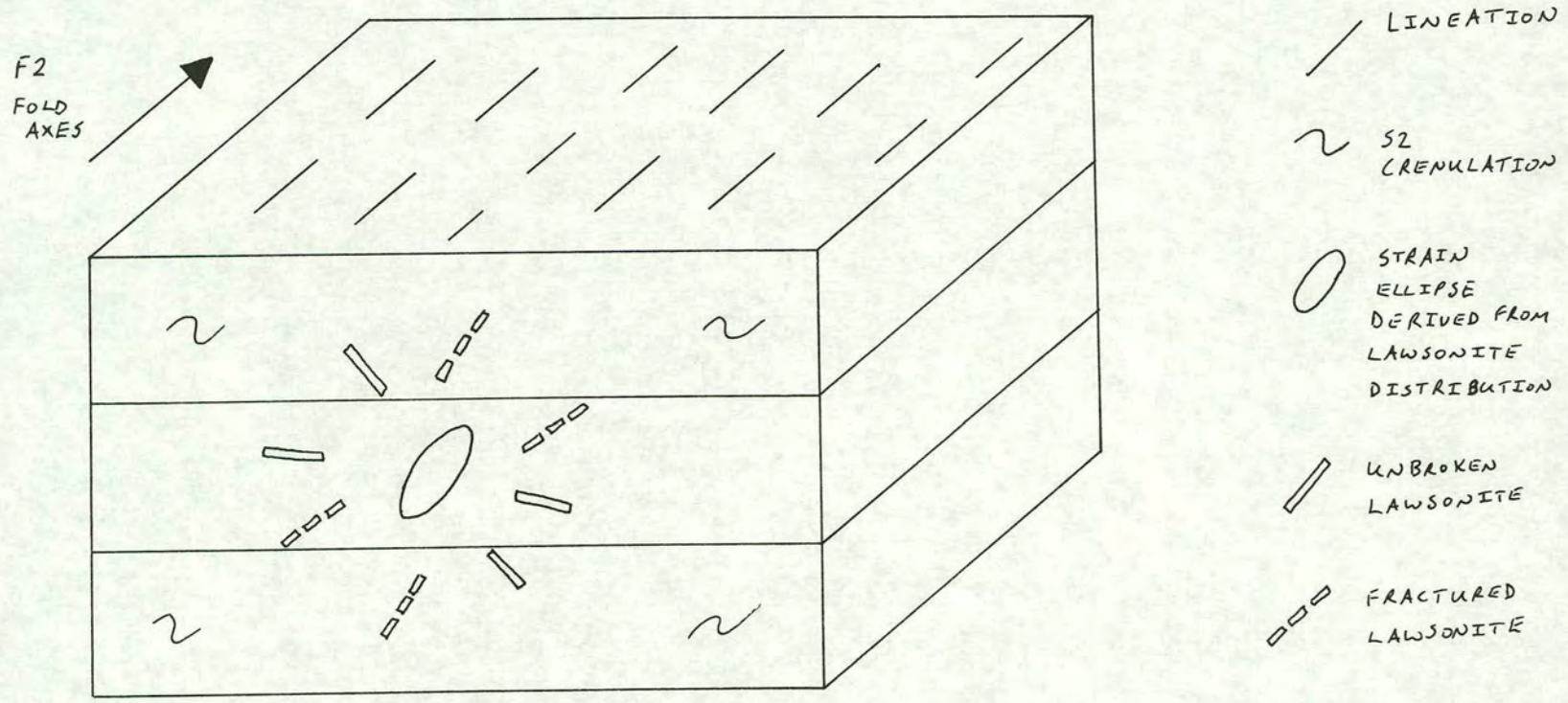

Figure 5.10 Schematic diagram showing the geometric relationships between structural elements and strain indicators in the C.T.O.

5.2.2 Overhanging Outcrop

The Overhanging Outcrop (O.H.O.) is a large outcrop of greyschist exposing a 5m thick section in two mutually perpendicular cliff faces on the north coast of Marmaris Bay (Figure 5.11). Both faces cut the bedding and schistosity at a high angle. As in the C.T.O. one face is clearly coincident with steeply dipping laterally continuous quartz vein (Figure 5.12).

The schists display typical characteristics similar to those noted in the C.T.O. Well preserved primary layering is clearly visible in the face perpendicular to the vein (Figure 5.13) but is difficult to discern in the vein face itself. It is accompanied by a strongly developed S1 foliation sub-parallel to layering. No large scale folding of the S1/S0 is visible in either face of the outcrop. However, a strongly developed asymmetric S2 crenulation is often evident. In general, it seems more strongly developed than in the C.T.O. Nevertheless, its intensity is still highly variable and areas exist in which it is apparently absent.

Remnants of the steeply dipping vein are present on the seaward face of the outcrop as discontinuous patches of quartz up to 5 cm thick. Overall the vein appears identical in character to those identified in the C.T.O. but exposed over a larger area. It is essentially planar with only small variation in dip over the outcrop and cuts bedding, schistosity and at a high angle. The strike of the surface is almost identical to that of the veins in the C.T.O. but its dip is slightly steeper. In the field it seems essentially undeformed. The similarity in features suggest that it is of the same generation if not actually synchronous with the veins in the C.T.O.

The schists contain numerous deformed quartz bodies at a high angle to the upright vein interpreted as the remnants of earlier, pre- or syn-deformational quartz veins. The take the form of discontinuous lenses parallel to the S1 and occasional rootless fold hinges. They range in size from mm thick micro-veins to larger boudins

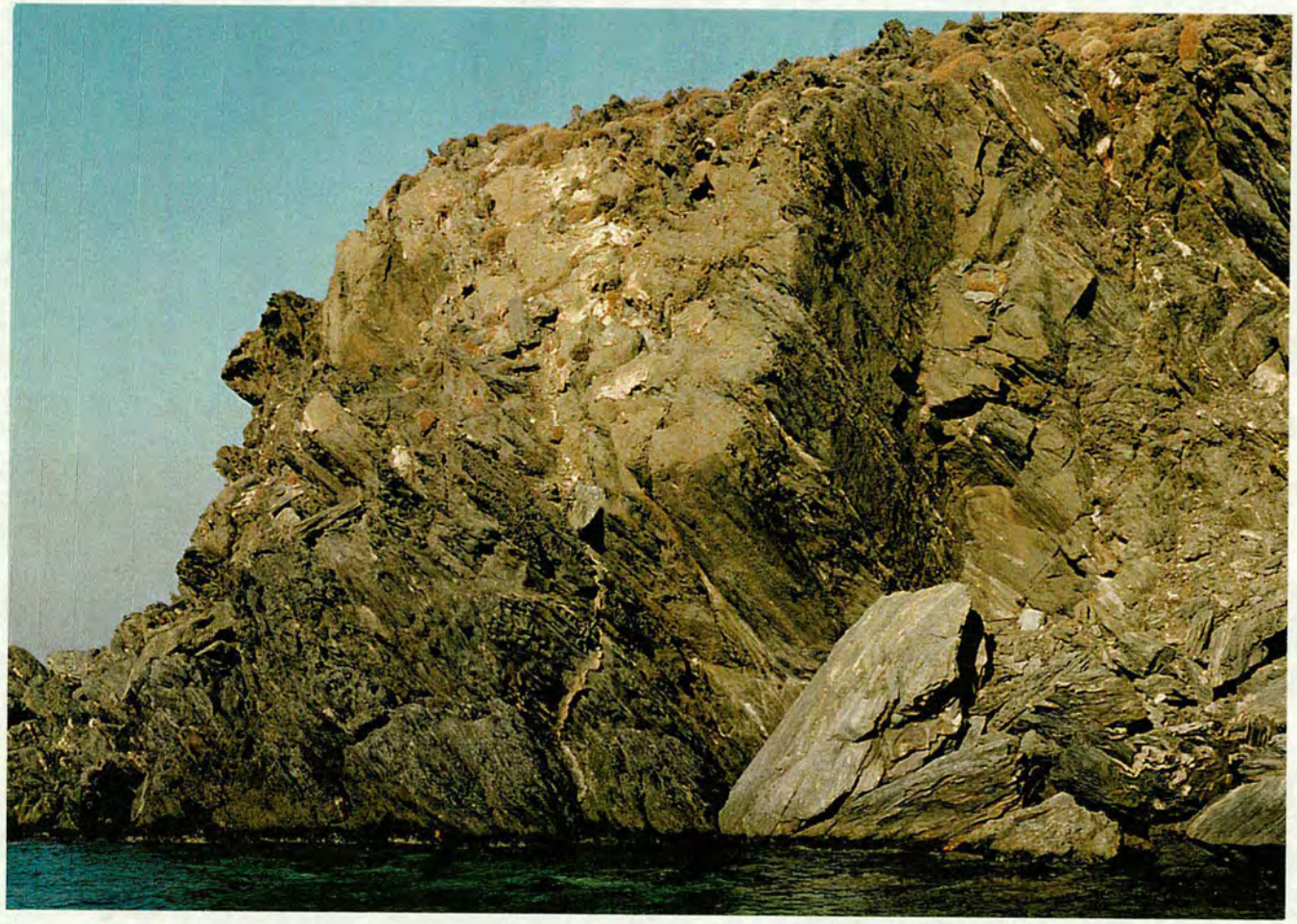

Figure 5.11 Large scale photograph of the O.H.O. showing the two mutually perpendicular faces at a high angle to the compositional layering.

Figure 5.12 Face of the O.H.O. coincident with the planar quartz vein, remnants of which still adhere to the face. The dashed line on the overlay marks the margin of the lawsonite-rich zone associated with the deformed vein at a high angle to the planar vein.

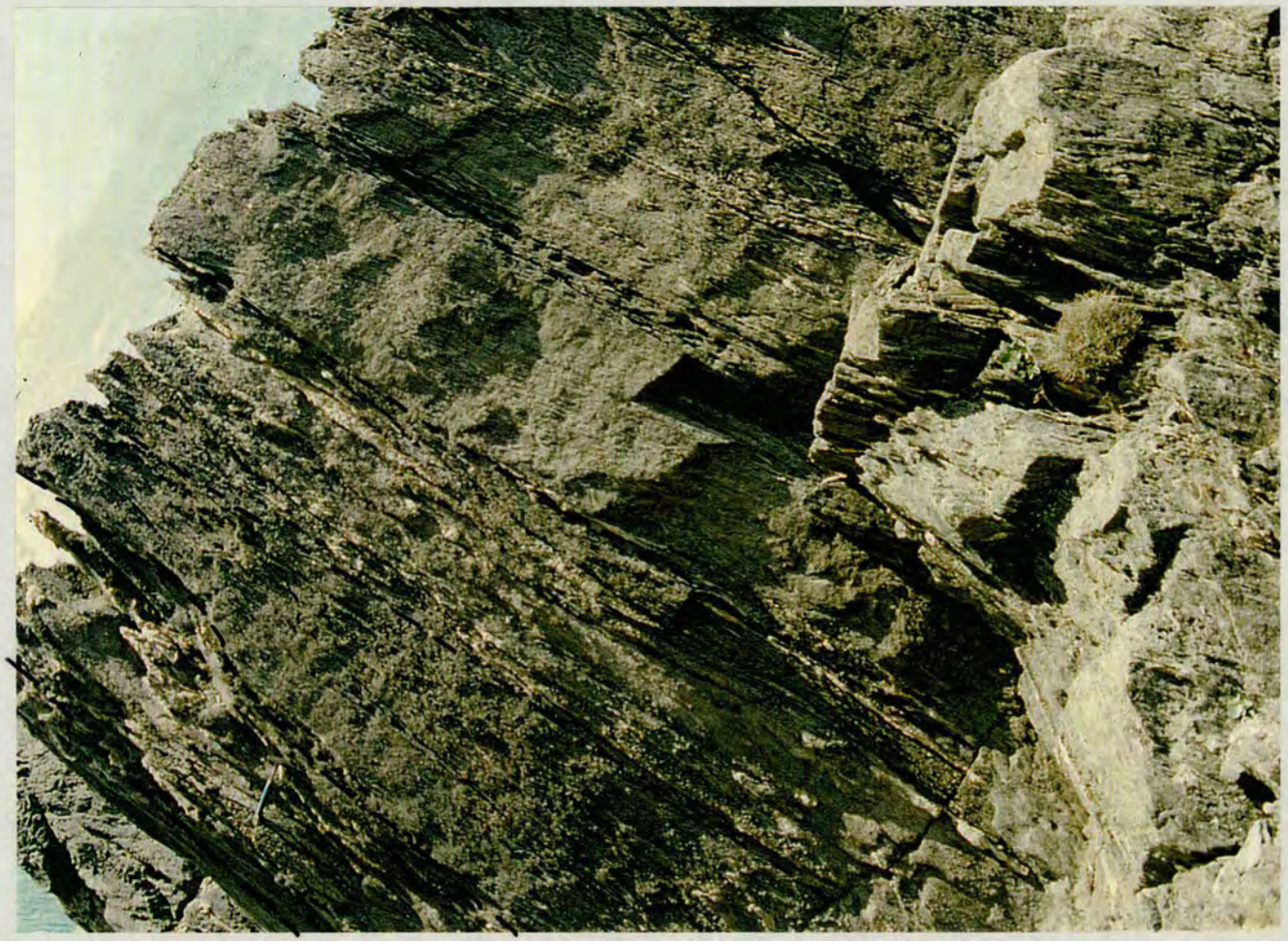

Figure 5.13 Face of the O.H.O. perpendicular to the planar vein. The dashed line on the overlay marks the margin of the lawsonite-rich zone associated with strongly deformed quartz veins.

up to 2 cm thick. In the majority of cases the veins seem limited in extent but in the face perpendicular to the upright vein the remains of two larger quartz veins are visible as horizons containing numerous enechelon quartz lenses running across the width of the face parallel to S1 and layering (Figure 5.13).

Lawsonite distribution

The distribution of lawsonite in the O.H.O. shares many features with that in the C.T.O. As in the latter, there is clearly a spatial relationship between the upright quartz vein and a significant proportion of the lawsonite in the schists which in turn suggests a genetic relationship. Where remnants of the vein adhere to the face a lawsonite-rich zone several cm thick is invariably present in the schists immediately adjacent to its margin (Figure 5.14). Some of the vein quartz patches also appear to preserve traces of an identical lawsonite-rich zone on the opposite side of the vein. These features apparently record the symmetrical growth of vein related lawsonite within the schists on both sides of the upright vein.

The distribution of lawsonite in the schists adjacent to the vein display similar characteristics to that described in the C.T.O. Where the remains of the upright vein are absent varying thickness' of schist have been eroded from the face. This has resulted in the removal of the most lawsonite-rich zone immediately adjacent to the vein over the majority of the face and exposed schists with greatly varying modal proportions of lawsonite. In some horizons the concentration of lawsonite is limited the zone immediately adjacent to the vein while in others it decreases regularly with distance from the vein. In others the concentration of lawsonite remains uniformly high over the length of the observed section. As in the C.T.O. the variation in the modal proportion of lawsonite within and between layers may be explained by infiltration of the schists by a lawsonite generating fluid coupled with variation in permeability to this fluid and susceptibility to lawsonite growth in differing horizons of the greyschists.

Figure 5.14 Lawsonite-rich zone at the contact between the planar quartz vein and the greyschists.

Figure 5.15 Lawsonite-rich margin on a deformed quartz body in the upper of the two lawsonite-rich zones perpendicular to the planar vein.

This relationship between the upright veining and lawsonite growth is supported by the presence of anastomosing micro-cracks within the vein itself oriented sub-parallel to the vein walls and containing fine-grained clino-zoisite and mica. These phases are interpreted as the product of lawsonite breakdown reactions and thus record the precipitation of lawsonite within the vein itself. In one example, a single, subhedral rhomb of fresh lawsonite entirely surrounded by quartz is preserved in the ground mass of the vein.

However, in contrast to the C.T.O. lawsonite growth can also be seen to be spatially related to strongly deformed quartz bodies at a high angle to the upright vein. At the eastern end of the vein face two more deeply eroded areas expose schists with a generally high concentration of lawsonite (Figure 5.12). Closer examination of these areas reveals that the lawsonite is concentrated in narrow horizons sub-parallel to bedding and S1 which form protruding ribs separated by more deeply eroded, more lawsonite poor horizons. In both zones the lawsonite-rich horizons appear coincident with discontinuous deformed quartz bodies sub-parallel to bedding and S1 (Figure 5.15). Both zones are exposed in the vertical face perpendicular to the vein face as laterally continuos zones of discontinuous enechelon quartz boudins sub-parallel to the S1/S0 and each other (Figure 5.13). They exhibit a uniformly high concentration of lawsonite across the entire width of the face. On a small scale this is clearly most highly concentrated in selvages immediately adjacent to individual quartz bodies.

Timing of lawsonite growth.

From the distribution of lawsonite it is clear that lawsonite growth in the O.H.O. is related to both deformed and undeformed quartz veins. It seems most likely that the two vein types represent two discrete episodes of infiltration. The only alternative hypothesis is that they are synchronous but that the planar vein is protected from deformation by virtue of its orientation. Given the intense deformation of the other veins this scenario seems unlikely.

As in the C.T.O. the planar vein seems undeformed on a large scale. Unlike the C.T.O. it is not possible to use the distribution and appearance of the lawsonite in the face to assess the extent of deformation after the formation of the vein. However, the quartz which forms the vein exhibits undulose extinction, deformation lamellae and sub-grain formation indicating that it has experienced intense crystal plastic deformation. The presence of lawsonite within the vein and clear vein related lawsonite growth in the schists show that it formed at the peak of the blueschist metamorphism which is contemporaneous with the peak of the syn-blueschist deformation. These factors combined with the similarities in morphology and orientation suggest that the upright veins in both the C.T.O. and O.H.O. grew synchronously at a late stage in the blueschist event.

The intense deformation of the other veins suggest that they grew significantly earlier in the syn-blueschist deformation although the fact that they too generate lawsonite indicates that they formed under similar P and T conditions to those during the formation of the undeformed veins. However, it is difficult to identify their timing of growth more accurately. as noted earlier (section 3.3.2 *Origin of the foliation*) it is often difficult to determine the timing of deformation of particular bodies due to the essentially continuos nature of the syn-blueschist deformation. The deformation may be ascribed to the syn-S1 flattening or the F2 folding event or a combination of the two. The deformed veins occasionally contain rootless fold hinges with axes sub-parallel to those of S2 folds however this may result from the deformation of quartz bodies already rotated into parallelism with the S1 during and earlier flattening phase of the deformation. Lawsonites associated with the deformed veins typically exhibit well developed internal fabrics with straight cores and curved rims. If such fabrics are the result of porphyroblast rotation as seems most likely then at least the later stages of growth must have occurred during non-coaxial deformation.

5.2.3 Gria Spilia Fold

At the lower boundary of the Gria Spilia Meta-igneous Block the apparently sedimentary boundary with the greyschists is folded into a single fairly tight fold (Figure 3.6). The greyschists exposed in the core of the fold are typically dark grey and graphitic with well developed bimodal quartz and mica layering.

As noted previously, the schist in the lee of the G.S.M.B. appear to be protected from the effects of the early flattening phase of the deformation and thus do not possess the penetrative S1 present in the rest of the greyschists. Instead the greyschist in the core of the fold exhibits a weak foliation parallel to the axial plane of the fold. This is the equivalent of the S2 crenulation cleavage in the rest of the L.G.S.U.

The gneisses in contact with the greyschists are intermediate to basic in composition. A glaucophane -rich layer is intermittently present along the contact between the schists and the gneisses. It is probably a less well developed example of the striking metasomatic rind present along other sections of the boundary between the greyschists and the G.S.M.B. As in the adjacent schist the gneisses at the margin of the block possess a weak S2 cleavage axial planar to the fold.

Lawsonite Distribution

The most striking feature of the outcrop is an clear zone of lawsonite enrichment in the margin of the G.S.M.B. Obvious sub-hedral to euhedral lawsonite pseudomorphs increase in both size and concentration toward the contact with the schist over a distance of 25 to 35 cm (Figure 5.16). Outside this zone the modal proportion of lawsonite in the gneisses appears to be controlled by their bulk composition.

Figure 5.16 Lawsonite-rich zone with the margin of the Gria Spilia Meta-Igneous body at its contact with the greyschists.

The schists within the core of the fold are all lawsonite bearing . However, there is no increase in lawsonite concentration within the schist adjacent to the gniesses relative to those in the fold core.

There is little or no veining in either the schist or the gneisses. Occasional quartz lenses up to 1 cm thick and 20 cm long orientated axial planar to the fold are present in the schist near the boundary with the gneisses. Some cross over the boundary with the gneiss. However, there is no spatial relationship between these veins and the concentration of lawsonite in either the schist or the gneisses.

These observations suggest that the lawsonite growth in the margin of the gniesses is the result of their infiltration by a fluid derived from the schists. The only alternative is the possibility that the lawsonite-rich zone results from the isochemical metamorphism of a chemically altered rind formed on the gneiss olistolith during near surface weathering. However. this second possibility is discounted as it appears incompatible with geochemical analysis of the lawsonite-rich zone.

The uniform and continuous nature of the enriched zone suggests that in this case the fluid infiltration must be pervasive rather than channelized. The presence of the lawsonite enrichment in the schist rather than gniesses also makes it likely that the fluids causing the lawsonite growth are derived from the schist rather than the gniesses. This seems to rule out any possibility that the fluid responsible for lawsonite growth in the rest of the L.G.S.U. is derived from the G.S.M.B.

Timing of lawsonite growth

The lawsonites present in the margin of the G.S.M.B. contain apparently isotropic internal fabrics which indicate that their growth predates the formation of the axial planar fabric present in the matrix. Thus, their growth must either pre-date the folding or occur relatively early in the formation of the fold.

5.2.4 Calc-Silicate Horizon

On the north side of Marmaris bay 20m up section from the O.H.O. a small outcrop exposes a 15 cm thick calc silicate horizon surrounded by typical graphitic grey schists with a strong S1 foliation parallel to bedding and a weakly developed S2 crenulation with axial plane at high angle to layering (Figure 5.17). It seem to have experienced a small amount of boudinage typical of calc-silicate horizons in the greyschists and is now present as a number of slightly rounded sub-rectangular blocks which the schist wrap around.

The exposed faces of the calc silicate blocks are coated with layer of quartz up to 1 cm thick. This quartz veining appears extends a short distance along the joints in the calc-silicate layer produced by the boudinaging. However it does not appear to extend into the schists.

Lawsonite distribution

Large pale coloured sub to euhedral rhombs of lawsonite up to 3 cm in size are present within the vein quartz coating the calc-silicate blocks (Figure 5.18). They appear to be most concentrated at the corner of the blocks where the vein meets the contact between the calc-silicate layer and the schists. Sectioning of one of the blocks reveals that similar lawsonite pseudomorphs are present along the contact between the calc-silicate layer and the schists for 10 to 15 cm from the intersection with the vein. they occur within the margin of the calc-silicate layer and the schists With increasing distance from the vein both the size and concentration of the lawsonite pseudomorphs decrease markedly. Away from the calc-silicate layer the schist appear virtually lawsonite-free.

The boundary between the calc-silicate layer and the schists is also marked by a change in colour of the schists. Approaching the contact they gradually change

Figure 5.17 Quartz coated face of the calc-silicate horizon exposed adjacent to more prominent graphitic schists.

Figure 5.18 Vein generated lawsonite at the contact between the quartz vein and the calc-silicate horizon.

from their typical dark grey colouration to a silvery grey-green colour over a distance of 5 to 10 cm.

The distribution of lawsonite in this outcrop once again suggest that it is related to quartz veining. However, in this example the fluid seems to have taken advantage of a distinct lithological boundary in order to infiltrate the schist from the vein.

Timing of veining and lawsonite growth

Thin sections of the veins reveal strongly undulose extinction, deformation lamellae and sub-grain formation which indicate that it has experienced significant crystal plastic deformation and show that its growth predates the end of the blueschist deformation. On a larger scale it displays no evidence of deformation however this may be due to the relative strength of the calc-silicate layer in which it occurs. It may also be due to growth in a relatively late stage of the deformation in which case it may be of the same generation as the upright veins in the C.T.O. and O.H.O. Such interpretation may be supported by the similarity in the orientation of the vein (30° to 160°) with those in the other outcrops.

5.2.5 Other Outcrops

In addition to the outcrops described above, a number of smaller quartz bodies were noted in the L.G.S.U. which attest to the wide spread nature of the lawsonite infiltration event. These take the form of individual quartz boudins intrafolial to the S1 foliation associated with lawsonite-rich fringes in the surrounding schists (Figure 5.19). As in the larger examples they indicate syn-deformational lawsonite growth related to syn-deformational quartz veins.

Figure 5.19 Small quartz boudin associated with a high concentration of pale pink lawsonite in the adjacent schists.

5.3 Ca-Al Silicate Distribution in the U.G.S.U

5.3.1 Pathside Outcrop

On the eastern side of the path along the Panavlies Ridge by the western wedge of a walled enclosure a large outcrop exposes a 3m thick section of intensely deformed greyschists (Figure 5.20). The only visible trace of the original sedimentary layering are boudinaged and microfolded remains of more quartz-rich interlayers. More micaceous layers exhibit a flat lying penetrative S2 transposition foliation. No larger scale folding of the layering is visible.

The schists contain numerous deformed quartz bodies in the form of lens shaped boudins oriented sub-parallel to the S2 and occasional rootless fold hinges to which the S2 is axial planar. These obviously represent the remains of previously laterally continuous quartz veins extensively disrupted during the transposition event.

Distribution of Ca-Al silicates.

The majority of the schists in the outcrop are lawsonite bearing to some extent. However, the variation in the modal proportion of lawsonite is clearly spatially related to some of the deformed quartz bodies present in the schists. Many of them are associated with dense concentrations of euhedral lawsonite pseudomorphs in the adjacent schists (Figures 5.21 and 5.22). The concentration of lawsonite within the schists decreases markedly with increasing distance from the margin of the bodies.

Those quartz bodies associated with lawsonite growth appear to represent the remains of one or more pre-or syn-deformational quartz veins (Figure 5.20). One set forms a discontinuous horizon running diagonally across the outcrop at an angle to the S2 foliation. All the boudins have well developed lawsonite haloes which often

Figure 5.20 Section of intensely deformed greyschist exposed in the pathside outcrop. The overlay marks the position of the deformed quartz boudin. The dashed line marks the inferred extent of the previously continuous quart vein and associated lawsonite-rich schists.

Figure 5.21 Deformed quartz boudin and associated lawsonite growth in the schists.

Figure 5.22 En echelon quartz lenses and associated lawsonite growth in the adjacent schists.

continue into the schist beyond the end of the quartz boudins, forming tails parallel to the plane of the vein set. Occasionally clots of lawsonite pseudomorphs occur without associated vein quartz within the schists and form discontinuous links between adjacent boudins. These may be related to other quartz bodies below the erosion surface.

A second horizon exhibiting a high concentration of lawsonite is present in a zone running across the lower part of the outcrop approximately parallel to the S2 foliation. It contains three elongate boudins of quartz up to 5 cm thick which are associated with a continuous lawsonite-rich zone up to 10 cm thick in the adjacent schists.

These deformed quartz veins are viewed as roughly analogous to the lawsonite generating quartz veins in the L.G.S.U. However, they have been disrupted by the more intense folding event in the U.G.S.U. The remnants of the quartz veins retain their distinctive lawsonite-rich margins but any finer scale variation in lawsonite concentration in the adjacent schists has been destroyed along with the primary compositional layering. Nevertheless, the schists within the outcrop are generally lawsonite bearing and it is possible that a larger proportion of the lawsonite is related to the veining than is immediately apparent.

Timing of veining and lawsonite growth.

The intense deformation of the veins indicate that they are pre-or syn-deformational relative to the transposition event in the U.G.S.U. However, examination of internal fabrics allows the timing to be more accurately determined. Porphyroblasts contain well developed straight inclusion fabrics discordant with the S2 fabric in the matrix and truncated by it. They are attributed to the overgrowth of the S1 foliation followed by post-growth rotation of the porphyroblasts relative to the external fabric. Thus, the veining and lawsonite growth must predate the transposition event.

5.3.2 Low Strain Zone

A small outcrop exposes an area of schist which has experienced considerably lower strain than the majority of the U.G.S.U. during the S2 transposition event (Figure 5.23). It retains the typical fine scale sedimentary layering and parallel S1 foliation present throughout the L.G.S.U. but largely destroyed in the U.G.S.U. this has been folded into a tight, metre-scale F2 fold. In the hinge regions of the fold the S1 is strongly crenulated but on the limbs the crenulation is relatively weak. In general the state of strain associated with the F2 is comparable with that in the most strongly deformed areas of the L.G.S.U. The outcrop is also cut by a later extensional S3 crenulation which gives it a characteristic blocky appearance.

The schists contain two distinct generations of quartz veins. The earliest veins are parallel to and folded with the primary layering and S1 and are clearly pre-deformational or syn-S1 in age. However, another laterally continuous veins clearly cross-cuts the primary layering and the S1. Nevertheless it has been strongly folded during the F2 folding. This folding is accompanied by attenuation of the fold limbs and thickening of the hinge regions. The angular relations between the limbs of the folded quartz veins and the layering that it crosscuts indicates that the growth of the vein was synchronous with the F2 folding in the schists.

Distribution of Ca-Al silicates.

The majority of the outcrop contains sparsely distributed euhedral porphyroblast with a even distribution. However, there is a clear concentration of lawsonite associated with the syn-S2 vein. Intermittent zones with very high concentrations of lawsonite are found within the schist immediately adjacent to the vein (Figure 5.24). The discontinuous nature of the lawsonite-rich rind appears to due to post growth extension of the vein. While the more ductile quartz vein has extended plastically the lawsonite -rich fringe has been boudinaged.

Figure 5.23 Low strain zone preserving a tight fold of primary layering. It is cut by a deformed quartz vein. The angular relationship between the vein and bedding suggest that it is syn-deformational with the fold.

Figure 5.24 Close-up of section of syn-deformational quartz vein showing associated lawsonite growth in adjacent schist.

Figure 5.25 Boudinaged section of syn-deformational quartz vein containing some epidote.

Further along the vein a larger boudin of quartz contains green prismatic crystals of epidote (Figure 5.25). The presence of the epidote may be responsible for the presence of the boudin itself as it will stop this portion of the vein deforming plastically as readily as pure quartz.

Timing of the veining

As noted above the angular relationship between the lawsonite generating vein indicates the it is synchronous with the formation of the F2 fold in the schists.

5.3.3 Mega Boudin 1

To the east of the path from Kambos along the Panavlies Ridge approximately 100m after the last wall a large outcrop of greyschist contains an obvious meta-carbonate boudin. A 3m long section of the boudin is exposed (Figure 5.26). At the western end of the outcrop it is truncated by a vertical face, it then narrows considerably before widening then eventually tapering out.

It is surrounded by typical grey schists with a penetrative S2 transposition cleavage which wraps around the margin of the boudin. The boudin itself seems largely unaffected by the F2 folding. Rare, small scale folds are present at the margin with the schists but no larger scale folding is apparent.

Distribution of Ca-Al silicates

The meta-carbonate boudin contains numerous crystalline masses containing high concentrations of epidote and / or more rarely lawsonite in a matrix of quartz. Their modal composition varies considerably. Most commonly they are composed of green prismatic epidote set in a groundmass of quartz. However, some larger quartz

Figure 5.26 Large meta-carbonate boudin surrounded by intensely deformed schist with penetrative S2 cleavage. The overlay marks the boundary of the boudinaged layer (dashed line), and smaller boundins in the schists (stippled areas).

boudins containing euhedral pseudomorphs after lawsonite are present. they may also contain subsidiary amounts of calcite, chlorite and chloritoid.

The morphology of the bodies vary considerably. Some take the form of large quartz-rich boudins containing coarse crystals of epidote and / or lawsonite or more elongate quartz bodies with fringes of epidote along their contact with the host rock (Figures 5.27 and 5.28). Others consist of thin veins composed almost entirely of epidote with only minor amounts of quartz. These smaller veins are often continuous with the larger bodies. there seems little doubt that the more laterally continuous quartz-rich bodies are the remains of deformed and boudinaged veins (Figure 5.29).

However, some bodies are more irregular. In one of the more epidote rich zones they appear to form an approximately radial set of irregular veinlets (Figure 5.30). This arrangement seems difficult to reconcile with a simple model of originally planar quartz veins crosscutting the meta-carbonate body. Instead the veins appear to infill an irregular set of fractures. This fracturing of the body may be related to the extensional strain that causes the boudinage. Such an interpretation is consistent with its location near a constriction in the boudin which would represent a zone of dilatancy during the boudinaging event.

Within the schist immediately below the mega-boudin two smaller boudins are present (Figure 5.26). The lower is a 20 cm long lens of meta-carbonate material identical to that in the larger body (Figure 5.31). In its core it contains a deformed mass of epidote + lawsonite + quartz identical to those in the described above. 30 cm above this is a 15 cm long lens of quartz containing of green prismatic epidote (Figure 5.32). In both cases the S2 foliation within the schist wraps around the bodies. At both ends of the quartz lens folded tails of quartz extend into the schist before tapering out and disappearing. The adjacent schist contain numerous enechelon quartz veinlets and numerous pseudomorphs after lawsonite.

Figure 5.27 Large quartz boudin containing lawsonite and epidote.

Figure 5.28 Close-up of boudin containing prismatic epidote from core of the meta-carbonate boudin.

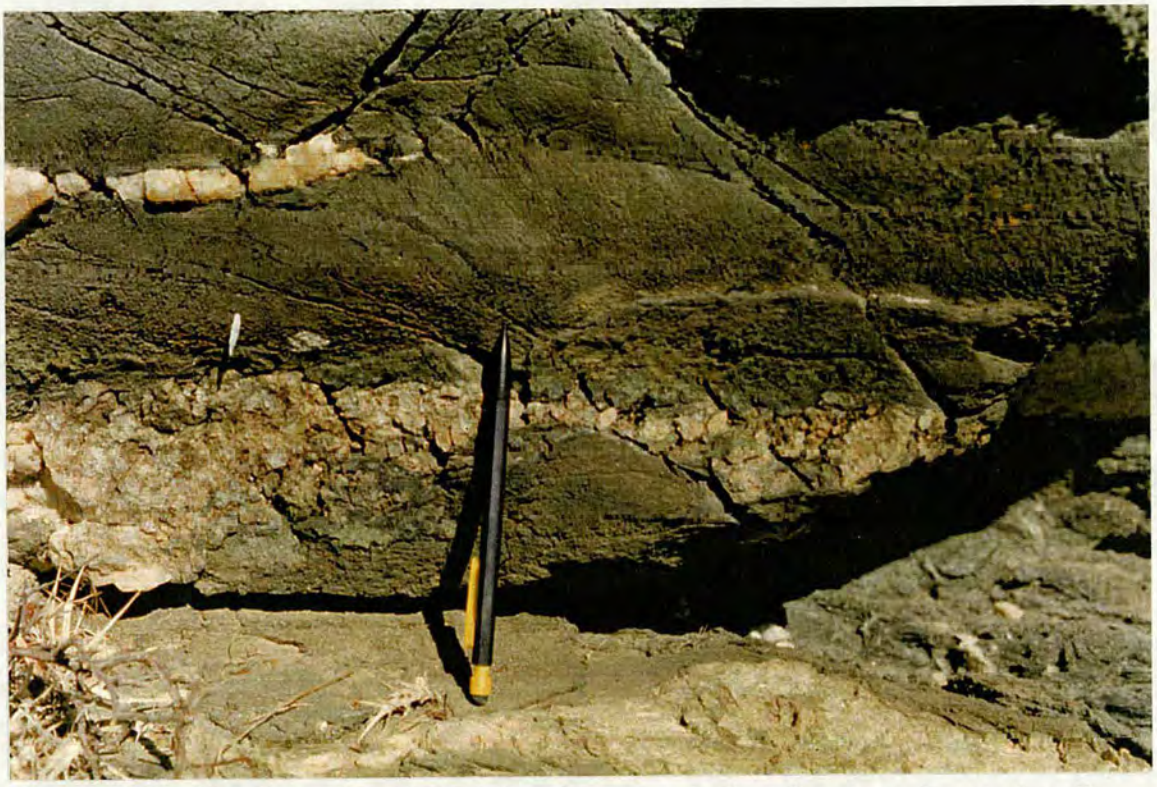

Figure 5.29 Boudinaged epidote-rich vein near margin of meta-carbonate boudin and schists.

Figure 5.30 Irregular radiating epidote veinlets within the meta-carbonate boudin.

Figure 5.31 Small meta-carbonate boudin in schist below larger body, containing deformed epidote and quartz mass.

Figure 5.32 Epidote bearing quartz boudin with schist below meta-carbonate boudin.

The presence of these bodies in the adjacent schists indicate that the Ca Al-rich veining was not limited to the mega boudin. They show that the epidote and lawsonite bearing veins were present in the schist before being largely destroyed by the intense S2 transposition event.

Timing of the veining

The timing of the vein formation is difficult to determine accurately. The deformation of the veins inside and outside the boudin clearly indicate that they predate that F2 folding. However, the intense nature of this event has destroyed relationships which might have allowed a more exact dating and no porphyroblast internal fabrics are present which might be used to estimate timing of growth.

If some of the veining is related to boudinage of the meta-carbonate body as suggested then this might indicate growth during a relatively early stage of the syn-blueschist deformation. Observations in the L.G.S.U. indicate that boudinage of calc-silicate layers there occurs during the formation of the S1.

5.3.4 Mega Boudin 2

At the far end of the Panavlies Ridge an outcrop exposes a strongly boudinaged meta-carbonate layer. It is surrounded by greyschists with a penetrative S2 foliation which wraps around the margin of the boudinaged layer. In low strain patches adjacent to the boudins the S1 foliation is preserved. Away from the boudins the S2 is intermittently folded by open upright folds associated with the Mavro Mitia Monocline.

Distribution of Ca-Al silicates

At one end of a metacarbonate boudin a large calc-silicate-rich mass 2m long and up to 30 cm thick is present at the boundary with the surrounding greyschists. it is largely composed large euhedral lawsonites up to 5 cm long and coarse bundles of

prismatic epidote in a matrix of quartz (Figure 5.33). In addition it contains amorphous masses of dark green soft chlorite intergrown with minor amounts of chloritoid and garnet. Within the boudin itself are smaller elongate boudins / veinlets with an identical mineralogy aligned sub parallel to the larger boudin and the contact with the schists. One boudin cut by a 1.5 cm wide vein composed of prismatic epidote crystals arranged perpendicular to the vein boundary. 3m to the right at the nose of another boudin there is a high concentration of crystalline masses with an identical mineralogy (Figure 5.34).

These veins are similar in appearance, composition and situation to those in the previously described outcrop. In general the boudins, and hence the veins, are more strongly deformed.

Timing of veining

It is difficult to precisely date the timing of the veining .However, their deformation indicates that they pre-date the transposition event in the U.G.S.U. If the veining is associated with the boudinage itself and we assume that the boudinage of more competent horizons is approximately synchronous throughout the greyschist then this would indicate a syn-S1 timing for vein formation.

5.3.5 Other Outcrops

As well as those outcrops noted above, numerous other locations within the U.G.S.U. exhibit significant Ca-Al silicate growth both within deformed quartz veins themselves and within the adjacent schists. They vary from large apparently isolated boudins-rich in lawsonite and/or epidote (Figure 5.35) to areas of en-echelon quartz lenses with lawsonite-rich fringes apparently representing the remains of more laterally continuous quartz vein systems (Figure 5.36). In all cases the quartz bodies

Figure 5.33 Large lawsonite and epidote bearing boudin at boundary between schist and boudinaged calc-silicate layer.

Figure 5.34 Irregular epidote and lawsonite veinlets at nose of boudin in same layer as figure 5.33.

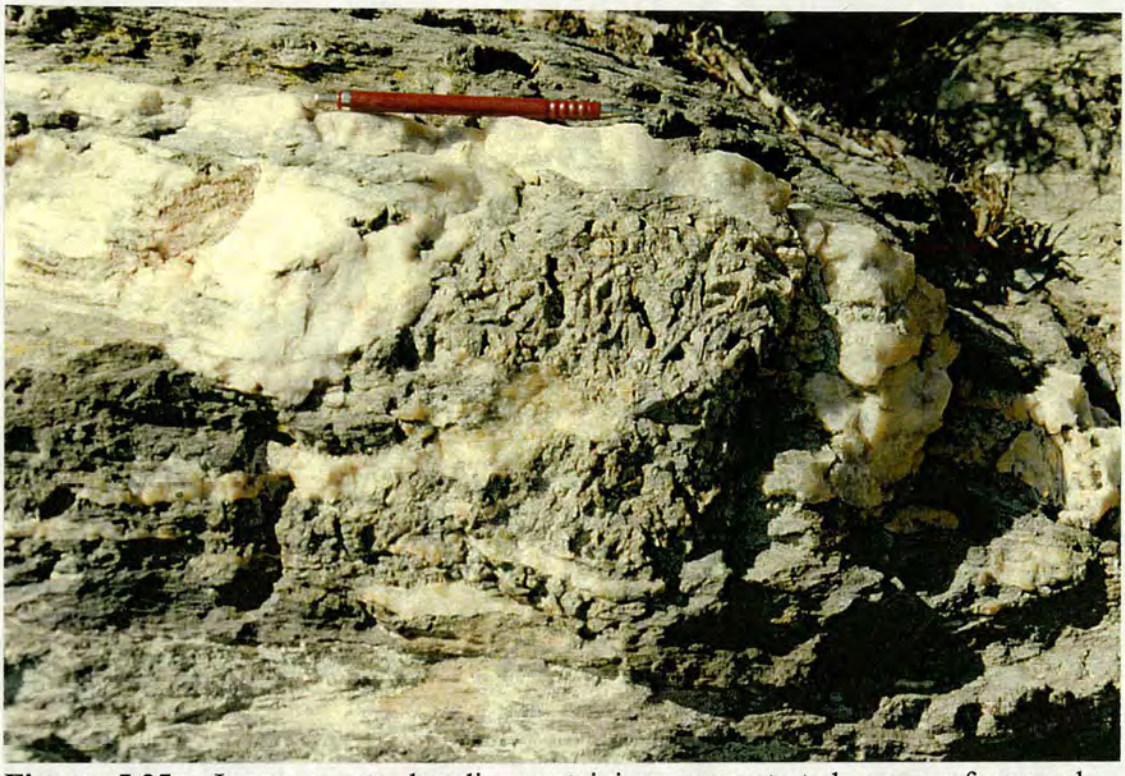

Figure 5.35 Large quartz boudin containing concentrated mass of coarsely crystalline epidote in its core.

Figure 5.36 The remains of an intensely deformed quartz vein with associated lawsonite development in the adjacent schist.

have been intensely deformed and clearly pre-date or are synchronous with the transposition event.

5.4 Summary

The field observations described above clearly indicate that a significant proportion of the lawsonite in both the L.G.S.U. and U.G.S.U. is spatially related to syn-deformational quartz veins. This in turn suggests that the growth of this phase is at least partially externally controlled by an infiltrating fluid.

All veins are syn-deformational relative to the syn-blueschist deformation. However, the degree of strain they display varies considerably. Where veins are intensly deformed it is impossible to establish the exact timing of formation relative to the strain history. However, two largely undeformed planar veins in the LGSU are clearly synchronous with the folding event in that area. This is consistent with the interpretion of the lawsonite internal fabrics (chapter 4) which suggests that the lawsonite growth in different of parts the greyschists is broadly synchronous with the earliest stages of the second phase of the deformation in a particular area.

The presence of the veins indicates that for much of the time this infiltration event is highly channelised. However, the growth of lawsonite in the schists adjacent to many of the veins indicates that the fluid is able to pervasively infiltrate parts of the schists for considerable distances away from the vein margins. The extent to which the fluids infiltrate the schists seems to be at least partially controlled by the composition of individual greyschist horizons.

CHAPTER 6

NATURE OF THE FLUID CONTROL OF LAWSONITE GROWTH

6.1 Introduction

In the previous chapter, field data was presented which shows that a significant proportion of the Ca-Al silicates in the greyschist units are spatially related to deformed quartz veins. The veins themselves may contain epidote and/or lawsonite while the immediately adjacent schists typically contain high concentrations of lawsonite. The increased concentration of lawsonite in the schists adjacent to the veins suggests that its growth is at least locally externally controlled by vein-derived fluids infiltrating the schists. The aim of this chapter is to elucidate as far as possible the nature and properties of the controlling mechanism.

Previous studies on the Syros blueschists (Ridley 1982, Barr 1990) have briefly considered the possibility that lawsonite growth is externally controlled without conclusively identifying the nature of this control. Both authors discuss possible lawsonite generating reactions which are consistent with some form of fluid driven external control and thus might account for the idiosyncratic distribution of lawsonite in the meta-sediments.

Identification of prograde reactions is difficult in the meta-sediments. No reaction textures are visible in thin section. All assemblages are in textural equilibrium at similar P and T and no intermediate steps in their development are preserved. Instead both Ridley and Barr base their analysis on the reasonable assumption that, with the exception of movement of H_2O-CO_2 fluids, the lawsonite generating reactions are isochemical and thus lawsonite must be derived from a pre-existing calcic phase.

Ridley (1982) suggests lawsonite may be generated from calcite by reactions of the form:

calcite + muscovite + H_2O = lawsonite + CO_2

Experimental studies show that lawsonite + quartz is only stable in the presence of extremely water-rich fluids (Nitsch 1972). Thus, under closed system conditions the

production of CO_2 will inhibit reaction progress and limit the quantity of lawsonite that can be generated. However, if the system is open and any CO_2 produced is flushed away by an infiltrating water-rich fluid then the reaction will continue to completion. Hence, significant growth of lawsonite by this reaction is dependent on infiltration by externally derived fluids.

Barr (1990) proposes two alternative lawsonite generating reactions. Within graphite-bearing schists she suggests that its growth may be the result of *in situ* graphite 'burning' coupled with the reduction of Fe^{3+} bearing epidote to Fe^{2+} bearing almandine garnet e.g.

$$24 \text{ epd} + 6 \text{ C} + SiO_2 = 11 \text{ gross} + 9 \text{ law} + 8 \text{ alm} + 3 H_2O + 6 CO_2$$

This reaction is accompanied by a simultaneous reaction in graphite-free schists which utilises the CO_2 generated in the graphite-bearing schists.

$$2 \text{ epd} + 5 H_2O + CO_2 = 3 \text{ lawsonite} + \text{calcite}$$

The dependence of the reaction on infiltration by a CO_2 bearing fluid would explain the element of external control evident in the lawsonite distribution, provided that the CO_2 could be channelled to the graphite-free schists.

However, none of these reactions is applicable in the outcrops considered in this study. All involve calcite as either a reactant or product while, with the exception of occasional meta-carbonate horizons, the greyschist assemblages are carbonate free. In fact it is clear that the vein-related lawsonite does not grow at the expense of a calcium-bearing precursor. Lawsonite is the only dominantly calcic phase present in the schists other than epidote which is almost entirely confined to the vein assemblages. Where lawsonite concentration decreases away from veins there is no reciprocal increase in any other calcium-bearing mineral.

If lawsonite does not grow at the expense of another calcic phase then the calcium it contains must be derived from an alternative source. The only possible solution is that the lawsonite generating process is metasomatic and involves the addition of significant quantities of calcium to the schists from the vein fluids. The

presence of Ca-Al silicates within many of the veins indicates that the fluids are calcium bearing.

In order to confirm the metasomatic nature of the lawsonite generating process a number of sections displaying clear gradients in lawsonite concentration were analysed to assess the gains and losses of both major and minor elements and identify the associated changes in mineralogy. All but one come from the Cedar Tree Outcrop in the L.G.S.U. This outcrop was selected as it displays the least post-veining deformation and thus the least disruption to the metasomatic zones adjacent to the veins. In addition the schists it is composed of exhibit little or no post blueschist alteration except for the pseudomorphing of the majority of lawsonites. All sections are perpendicular to the planar quartz veins and parallel to primary compositional layering. The other analysed section was across the zone of lawsonite enrichment in the margin of the Gria Spilia Igneous body. It is orientated perpendicular to its contact with the surrounding greyschists. Each section was divided into a series of contiguous samples each of which were analysed using X.R.F. for the major elements Si, Al, Fe, Mg, Ca, Na, K, Ti, Mn, P and the trace elements Nb, Zr, Y, Sr, Rb, Th, Pb, Zn, Cu, Ni, Cr, Ce, Nd, La, V, Ba, Sc.

6.2 Quantitative analysis of metasomatism using the Isocon method

The quantitative evaluation of the losses and gains of different elements during a metasomatic event is impossible solely from comparison of chemical analyses of altered and un-altered samples. The data is invariably expressed in the form of concentrations, i.e. wt% for major elements and ppm for trace elements. Therefore, addition or removal of any element will cause reciprocal variation in all other elemental concentrations, generally referred to as the closure problem.

Thus, it is essential to introduce a further independent constraint to calculations. The most widely used method is to assume that one or more elements will remain immobile during the metasomatism. Thus, their concentration will vary

only by dilution or concentration. Having identified such immobile elements it is possible to determine the extent of gains or losses of mobile elements by comparison.

The identification of immobile components is difficult, especially at high temperatures and pressures. The elements most commonly thought to be immobile are Al, and high field strength elements (H.F.S.E.) such as Ti and Zr. However, there is no reason to assume that any of them are immobile during the development of the veins under consideration. Aluminium is clearly transported in the fluid as aluminous minerals are present in the veins. Studies on veins forming under similar PT conditions and with similar fluid compositions show that Ti, Zr and a wide range of other trace elements are mobile (Philippot and Selverstone 1991, Getty and Selverstone 1994).

Instead, mass balance models can be used to elucidate the behaviour of individual components. This study uses the Isocon Method described by Grant (1986) and developed from Gresens (1967) equation for metasomatic alteration. The latter allows the calculation of losses and gains from chemical analyses and specific gravities of altered and unaltered equivalents based on the assumption that some elements are immobile during the metasomatism. Grant (1986) modifies Gresens equation and obtains the simplified solution:

$$C_i^A = \frac{M^o}{M^A}\left(C_i^o + \Delta C_i\right)$$

where C_i^A is the concentration of element i in the altered sample, C_i^O the concentration of element i in the unaltered sample, M^O the mass of the unaltered sample, M^A the mass of the altered sample and ΔC_i the change in concentration of i during the metasomatism. A relationship of this form can be written for each component. For a single metasomatic event $\left(M^O/M^A\right)$ is constant

For immobile elements $\Delta C_i = 0$ and therefore their concentrations in the altered and unaltered samples are related by the expression:

$$C_i^A = \left(\frac{M^O}{M^A}\right) C_i^O$$

Thus, on a plot of C_i^A against C_i^O all immobile elements will plot on a straight line through the origin. (Figure 6.1). Grant (1986) terms this line the 'isocon' for the alteration. The gradient of the isocon is $\left(M^O/M^A\right)$ and indicates whether mass is lost, gained or conserved during the alteration.

Components which have been gained and lost during the metasomatism will plot above and below the isocon line respectively (Figure 6.1). The distance between the point for any mobile component and the isocon is directly proportional to the extent of addition or loss. The percentage change in concentration is easily calculated from the plot.

As it is useful to plot both major and minor components on the same plot the data often covers a large numerical range. However it is possible to scale all the data to produce a more manageable range of values. As long as both the altered and unaltered concentrations of a particular component are multiplied by the same factor it does not affect the interpretation of the isocon plot.

Only two assumptions are inherent in the application of the Isocon method. The two analysed rocks must clearly represent altered and unaltered equivalents and the metasomatic change must be pervasive on the scale of the samples analysed.

6.3 Application of the Isocon Method to the Present Study

An isocon plot was derived from each of the metasomatic sections analysed by plotting the most altered sample against the least altered sample. Using an identical technique to Olsen and Grant 1991, all major elements were scaled to a value of C^O = 30 wt% and all minor elements to a value of C^O = 20 ppm. As well as making the diagrams more concise and aiding interpretation, this corrects, but does

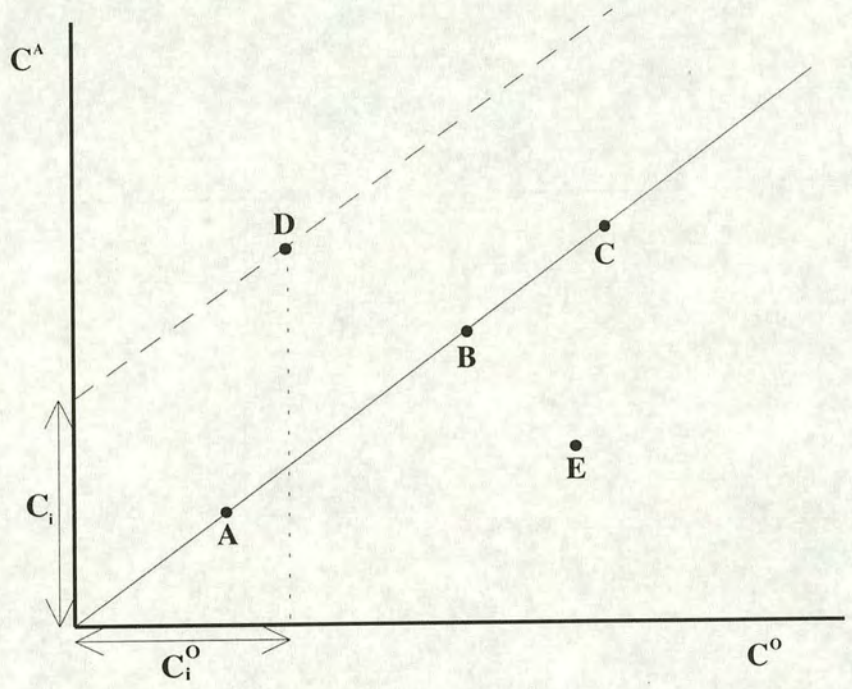

Figure 6.1 Diagram showing an ideal isocon plot. Components A, B and C are immobile during the alteration and thus fall on a straight line passing through the origin, the isocon. The slope of the isocon is M_o / M_a and thus gives the overall change in mass resulting from the alteration. Components D and E have been added and removed respectively during the alteration. The percentage change in concentration of component D is given by C_i / C_o.

not eliminate, the tendency to give greater weighting to variation in components with higher concentrations when choosing isocons.

As noted above, components which were immobile during the metasomatism should fall on a single straight line through the origin, namely the isocon. Given that both the major and minor elements are normalised to single values of C^o then the points for all immobile major elements should plot at the same point and those for all immobile minor elements at another. However, when the method is applied to real data, uncertainties typically cause some scattering of the data points around the true isocon.

Grant and Olsen (1991) suggest four possible sources of uncertainty :-

- the choice of the protolith
- the choice of the altered rock
- the degree to which a component is truly immobile
- analytical errors

Of these potential sources of error they suggest the first two are by far the most serious.

In order to produce meaningful results from the isocon method it is essential that the unaltered sample is as nearly as possible the compositional equivalent of the protolith of the altered sample. When choosing the samples for this study every effort was taken to satisfy this requirement. Samples were taken from the opposite ends of sections showing clear gradients in lawsonite concentration which are orientated parallel to compositional layering. However, the greyschists invariably display primary layering on a scale far smaller than the size of the analysed samples. Given this small scale compositional variation it is unlikely that the sample used as the protolith represents the exact pre-metasomatic equivalent of the altered sample. This factor alone probably accounts for the vast majority if the uncertainty in the plots. Nevertheless as long as the uncertainties are small then the data points for immobile components will still plot over a relatively small area and the isocon for the alteration can be accurately defined. This appears to be true of the examples in this study.

However, the scatter in the data does mean that the identification of immobile components and the exact positioning of the isocon is often open to a degree of interpretation. In general it is relatively easy to identity those elements which have experienced large losses or gains during any alteration. However, it is difficult to distinguish between other elements which may have been immobile or experienced small losses or gains. Grant and Olsen (1991) briefly consider the use of statistical methods in choosing isocons but conclude that most methods are inapplicable and that those that are applicable offer little advantage over visual inspection.

In this study we have the advantage that the samples that are used to derive the plots form the opposite ends of continuous or semi-continuous sections through metasomatic zones. Thus it is possible to examine the incremental variation in concentration of components along the sections. In particular, ratios between immobile elements should experience no systematic variation with increasing alteration, while ratios between mobile and immobile elements will show systematic increases or decreases in magnitude even if the gains or losses of the mobile elements are relatively small. In addition, an understanding of compositional variation in unaltered greyschist samples allows us to, at least partially, assess the extent to which any irregularities in variation along sections can be attributed to pre-alteration compositional variations within the sections.

Thus, for this study immobile components are largely identified by visual inspection with some additional help from other geochemical data where possible. Isocons are then placed through the centre of the group of apparently immobile components. Where there is more than one possible choice of isocon for a particular section the effect of the choice on conclusion is discussed. However, where the placing of the isocon may be based on the distribution of either major or minor elements that for the one for the major elements is generally preferred.

6.4 Results of the Geochemical Analysis of Sections from the Greyschists.

6.4.1 Sections of sample 92/20

Sample 92/20 was taken from the southern end of the C.T.O. and contains a complete section of the schists between the two upright quartz veins. Two large blocks were cut from the sample to provide parallel sections perpendicular to the veins for geochemical analysis 92/20 section 1 and 92/20 section 2. Each was then sub-divided into ~5 mm thick, sub-rectangular slabs with faces parallel to the veins/schist contact (Figure 6.2). Dividing the samples in this fashion allows analysis of the compositional variation on a fine scale parallel to the layering and perpendicular to the vein while minimising the effect of small scale pre-metasomatic compositional variation arising from the layering itself, as many small layers are averaged in each analysis.

Field observations suggest lawsonite concentration in the sample is spatially related to the veins. This is confirmed by measurement of lawsonite concentration in the sections cut for geochemical analysis. The faces of the blocks were polished and the area of lawsonite on each face measured. The resulting value was then divided by the total area of the face and values for the two faces of each individual block averaged. This is then converted to a volume fraction. As the lawsonite porphyroblasts are large, euhedral rhombs which contrast strongly with the schist matrix this provides a simple measurement of the modal proportion of lawsonite in each block. The resulting data shows that in both sections the concentration of lawsonite in the schists decreases markedly away from vein 2 before the rising again toward vein 1 (Figure 6.3). Thus for geochemical analysis each section can be divided into two sub-sections showing an overall decrease in lawsonite concentration with increasing distance from a vein.

Preliminary examination of geochemical data (Tables 6.1 & 6.2) reveals that the variation in lawsonite concentration within the sample is accompanied by

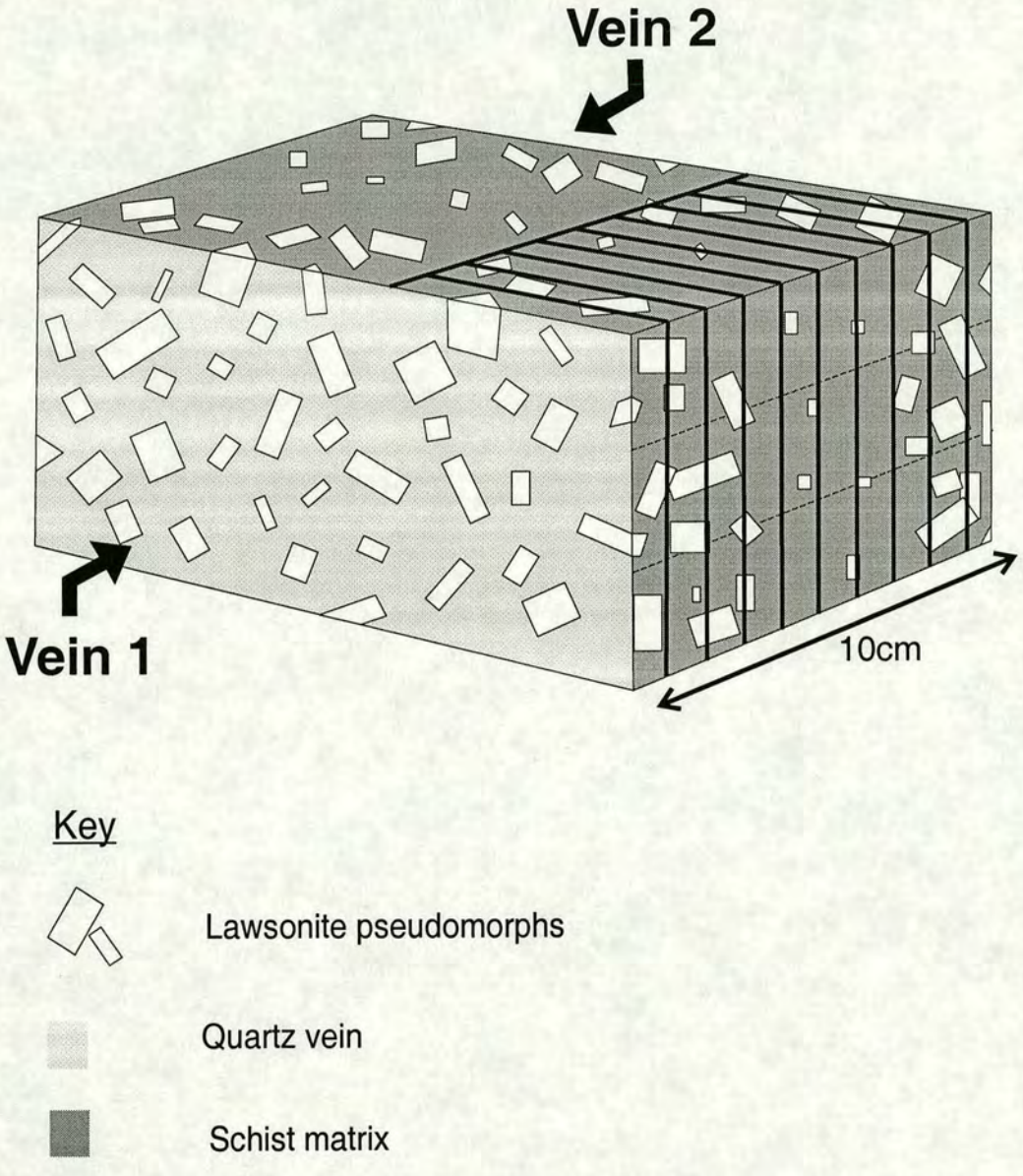

Figure 6.2 Schematic block diagram showing the orientation of the samples within the sections from sample 92-20 relative to the upright quartz veins and the distribution of lawsonite.

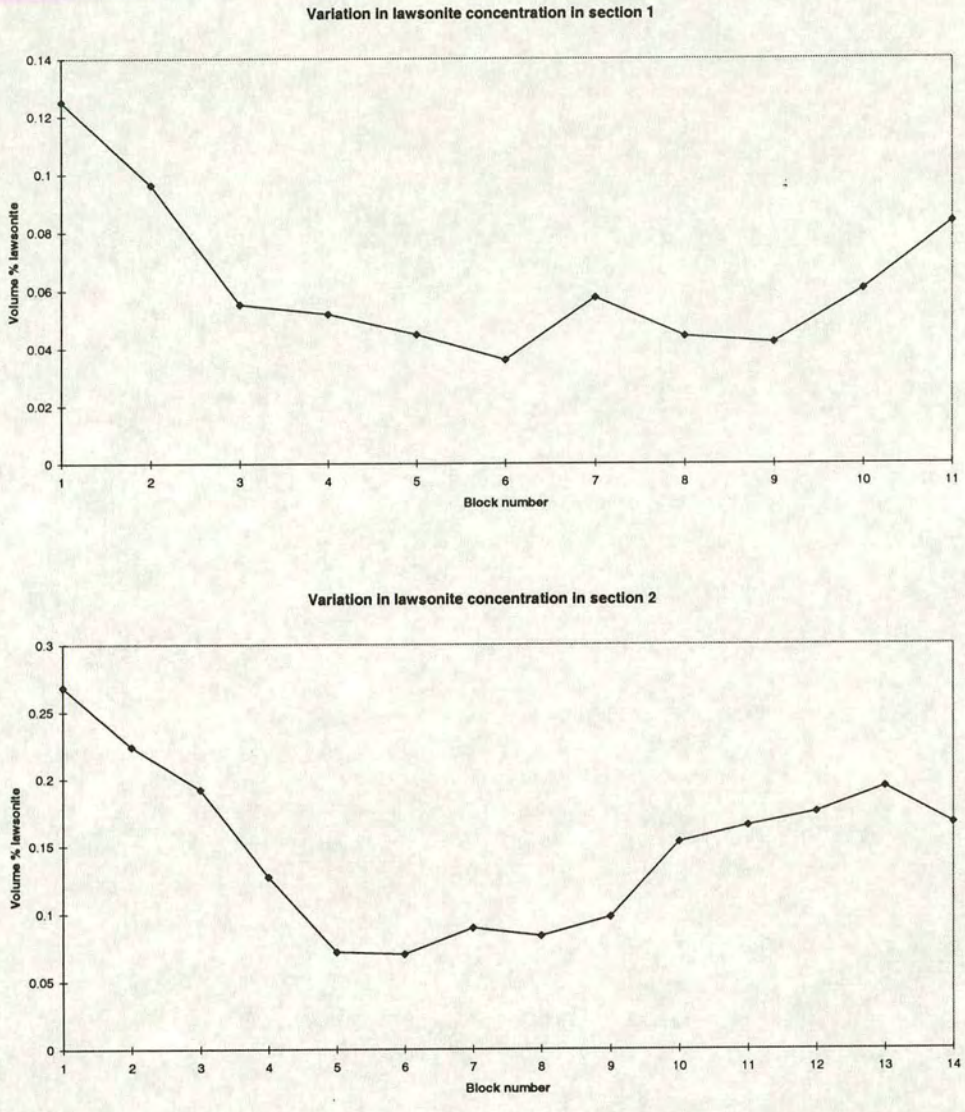

Figure 6.3 Plots showing the variation in the volume % lawsonite along the sections from sample 92-20. Blocks at either end of the plots are those closest to the upright veins.

Sample	SiO2	Al2O3	Fe2O3	MgO	CaO	Na2O	K2O	TiO2	MnO	P2O5	LOI	Total
SI/2	50.31	20.13	8.66	6.06	5.40	1.97	2.544	1.033	0.091	0.051	3.98	100.23
SI/3	50.96	19.47	8.97	6.44	4.67	2.00	2.685	1.027	0.093	0.067	3.71	100.09
SI/4	51.43	19.13	8.74	6.27	4.66	2.20	2.577	0.996	0.087	0.078	3.65	99.82
S1/5	52.20	18.46	8.63	6.26	4.41	2.57	2.503	0.991	0.078	0.101	3.55	99.75
SI/6	52.37	18.25	8.77	6.39	4.16	2.59	2.603	0.993	0.083	0.090	3.41	99.70
SI/7	52.27	18.60	8.46	6.09	5.03	2.24	2.276	0.994	0.080	0.088	3.47	99.60
SI/8	52.65	18.40	8.65	6.35	4.54	2.26	2.348	0.973	0.082	0.079	3.55	99.87
SI/9	52.26	18.88	8.55	6.17	4.97	2.16	2.273	0.986	0.083	0.075	3.64	100.05
SI/10	51.24	19.87	8.15	5.58	6.24	1.92	1.983	0.963	0.089	0.071	3.88	99.99

Sample	Nb	Zr	Y	Sr	Rb	Th	Pb	Zn	Cu	Ni	Cr	Ce	Nd	La	V	Ba	Sc
SI/2	20.0	220.4	33.6	372.7	109.4	13.5	23.6	128.5	46.1	291.3	629.6	80.3	29.3	31.1	213.1	325.2	24.7
SI/3	20.9	220.2	33.6	292.8	115.7	14.1	21.1	135.0	38.7	297.8	625.4	73.0	32.3	33.6	197.1	353.6	27.1
SI/4	20.2	218.0	32.9	284.2	110.8	13.7	18.1	135.2	36.8	291.7	608.4	82.3	31.6	30.3	197.7	330.6	27.5
S1/5	19.3	211.8	32.0	258.0	106.2	13.6	16.5	135.0	35.3	284.9	588.8	71.2	29.9	28.2	193.0	324.3	26.4
SI/6	19.3	213.7	31.7	230.8	111.9	13.2	17.1	137.3	32.0	287.0	612.9	74.4	28.9	31.3	185.5	344.3	24.6
SI/7	18.9	215.3	32.7	316.3	97.0	12.3	20.7	131.7	37.6	273.9	616.5	70.0	28.0	28.7	195.5	291.0	25.8
SI/8	19.7	220.3	33.0	285.4	101.2	12.2	19.5	137.1	40.9	284.5	623.6	79.1	32.8	31.1	188.8	299.3	26.7
SI/9	19.3	225.5	34.0	329.1	97.8	13.5	19.9	131.4	39.6	277.6	669.5	77.4	28.9	32.5	193.3	290.6	27.4
SI/10	18.5	223.6	36.6	465.1	84.8	12.8	26.1	120.8	48.9	268.4	673.2	72.6	33.2	31.0	210.3	262.4	21.4

Table 6.1 XRF data for the samples from 92/20 section 1.

Sample	SiO2	Al2O3	Fe2O3	MgO	CaO	Na2O	K2O	TiO2	MnO	P2O5	LOI	Total
S2-2	49.90	20.51	7.34	4.98	7.20	2.17	1.864	0.998	0.080	0.063	4.43	99.54
S2-3	50.73	19.87	7.81	5.42	6.56	1.95	1.844	0.985	0.086	0.076	4.30	99.62
S2-4	51.42	19.20	8.44	6.02	5.44	1.94	2.112	0.997	0.084	0.088	4.17	99.91
S2-5	51.52	18.89	8.77	6.46	4.93	2.06	2.233	1.013	0.085	0.091	4.18	100.23
S2-6	51.31	18.73	8.85	6.39	4.89	1.98	2.138	0.960	0.093	0.093	4.03	99.48
S2-7	51.74	18.48	8.68	6.27	5.02	2.34	2.062	0.958	0.089	0.112	4.09	99.84
S2-8	52.53	18.15	8.72	6.38	4.71	2.29	2.191	0.959	0.087	0.106	3.73	99.85
S2-9	51.70	18.60	8.57	6.18	5.15	2.19	2.102	0.973	0.093	0.107	4.10	99.76
S2-10	50.40	19.37	8.37	5.93	5.81	2.26	2.092	1.004	0.092	0.119	4.23	99.67
S2-11	49.26	20.01	8.12	5.84	5.96	2.13	2.137	1.009	0.081	0.102	4.31	98.96
S2-12	48.86	21.05	8.14	5.63	6.53	2.29	2.117	1.068	0.090	0.095	4.17	100.04
S2-13	48.44	21.29	7.83	5.49	6.60	2.14	2.172	1.024	0.088	0.091	4.46	99.61

Sample	Nb	Zr	Y	Sr	Rb	Th	Pb	Zn	Cu	Ni	Cr	Ce	Nd	La	V	Ba	Sc
S2-2	18.9	209.1	31.9	586.8	78.5	11.6	53.0	107.5	59.0	259.5	628.4	75.5	32.4	31.5	225.4	235.6	20.5
S2-3	18.2	211.7	32.6	490.7	77.8	11.5	37.0	116.0	48.7	261.8	610.2	78.1	31.7	35.3	219.1	237.3	25.6
S2-4	19.4	213.3	30.8	374.1	90.5	14.7	30.2	131.1	44.5	280.4	636.5	81.1	32.2	33.8	196.6	277.3	23.5
S2-5	19.6	217.7	30.1	318.7	94.6	12.2	25.1	141.7	41.6	293.5	627.8	81.9	32.6	23.9	194.8	284.9	24.6
S2-6	19.1	210.3	30.9	307.9	90.4	12.1	23.2	140.2	40.1	288.9	614.4	78.5	30.3	25.7	192.8	273.1	22.6
S2-7	18.7	209.5	30.3	320.5	88.6	12.1	22.5	138.2	37.5	280.1	607.4	67.0	27.0	26.2	185.1	260.6	23.4
S2-8	19.3	215.5	30.0	283.8	93.7	12.0	19.9	138.3	35.2	274.7	609.3	72.8	29.6	27.0	183.9	272.3	26.7
S2-9	18.7	217.2	30.6	335.0	89.0	11.9	21.7	135.4	37.2	271.4	610.7	74.3	32.4	28.7	190.9	263.7	23.8
S2-10	19.6	229.1	32.5	386.0	88.7	13.7	22.8	129.9	41.4	268.7	616.0	82.3	36.0	32.4	199.5	258.9	26.2
S2-11	19.8	224.7	32.0	459.2	91.8	13.4	24.4	128.3	45.2	273.3	619.2	81.2	33.9	31.9	215.0	282.5	24.7
S2-12	20.3	232.0	34.7	505.8	89.6	14.2	28.8	119.4	49.8	260.5	617.8	91.0	35.1	35.6	227.8	277.4	25.0
S2-13	19.8	228.0	34.3	543.3	91.7	13.5	29.0	116.7	51.7	254.8	612.5	91.0	33.9	38.5	226.3	283.4	24.4

Table 6.2 XRF data for the samples from 92/20 section 2.

systematic variation in bulk rock composition confirming the hypothesis that lawsonite growth is the result of major element metasomatic alteration. By far the most significant change is the increase in wt% CaO with increasing lawsonite concentration. A plot of wt% CaO against lawsonite concentration reveals a strong correlation between the two variables (Figure 6.4) and suggests that the concentration of Ca provides a reliable index of the extent of alteration. Thus, the change in concentration of other elements with increasing alteration can be assessed by plotting their concentration against that of calcium. Such plots show that the growth of lawsonite is accompanied by a increase in wt% Al (Figure 6.5b) but a decrease in the concentration of Si, Fe, Mg, Na, K and P (Figures 6.5a, c, d, e, and f). In contrast, Mn and Ti display no regular variation with concentration of CaO (Figures 6.5g and h). The majority of the trace elements also exhibit no obvious correlation with wt% CaO. However, plots suggest that the alteration is accompanied by increases in concentration of Y, Sr, Rb, Pb, Cu, Cr and V and decreases in the concentration of Zn and Sc.

While these plots clearly show that the growth of vein related lawsonite is the result of metasomatic alteration involving systematic variation in bulk rock composition they do not reveal which components are added or removed nor the magnitude of gains and losses. The closure effect means that variation in the concentration of any single component will cause a change in the concentration of all others. Even those elements which are immobile during the alteration will vary in concentration as long as the net change in mass is not zero. Therefore, in order to assess the behaviour of individual components and to quantify any losses or gains the compositional variation was further analysed using the isocon method. Two isocon plots were derived from each of the sections by plotting the samples adjacent to the veins against the least altered samples in their respective sections, i.e. those with the lowest wt% CaO. The resulting isocon plots are shown in Figures 6.6 to 6.9 and their interpretation described in the following sections. The characteristics of the alteration evident in sample 92-20 are then summarised in a further section.

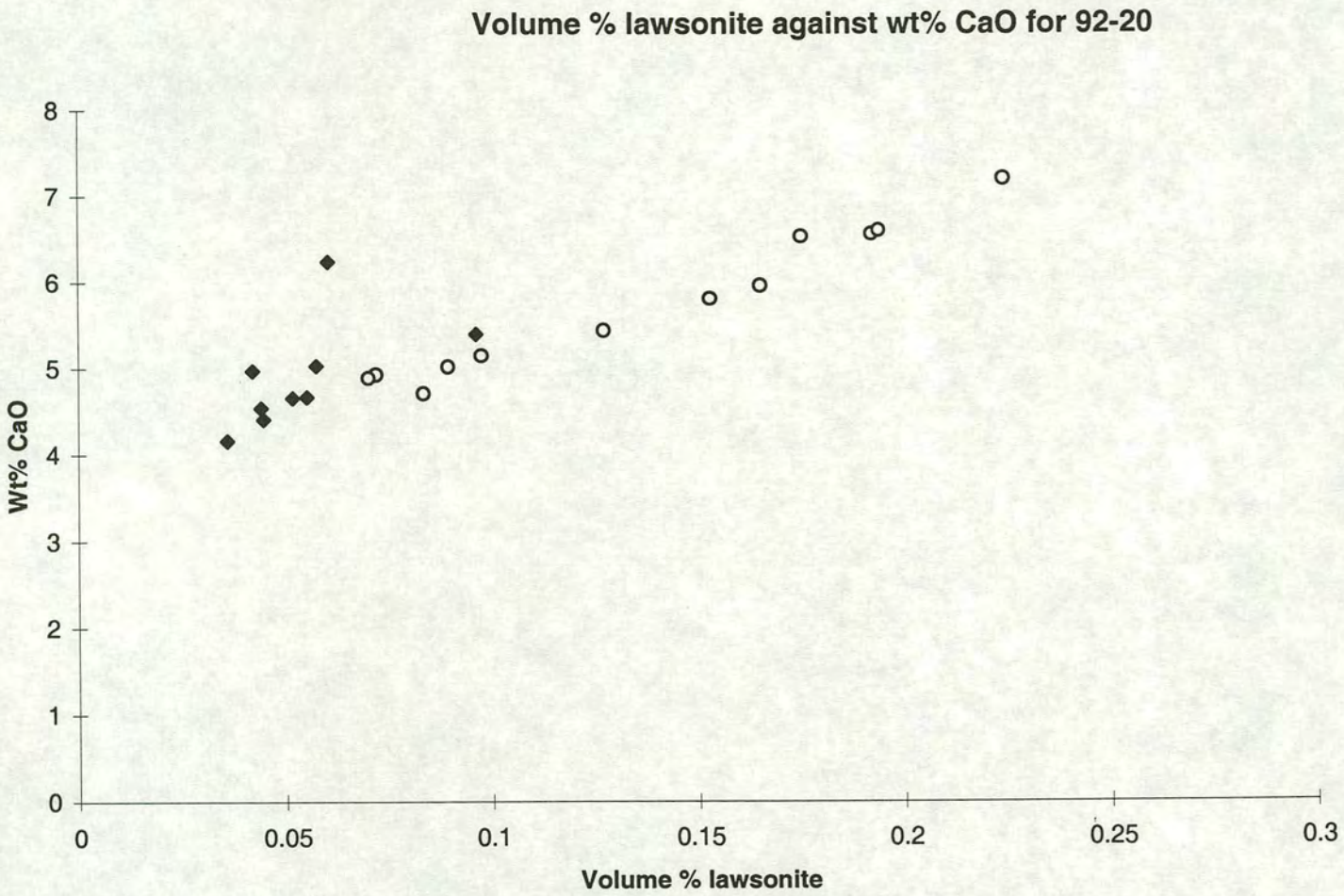

Figure 6.4 Plot showing the close correlation between the concentration of Ca and lawsonite content in the sections from sample 92-20.

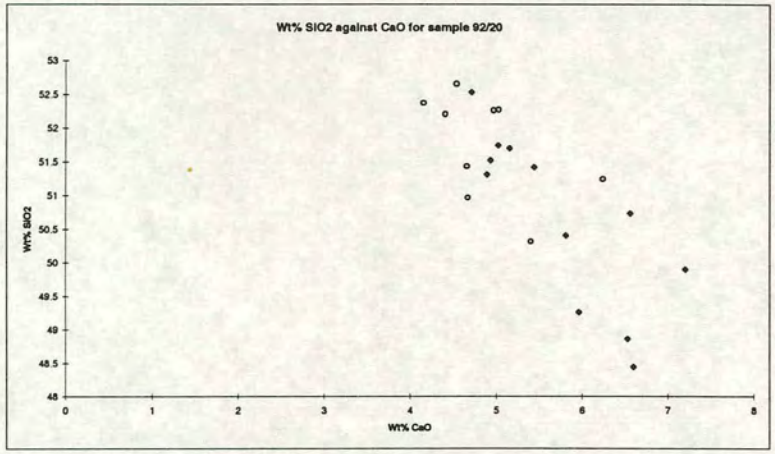

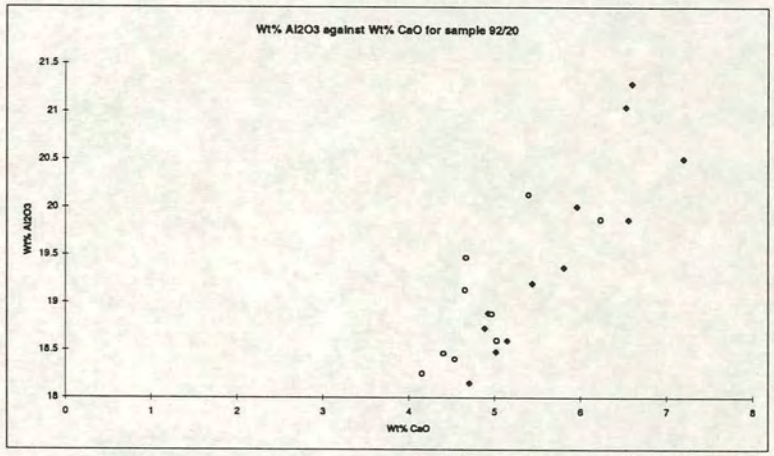

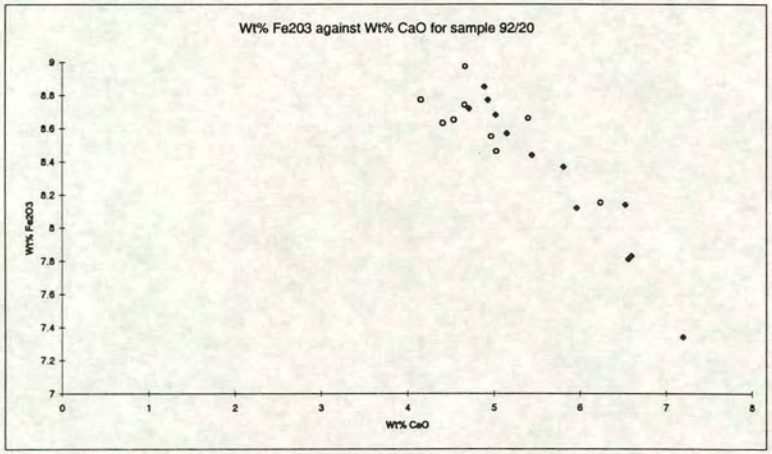

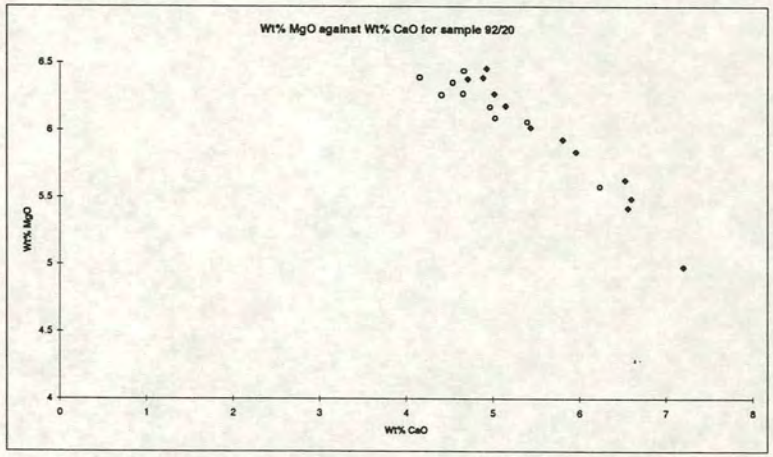

Figure 6.5 (a to d) Series of plots illustrating the variation in concentration of the major elements in sample 92-20 with increasing alteration. This is measured by increasing calcium concentration.

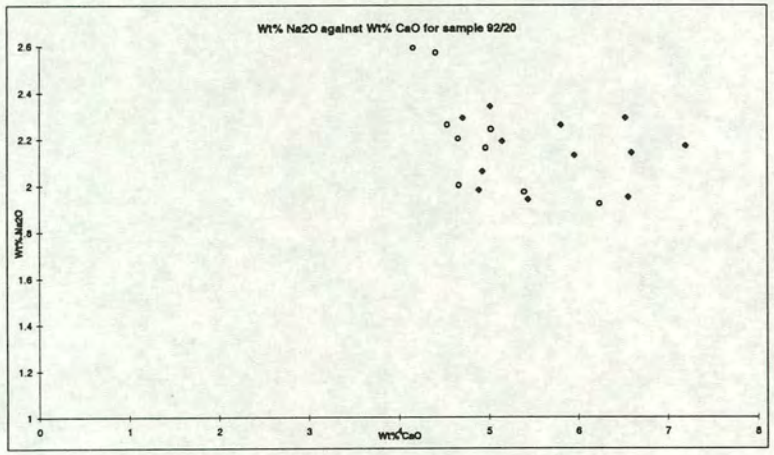

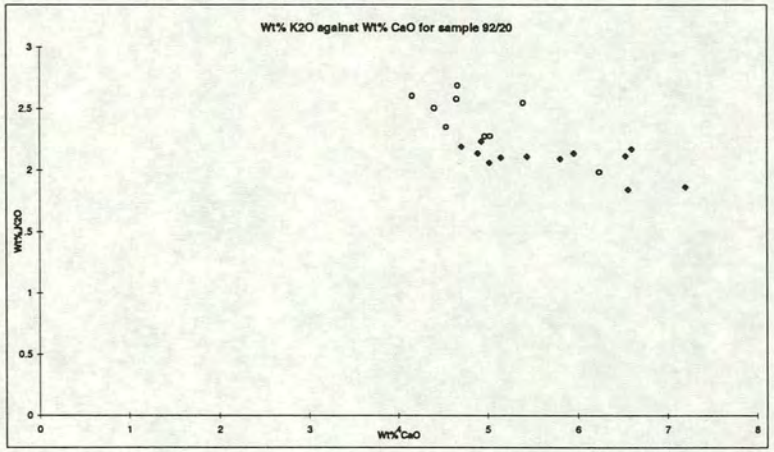

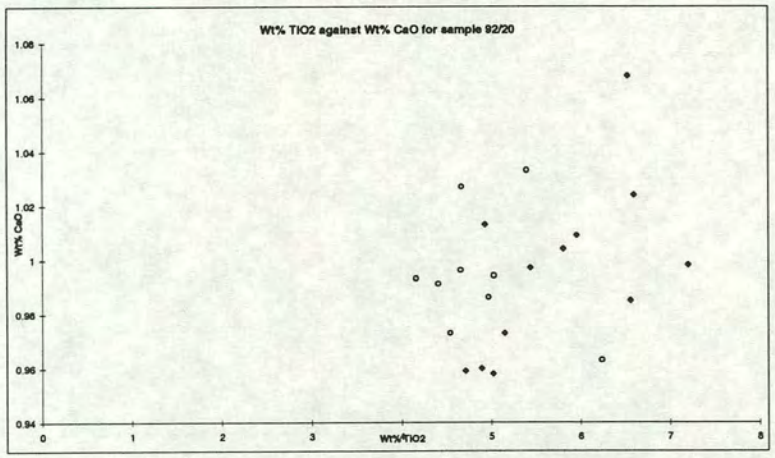

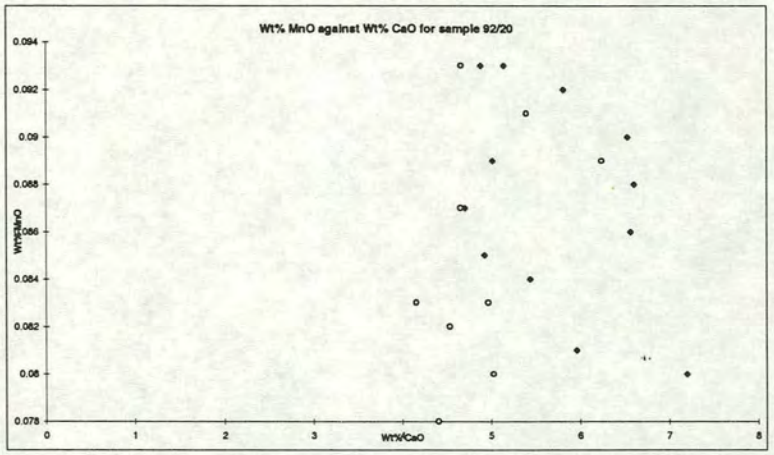

Figure 6.5 (e to h) Series of plots illustrating the variation in concentration of the major elements in sample 92-20 with increasing alteration. This is measured by increasing calcium concentration.

Fig 6.6 : 92/20 S1-6 against 92/20 S1-2

The isocon for the plot 92/20 S1-6 against 92/20 S1-2 can be defined by the distribution of either the major or trace elements (Figure 6.6a).

The behaviour of the major elements suggests that best fit isocon is defined by the position of the data points for Fe, K and Si. The plot clearly indicates that the alteration involves significant gains in Ca and losses of Na and P. The remaining elements can then be considered to be mobile or immobile depending on the degree of uncertainty assumed and the positioning of the isocon. However, if the scatter is merely the result of uncertainties and all the elements are immobile one would not expect them to display any systematic relative variation other than can be explained by original compositional variation. Examination of the incremental changes along the sections shows that this is clearly not the case. Al, Ti both show regular increases in concentration with increasing alteration while Si shows a regular decrease in concentration. Fe, Mg, K and Mn exhibit somewhat irregular but similar profiles. The similarity suggests that the irregular variation is the result of pre-alteration compositional variation as their concentrations exhibit a positive correlation in the unaltered grey schists. However, the ratios of Fe, Mg and K to Mn show a general decrease along the profiles indicating that concentration of Mn increases relative to the other components with increasing alteration. Similarly, the ratios Fe and K to Mg show a general increase with increasing alteration indicating a decrease in Mg concentration relative to Fe and K. Overall these factors suggest that the relative distribution of the points on the plot is a true measure of differing behaviour during the metasomatism rather than being the solely the result of uncertainties in the data. The variation is interpreted as being the result of addition of Al, Mn and Ti and the removal of Mg while Fe, Si and K remain immobile during the alteration.

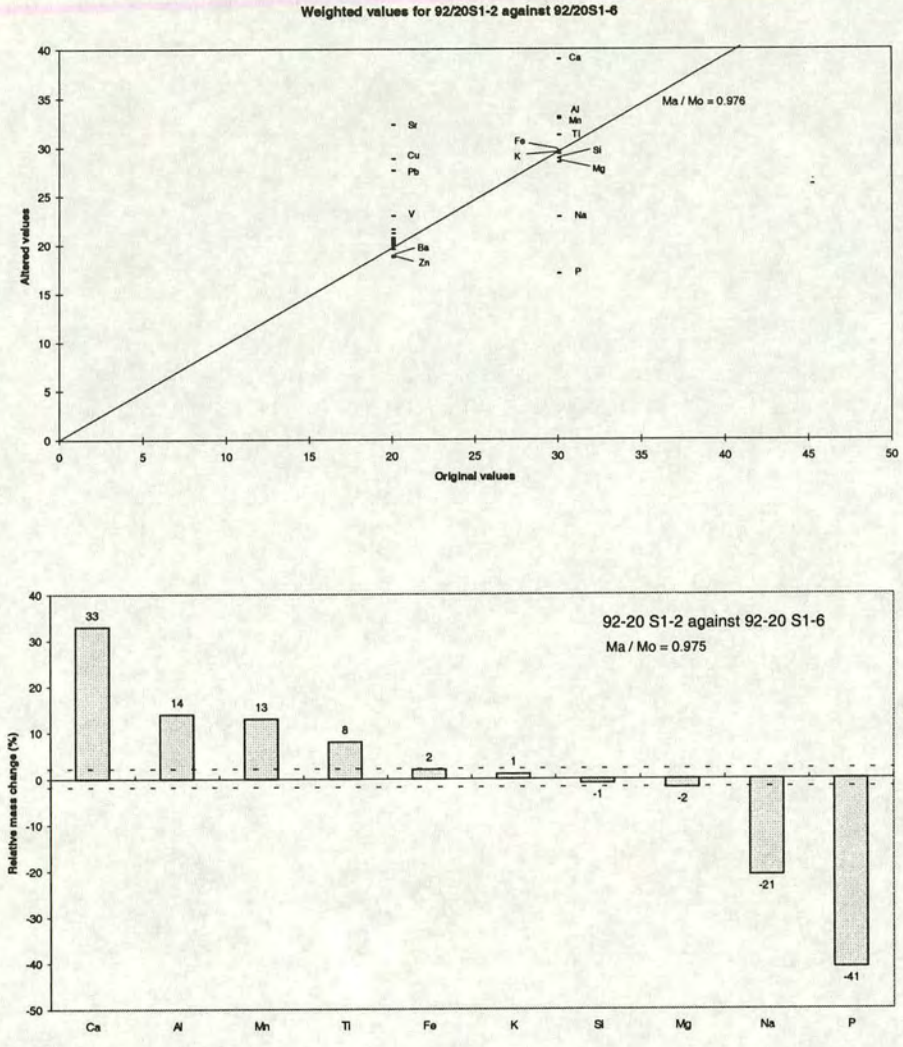

Figure 6.6 (a) Isocon plot used to determine the relative losses and gains of components between samples 92-20 S1-2 and 92-20 S1-6. The isocon shown is based on the assumption that Fe, Si and K are immobile. (b) Histogram illustrating the relative mass change of the major elements.

Overall, the choice of Fe, Si and K as immobile elements suggests that the alteration in the section is the result of gains in Ca, Al, Mn, Ti, Sr, Cu, Pb and V and the loss of Na, P, Mg, Ba and Zn with an overall gain in mass of 2.5%.

However as noted above a second possible isocon can be postulated by considering the distribution of the trace elements on the plot. This is simply placed through the most densely packed set of data points for the trace elements. While the isocon for the trace elements plots relatively close to that for the majors it makes significant changes to the apparent nature of the alteration. Most importantly it would suggest that Fe, Si, and K have been lost rather than being immobile. In addition it suggests that alteration involves a mass decrease of ~1.5%.

In general, the isocon defined by major elements is preferred. If the distribution of Fe, Si and K resulted from differing degrees of removal one might expect their relative concentrations to exhibit some degree of systematic variation with increasing alteration. However, they do not. Nevertheless, it is possible that the true isocon for the alteration falls somewhere between the two and that the apparently immobile major elements do experience some small losses.

Fig 6.7 : 92/20S1-6 against 92/20S1-10

The distribution of components on the plot for 92/20S1-6 against 92/20S1-10 is broadly similar to that on the plot for 92/2092/20 S1-6 against 92/20 S1-2 but with some significant variation. Overall it is interpreted in a similar fashion.

The behaviour of the major elements suggests that the best fit isocon is defined by the position of the data points for Fe, Ti and Si. Unlike the previous sample this agrees almost exactly with the distribution of trace elements. All major elements display regular variation with increasing alteration with the exception of the values for sample 92/20S1-9 which plot slightly off the overall trend. Nevertheless the relative concentrations of the components in this sample are consistent with the

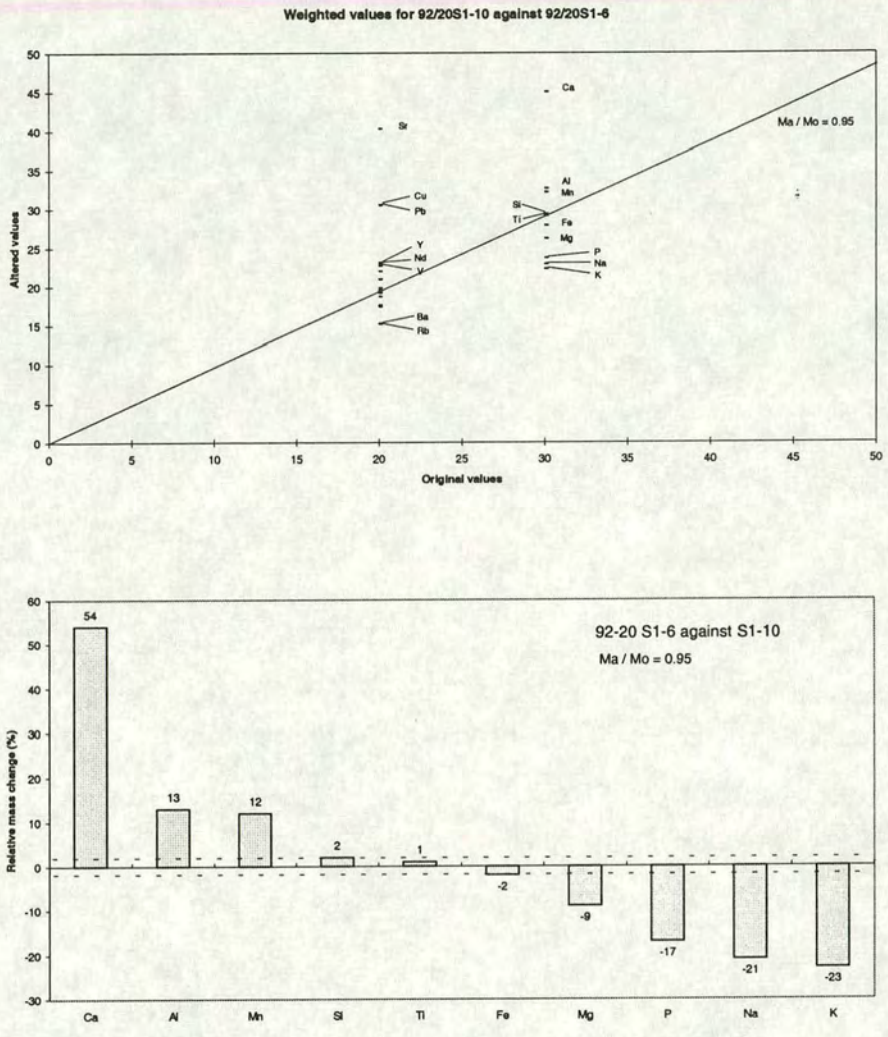

Figure 6.7 (a) Isocon plot used to determine the relative losses and gains of components between samples 92-20 S1-6 and 92-20 S1-10. The isocon shown is based on the assumption that Fe, Si and Ti are immobile. (b) Histogram illustrating the relative mass change of the major elements.

overall variation suggested by the isocon plot. Those components added during the alteration show lower concentrations than expected while immobile components and those lost during the alteration show higher values. Thus it appears to displays a relatively lower degree of alteration than would be expected for its position in the section. Ca, Al and Mn all exhibit general increases in concentration with increasing alteration and have clearly been added during the metasomatism. P, Na and K display almost identically shaped profiles showing a decrease in concentration. Their distribution suggests that this is the result of removal during the alteration. Thus the best candidates for components which are immobile during the metasomatism are Si, Ti, Fe and Mg. However, the ratio of Fe to Mg exhibits a systematic increase in magnitude suggesting that Mg is lost during the alteration.

Thus the plot suggests that the alteration in the section is the result of the addition of Ca, Al, Mn, Sr, Cu, Pb, Y, V, and Nd and the removal of P, K, Na, Zn, Sc, Ba, Rb with an overall mass increase of ~4%.

Fig 6.8 : 92/20S2-8 against 92/20S2-2

The isocon for 92/20S2-8 against 92/20S2-2 may be chosen by using the major or minor elements.

Using major elements the best fit isocon is defined by the data points for Fe, K, Mn, Na and Si. Ca, Al, and Ti all exhibit steady increases in concentration with increasing alteration. This coupled with the distribution of data points clearly indicates that they have been added during the metasomatism. Similarly the concentration of P decreases steadily with increasing alteration indicating that it has been removed from the metasomatism. The ratios of Mg to Fe and K show a systematic increase with increasing alteration indicating that Mg is lost during the metasomatism. In contrast, the ratios of Si, Na, Mn, K, Fe with each other display no systematic variations. This is consistent with these elements being immobile during the alteration.

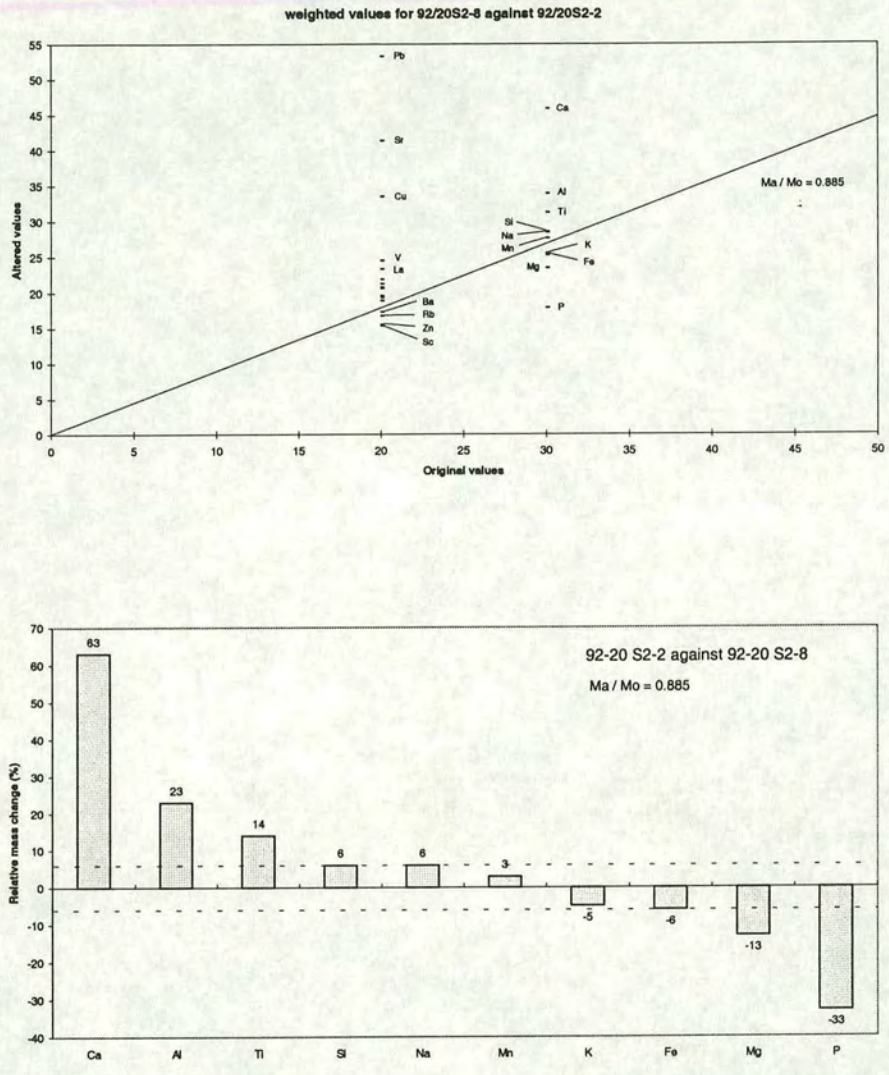

Figure 6.8 (a) Isocon plot used to determine the relative losses and gains of components between samples 92-20 S2-2 and 92-20 S2-8. The isocon shown is based on the assumption that Fe, Si, Mn, Na and K are immobile. (b) Histogram illustrating the relative mass change of the major elements.

In summary, choosing an isocon on the basis of major element distribution suggests that the alteration in this section involves the addition of Ca, Al, Mn, Pb, Sr, Cu, V, and La and the removal of Mg, P, Ba, Rb, Zn, Sc with an overall mass increase of ~12%.

Fig 6.9 92/20S2-8 against 92/20S2-13

As above, isocon for a plot of 92/20S2-8 against 92/20S2-13 may be chosen using the distribution of either the major or minor components.

Using the major elements the best fit isocon is defined by bisecting the range defined by the data points for Mn, K, Na, Si and Fe. Both Ca and Al show incremental increases in concentration with distance toward the vein and have clearly been added during the metasomatism. Ti has a similar shaped profile with the exception of an anomalously high value in sample 92/29S2-12 and is also assumed to be added. All other components show net decreases in concentration with increasing alteration. Si, Fe and Mg all have similar steeply sloped profiles with almost constant gradients and thus at first sight appear to exhibit similar behaviour during the alteration. However the ratios of both Si and Fe to Mg show increases with increasing alteration suggesting that Mg is lost during the alteration. In contrast the ration of Si to Fe shows no regular variation. The concentration of P also decreases regularly toward the vein with the exception of a peak in concentration in 92-20S2-9 and is clearly lost during the alteration. All other components have unique, very irregularly shaped profiles which shed no real light on their behaviour. However, their distribution on the isocon plot suggests that they are .relatively immobile during the alteration.

In summary, fitting the isocon to the major elements suggests that the alteration in this section is the results from the addition of Ca, Al, Ti, Sr, Cu, Pb, La, Ce and V and the removal of Mg, P and Zn with an overall gain in mass of ~ 4.5%. However, the large range over which the data points for the apparently immobile

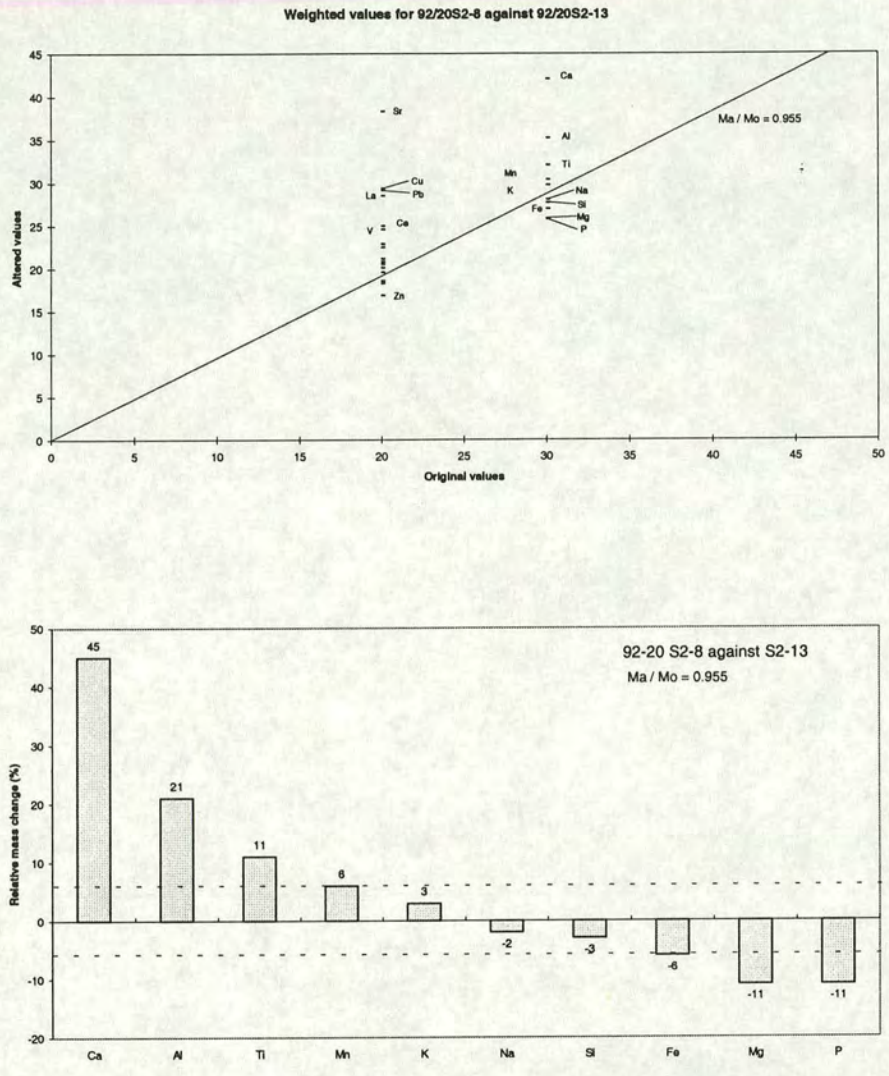

Figure 6.9 (a) Isocon plot used to determine the relative losses and gains of components between samples 92-20 S1-8 and 92-20 S1-13. The isocon shown is based on the assumption that Fe, Si, Na, Mn and K are immobile. (b) Histogram illustrating the relative mass change of the major elements.

elements fall suggests that there is considerable uncertainty in the positioning of the isocon.

Alternatively, the isocon can be positioned on the basis of the distribution of the data points for the minor elements. This would suggest that all the major elements are mobile to some extent during the alteration with Fe Si, Na, K, and Mn all experiencing some degree of loss rather than being immobile. However, there is no reason to believe that such a conclusion is more valid or likely than the positioning of the isocon using the major elements. As in other examples there is no systematic variation in the in the ratios of the apparently immobile elements which would be expected if their distribution is the result of differing degrees of removal during the alteration.

Summary of data from sections from 92-20

Table 6.3 summarises the relative changes in mass of the major elements identified in the four sections from sample 92-20. Comparison of the results shows that the majority of the major elements display identical behaviour in most if not all the sections and gives a clear picture of the characteristics of the alteration accompanying the growth of lawsonite.

In all four sections the metasomatism is dominated by the addition of Ca and, to lesser degree, Al. This is accompanied by the removal of P and smaller but significant reductions in the concentration of Mg. Both Fe and Si appear to be immobile during the alteration.

The apparent behaviour of the other components displays some variation from section to section. However, this variation is not entirely random. Mn and Ti display similar characteristics and the plots suggest that they are either added during the alteration or are immobile. Similarly the plots suggest that K and Na are either removed during the alteration or remain immobile. Significantly, these elements have

low absolute concentrations. Thus, interpretation of their behaviour is more susceptible to errors caused by even small pre-alteration compositional variation, especially if losses or gains are themselves small in magnitude.

	92-20 S1-6 v 2	92-20 S1-6 v 10	92-20 S2-8 v 2	92-20 S2-8 v 13
Al	+	+	+	+
Fe	0	0	0	0
Si	0	0	0	0
Mg	-	-	-	-
Ca	+	+	+	+
Na	-	-	0	0
K	0	-	0	0
Ti	+	0	+	+
Mn	+	0	+	0
P	-	-	-	-

Table 6.3 Summary of the apparent behaviour of the major elements during the alteration of sample 92-20. (+ indicates element is gained, - that it is lost and 0 that it is immobile.

The isocon plots also suggest that the alteration in all four sections result in a net gain in mass of up to 11.5%.

The behaviour of the minor elements is a little more variable. For three out of the four sections their distribution is apparently incompatible with the position of the best fit isocon for the major elements. In these sections the chosen isocon suggests that the vast majority of minor elements are added during the metasomatism and the alteration involves a small net decrease in mass. Nevertheless, it is clear that the alteration in all four sections involves the addition of significant amounts of Sr, Pb,

V, and Cu, and the removal of Zn. More than one of the sections also suggest that this may be accompanied by the addition of Nd, La and Y and the removal of Sc, Ba and Rb.

6.4.2 Section 92-33

Section 92-33 consists of three samples taken from a single compositional layer oriented approximately perpendicular to the larger of the planar quartz veins in the C.T.O. Sample 92-33A was taken from immediately adjacent to the vein while 92-33B and 92-33C were 15 cm and 25 cm away from the vein respectively.

Preliminary examination of the geochemical data shows that there are large differences in composition between samples 92-33A and 92-33B but little difference in composition between samples 92-33B and 92-33C (Table 6.4). This suggests that while sample 92-33A has been altered during the vein related metasomatism samples 92-33B and 92-33C have not.

In order to assess the losses and gains of components accompanying the alteration an isocon plot was derived by plotting 92-33A, the altered sample, against 92-33B as the unaltered sample (Figure 6.10). As there is a minimum of pre-metasomatic compositional variation within the section identification of the best fit isocon is relatively simple. It clearly falls through a tightly packed group of data points defined by those for Na, Mg, Fe, Ti and P suggesting that these components are immobile during the alteration. This choice of isocon also agrees well with the distribution of data points for the minor elements. It suggests that the alteration is the result of the addition of Ca, Al, Mn, Sr and Pb and the loss of Si, K and Rb with an overall decrease in mass of ~2%.

This alteration shares many characteristics with that described in sample 92-20. It involves the addition of Ca, Al, Mn, Sr and Pb, and the loss of K while Fe

Sample	SiO2	Al2O3	Fe2O3	MgO	CaO	Na2O	K2O	TiO2	MnO	P2O5	LOI	Total
92/33A	55.90	16.46	6.34	4.86	6.64	2.21	1.58	0.764	0.131	0.138	5.48	100.49
92/33B	60.86	13.99	6.64	5.05	3.81	2.23	2.37	0.764	0.098	0.134	4.03	99.98
92/33E	62.23	13.75	6.30	4.79	3.67	2.15	2.31	0.773	0.111	0.138	3.67	99.90

Sample	Nb	Zr	Y	Sr	Rb	Th	Pb	Zn	Cu	Ni	Cr	Ce	Nd	La	V	Ba	Sc
92/33A	14.2	185.1	28.0	418.7	65.8	8.4	31.1	91.5	22.7	222.0	655.8	44.9	19.7	20.9	177.1	222.7	21.1
92/33B	16.4	176.7	23.9	126.9	99.6	11.0	10.8	94.7	25.0	251.8	440.8	44.9	19.4	21.5	131.1	311.6	16.2
92/33E	16.4	194.2	24.5	123.2	98.4	10.9	10.1	91.3	25.2	243.3	564.5	51.1	23.5	27.5	127.3	285.4	16.5

Table 6.4 XRF data for the samples from section 92-33.

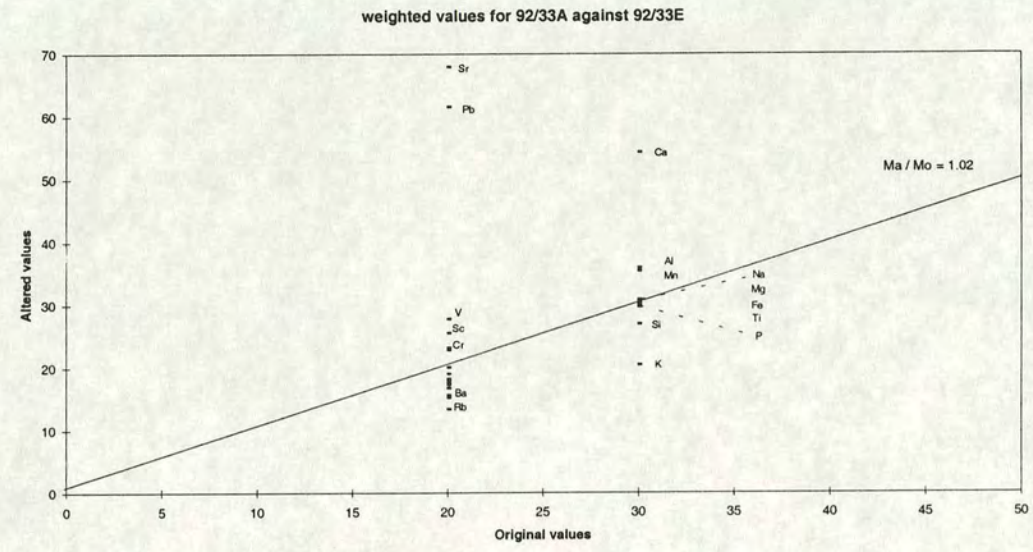

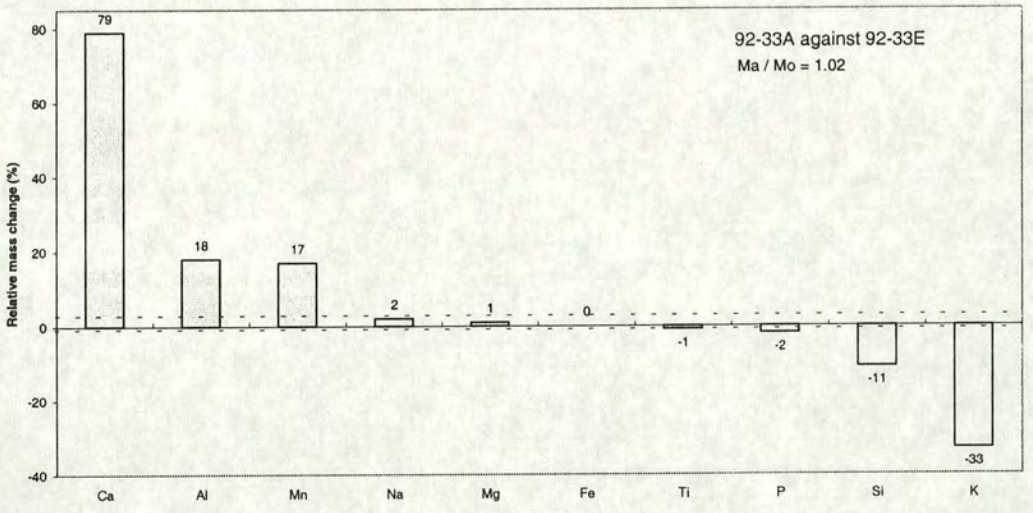

Figure 6.10 (a) Isocon plot used to determine the relative losses and gains of components between samples 92-33A and 92-33E. The isocon shown is based on the assumption that Fe, Na, Mg, P and Ti are immobile. (b) Histogram illustrating the relative mass change of the major elements.

remain immobile. However, it also displays some differences. Most significantly, Si is clearly lost rather than being immobile and the alteration involves a small net decrease in mass rather than a net increase in mass. In addition, both P and Mg appear to be immobile during the alteration rather than being lost.

6.4.3 Sample 93/84

Sample 93/84 is 20 cm long core drilled into the main face of the C.T.O. oriented perpendicular to the larger of the 2 upright veins and parallel to compositional layering (Figure 6.11). For geochemical analysis it was sub-divided into 4 equal sections designated 93/84A to D with 93/84A and 93/84D being closest and furthest from the vein respectively.

Once again initial observation of the geochemical data reveals large variations in the concentrations of both major and trace elements along the section (Table 6.5). Figure 6.12a is an isocon plot of 93-84D, the least altered sample, against 93-84A, the most altered sample. Data points for both the major and minor elements are spread over a considerable range with no obvious maximum density. Initial observation of the distribution of the data points for the major elements suggests three possible isocons. The most conservative choice is to assume the Al, Ti, Mn, Mg, Fe and Na are all immobile. This would suggest that the alteration is the result of the addition of Ca Sr, and Pb and the removal of Na, K, Si, P, and Rb (Fig 6.12b) with a net decrease in mass of ~17%. A second isocon can be positioned by assuming that the only elements immobile during the alteration are Fe and Mg. If this were the case then the alteration would involve the addition of Ca, Al, Ti and Mn and the loss of Na, K, Si, and P with a net decrease in mass of ~9%. Finally, it appears possible to fit an isocon to the group of data points for Al, Ti and Mn. This would indicate gain of Ca and loss of Mg, Fe, Na, K, Si and P with a net mass loss of ~22%.

However, whichever isocon is chosen the inferred alteration is significantly different from that identified in sample 92-20 but shares the same broad

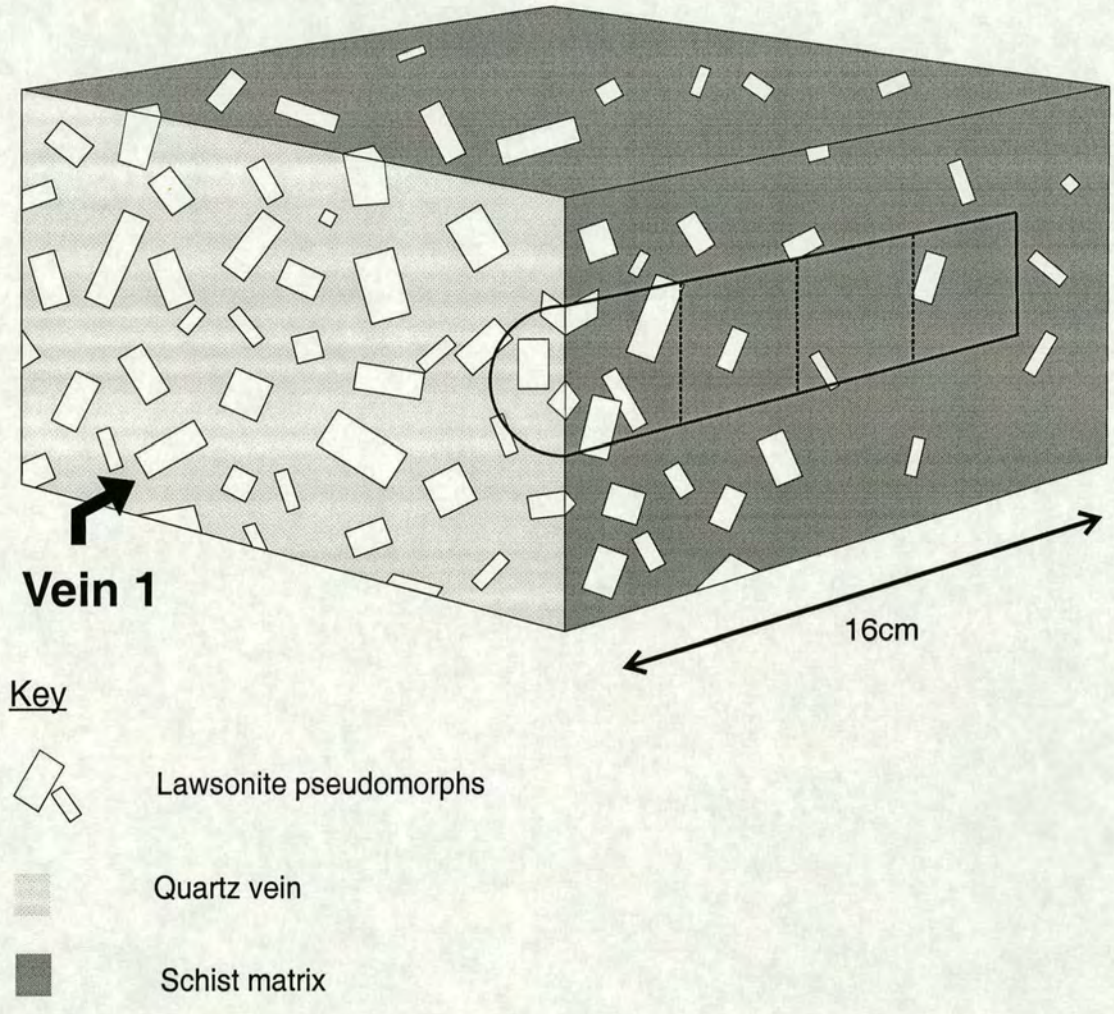

Figure 6.11 Schematic block diagram showing the orientation of the samples from core 93-84 relative to the upright quartz vein and the distribution of lawsonite.

sample	SiO2	Al2O3	Fe2O3	MgO	CaO	Na2O	K2O	TiO2	MnO	P2O5	LOI	Total
93/84A	52.31	16.76	7.42	5.53	6.38	2.69	2.043	0.850	0.112	0.113	5.47	99.67
93/84B	55.81	15.48	7.86	5.82	4.13	2.52	2.539	0.886	0.115	0.144	4.36	99.67
93/84C	57.10	15.11	7.89	5.64	4.13	2.73	2.249	0.778	0.120	0.143	3.93	99.81
93/84D	61.91	13.56	6.85	5.07	3.17	2.68	2.201	0.693	0.094	0.142	3.26	99.64

sample	Nb	Zr	Y	Sr	Rb	Th	Pb	Zn	Cu	Ni	Cr	Ce	Nd	La	V	Ba	Sc
93/84A	16.3	182.5	27.2	328.6	84.2	10.7	23.3	101.7	37.2	237.1	520.8	57.0	26.9	27.8	194.4	305.0	17.7
93/84B	18.9	186.5	25.0	138.8	107.7	10.9	11.0	111.3	35.4	256.0	501.5	62.7	25.0	31.1	167.1	336.3	17.8
93/84C	15.9	167.2	23.4	152.3	94.3	10.0	10.4	107.8	26.8	233.0	483.2	49.7	22.4	21.4	163.3	318.2	18.6
93/84D	13.6	147.9	20.7	115.5	92.0	7.5	8.7	97.9	27.9	213.0	534.5	42.9	19.5	20.5	149.8	305.5	15.6

Table 6.5 XRF data for samples from core 93-84.

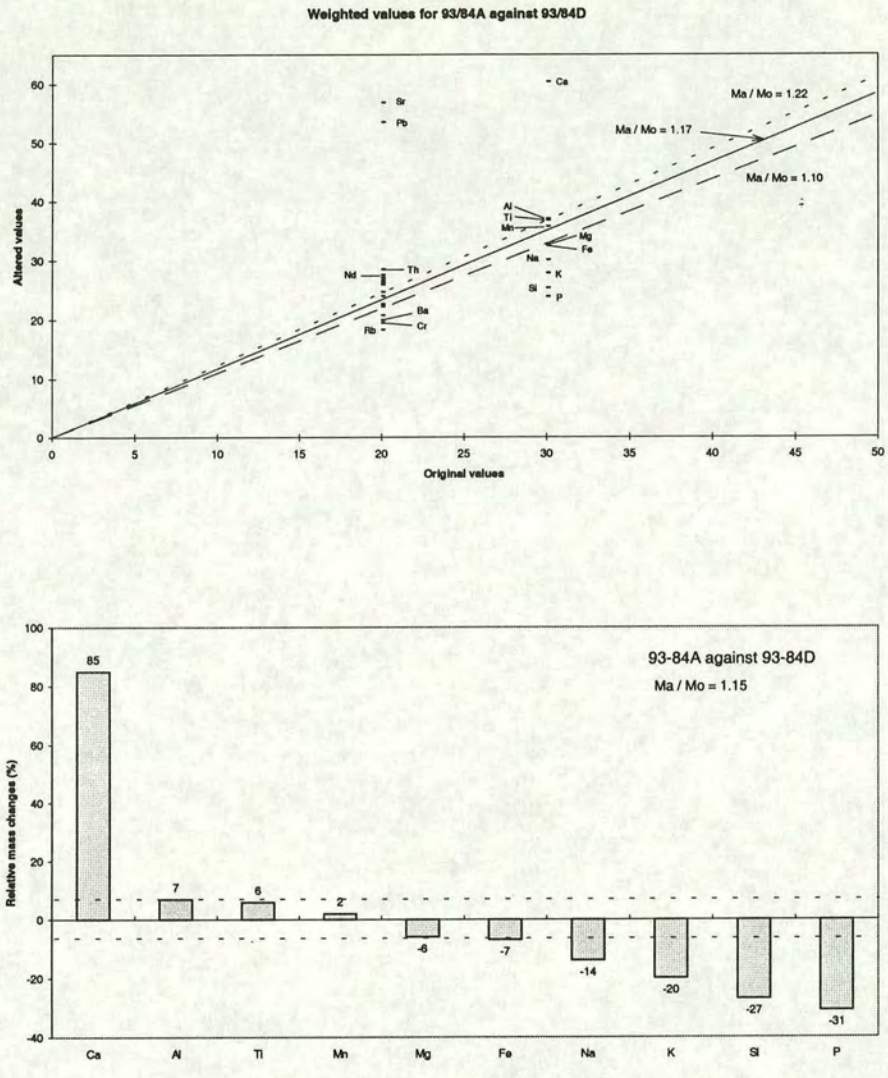

Figure 6.12 (a) Isocon plot used to determine the relative losses and gains of components between samples 93-84A and 93-84D. Three possible isocons are shown. Solid line : Al, Ti, Mn, Mg, Fe, Na assumed to be immobile. Short dashed line : Al, Ti and Mn assumed to be immobile. Long dashed line Fe amd Mg assumed to be immobile. (b) Histogram illustrating the relative mass change of the major elements assuming that the solid line is the true isocon.

characteristics as that identified in section 92-33. Once again it clearly involves the loss of Si and results in net loss of mass.

As in the sections from sample 92-20 the incremental variation in concentration of components was examined to try to clarify the behaviour of individual elements. Plots of concentration of the components against distance from the vein show that this variation is far from regular along the sections (Figure 6.13). While there are large changes in composition between samples A and B and between samples C and D there is relatively little change in composition between samples B and C. In addition the relative changes in concentration of components between samples A and B and between samples C and D are different.

This apparent irregularity in the behaviour of the major elements might be explained by pre-metasomatic compositional variation in the schists, variation in the nature of the alteration process with distance from the veins or a combination of the two factors.

There is a high concentration of vein-related lawsonite in 93-84A and it seems clear that the changes in composition between samples A and B are the result of the vein related metasomatism identified in other sections. Figure 6.14 shows the isocon plot for 93-84A against 93-84B.. Using the distribution of the major elements the best fit isocon clearly falls through the group of data points for Si, Fe, Mg, Ti and Mn. These components are thus assumed to be immobile during this stage of the alteration. This isocon also fits well with the distribution of data points for the minor elements. It suggests that the alteration involves the addition of Ca, Al, Na, Sr, Pb and V and the loss of P, K and Rb accompanied by a net mass gain of ~10%. However the apparent increase in Na appears to be due to an anomalously low value in sample B and may not represent a real increase during the alteration. Significantly, this is almost identical in nature to the alteration identified in the sections from sample 92-20.

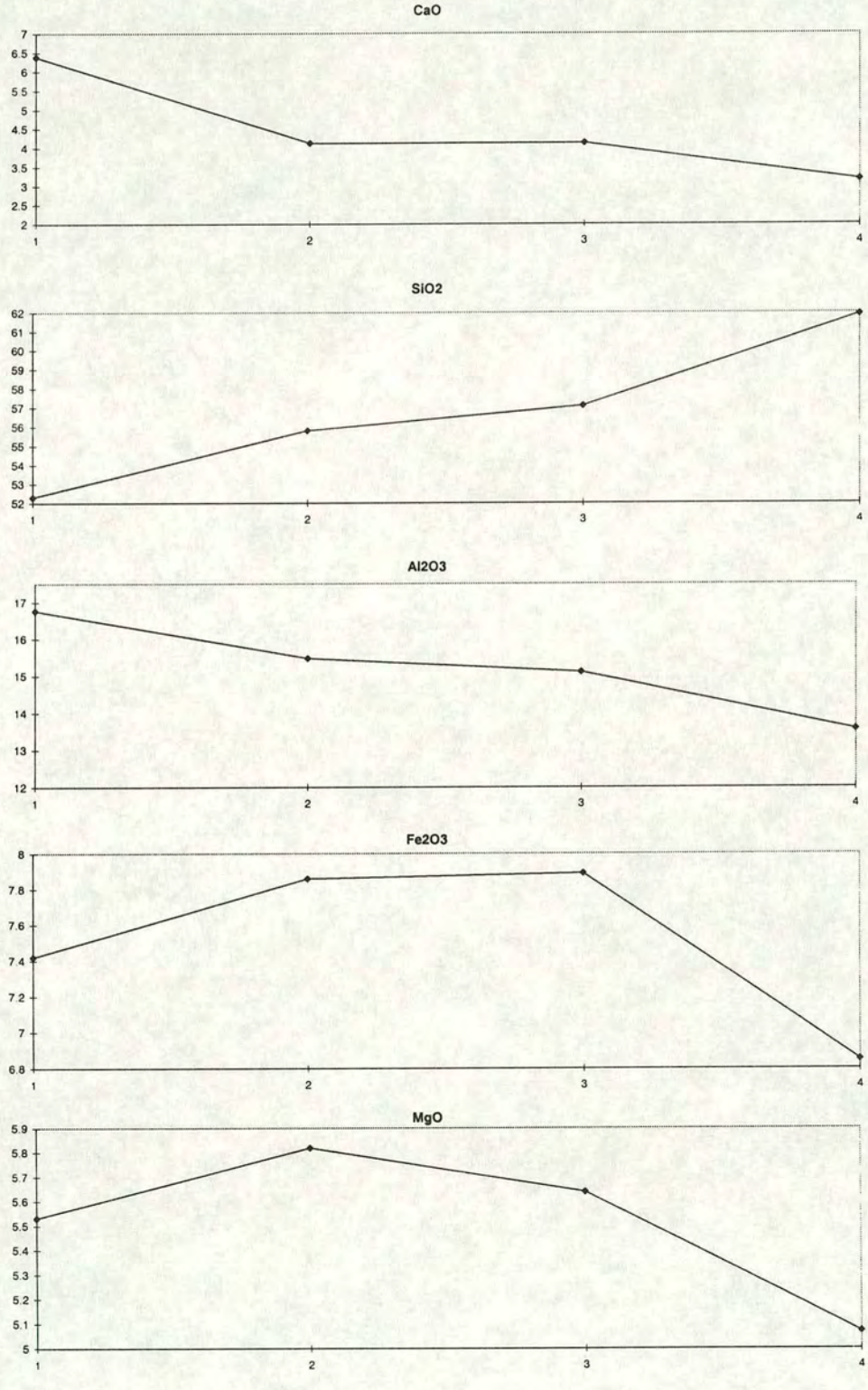

Figure 6.13a Series of plots showing the incremental variation in concentration of the major elements in section 93-84 with increasing distance from the vein.

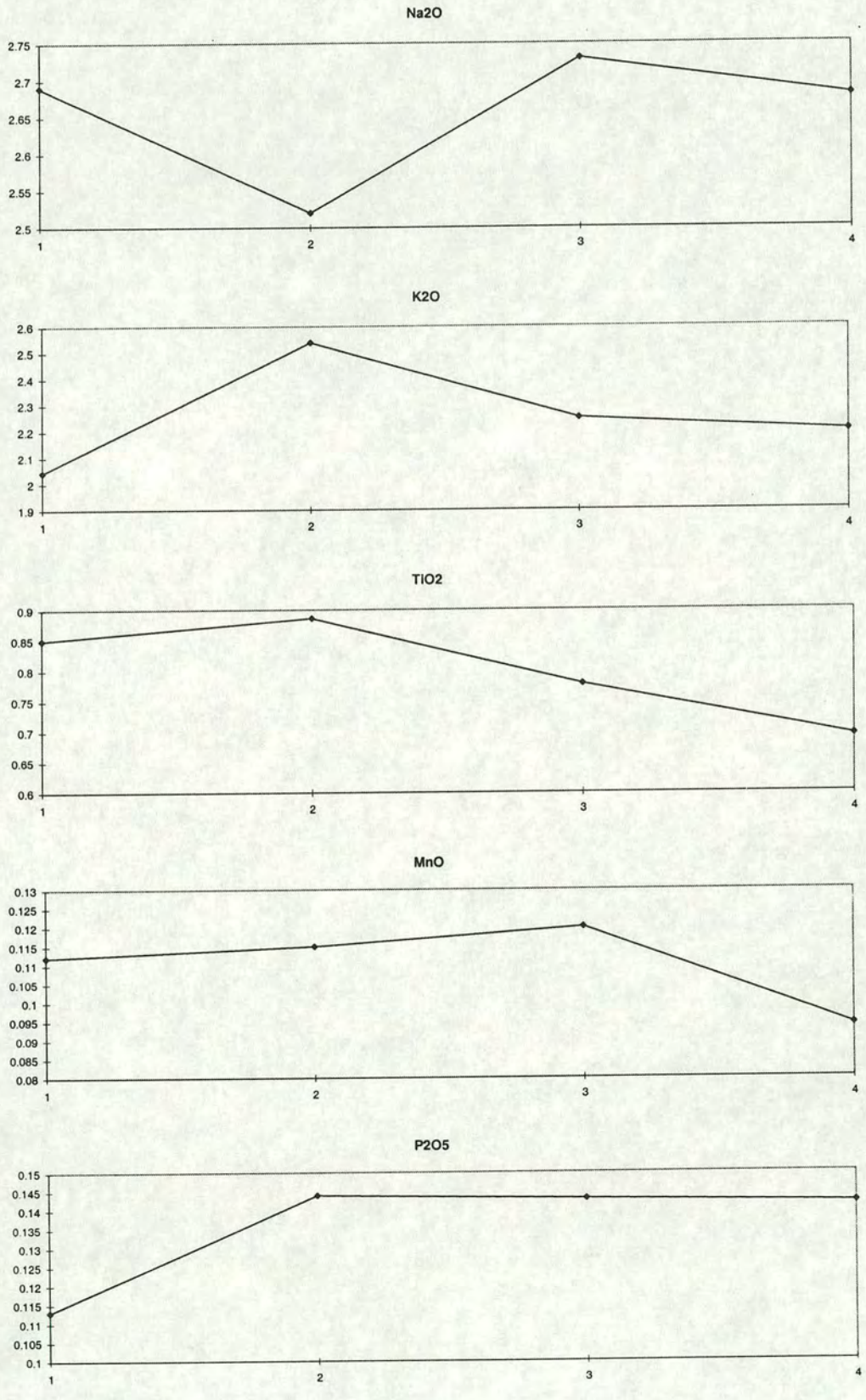

Figure 6.13b Series of plots showing the incremental variation in concentration of the major elements in section 93-84 with increasing distance from the vein.

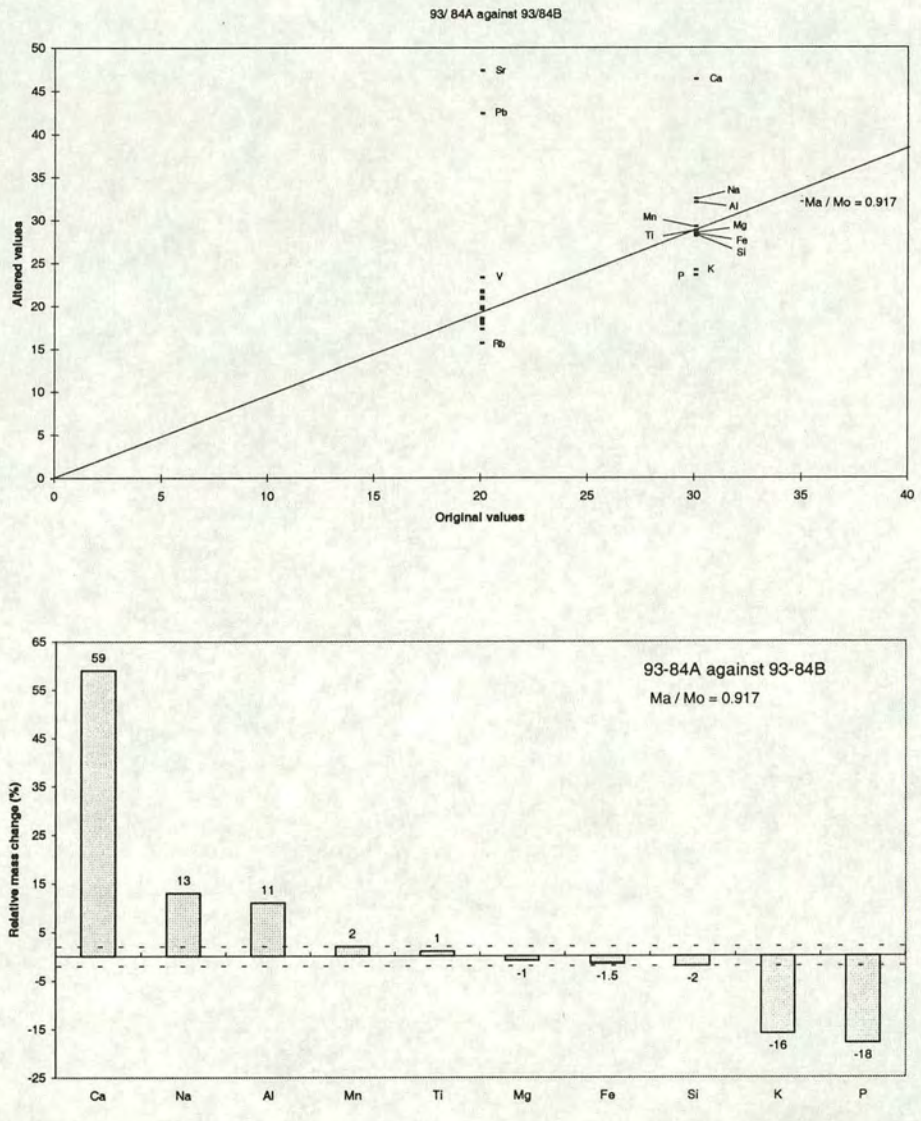

Figure 6.14 (a) Isocon plot used to determine the relative losses and gains of components between samples 93-84A and 93-84B. The isocon shown is based on the assumption that Fe, Si, Mg, Mn and Ti are immobile. (b) Histogram illustrating the relative mass change of the major elements.

In contrast, preliminary examination of data suggests that the difference in concentration of components between samples C and D could be the result of pre-metasomatic compositional variation. Plots show that the compositional change from C to D consists of a large increase in Si concentration coupled with a decrease in the concentration of all other components. The closure effect ensures that an increase in the concentration of any component will cause a decrease in the concentration of all others. Thus the decrease in the concentration of other components may simply reflect the increase in the concentration of Si. Of all minerals in the grey schists quartz displays the most heterogeneous distribution often occurring in small scale S1 parallel segregations.

However, if the difference in composition between C and D were merely the result of a higher content of quartz in D relative to C then an isocon plot would simply indicate a 'loss' of Si while all other elements were apparently 'immobile'. Instead, such a plot (Figure 6.15) indicates that change in composition from D to C is the result of the loss of K, P, and Na as well as Si and the gain of Ca and Mn while Fe, Ti, Al and Mn all remain immobile. This strongly suggests that this part of the section is also affected by the vein related metasomatism. However, the alteration displays some significant differences to that identified in other plots. Unlike the alteration in sample 92-20 and that between 93-84A and B Si is lost rather than being immobile, Al is immobile rather than being gained and there is an overall loss in mass rather than a net gain. Similarly, the data for 92-33 suggests that Al is being added rather than being immobile.

While there are large changes in composition between sample A and B and between samples C and D which can be ascribed to major element metasomatism there is little difference in composition between samples B and C. An isocon plot supports this observation (Figure 6.16). At most it suggests increases in Ti and K and possibly a small loss of Na with all other elements immobile and no overall change in mass. All the apparently mobile elements have small absolute concentrations and are thus more susceptible to errors caused by original compositional variation. Overall it

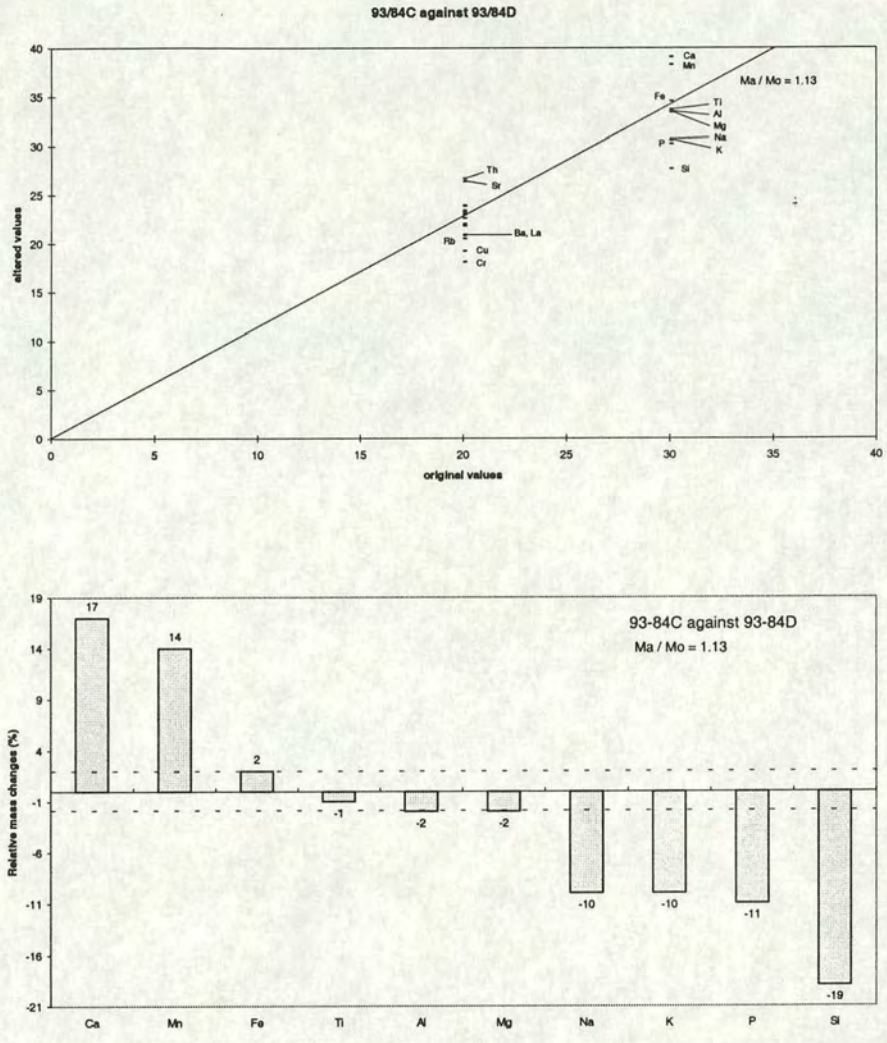

Figure 6.15 (a) Isocon plot used to determine the relative losses and gains of components between samples 93-84C and 93-84D. The isocon shown is based on the assumption that Fe, Al, Mn and Ti are immobile. (b) Histogram illustrating the relative mass change of the major elements.

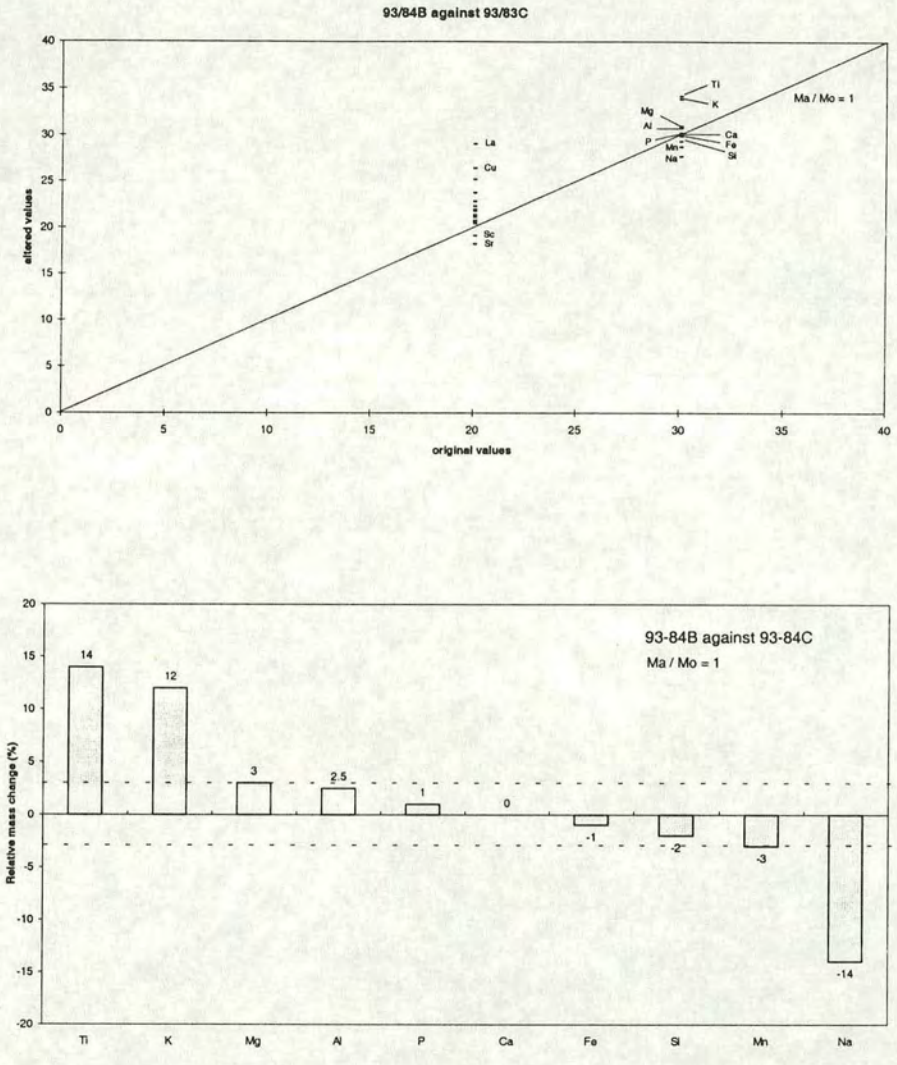

Figure 6.16 (a) Isocon plot used to determine the relative losses and gains of components between samples 93-84B and 93-84C. The isocon shown is based on the assumption all elements other than Ti, K, and Na are immobile. (b) Histogram illustrating the relative mass change of the major elements.

seems likely that there is no significant gain or loss of components over the interval defined by samples B and C.

Thus, examination of the compositional variation in section 93-84 indicates that it contains two portions in which significant major element metasomatism is evident separated by third in which no significant gains or losses of elements occurred. In addition, it reveals that the nature of the alteration in the two metasomatised zones is different. In the zone immediately adjacent to the vein the alteration involved the addition of Ca, Al, Sr, Pb and V and the loss K, P and Rb with an overall gain in mass of ~8%. In the other zone of alteration it involved the addition of Ca, Mn, Sr and the loss of Na, K, P, and Si. Thus there appears to be variation in the nature of the alteration with distance from the vein.

The combined effect of the two zones of alteration is the addition of Ca, Al, Mn, Sr, Pb and V and the removal of Si, Na, K and P. Thus, the best fit isocon for the total alteration (Figure 6.12) appears to be that which assumes that only Fe and Mg are totally immobile during the alteration. The only element whose behaviour is apparently inconsistent with this choice is Ti which appears to be immobile in both of the alteration zones but which appears to show a net increase in concentration during the alteration as a whole. Significantly, these overall gains and losses are almost identical to those identified in section 92-33.

Spatial variation in the nature of the alteration would also explain the differences between the overall gains and losses in sections 93-33 and 93-84. While the latter longer sections record the effects of both zones of the alteration, the shorter sections from the former only record the effects of the alteration in the zone nearest the vein.

6.4.4 Core Section: Samples 93-56 to 93-63

This is the longest section through the alteration zone adjacent to the upright vein. Eight parallel cores were drilled in the top of the C.T.O. each parallel to the contact between the upright vein and the schists (Figure 6.17). They are numbered from 93-56 to 93-63 with 93-56 closest to the vein. The cores are evenly spaced approximately 5 cm apart except for the two samples closest to the vein which are close to the vein.

In order to assess the variation in lawsonite concentration within the section each core section was halved parallel to its length and the cut faces polished. The area of lawsonite on each face was then measured and modal proportion of lawsonite estimated for each sample as for sample 92-20. A plot of lawsonite concentration against distance reveals a rapid decrease in lawsonite concentration with distance in the samples closest to the vein but further from the vein the trend is more irregular (Figure 6.18). However, the geochemical data shows that the concentration of Ca decreases fairly regularly away from the vein across the entire width of the section. In other sections wt% CaO has been shown to be an good index of lawsonite content (section 6.4.1) and thus it appears to indicate that the lawsonite concentration continues to decrease along the section. The fact that this decrease is not discernible in Figure 6.18 is probably due to a greater degree of uncertainty in the measurement of modal proportion of lawsonite in this section relative to that in sections from 92-20. The area of the individual faces measured is considerably smaller and it was only possible to measure one face per sample rather than two.

Plots of concentration of the components against distance from the vein show that the decrease in lawsonite concentration is accompanied by significant compositional variation (Table 6.6 & Figure 6.19). All profiles are affected by the presence of an S1 parallel quartz vein in samples 58, 59 and 60 which increases the overall wt% SiO_2 and thus, due to the closure effect, decreases the concentration of all other components except P. The increase in the P concentration presumably indicates the presence of apatite in the veins. Ignoring this factor the variation in

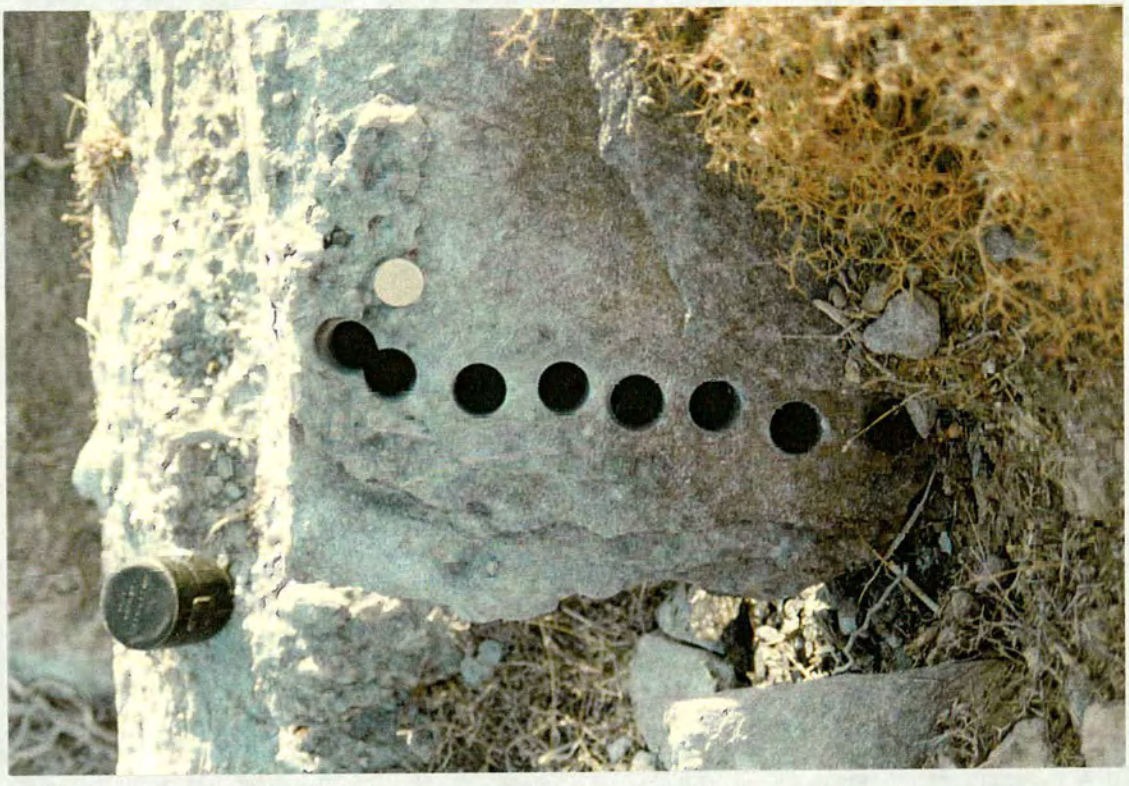

Figure 6.17 Photograph of the upper surface of the C.T.O. illustrating the position of the core section samples relative to the planar quartz vein.

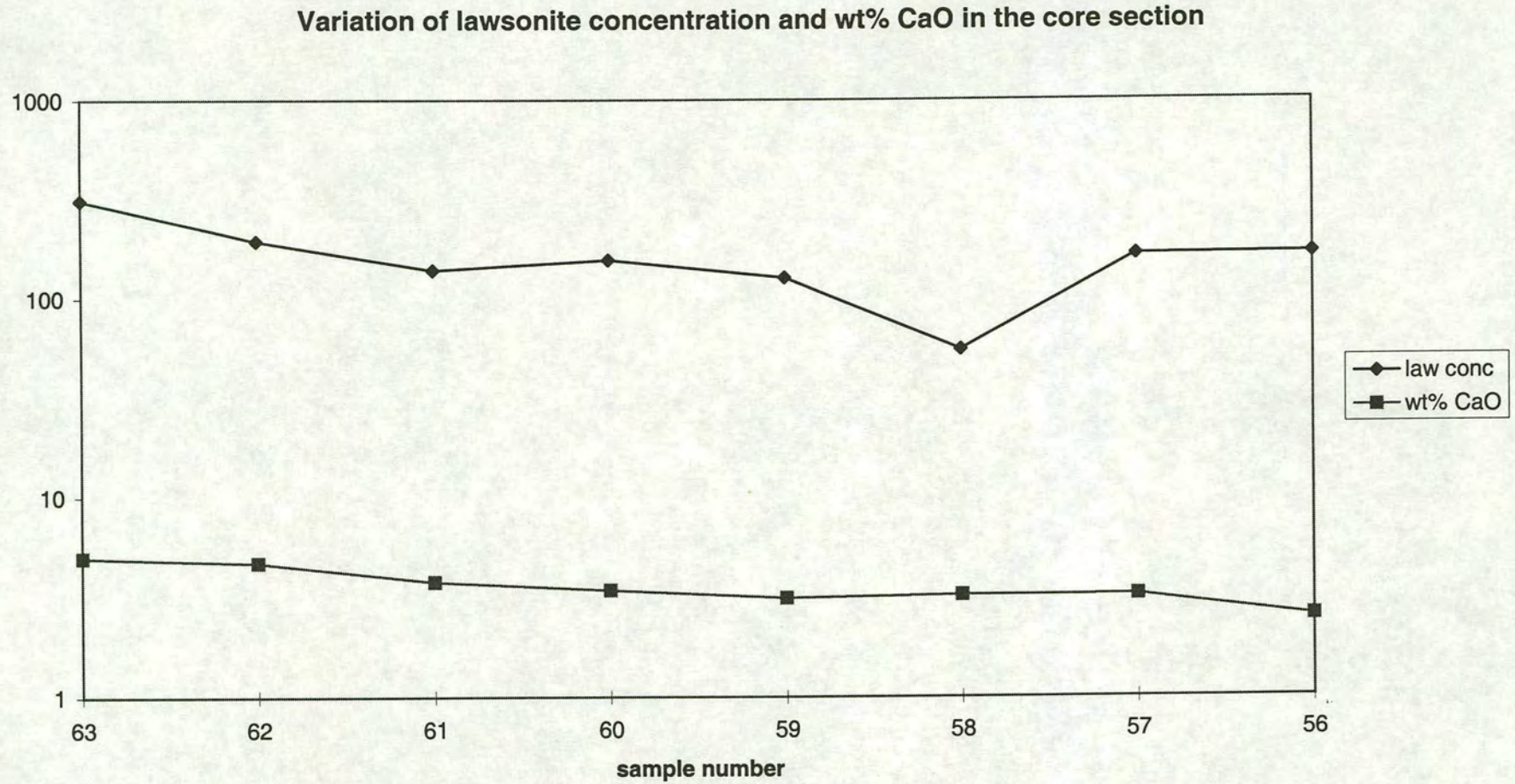

Figure 6.18 Plot illustrating the change in concentration of lawsonite within the core section and the accompanying change in concentration of Ca.

sample	SiO2	Al2O3	Fe2O3	MgO	CaO	Na2O	K2O	TiO2	MnO	P2O5	LOI	TOTAL
93/56	62.65	13.80	6.54	5.00	2.53	2.68	2.359	0.756	0.097	0.149	3.00	99.57
93/57	61.62	14.06	6.39	4.94	3.24	2.59	2.304	0.788	0.099	0.144	3.46	99.64
93/58	63.10	13.38	6.23	4.66	3.23	2.44	2.231	0.727	0.101	0.151	3.34	99.58
93/59	62.94	13.13	6.34	4.84	3.12	2.48	2.268	0.702	0.099	0.144	3.60	99.65
93/60	63.01	13.18	6.23	4.79	3.42	2.53	2.120	0.722	0.092	0.140	3.63	99.87
93/61	59.85	14.24	6.80	5.06	3.77	2.57	2.362	0.800	0.100	0.137	4.03	99.72
93/62	58.06	14.39	6.86	5.16	4.69	2.43	2.255	0.803	0.108	0.129	4.90	99.78
93/63	57.83	14.62	6.87	5.09	4.97	2.35	2.014	0.764	0.111	0.129	4.85	99.59

sample	Nb	Zr	Y	Sr	Rb	Th	Pb	Zn	Cu	Ni	Cr	Ce	Nd	La	V	Ba	Sc
93/56	15.4	178.9	25.1	92.1	97.2	8.7	10.4	96.4	30.0	231.9	519.2	47.7	18.9	24.2	133.8	272.6	15.5
93/57	15.8	186.5	26.5	125.6	94.9	8.9	11.7	94.3	27.2	231.5	547.4	52.3	21.6	28.9	140.0	263.2	15.5
93/58	14.7	175.8	25.6	120.7	91.8	8.5	10.0	86.4	24.3	217.9	539.1	51.1	22.8	24.9	136.1	244.2	15.1
93/59	14.6	173.1	23.8	101.7	93.4	7.9	8.9	90.7	22.0	222.3	519.9	45.2	22.7	24.6	131.4	271.0	16.9
93/60	14.8	171.7	23.9	129.0	87.8	7.9	9.1	88.8	21.7	223.1	542.0	52.6	19.6	23.5	134.6	243.9	15.3
93/61	16.9	190.2	26.3	139.3	97.4	8.5	9.5	96.5	24.7	235.5	571.3	57.2	23.2	24.1	146.4	275.4	17.3
93/62	16.9	194.9	26.4	180.5	94.0	8.9	11.3	95.5	32.6	237.6	568.6	57.9	23.5	32.7	150.3	269.5	18.5
93/63	16.1	190.7	27.1	236.5	83.9	8.2	14.1	95.9	31.3	243.1	581.9	53.6	23.1	30.8	158.1	258.9	20.5

Table 6.6 XRF data for samples from the core section.

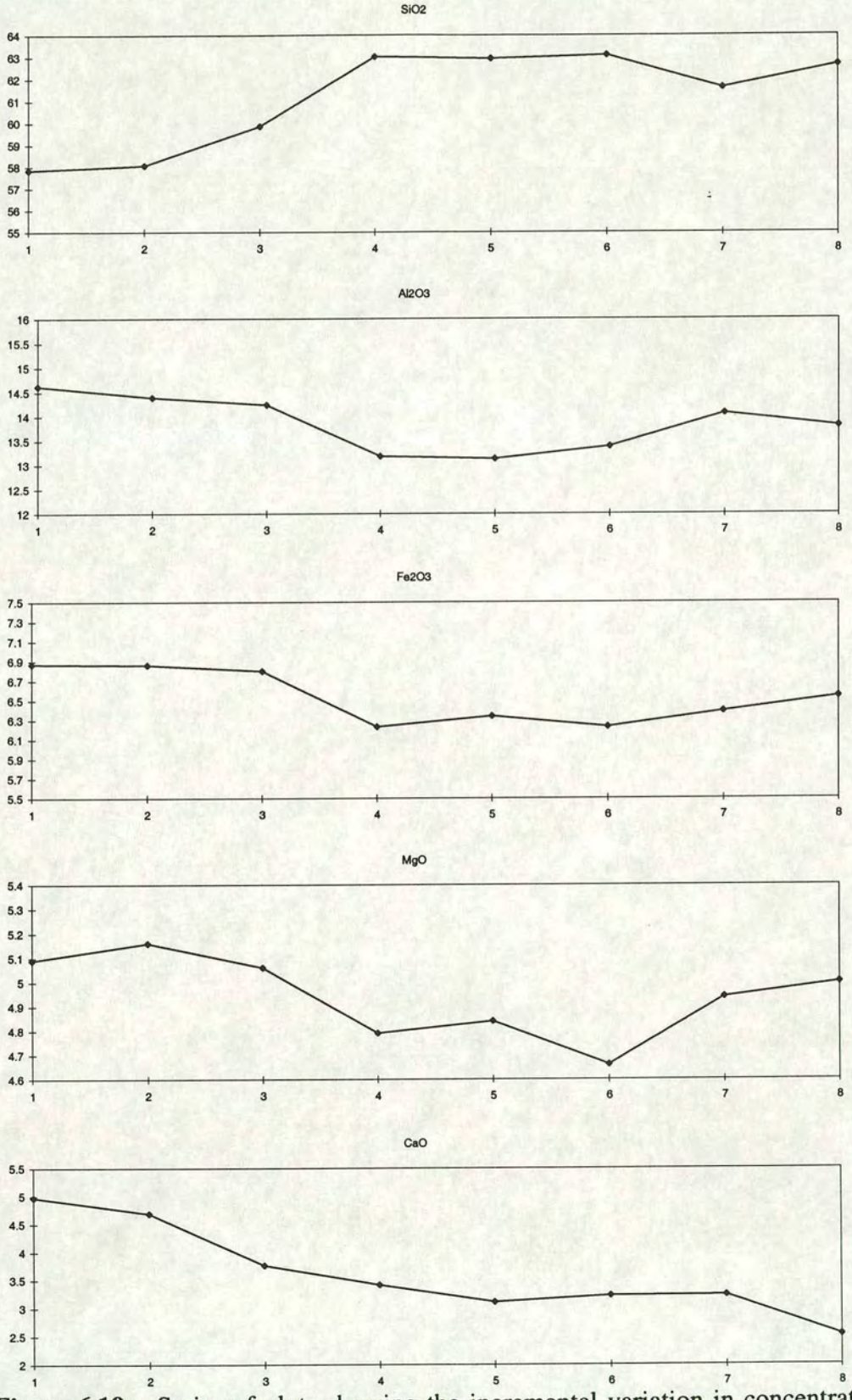

Figure 6.19a Series of plots showing the incremental variation in concentration of the major elements in the core section with increasing distance from the vein.

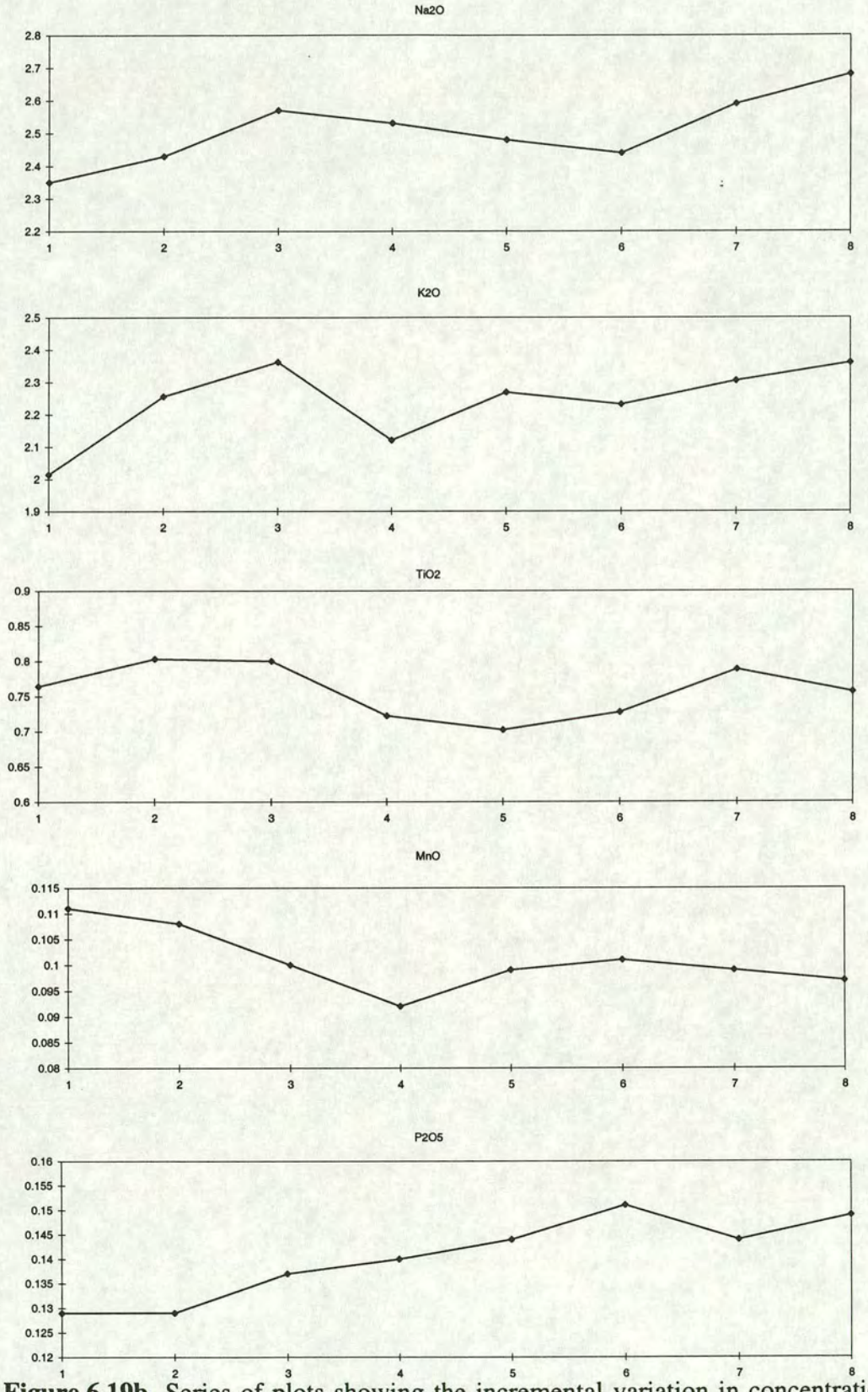

Figure 6.19b Series of plots showing the incremental variation in concentration of the major elements in the core section with increasing distance from the vein.

concentration of most major elements with distance along the section is fairly regular. The concentrations of Ca, Al and Mn all increase incrementally toward the vein. Fe, Mg, and Ti have less regular profiles resulting in small net increase in concentration with increasing alteration. Si, P and Na all display regular decrease s toward the vein. K displays a similar decrease but its but its trend is more irregular.

Figure 6.20 is an isocon plot for 93-63 against 93-56 and illustrates the total losses and gains of components along the section. Fitting an isocon to the distribution of the major elements suggests that Al, Fe, Mg and Ti are immobile during the alteration. Such an isocon also fits quite well with the distribution of the data points for the minor elements. It would suggest that the change in composition along the section is the result of a gain of Ca and Mn and a loss of Si, Na, P, and K with an overall loss in mass of ~3%.

However, if the interpretation of the data from sample 93-84 is correct and there is variation in the nature of the alteration with distance from the vein then it should be possible to identify these zones in this section as well. Finer scale examination of the data suggests that this is indeed the case.

Figures 6.21 shows an isocon plot for 93-62 against 93-63 illustrating the changes in composition between the two samples closest to the vein. While the overall losses and gains of components are small the best fit isocon suggests that Al is added during the alteration while Si is immobile and there is a small net increase in mass. This contrasts with the alteration in the rest of the section as illustrated in an isocon plot for 93-56 against 93-62 Figure 6.22. This plot suggests that Al is immobile in this portion of the section while Si is lost and the alteration results in an significant net decrease in mass. This agrees with the observations on sample 93-84 and supports the conclusion that there is spatial variation in the nature of the metasomatism

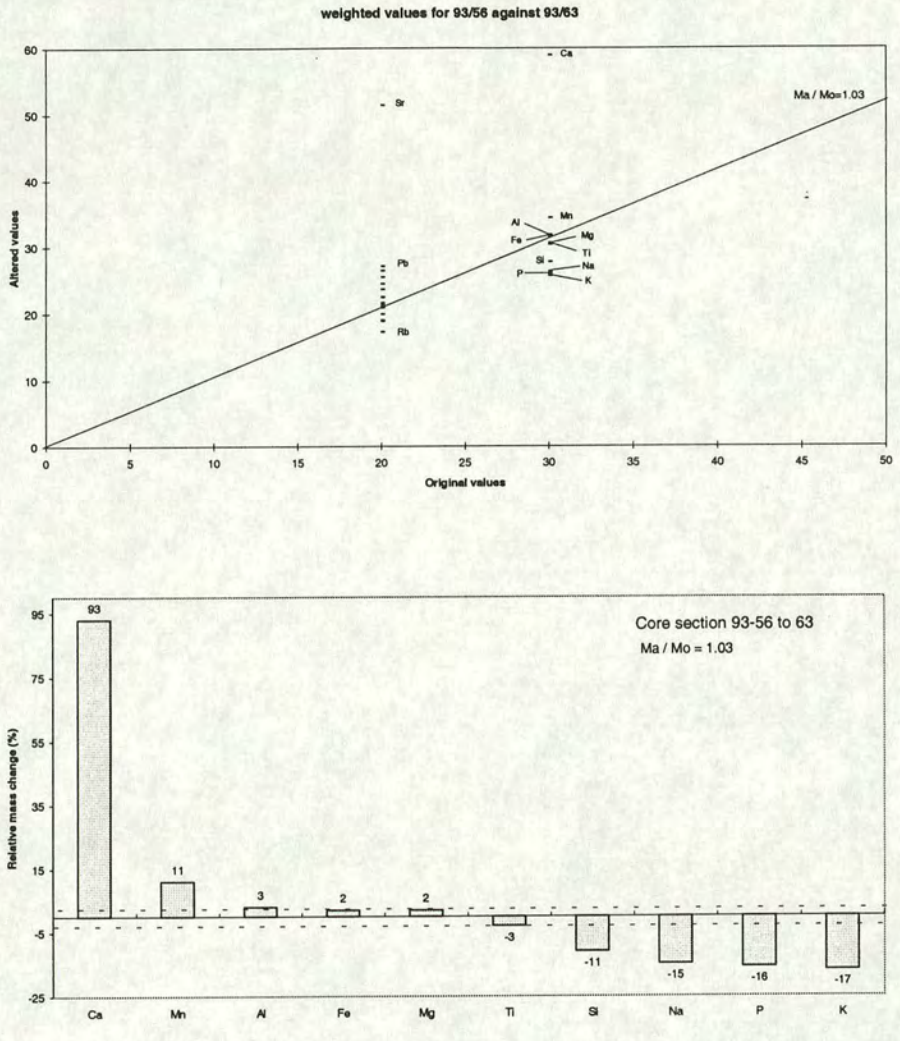

Figure 6.20 (a) Isocon plot used to determine the relative losses and gains of components between samples 93-56 and 93-63. The isocon shown is based on the assumption Al, Fe, Mg and Ti are immobile. (b) Histogram illustrating the relative mass change of the major elements.

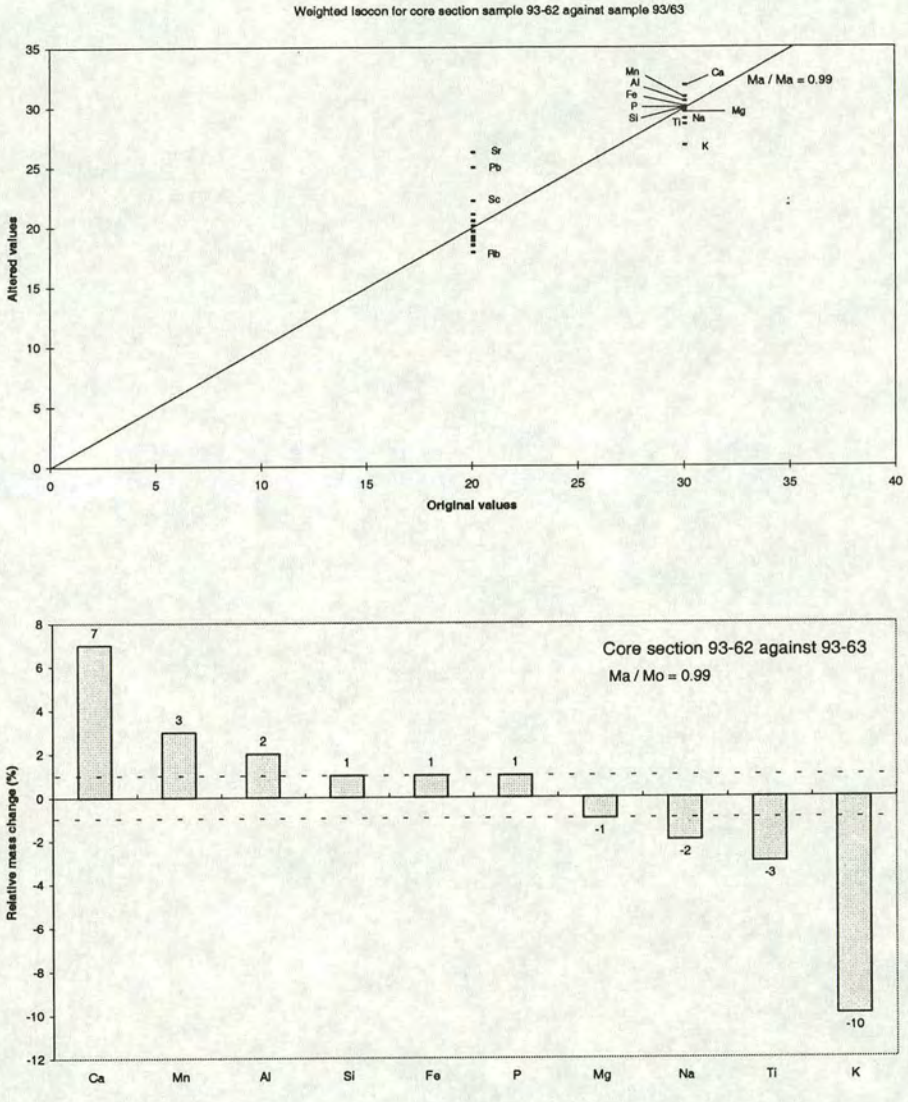

Figure 6.21 (a) Isocon plot used to determine the relative losses and gains of components between samples 93-62 and 93-63. The isocon shown is based on the assumption Fe, Mg, Si, and P are immobile. (b) Histogram illustrating the relative mass change of the major elements.

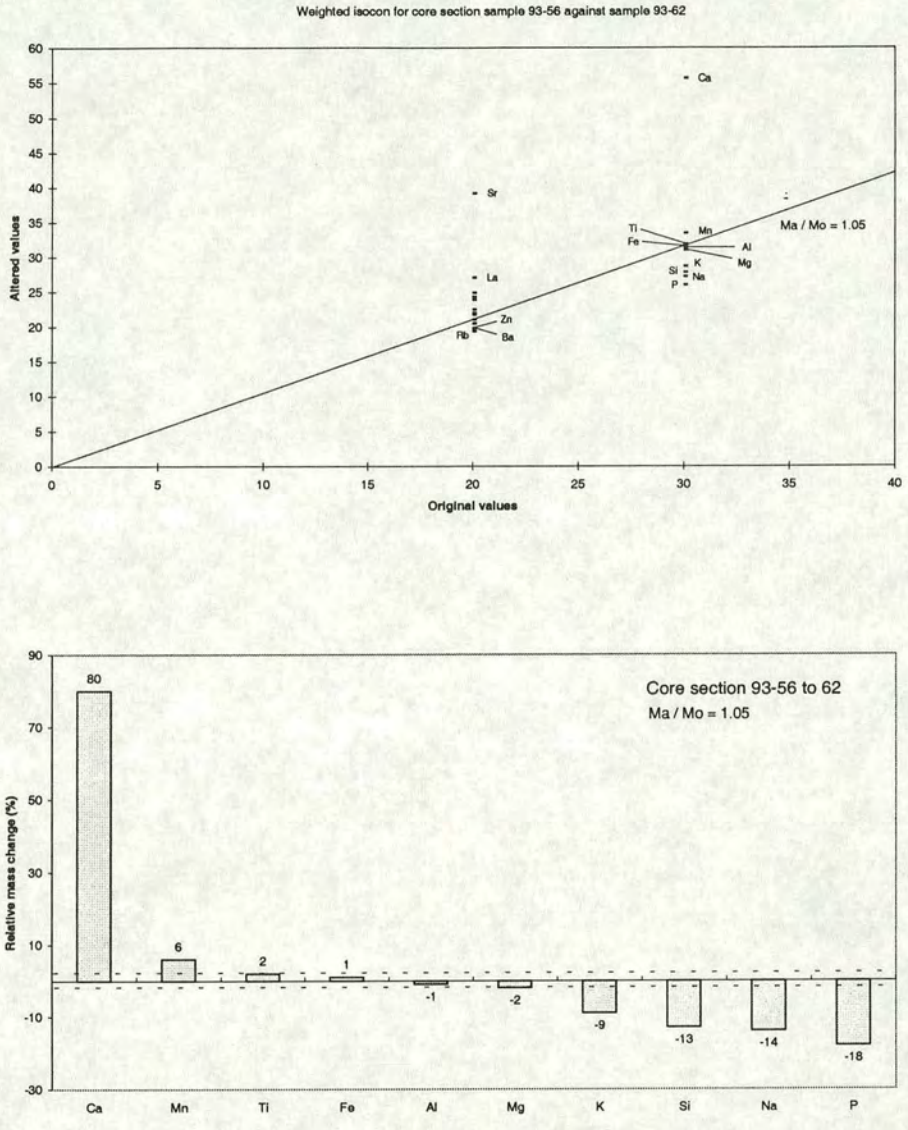

Figure 6.22 (a) Isocon plot used to determine the relative losses and gains of components between samples 93-56 and 93-62. The isocon shown is based on the assumption Fe, Mg, Al, and Ti are immobile. (b) Histogram illustrating the relative mass change of the major elements.

6.4.5 Summary of Characteristics of Metasomatism in the C.T.O

Geochemical analysis of sections from the C.T.O. show that vein related lawsonite growth is the result of major element metasomatism. The most significant features of this alteration are the addition of Ca and Al and the removal of Si, P, Na and K. In addition it may involve the addition of small quantities of Mn and/or Ti and the removal of small quantities of Mg. Fe is the only major element which seems to be totally immobile during the metasomatism. Overall the alteration results in a significant net loss of mass.

Closer examination reveals that the total alteration is the result of two distinct zones of alteration. These are distinguished by changes in the apparent behaviour of Si and Al with distance from the vein. In the zone immediately adjacent to the vein silica appears to be effectively immobile during the metasomatism while Al is added to the schists. In contrast, further from the vein Si is removed while aluminium appears to be immobile. in this light it appears more realistic to describe the silica as 'conserved' near the vein implying that it could have been mobile but that the net flux in has been balanced by the net flux out. Other major elements behave in a broadly similar way in both sections with the exception of Mg which seems to be removed from some sections adjacent to the vein but immobile in those further from the vein and Ti which seems to be added in some sections adjacent to the vein but immobile in those further from the vein.

The alteration also involves some significant gains and losses of minor elements. In particular both zones of alteration involve the addition of proportionately large quantities of Sr and Pb. In addition, the alteration adjacent to the vein may involve the addition of both V and Cu. Rb, Ba and Zn are all commonly lost during the alteration.

6.5 Relationship Between Metasomatism and Mineralogy in the Greyschists

The changes in bulk rock composition along metasomatic sections must be reflected in variations in mineralogy. This variation in turn must be the result of reactions between the original schist minerals and the infiltrating fluid. The most obvious result of these reactions is the generation of large volumes of lawsonite and therefore the dominant reactions are probably those generating the lawsonite. However, it is possible that other less volumetrically significant reactions also take place.

6.5.1 Possible Lawsonite Generating Reactions

Examination of geochemical variation in the metasomatised sections suggests a limited number of possible lawsonite generating reactions. In all the sections the alteration involves the loss of K and/or Na. This suggests that the reactions accompanying the alteration in these sections involve the breakdown of a phase or phases rich in one of these components.

The only K bearing phase in the schists is muscovite. Thus, in those sections showing K loss muscovite must be a reactant. The simplest reaction between a calcium-rich fluid and muscovite to generate lawsonite takes the form:-

$$3\ Ca^{2+} + 1\ \text{muscovite} + 1\ H_20 = 3\ \text{lawsonite} + 2\ K^+ + 4H^+$$

In volumetric terms this would suggest that 1 cm^3 of lawsonite results from the reaction of 0.46 cm^3 of muscovite. However, this assumes that the K-bearing mica is muscovite while all those analysed from the greyschist are phengitic. This would result in a slightly smaller muscovite to lawsonite ratio and the loss of some Si during the alteration. In addition the K mica contains small but significant amounts of Mg and Fe which would be liberated during the reaction. This might explain the loss of Mg evident in some sections.

The schist contain two Na bearing phases, paragonite and glaucophane. Where sections show a loss in Na one or both of these phases must be breaking down. An identical lawsonite generating reaction to that for muscovite can be written for paragonite.

$$3\ Ca^{2+} + 1\ \text{paragonite} + 1\ H_20 = 3\ \text{lawsonite} + 2\ Na^{+} + 4H^{+}$$

In volumetric terms this would suggest that production of 1 cm^3 lawsonite involves the reaction 0.46 cm^3 of paragonite. Probe analysis of paragonite composition shows that they contain minimal amounts of Fe and Mg and equal proportions of Si and Al so unlike muscovite its breakdown would not involve the loss of Fe, Mg or Si.

Identifying possible glaucophane breakdown reactions which are compatible with the characteristics of the alteration is more difficult. A simple reaction between a calcium-bearing fluid and glaucophane of the same as that found in the greyschists would require the loss of large quantities of Fe, Mg and Si.

$$32\ C^{a2+} + 32\ \text{glaucophane} + 32\ H_20 =$$
$$32\ \text{lawsonite} + 64\ Mg^{2+} + 32\ Fe^{2+} + 192\ Si^{4+}$$

However, none of the sections appear to record any loss of iron during the deformation. Thus if lawsonite is generated by a reaction involving glaucophane breakdown the Fe released must be retained in the system. This would be achieved if glaucophane breakdown was accompanied by the formation of chlorite. A possible reaction is

$$32\ Ca^{2+} + 32\ \text{glaucophane} + 8\ \text{muscovite} + 64\ H_20 =$$
$$32\ \text{lawsonite} + 10\ \text{chlorite} + 16\ K^{+} + 64\ Na^{+}\ 185\ Si^{4+}$$

Part or all of the muscovite could be replaced with paragonite. Such a reaction would explain the loss of Si and Na and/or K without requiring the loss of Fe. In volumetric terms it suggests that the formation of 1 cm^3 lawsonite will be accompanied by the production of 0.65 cm^3 of chlorite and the breakdown of 2.57 cm^3 of glaucophane and 0.35 cm^3 of muscovite.

While the above reactions might explain the loss of Na, K, and possibly Si they do not account for the addition of Al in the zone closest to the vein. The

simplest way to account for this is to assume that Ca and Al in the fluid combine directly with a source of Si to form lawsonite. The Si involved in the reaction may be in the form of quartz or Si released by other reactions. However, it must be locally sourced or the reaction would result in an increase in Si concentration with increasing alteration while the geochemical analysis shows that it is conserved within this zone. If the reaction involves quartz i.e.

$$1\ Ca^{2+} + 2\ Al^{3+} + 7\ \text{quartz} + 2\ H_2O = 1\ \text{lawsonite}$$

then the formation of 1 cm^3 lawsonite would result in the loss of 1.57 cm^3 quartz.

A combination of some or all of the above reactions would explain the growth of lawsonite and the attendant variations in bulk rock composition. In order to test their applicability the variation in mineralogy of the analysed sections was examined and the effects of the model reactions were quantitatively compared with the results of the geochemical analysis.

6.5.2 Mineralogical Variation During the Alteration

Thin-sections from the analysed samples were point-counted in an attempt to characterise and quantify the changes in mineralogy accompanying the metasomatism. However, it proved difficult to obtain meaningful results. The large size of the lawsonite porphyroblasts relative to other phases and the presence of compositional domains such as pressure shadows means that as large an area as possible must be point-counted in order to produce a true estimate of the modal proportions of the phases. However, the greyschists exhibit small-scale primary compositional layering with the thickness of individual layers varying considerably over small distances. Thus, if a thin-section covers more than one compositional layer it is difficult to distinguish variation in modal proportions of minerals due to the alteration from that due to primary compositional variation.

However, detailed point counting of thin-sections from sample 93-84 enabled some estimates of the mineralogical variation to be obtained. This sample appears to

be confined to a single, relatively homogenous horizon so primary compositional variation has no effect. Sections from the opposite ends of the sample were analysed to ensure that the differences in mineralogy would be as large as possible. As large an area of each section as possible was measured in order to minimise the effect of the size of lawsonite porphyroblasts and sub-thin section scale compositional domains. The results are summarised in Table 6.7.

	Section 93-84A	Section 93-84D
Glaucophane	31.9	30.7
Quartz	11.8	19.0
White mica	19.3	22.3
Lawsonite	24.3	15.5
Garnet	6.8	8.3
Sphene	1.1	1.2
Chlorite	1.7	1.3
Calcite	2.4	1.2
Others	0.3	0.1

Table 6.7 Results of point counting of thin sections from section 93-84.

The largest individual differences between the two samples are the gain in lawsonite and the loss of quartz. The latter suggests that the loss of silica during the alteration is the result of the dissolution of quartz rather than the release of Si during a reaction.

Significantly, the data shows that the concentration of glaucophane remains approximately constant and if anything increases slightly with increasing alteration. This coupled with the insignificant increase in chlorite concentration indicates that the lawsonite generating reaction does not involve the breakdown of glaucophane.

Given the loss of Na and K during the alteration this suggests that the lawsonite growth is the result of reactions between the infiltrating fluid and muscovite and paragonite. Such a mechanism is supported by the drop in concentration of mica with increasing lawsonite concentration. Comparison of the volumetric ratios of mica to lawsonite in the model reaction to the actual ration suggests that the loss of mica is slightly too small. However, at least part of the lawsonite must be the result of the reaction between Ca, Al and Si. This would adequately explain the discrepancy.

The involvement of mica in the lawsonite generating reaction is also reflected in the distribution of minerals on a finer scale. By subdividing the point counting data for each of the thin sections it is possible compare the composition of sub-thin-section scale domains. It is clear that in both 93-84A and 93-84B areas with the highest concentration of lawsonite also have the lowest concentrations of mica (Figure 6.23a and Figure 6.24a). This is consistent with models of porphyroblasts growth that suggests that they will be surrounded by regions depleted in the phases which breakdown during their formation. As would be expected the effect is more pronounced in 93-84 where the schists are more strongly altered. In contrast, the concentration of glaucophane appears to independent of lawsonite concentration in both sections (Figure 6.23b and Figure 6.24b). This is consistent with it being inert during the lawsonite generating reaction. The behaviour of quartz appears to be different in the sections. In 93-84A its concentration seems to be approximately constant with varying lawsonite concentration and by inference it is not involved in the reaction (Figure 6.23c). However, in 93-84D the concentration of quartz appears to decrease with increasing lawsonite concentration (Figure 6.24c). This is consistent with the loss of quartz evident from 93-84D to 93-84A and the loss of silica during the first stage of the alteration. However, if this is a real effect one would expect it to be reflected in the distribution of quartz in sample 93-84D.

Unfortunately, while it is possible to measure the overall change in concentration of mica by point counting it is not possible to distinguish between

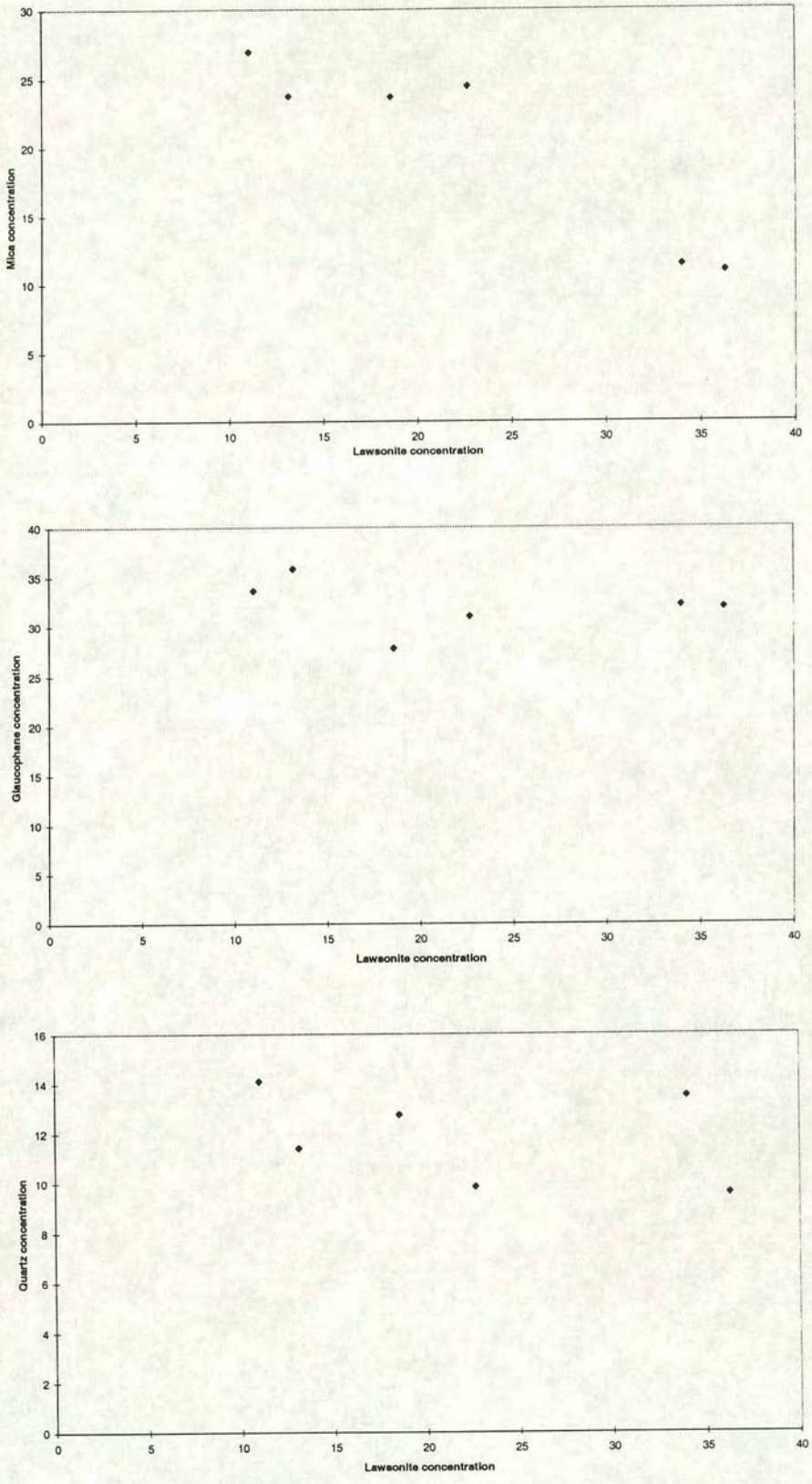

Figure 6.23 Plots illustrating the variation in concentration of other minerals with varying concentration of lawsonite in sub-thin-section scale domains of a section from 93-84A.

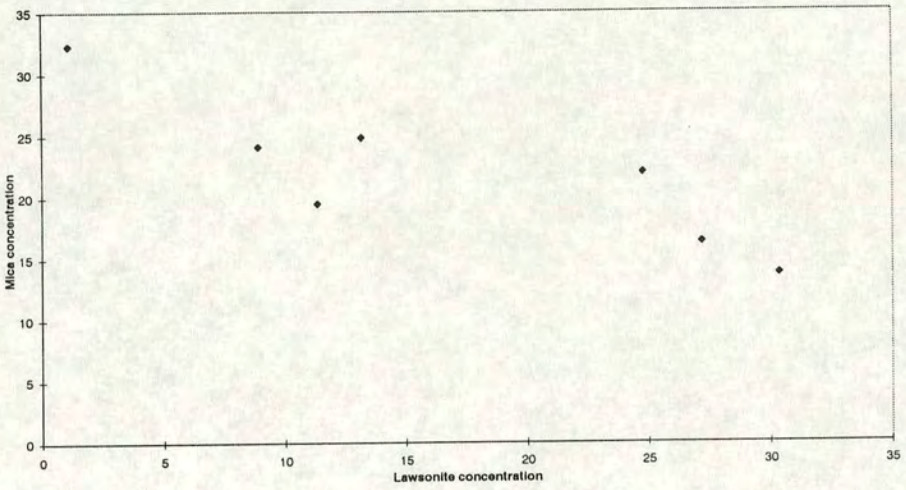

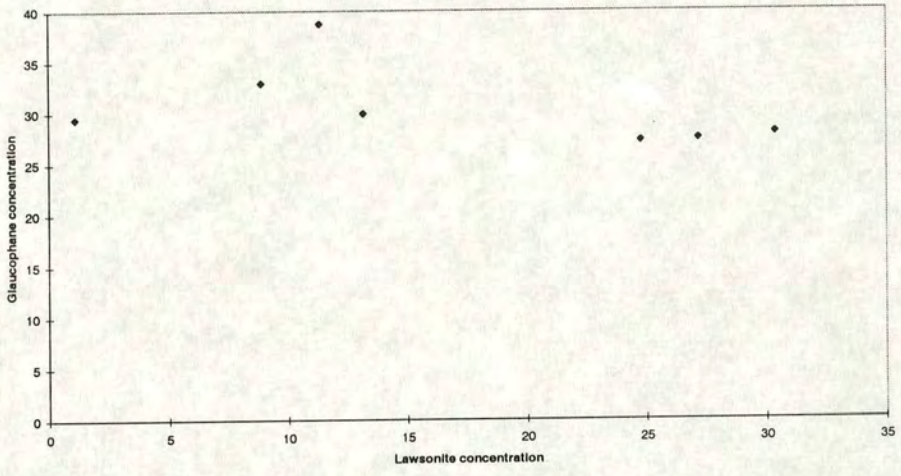

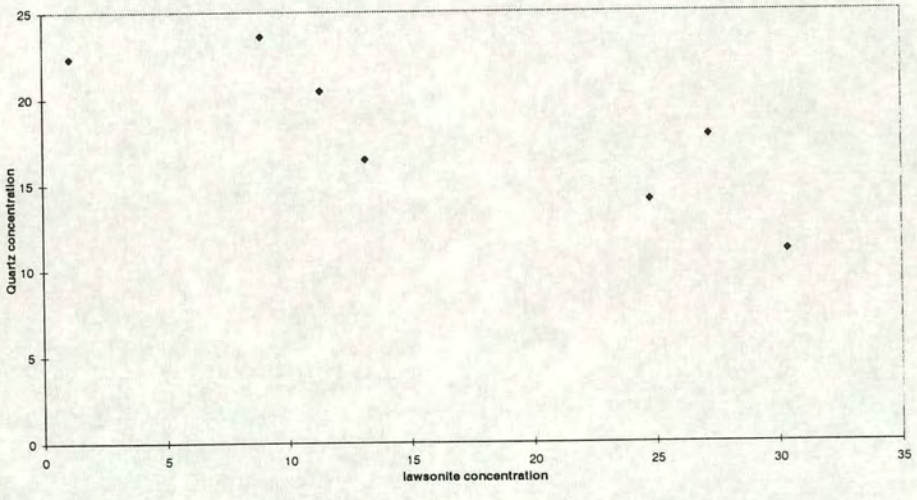

Figure 6.24 Plots illustrating the variation in concentration of other minerals with varying concentration of lawsonite in sub-thin-section scale domains of a section from 93-84D.

muscovite and paragonite. An attempt to stain slides proved un-successful. XRD. confirms that the schists contain paragonite. However, quantitative analysis by this method is difficult. It is further complicated by the presence of paragonite in the lawsonite pseudomorphs. Thus, it appears impossible to determine the relative changes in concentration of paragonite and muscovite during the alteration.

6.5.3 Synthesis

The changes in composition adjacent to the veins is due to interaction between the schists and the infiltrating fluid with the major mineralogical result being the growth of lawsonite. However, while the growth of lawsonite continues throughout the metasomatised zone the nature of the metasomatism changes. This suggests in turn that the nature of the reaction(s) between the fluid and the schists changes.

In the schists further from the vein the alteration is dominated by the addition of Ca and the loss of Si and K and/or Na. Point counting suggests that the lawsonite grows at the expense of white mica thus the gain in Ca and loss of alkalis is attributed to a reaction between the Ca-rich fluid and paragonite and muscovite of the form :

$3\ Ca^{2+} + 1$ muscovite $+ 1\ H_20 = 3$ lawsonite $+ 2\ K^+$

$3\ Ca^{2+} + 1$ paragonite $+ 1\ H_20 = 3$ lawsonite $+ 2\ Na^+$

Unfortunately no relevant activity plots were found for the PT conditions of metamorphism. However, the reactions are consistent with the variation in mineral stability with Ca and K activity in a coexisting fluid at similar pressures but lower temperatures.

Loss of silica during the alteration is ascribed to the loss of quartz indicated by the point counting. This is probably simply the result of dissolution of quartz in the infiltrating fluid which suggests that it is undersaturated in silica. similarly the loss of P must be due to the dissolution of apatite, presumably because the fluid is

undersaturated in P. Ca liberated in this process is assumed to be consumed by the lawsonite generating reaction.

In the zone immediately adjacent to the vein Ca and Al are added to the schists and P and Na and/or K are lost but Si appears to be immobile. Loss of alkalis suggests that the mica breakdown reactions also occur in this zone and account for at least part of the added. Similarly, the loss of P suggests that the dissolution of P continues.

However, the addition of Al indicates that a further reaction must be taking place. The only phase which appears to increase in concentration during the alteration is lawsonite and this must be the destination for the Al added. Thus it is suggested additional lawsonite growth is caused by the reaction

$$1\ Ca^{2+} + 2\ Al^{3+} + 7\ SiO_2 + 2\ H_2O = 1\ \text{lawsonite}$$

It seems likely that the source of silica is that dissolved in the fluid and the growth of lawsonite by this process is essentially due to its precipitation from the fluid.

Furthermore, the dissolution of quartz must also occur in this zone or Si would be added during the alteration. Instead the dissolution of quartz must be approximately balanced by the fixing of Si in lawsonite thus resulting in the apparent immobility of Si.

Both Mn and Ti show some degree of addition in some sections. The addition of Ti is probably explained by limited growth of sphene however the addition of Mn is more problematical. The majority of manganese is concentrated in the garnets but there is no evidence of garnet growth during the metasomatism.

Of the minor elements, Sr and Pb readily substitute for Ca and are probably present in the lawsonites. It is also possible that the Cu substitutes for Ca. V will substitute for Al and it is apparently only added in those zones of the alteration in which al is added. Rb and Ba substitute for K and there loss is clearly related to the

loss of this element. Similarly the loss of zinc is limited to those sections showing a loss of Mg.

6.5.4 Quantitative Comparison of Compositional Data with Possible Lawsonite Generating Reactions

Point counting data appears to confirm that much of the vein-related lawsonite growth is the result of a reaction between the infiltrating fluid and mica. During the second stage of the alteration this must be accompanied by a further reaction in order to explain the gain in Al. As noted above it is possible to write fairly simple equations for such reactions (section 6.5.1). These in turn provide simple predictions for the amount of Na and/or K which should be lost due to the addition of a given amount of Ca and Al. Thus, the reaction of 3 moles of CaO with mica will release 1 mole of K_2O or Na_2O. Similarly, the addition of 1 mole of Al_2O_3 to the schists in the form of lawsonite requires reaction the addition of 1 mole of CaO.

The isocon analysis should provide a measure of the absolute amount of each component added or removed during the alteration in a particular section. Thus, it is possible to compare the mass changes predicted by the model reactions with those observed. This is done by comparing the actual amount of Ca added with the amount of Ca addition consistent with the gain in Al and loss of K and / or Na for each section. The results are summarised in table 6.8.

Examination of the data clearly indicates that there are large differences between the model and observed data for the vast majority of the sections. In some cases the amount of Ca added is half or double that predicted by the addition of Al and loss of Na and K.

The lack of consistency between the observed and predicted results may by due to either an incorrect choice of reactions or uncertainties in the results of the isocon analysis. However, if the former were true one might expect the error between

Section	Amount of Ca added (mol)	Ca consumed by reaction with Al (mol)	Ca consumed by reaction with Mu(mol)	Ca consumed by reaction with Pg(mol)	Discrepancy in amount of Ca (mol)
92-20 S1-6 to 2	0.024	0.023	0	0.0276	-0.0266
92-20 S1-6 to 10	0.04	0.023	0.0192	0.26	-0.0282
92-20 S2-8 to 2	0.053	0.041	0	0	+0.012
92-20 S2-8 to 13	0.038	0.037	0	0	+0.001
93-84B to A	0.044	0.017	0.0132	0	+0.0138
93-84C to D	0.00963	0	0.0069	0.0132	-0.01047
coresection 93-62 to 63	0.0059	0.0028	0.006	0.00234	-0.00524
coresection 93-56 to 62					

Table 6.8 Comparison of the gain in Ca content measured and that predicted by the loss of other elements if the inferred reactions are correct.

the observed and predicted results to be more regular. Instead it appears to be random in nature. Furthermore it is difficult to suggest any other possible reactions given the relatively limited number of possible reactions and the mineralogical variation identified by point counting.

Instead it seems far more likely that the discrepancy is due to uncertainties associated with the isocon analysis. As noted above this may be due largely to the pre-metasomatic compositional variation within the sections. In addition there will may be some errors due to uncertainty in the positioning of the isocons. Thus, while the isocon analysis seems to provide a good qualitative measure of the relative mass changes during the alteration uncertainties in the method mean that it cannot be used for accurate quantitative analysis.

6.6 Section From Margin of Gria Spilia Body

In order to assess changes of composition accompanying lawsonite growth in the margin of the Gria Spilia Meta-igneous Body (G.S.M.B) a 20 cm long section perpendicular to its contact with the schists was analysed. The section was sub-divided into five samples with 92-160A closest to the schist contact and 92-160E furthest from it. However, sample 92-160A contains a portion of the glaucophane-rich metasomatic rind intermittently present along the contact between the schists and the G.S.M.B. This significantly affects the composition of the sample and means that the changes in concentration of the major elements between sample A and B do not conform to the trends evident in the rest of the section. Therefore the sample was ignored during the quantitative analysis of the compositional change and an isocon plot was produced by plotting 92-160B against 92-160E (Figure 6.25).

Preliminary examination of the isocon plot suggests that the alteration is the result of the addition of Ca, K, Rb and Pb and the loss of Na. The data points for all other major elements plot over a fairly narrow range and based on this distribution alone appear to be immobile during the alteration. This also agrees well with the

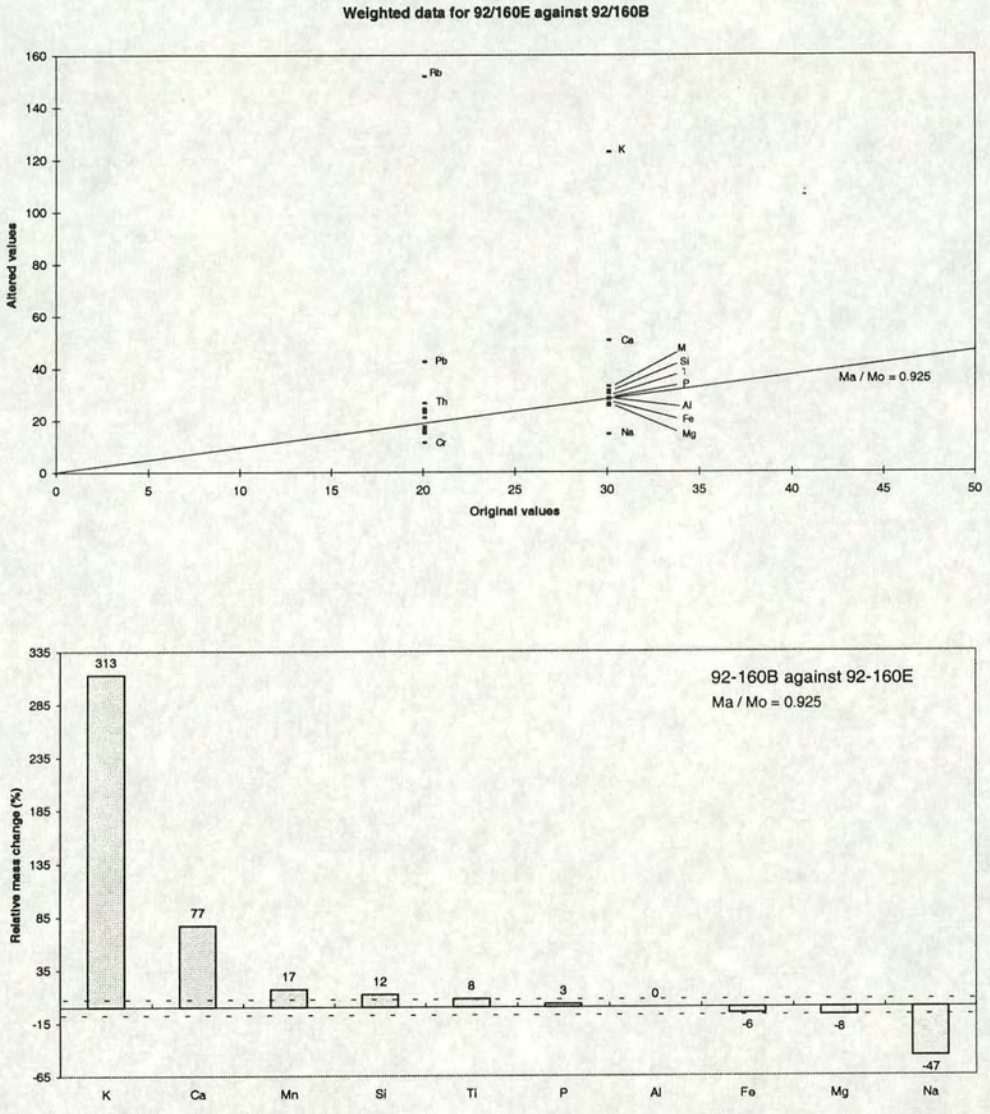

Figure 6.25 (a) Isocon plot used to determine the relative losses and gains of components between samples 92-160B and 92-160E. The isocon shown is based on the assumption Fe, Mg, and Al, are immobile. (b) Histogram illustrating the relative mass change of the major elements.

distribution of the data points for the minor elements. However, examination of plots showing the variation in concentration of the major elements with distance along the section (Figure 6.26) shows that while Al, Fe and Mg all display regular decreases in concentration with increasing alteration, Si and Mn appear to display generally increasing trends with increasing alteration. The ratios of both Si and Mn to Fe, Mg and Al all increase with increasing alteration. On these grounds it is impossible that both these groups of elements are immobile during the metasomatism. Instead either Si and Mn must be added or Fe, Mg and Al lost. There is no conclusive evidence to support either model. However, taking into account the characteristics of the alteration in the greyschists it seems more likely that Fe is immobile during the alteration. Thus the overall alteration as indicated by the isocon plots involves the addition of K, Ca, Si and Mn and the loss of Na with an overall gain in mass of ~2%.

In the greyschist the nature of the alteration varies with distance from the vein. However, there is no evidence that this is the case in margin of the G.S.M.B. The relative changes in mass between samples 92-160C and 92-160B are almost identical in nature to those evident in the rest of the section.

The most startling difference between the alteration evident in the greyschists and that identified in the margin of the G.S.M.B. is the apparent addition of very large amounts of K. However, it appears most likely that this is the result of addition of K during the lawsonite pseudomorphing event. Thus, it is unrelated to the metasomatism accompanying the growth of the lawsonite. However, it does obscure any loss of K which may be associated with lawsonite-generating reaction.

Attempts to measure changes in modal mineralogy accompanying the alteration and thus identify possible reactions proved unsuccessful.

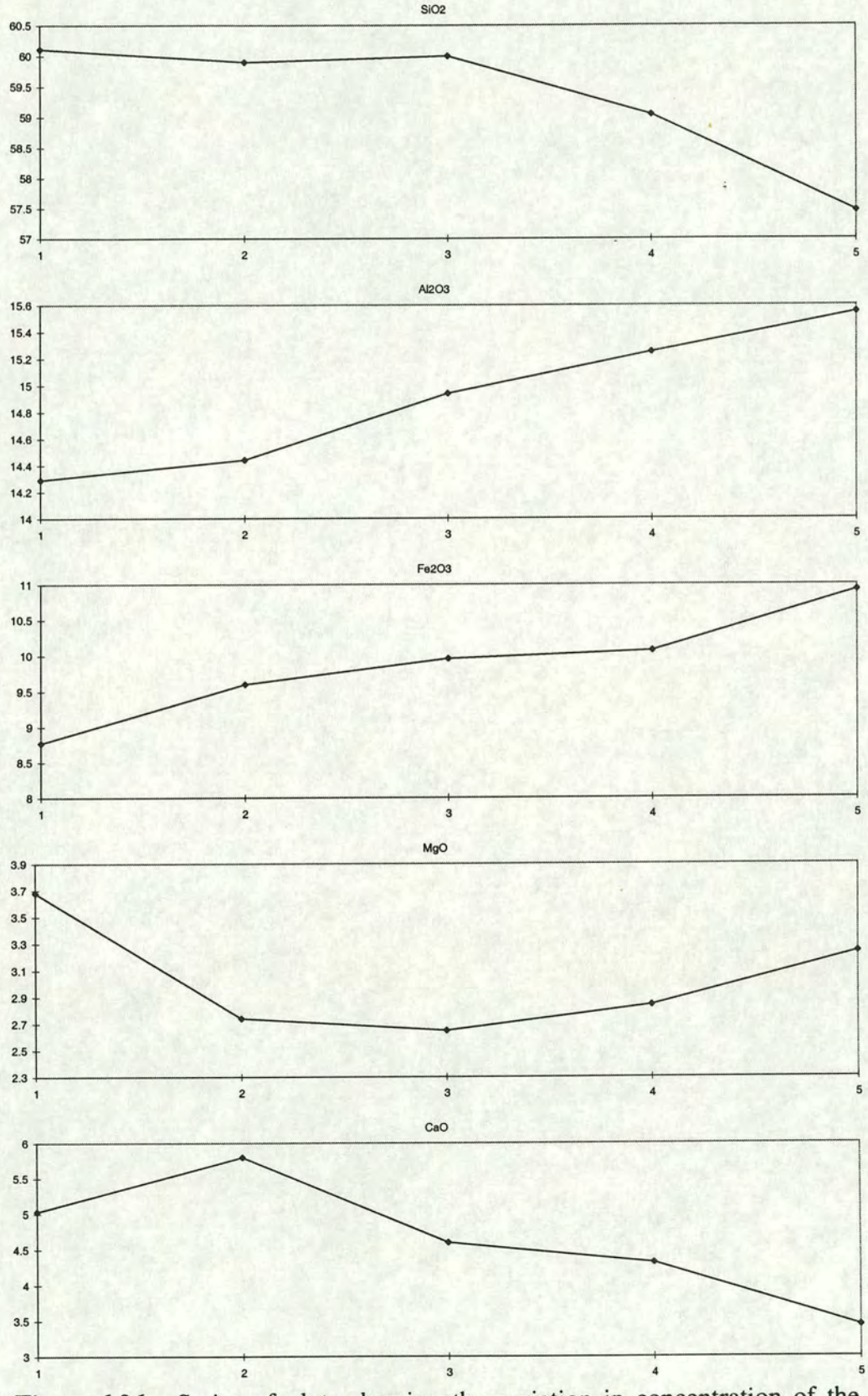

Figure 6.26a Series of plots showing the variation in concentration of the major elements within samples 92-160 A to E with increasing distance from the schists / gneiss contact.

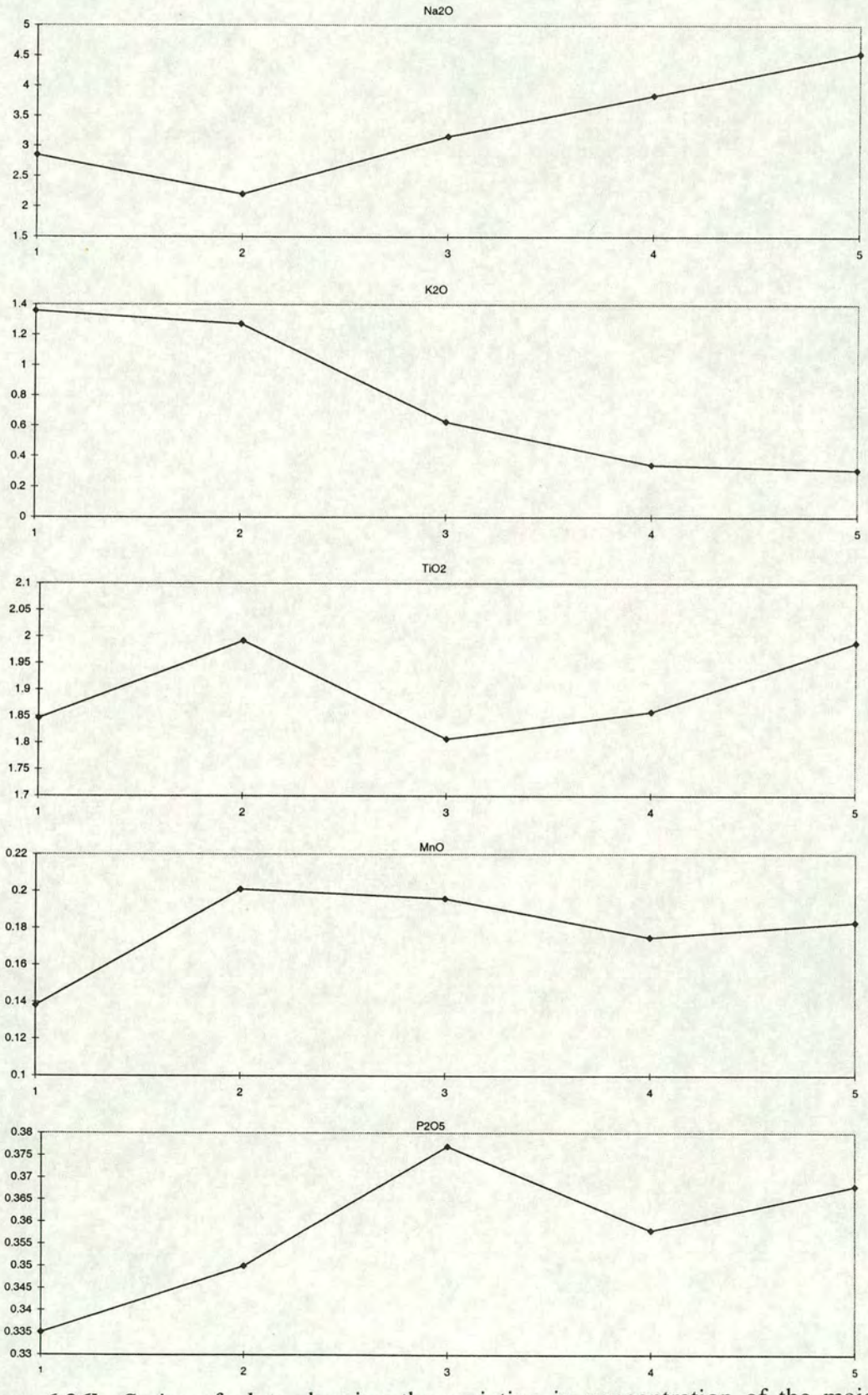

Figure 6.26b Series of plots showing the variation in concentration of the major elements within samples 92-160 A to E with increasing distance from the schists / gneiss contact.

6.7 Conclusions

1) Vein-related lawsonite growth in both the greyschists and the margin of the GSMB is the result of major element metasomatism.

2) In the greyschists this alteration involves two processes. The first is a reaction between the fluid and micas within the wall rocks to produce lawsonite. This results in the addition of Ca to the altered schists and the loss of alkalis to the fluid. It is accompanied by the loss of Si due to dissolution of quartz. Overall it results in a loss of mass. In a zone immediately adjacent to the vein this reactions is apparently accompanied by the direct precipitation of lawsonite. This results in the addition of Ca and Al to the schist. Within the zone where direct precipitation occurs the Si content of the schists is conserved probably due to an approximate balance between the amount removed by the dissolution of quartz and that added by the precipitation of lawsonite.

The metasomatism in the margin of the GSMB is the result of a single process. it involves the addition of Ca, Si and Mn and the loss of Na. It is possible that it also involves the loss of K however its behaviour is masked by a large gain in K associated with the lawsonite pseudomorphing event. Overall the alteration results in a gain in mass.

CHAPTER 7

STABLE ISOTOPIC ANALYSIS OF THE INFILTRATION EVENT

7.1 Introduction

Numerous fluid-rock interaction studies have shown that stable isotopic analysis is a powerful tool for the investigation fluid infiltration during regional metamorphism. The scale of isotopic equilibrium may provide a measure of the scale of fluid transport. Identification of isotopic fronts allows direct measurement of the magnitude of fluid fluxes. The isotopic composition of the infiltrating fluid may indicate its source.

Examination of the distribution of lawsonite in the greyschists indicates that the highest concentrations are related to a fluid infiltration event, traces of which are evident as syn-deformational quartz veins. Geochemical analysis confirms this relationship and shows that it is the result of major element metasomatism which effects the schists at least 40 cm from the contact with the vein. However, neither method reveals the true extent of the infiltration, nor how much of the lawsonite that is not clearly spatially related to veins has grown as a result of metasomatic alteration.

Investigation of stable isotopic variation in the greyschists and veins might allow the full extent of the lawsonite-generating fluid infiltration event to be estimated. In particular, it may provide a method of estimating how much of the lawsonite growth in the greyschists can be attributed to the infiltration In addition, it could provide information on fluid/rock ratios and the source of the infiltrating fluid.

7.2 Theoretical basis for stable isotopic analysis of fluid infiltration

An infiltrating fluid will exchange stable isotopes with those parts of the country rock with which it comes into contact until the rock and fluid are in isotopic equilibrium. The extent to which this process alters the stable isotopic composition of the infiltrated rocks is controlled by three factors :-

- the fluid/rock ratio
- the difference between the isotopic composition of the infiltrating fluid and that of the rocks it infiltrates.
- the nature of the pathways along which the fluid flows.

An understanding of the details of this control allows information about the nature of a fluid infiltration event to be deduced from the variation of stable isotopic composition within the infiltrated unit / terrane / area.

(A) Fluid Rock ratio

If the volume of infiltrating fluid is small relative to the volume of rock with which it interacts rocks then the rocks may buffer the isotopic composition of the fluid. In such cases, the infiltrated rocks will retain their original isotopic compositions and it will therefore be impossible to distinguish them from their uninfiltrated counterparts using stable isotopic analysis. However, if the fluid rock ratios are sufficiently large the stable isotopic exchange will result in a shift in the stable isotopic compositions from their initial values toward that of the fluid. In such circumstances it may be possible to distinguish infiltrated rocks from uninfiltrated rocks on the basis of their stable isotopic compositions.

(B) Composition of fluid

The fluid/rock ratio necessary to produce a measurable shift in the stable isotopic composition of infiltrated rocks is dependent on the difference between their initial isotopic composition and that of the infiltrating fluid. If the difference is large relatively small fluid/rock ratios may result in significant shifts in the stable isotopic composition. However, if the difference is small much larger fluid/rock ratios are required to produce any measurable change. Even if the rocks completely re-equilibrate with such a fluid the small difference in compositions mean it may be difficult to distinguish isotopically the infiltrated rocks from their uninfiltrated counterparts.

(C) Pattern of fluid flow

The pattern of fluid flow within an infiltrated body is controlled by the nature of the permeability. This is typically defined with reference to two widely used concepts, pervasive flow and channelised flow. However, care must be taken in when applying these terms, particularly in relation to the scale of observation (see Kohn & Valley 1994, Oliver 1996 for discussion).

In this study pervasive flow is used to describe fluid transport along a network of grain edges / boundaries and / or microcracks / microveins. In such a fluid regime the infiltrating fluid will interact with all parts of the rock volume. If fluid rock ratios are sufficiently large this will result in complete homogenisation of stable isotopic values within the infiltrated area.

Channelised fluid flow occurs when variation in permeability causes segregation of the infiltrating fluid into discrete zones such that some parts of an infiltrated area interact with an externally derived fluid while others do not. Within those parts of an area that do interact with the fluid stable isotopic values may be completely homogenised. However, the uninfiltrated parts will retain their original isotopic values and therefore and primary isotopic heterogeneity. Thus it may be possible to distinguish those parts of a terrane that have been infiltrated from those that have not on the basis of their isotopic heterogeneity.

Channelisation may be evident on a range of scales. Typical fluid channels include veins, lithological contacts, specific lithological layers and shear zones. It is crucial to note that the distinction between channelised and pervasive flow is largely a question of scale. While the fluid infiltration event in a particular terrane may be channelised on a large scale smaller parts of the area may experience pervasive flow.

7.3 Application of stable isotopic analysis to the lawsonite-generating event

As noted above the pattern of stable isotopic alteration resulting form an infiltration event is critically dependent on the pattern of fluid flow, fluid rock ratios and the difference in composition between the isotopic composition infiltrating fluid and that of the rock it infiltrates. Some inferences about the pattern of fluid flow during the lawsonite generating event can be already be drawn from the observations from the vein outcrops documented in chapter 5.

The presence of quartz veins clearly indicates that much of the fluid flow during the lawsonite-generating event was focused along discrete fractures. However, the alteration of the adjacent schists indicates that at least some of the wall rocks were pervasively infiltrated by the fluid. The extent of the alteration varies considerably in different compositional horizons. In some of the layers rocks 40 cm from the vein schist / contact have clearly been altered by the fluid. In others lawsonite growth is limited to the vein schist contact and the layers are essentially unaltered. As these layers have an identical mineralogy to the altered layers, including abundant mica, the lack of alteration implies that they have experienced a lower fluid flux although not necessarily no infiltartion at all. This suggests that there was significant variation in the permeability of the schists to the vein fluid and that the fluid infiltration was channelised on the scale of individual compositional horizons.

If the volume of fluid entering the schists from the vein were large and the oxygen isotopic composition of the vein fluid was sufficiently different to that of the infiltrated schists one would expect the metasomatism to be accompanied by a recognisable shift in the stable isotopic composition of the schists. Like the metasomatism the extent of this oxygen isotopic alteration would be influenced by the variation permeability. However, it seems unlikely that the limit of the oxygen isotopic alteration will exactly match the limit of the metasomatism within a particular unit. Different types of alteration fronts driven by the same fluid may travel

at significantly different velocities (Bickle and Baker 1989). If the isotopic front travelled at a faster velocity than the metasomatism then it might be possible to trace the effects of the fluid infiltration on a larger scale than is possible using the metasomatism alone. Even if schists were not metasomatised by the fluid they might preserve a record of their infiltration. However, it should be noted that this would still only place a lower limit on the extent of the infiltration as once the fluid has reached isotopic equilibrium with the schists it can continue to infiltrate without leaving an isotopic signature. If the oxygen isotopic signature of the infiltration were sufficiently distinct it might also be possible to identify units containing vein-related lawsonite which is not obviously related to quartz veins on the basis of their oxygen isotopic composition.

However, if the volume of fluid entering the schists from the vein were small and/or the oxygen isotopic composition of the vein fluid was similar to that of the schists then the infiltration may not have caused any resetting of oxygen stable isotopic compositions. If this were the case even the metasomatised schists would retain their original isotopic compositions and no widespread homogenisation of stable isotopic values would be observed. As a result the pattern of stable isotopic composition within the schists would provide no insight into the extent of the lawsonite generating fluid infiltration event.

7.4 Sample preparation and analytical method

Given the lack of carbonate in the veins and schists the simplest method for assessing stable isotopic variation in the greyschists is to analyse quartz separates from both schists and veins.

Samples for analysis were crushed by hand using a percussion mortar and sieved to obtain a grain size of approximately 200 microns. Other minerals were separated from the quartz by repeated use of a magnetic separator. The quartz fraction was treated overnight with conc. HCl to ensure that any carbonate present

was destroyed. The samples were then rinsed with deionized water and dried. Finally, all samples were hand picked to remove any remaining impurities.

Samples were analysed at the Scottish Universities Reactor and Research Centre, East Kilbride. Oxygen was extracted using ClF_3 and converted to CO2 by reaction with a heated carbon rod. The oxygen isotopic composition was then measured with a VGR SIRA 10 mass spectrometer. Every fifth sample was duplicated. The maximum observed error was 0.3 per mil. Error bars consistent with this shown on all plots.

7.5 Statistical analysis

Given the small size of most of the data sets meaningful statistical analysis of the data was often impossible. Where mention is made of the use of a statistical test this refers to the Kruskal-Wallis test of one way variance described on page 79 of Cheeney (1983).

7.6 Results of the Isotopic Analysis

The results of the isotopic analysis are summarised in Table 7.1, and considered in more detail in the following sections.

Table 7.1 Data from oxygen isotope analysis of quartz separates from a range of schists and veins from the greyschists.

Sample Type	**Sample No**	$\delta^{18}O(^{o}/_{oo})$
C.T.O. samples		
Planar quartz vein	92-23	18.2
	92-28AQ	18.4
	92-24A	18.1
S1 \\ quartz veins	92-25A	17.7
	92-25B	17.2
	93-73	17.9
Lawsonite-rich schists	92-28A	18.6
	92-28C	18.7
	92-28E	18.6
Lawsonite-poor schists	92-30A	18.1
	92-30B	18.4
	92-30C	18.4
Core section	92-56	18.3
	92-57	18.6
	92-58	19.0
	92-59	18.3
	92-60	18.6
	92-61	18.5
	92-62	18.8

Sample Type	Sample No	$\delta^{18}O(^{o}/_{oo})$
Overhanging Outcrop		
Planar vein	93-93A	17.2
	93-93B	17.0
Horizon 1	92-63	18.7
	92-114	19.5
	92-100	19.1
Horizon 2	92-57	18.2
	92-96	17.7

Sample Type	Sample No	$\delta^{18}O(^{o}/_{oo})$
Other LGSU samples		
Margin of the Gria Spilia Body	92-160B	17.2
	92-160D	16.3
	92-160E	16.4
Graphitic schists	92-2	18.1
	92-3	18.4
	92-4	18.9
	92-6	18.9
	92-8	17.8
	92-35A	18.2
	92-45	17.9
	92-46	18.8
	92-50	18.3
	92-51A	18.6
	92-74	18.1
	92-131	17.6
	92-132	17.7
	92-133	17.2
	92-134	18.1
	92-135	18.3
Calc silicates	92-39	18.2
	92-40	18.2
	92-40Q	18.3
	92-41	17.8
	92-43	18.0

Sample Type	Sample No	$\delta^{18}O(^{o}/_{oo})$
U.G.S.U Samples		
Lawsonite + Quartz Bodies	93-6	19.9
	93-12	19.1
	93-19	18.5
	93-20	19.2
	93-52	19.1
	93-54	18.9
	93-LD4	18.2
	93-LD7	19.7
Quartz Absent Mega Boudins	93-LDL	18.3
	93-LDU	19.3
	93-43	19.0
	93-LD1	19.5
Graphitic schists		
	92-38	17.8
	93-51	18.6
	92-173	18.6
	92-175	18.2
	92-176	18.1
	92-177	18.8

7.6.1 Cedar Tree Outcrop

Initially the study focused on the Cedar Tree Outcrop in the L.G.S.U. As with geochemical analysis this was because this outcrop displays the clearest relationships between the growth of the lawsonite and veining and it has experienced relatively little post-metasomatic deformation and no post-blueschist alteration. Five groups of samples were analysed. Their distribution is illustrated in figure 7.1

I. *Core section.* The geochemistry of this section is described in the previous chapter. It is composed of a series of core samples drilled perpendicular to compositional layering which together form a section stretching 40 cm from the vein schist contact. The geochemical analyses indicate that it has been altered during the vein-related metasomatism and has therefore been infiltrated by the lawsonite-generating fluid.

II. *Altered horizon* These samples were taken from a single compositional layer and form a section perpendicular to the planar vein. The concentration of lawsonite shows a regular decrease with increasing distance from the vein / schist contact indicating that the section has been affected by the vein-related metasomatism and has therefore been infiltrated.

III. *Unaltered horizon* As in the case of the altered horizon these samples are taken from a single compositional layer. However, in contrast, the schists are very lawsonite-poor and geochemical analysis shows that they are unaffected by the metasomatism. These samples may or may not have been infiltrated by the fluid.

IV. *Planar vein.* These were samples taken from the planar vein itself.

The results of the analysis are summarised in figure 7.2

Taking into account the estimated analytical uncertainties the values obtained from the groups of samples labelled unaltered schists and altered schists suggest that the stable isotopic compositions of individual schist layers are constant. In particular, there is no detectable systematic variation in composition with distance away from the vein over the length scale of the sections.

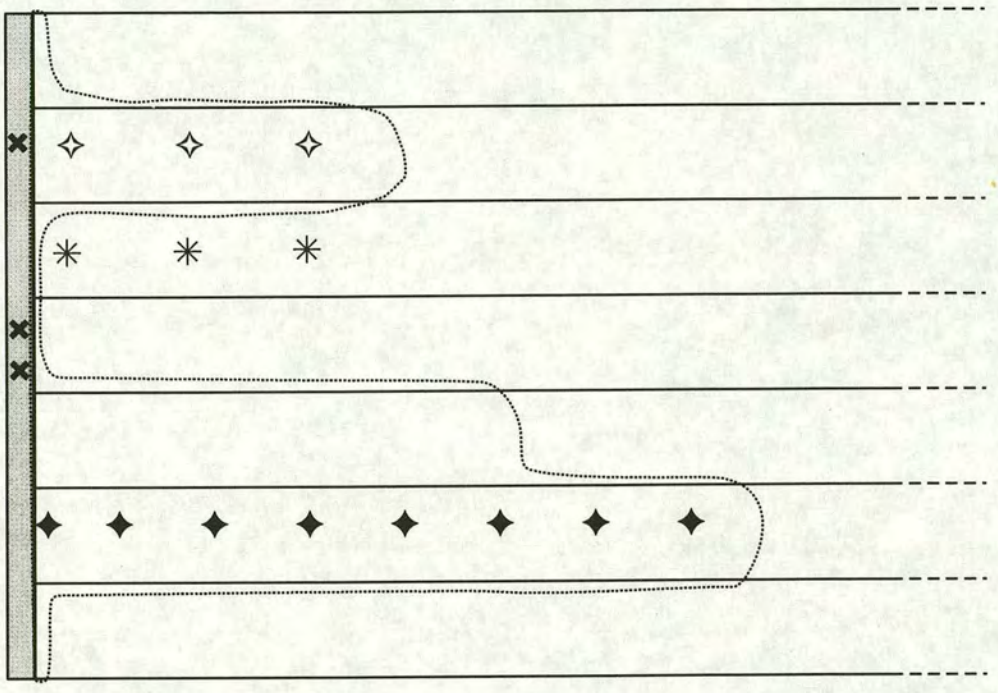

Key

- ✳ **Samples of unaltered horizon**
- ✧ **Samples of altered horizon**
- ✦ **Core-section samples**
- × **Samples of planar quartz vein**
- **Quartz vein**
- **Limit of metasomatism**

Figure 7.1 Schematic diagram showing the distribution of samples from the C.T.O. relative to the planar quartz veins. Not drawn to exact scale. Approximate dimensions of the diagram 75cm by 75cm.

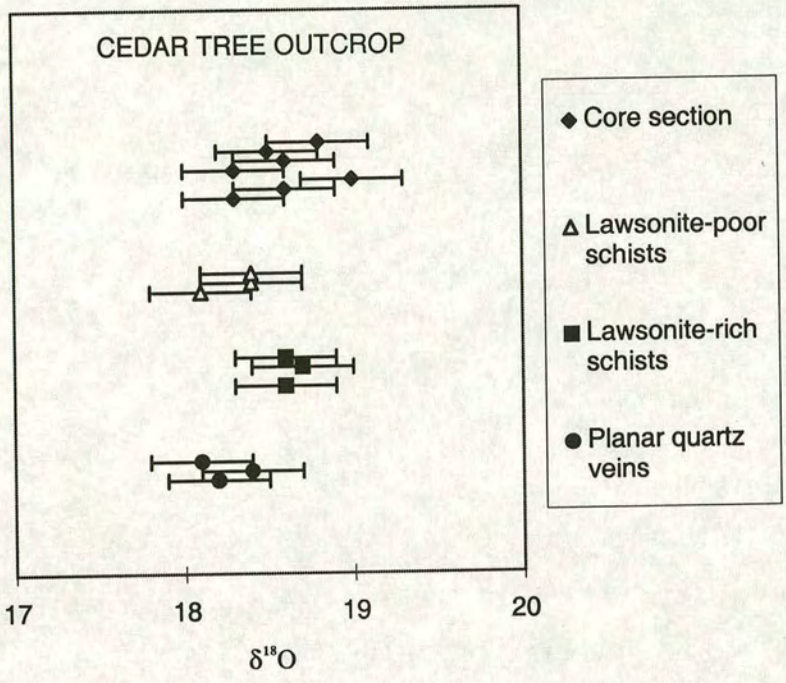

Figure 7.2 Plot showing the variation in oxygen stable isotopic composition displayed by quartz separates from samples from the Cedar Tree Outcrop.

The values obtained from the core section show a larger range which falls just outside that attributable to analytical error. However, once again there is no systematic variation with distance from the vein/schist contact. On these grounds it does not appear possible that the variation is a result of the infiltration. Instead the greater variation relative to the other sections may be attributed to the nature of the samples. Unlike the other two sections analysed the core section samples are cut perpendicular to layering and thus cross-cut a number of fine scale compositional layers. As the section is discontinuous it is difficult to ensure that every sample cuts exactly the same section through the lithological layering. This might explain the variation but would indicate that there is considerable variation in isotopic composition between adjacent compositional layers on a fine scale.

As might be expected simple statistical analysis indicates that there is no significant difference in isotopic composition between the two metasomatised sections but that the isotopic composition of both sections is significantly different from that of the un-metasomatised layer. However, the values obtained from these sections when compared with those obtained from the planar vein do not appear consistent with the hypothesis that the oxygen isotopes in the schists have re-equilibrated with the vein fluid. The values obtained from the vein are significantly different from those obtained from the metasomatised schists but not significantly different from those obtained from the un-metasomatised layer. If the metasomatised schists had re-equilibrated with the vein fluid then their oxygen isotopic composition should be that same as the vein. Instead it is the values obtained from the un-metasomatised schists that are indistinguishable from those in the vein. Taken in isolation the variation might suggest that the oxygen isotopes in the un-metasomatised layer have re-equilibrated with the vein fluid while those in the metasomatised schists have not. However, it is clearly impossible for the unmetasomatised schists to have been infiltrated by the vein fluid while the metasomatised schists were not.

Thus it seems that the only possible model of the fluid infiltration compatible with the isotopic data form the C.T.O. is one in which the schists buffer the composition of the fluid. Thus, the isotopic values obtained from the schists must represent original sedimentary values and the similarity between the value for the unaltered schists and the lawsonite-generating vein is coincidental. This would imply that the fluid fluxes responsible for the lawsonite-generating event are small and / or that the isotopic composition of the infiltrating fluid is close to that of the schists.

7.6.2 Over-hanging outcrop

Three groups of samples were analysed from the OHO with a view to comparing the isotopic composition of the planar lawsonite-generating vein and earlier deformed lawsonite-generating veins and assessing the degree of isotopic equilibrium between the veins and the schists. Their distribution is illustrated in figure 7.3.

Two groups were taken from the upper of the two domains containing discontinuous quartz bodies surrounded by lawsonite-rich schists which are interpreted as strongly deformed lawsonite generating veins (section 5.2.2). The most prominent features of the domain are two horizons of quartz boudins oriented parallel to layering and extending the width of the face perpendicular to the planar vein. It is unclear whether these represent the deformed remains of two separate veins or they are two portions of the same vein. A set of samples was analysed for each horizon. Three samples were taken from the lower one (horizon 1 in figure 7.3), a sample of schist adjacent to the planar vein and a sample of schist and a sample of the vein several metres away from the planar vein. Two samples were taken from the upper horizon (horizon 2 in figure 7.3), a sample of schist adjacent to the planar vein and a sample of the vein several metres from the planar vein. The remaining group of samples was taken from a portion of the planar vein adhering to the face of the outcrop. The values obtained are summarised in figure 7.4.

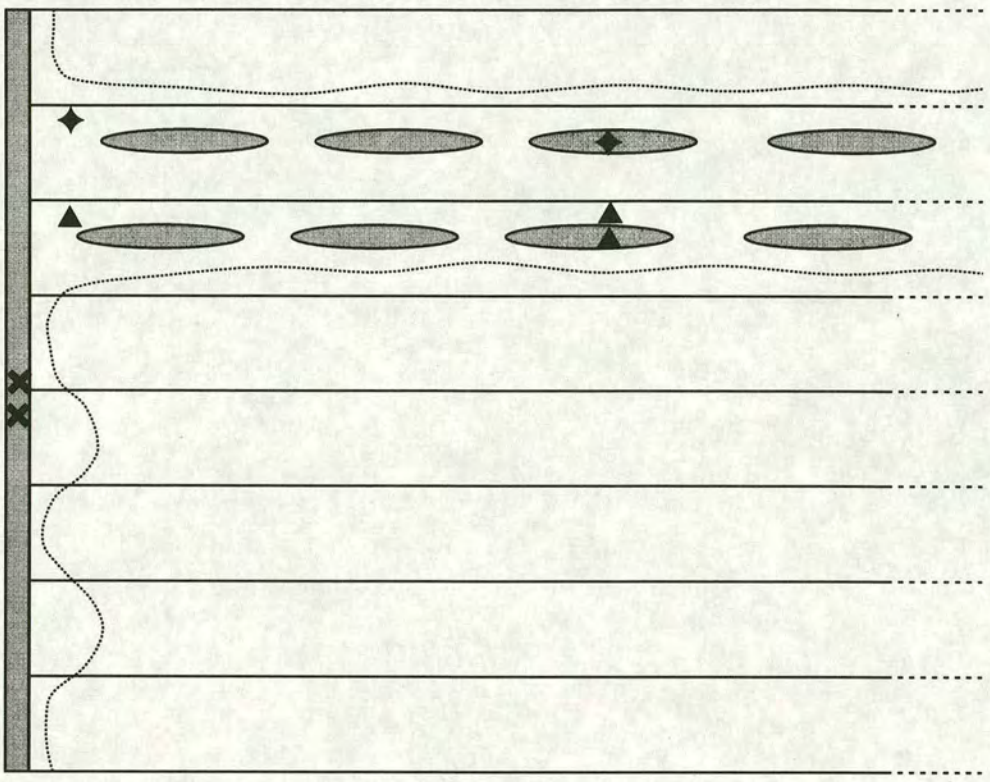

Key

✖ **Samples of planar quartz vein**

▲ **Samples of horizon 1**

✦ **Samples of horizon 2**

Quartz veins

Limit of metasomatism

Figure 7.3 Schematic diagram showing the distribution of samples taken from the Overhanging Outcrop relative to the planar quartz vein and lawsonite-rich horizons. Not drawn to exact scale. Approximate dimensions of diagram 4m by 4m.

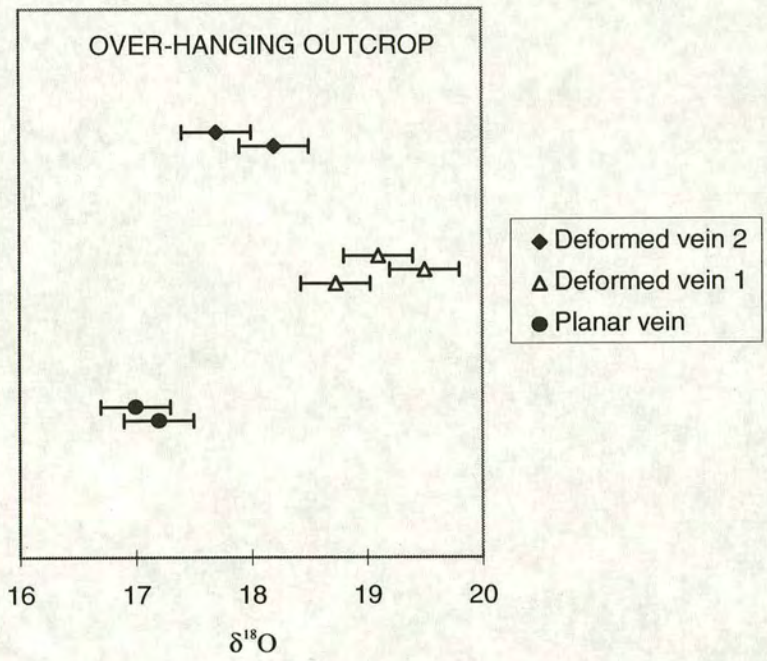

Figure 7.4 Plot showing the variation in oxygen stable isotopic composition displayed by quartz separates from samples from the Overhanging Outcrop.

Examination of the data shows that while the values for individual groups of samples are fairly similar there is considerable variation between the three groups. This pattern of variation appears to be consistent with either internal or external control of stable isotopic composition. If the values are internally controlled then the isotopic composition of the vein fluid will be locally buffered by the schists they cross cut and the variation in the composition of the veins will reflect primary isotopic heterogeneity in the sediments. Alternatively, if the isotopic composition of the vein fluid is externally controlled then variation in the composition of the veins will reflect variation in the composition of the infiltrating fluid. The similarity between the values for the veins and adjacent schists must then be due to alteration of original schist values by infiltration of fluid from the veins.

However, whichever model is correct it would be impossible to distinguish conclusively between infiltrated and un-infiltrated schists on the basis of their isotopic composition. If the isotopic composition is internally buffered then all schists will retain their original values. Even if the infiltrated schists have equilibrated with the fluid the range of values evident in the veins would mean that they would not display a sharply defined isotopic composition easily distinguished from the un-infiltrated schists.

7.6.3 Margin of the Gria Spilia Body

Three samples from the Gria Spilia Body were analysed forming a 20 cm long section through the lawsonite-rich zone at its margin. Geochemical analysis suggests that the lawsonite growth in this zone is the result of metasomatism associated with the infiltration of the meta-igneous gneisses by fluid from the greyschists.

The values obtained are lower than those found in the schists but much higher than the values obtained from unaltered igneous rocks. The highest value is found in the samples nearest the contact with the schists. These observations are consistent

with the suggestion that the block has been infiltrated by a relatively O^{18}-rich fluid sourced in the schists.

7.6.4 Other Samples From The LGSU

A further group of graphitic schist and calc silicate samples was analysed to assess the extent of isotopic variation over the LGSU as a whole. These were collected from widely scattered locations away from the identified vein systems. The results are summarised in figure 7.5.

The graphitic schists exhibit a fairly evenly distributed range of values from 17.2 to 18.9 while the calc silicates exhibit a narrower range of values from 17.8 to 18.3. Qualitative examination of the samples reveals no systematic relationship between the isotopic composition of samples and their lawsonite content.

These features are consistent with the suggestion that the isotopic composition of the schist and lawsonite generating veins are internally controlled and that the values obtained from the schist reflect primary sedimentary compositions. The range of compositions is identical to those found in the CTO and OHO. Other studies on similar lithologies from the Cyclades obtain similar magnitudes and ranges of isotopic composition and interpret them as representing primary sedimentary values (Matthews and Schliestedt, 1984; Schliestedt and Matthews, 1987; Schliestedt *et al,* 1987; Brocker *et al* 1993).

7.6.5 Samples From The UGSU

A collection of samples from the UGSU was analysed so that the isotopic composition of schists and veins and the degree of isotopic variation could be compared with that in the LGSU. These were divided into 3 groups, graphitic schists, veins containing Ca Al silicates or associated with their growth in adjacent schists, Ca-Al-silicate-absent veins. The values obtained are summarised in figure 7.6.

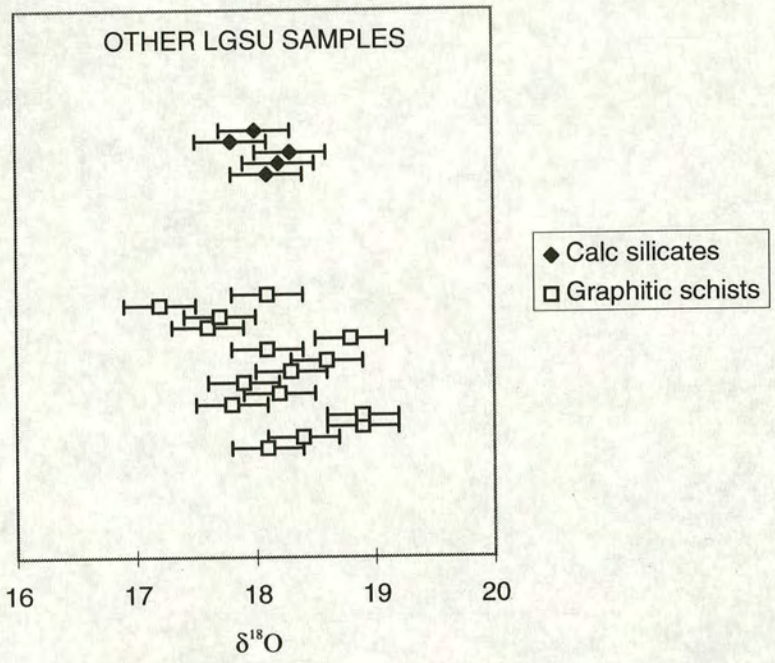

Figure 7.5 Plot showing the variation in oxygen stable isotopic composition displayed by quartz separates from samples from the Lower Greyschist Unit.

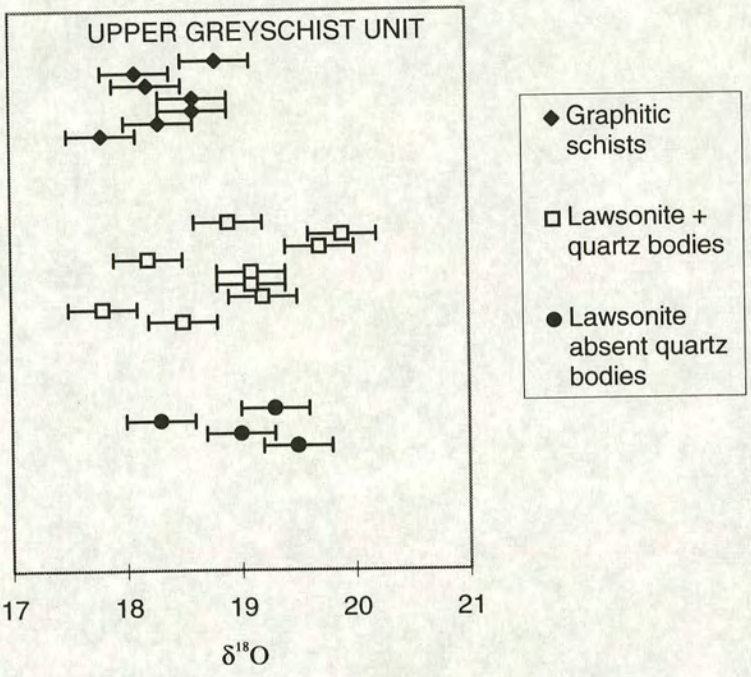

Figure 7.6 Plot showing the variation in oxygen stable isotopic composition displayed by quartz separates from samples from the Upper Greyschist Unit.

Both sets of veins display considerable ranges in composition and there is no statistically significant difference between the two groups. The schist samples have a the values for the veins are higher than those for the schists. The schist compositions are identical to those obtained from the schist from the LGSU. The veins have somewhat higher values than those found in the LGSU.

As in the LGSU the data seem most consistent with a regime in which the isotopic composition of the infiltrating fluid, represented by the values from the veins, is buffered by the rocks they infiltrate. The generally higher values found in the veins compared with those in the schists and those from the LGSU may be attributed to the high concentration of often thick carbonate-rich layers in the UGSU which are interpreted as impure marbles. Many of the vein samples are taken from quartz bodies within or near such horizons. Exchange of isotopes between these layers and the fluids would result in elevated values of $\delta^{18}O$

7.7 Summary

Oxygen isotope analysis reveals that the greyschists display a range of isotopic compositions identical to values of c. 17.5-20 $^{o}/_{oo}$ which have been interpreted as being of sedimentary origin. Ca-Al silicate generating veins also have a range in composition similar to that found in the schists though the lowest values (17 $\pm$ 0.3 $^{o}/_{oo}$) are found in veins. Schist adjacent to the veins which have clearly been infiltrated by fluid from the veins during the lawsonite generating event have values close to that for the veins but not exactly the same. These factors seem most consistent with a model in which the composition of the fluid in the veins is buffered by the schists. This in turn would suggest that the volume of fluid infiltrating the schists is relatively small.

The main aim of the stable isotopic study was to assess the extent of the lawsonite-generating infiltration event. Unfortunately, the results shed no light on

this. Identification of infiltrated layers requires that their isotopic composition is shifted by interaction with the fluid to a value easily distinguished from un-infiltrated layers. It is clear that this has not happened in the greyschists during the lawsonite-generating event.

CHAPTER 8

DISCUSSION AND IMPLICATION FOR OUR UNDERSTANDING OF FLUID FLOW IN SUBDUCTION ZONES

8.1 Introduction

The primary aim of this project was to investigate controls on the growth of calc-silicate minerals during the blueschist metamorphism on the island of Syros and in particular to reconcile the inferred need for extensive infiltration by an externally derived fluid to account for the growth of large volumes of lawsonite present with the lack of evidence for large scale fluid transport noted by Barr (1989). This was achieved by the discovery of a highly channelized, fracture-controlled fluid infiltration event which drives lawsonite growth in both metapelites and metabasites in northern Syros.

However, in addition to solving the immediate paradox the results of the project also offer an important insight into the fluid regime in subduction zones at lower crustal depths. In this chapter I argue that the lawsonite-generating event could be synchronous with and initiated by the transfer of the sediments from the down going plate to the accretionary wedge by underplating, and thus records the fluid regime at a critical point on the PTt path of the metasediments.

The implications of the results of this study will be discussed in this section. These include:-

- What is the source of the infiltrating fluid ?
- Did it acquire its characteristic composition at source or between the source and the site of the veins?
- To what degree is the scale and style of the fluid infiltration controlled by the deformation and lithological variation as distinct from the fluid generation mechanism itself?
- How is the timing of the infiltration event related to the deformation and/or tectonic processes occurring on a kilometre scale or larger?

8.2 Possible Sources for the Infiltrating Fluid

Fluids present during metamorphism are generally divided into two groups, internally derived fluids generated locally within the system under consideration and externally derived fluids which infiltrate the system from an external reservoir. The alteration associated with the veins indicates strong dis-equilibrium between fluid and the greyschists and suggests that the lawsonite-generating fluid is externally derived.

Several sources have been cited for externally derived fluids in metamorphic terranes in general. These include meteoric water, sea water, syn-sedimentary pore fluid, magmatic fluids and fluids liberated during metamorphic devolatilisation reactions. Given the depth at which the blueschist metamorphism takes residual uncombined water of sea or meteoric origin can be ruled out as it will have been expelled during compaction earlier in the burial history. Furthermore, there is no magmatic activity synchronous with the metamorphism which might produce the fluid component. On these grounds the only possible source for the fluid would seem to be devolatilisation reactions taking place in other adjacent reactive lithologies, or in regions of the subduction zone which are at higher T.

The chemistry of any externally-derived fluid should reflect the nature of its source and/or the path that it has followed since its formation. The chemical character of the lawsonite-generating fluid is fairly well constrained even though the solute contents are not known quantitatively. The mineral assemblages present in the metasomatic selvages adjacent to the lawsonite-generating veins require that the fluid is extremely water-rich (Barr, 1989). Geochemical analysis of the alteration is consistent with the fluid containing excess Ca, Al, Sr, Pb, V and Cu compared with the indigenous fluid in the rock since these elements are enriched as a result. The fluid is by the same argument poor in Si. Unfortunately, oxygen isotope analysis reveals that the fluids have equilibrated isotopically with the schists and have thus

lost their original stable isotopic signature which might have provided further information on their source.

The presence of the assemblages glaucophane + garnet + lawsonite and glaucophane + garnet + epidote indicate that the Syros rocks represent the highest grade portion of the blueschist facies. There is no textural evidence in the vein-bearing schists of any contemporaneous prograde fluid generating reaction. One looks therefore to inferred prograde reactions in deeper rocks. These will presumably be those involved in the transition from the blueschist facies to the eclogite facies. This involves a number of continuous reactions resulting in the breakdown of hydrous minerals such as lawsonite, chlorite and glaucophane and the formation of anhydrous phases such as garnet and omphacite with the release of water, e.g.:

$$Gln + Czo = Omp + Grt + Pg + Qtz + H_2O$$
$$Gln + Pg + Cal + Qtz = Omp + Grt + H_2O + CO_2$$
$$Gln + Lws = Omp + Grt + Pg + Qtz + H_2O$$

Complete eclogitization may result in almost total dehydration of a blueschist precursor. Typical blueschist metabasites contain ~3.5 wt% water while their eclogitic equivalents contain less than 0.8 wt% water (Peacock, 1993). Lawsonite with 5% H_2O is the dominant reservoir when present. Thus, the transition from blueschist facies assemblages with lawsonite to eclogite facies assemblages without in the rocks of the subducting slab would provide a source for large volumes of water-rich fluid at the depths of interest in a subduction zone environment (Peacock, 1993). The loss of epidote or clinozoisite and the reduction of the amphibole content in prograde sodic pyroxene- and garnet-forming reactions also generates fluid.

The transition from blueschist to eclogite facies assemblages is the result of increasing P and, more importantly T (Pognante 1991). However, the temperature at which it occurs is critically dependent on bulk-rock composition and μH_2O (Pognante

1991, Oh et al 1991). In particular, eclogite facies assemblages are stabilised at lower temperatures in rocks with low X_{Mg} and in systems with low μH_2O.

Incipient eclogitization has been identified in the Syros blueschists. Reaction textures in some gneissic metabasites lead Ridley (1984) to suggest that glaucophane and epidote are breaking down to garnet, omphacite, paragonite, quartz and water. He suggests that this is the result of up temperature metamorphism around peak conditions, although localised progress towards the overall textural equilibrium and variation in a_{SiO_2} during assemblage growth can also account for such textures in some cases. This is in agreement with studies in other areas which suggest that the reaction marks the boundary between the blueschist facies and the eclogite facies in metabasites (Reinsch 1979). The fact that this reaction texture is only observed in the more iron-rich metabasites is consistent with PT control being an important factor. The structural status of the products (i.e. their growth within the S1 S2 interval) suggest that the reaction is essentially synchronous with the lawsonite-generating metasomatism in the greyschists.

The fact that the Syros blueschists exhibit assemblages which could be regarded as reflecting the early stages of eclogitization, albeit only in rocks of certain compositions, suggests that, at the same time rocks deeper in the subduction zone and therefore at higher T will be undergoing a more intensive and pervasive eclogitization. At least part of the fluid generated during this process would be expected to migrate along the subduction shear zone and might therefore infiltrate rocks at higher levels. On these grounds it seems possible eclogitization of rocks at greater depths in the subduction zone might provide a credible source for the water-rich fluids involved in the lawsonite generating metasomatism. It does not by itself suggest why the process should be a discrete event in what is otherwise a continuous process. For that one needs to consider the structural evidence.

While the blueschist to eclogite transition might provide a source of water - rich fluids it does not account for the other characteristics of the infiltrating fluid.

Any fluid produced by a reaction which also generates quartz would be saturated with respect to silica. There is no recognised process involved in eclogitization which might release the large quantities of Ca present in the fluid though in principle a fluid leaving a glaucophane + Ca-Al-silicate reaction site at higher grade could be oversaturated in those phases relative to a lower grade region and precipitate the phase absent from the host. It is perhaps more likely that the fluid has been modified at some point on its flow path between its source and the point that it infiltrates the greyschists. A possible mechanism for this modification of the fluid is suggested by the striking similarity between the alteration identified in the greyschists and metasomatism commonly associated with serpentinized ultra-mafic bodies referred to as rodingization.

Rodingization may affect rocks of any composition that occur as inclusions within serpentinite bodies or at the boundary between serpentinite bodies other lithologies, including greywackes similar in bulk composition to the greyschists (Mittewede & Schandl 1992). It involves the growth of calc-silicate phases at the expense of Na and K-bearing phases and thus results in an overall gain in Ca and loss of alkalis. This is often accompanied by a decrease in the Si content of the protolith. Other components such as Al, Mg, Mn and P may also be mobile during the alteration. The exact nature of the alteration is controlled by the nature of the protolith.

Rodingization is attributed to reaction with a Ca-rich, silicate under-saturated fluid produced during serpentinization. Serpentinite forms by hydration of ultramafic rocks at relatively low temperatures and is thus dependent on the introduction of externally derived, water-bearing fluid. This process will significantly modify the composition of the infiltrating fluid. Simple reactions can be written to account for the production of serpentine minerals from olivine and other ferro-magnesian phases. However, the breakdown of pyroxenes releases calcium which cannot be accommodated in the serpentine minerals. If the fluid contains CO_2 then this may be precipitated as carbonate phases. Disseminated carbonate is common in many

serpentinites. However, if the fluid is CO_2-poor then the calcium may remain in solution and can therefore be transported with the fluid into other lithologies adjacent to the serpentinizing body. Furthermore, the silica under-saturated nature of the ultramafic will ensure that any dissolved silica will be removed by reactions to produce phases such as talc.

Direct evidence that such processes occur at shallow levels in the crust is provided by the identification of Ca-rich Si-poor waters in springs above actively serpentinizing bodies (Barnes et al 1967). Analysis of rodingites and associated serpentinites suggest that the upper PT limit for serpentinization is controlled by the stability of antigorite. At low to medium pressures antigorite breaks down to forsterite and talc at 500°C. However, experimental data suggests that at the pressures evident in the Syros metamorphism it is stable at considerably higher temperatures (Ulmer et al. 1994).

Thus it seems possible that the final composition of the fluid involved in the metasomatic growth of lawsonite is the result of its interaction with serpentinizing ultramafics. This would require that it passes through a fresh or partially altered ultramafic body on its flow path. This cannot be the serpentinite exposed in northern Syros as this was included in the sediments as detrital serpentinite prior to subduction. There are two possibilities, one is that the fluid is generated close to the Syros 'packet' but at higher grade and then mixes with a fluid source from much deeper which has 'seen' ultramafic in quantity. The other alternative is that ultramafic rocks are indeed directly in the path between the fluid source and the vein site.

8.3 Controls on the Extent of the Fluid Infiltration

As the importance of the role fluid phase in metamorphism has become increasingly apparent a considerable amount of effort has been expended in trying to identify the factors which control the mobility of fluids during metamorphism. In

other words the variables which control the permeability of rocks at depth within the crust. A number of factors have been cited in different studies. These include rock composition, structural fabrics, fluid composition and deformation. The overall pattern of permeability is typically a result of the interplay of two or more of these factors. Such models should be applicable to the lawsonite-generating infiltration event in the greyschists.

Two main sources of permeability have been identified in metamorphic rocks, a static interconnected porosity resulting form the presence of a network of tubules at triple grain boundaries in rocks in textural equilibrium which is referred to as intrinsic porosity and a dynamic porosity resulting from the hydro-fracturing of rocks on a variety of scales which is referred to as dynamic porosity (Oliver 1996).

Experimental studies have shown that the existence of an intrinsic porosity at a particular pressure and temperature is critically dependent on the composition of both the rock and the fluid (Holness and Graham 1991). Within a unit of uniform composition intrinsic permeability should result in pervasive fluid infiltration at a grain-scale. However, adjacent rocks of differing composition may act as aquifers and aquitards to the same fluid at the same P and T. In a heterogeneous unit this may result in channelisation fluid flow parallel to compositional layering.

Dynamic porosity is the result of the formation of fluid-filled fractures at elevated fluid pressures. The spacing of such fractures may vary considerably. At the finest scale it may result in pervasive infiltration similar in effect to grain boundary flow. However, in many areas it results in the channelisation of fluid flow in widely spaced fractures typically evident as veins. Fractures will form when the fluid pressure exceeds the sum minimum compressive strain and the tensile strength of the rock. Thus the stress field will control the orientation of the fractures. In addition, the presence of a strong foliation which significantly reduces the tensile strength of the rock may promote the formation of fractures.

The type of permeability present is also dependent on deformation. Intrinsic permeability requires that rocks are in textural equilibrium. High levels of ductile strain generally result in textural dis-equilibrium and therefore destroy any intrinsic permeability. Thus, during ductile deformation fluid infiltration is the result of the presence of dynamic permeability. If a rock contains a free fluid phase, in particular if fluid is being generated by dehydration reactions, then by destroying the intrinsic permeability and hence the ability of the fluid to escape, ductile deformation will elevate fluid pressures and promote the formation of a dynamic porosity. However, if the rock is essentially dry it will merely destroy the intrinsic permeability and render the rock impermeable, until a fluid phase is introduced.

These models of permeability seem consistent with the pattern of fluid flow in the greyschists. The greyschists are undergoing an intense ductile deformation throughout the lawsonite-generating event. Thus no intrinsic permeability would be expected and hydro-fracturing will be the sole permeability-generating process. However, no dehydration reactions are occurring within the greyschists and any fluid produced earlier in the metamorphism will have been driven out by the earlier stages of the deformation. Given this lack of a fluid phase no hydro-fracturing will occur in the main body of the schists and they will be impermeable. Where the lawsonite-generating fluid is introduced it will be focused into discrete fractures now evident as the quartz veins. As would be expected these veins form perpendicular to the maximum stretching direction defined by the dominant lineation parallel to the fold hinges.

Where the fluids do infiltrate the schists from the veins this too is the result of micro-fracturing. Observation shows that the extent of permeability in individual layers is the directly related to the strength of the S1 foliation which in turn is controlled by the modal proportion of mica. the more micaceous a horizon is the stronger the development of the foliation and the wider the alteration zone adjacent to the vein. This can be attributed to the fact that the foliation markedly reduces the tensile strength of the rock and hence promotes micro-fracturing.

8.4 Possible relationships between the fluid infiltration and subduction zone tectonic processes

The lawsonite-generating fluid infiltration event identified in the Syros greyschists occurs during the syn-blueschist deformation. Indeed the structural status of the lawsonite suggests that it is synchronous with a major change in the style of deformation. This deformation is the product of the subduction processes responsible for the metamorphism. Changes in the strain history reflect changes in larger scale tectonic processes. Thus, it appears that the timing of the fluid infiltartion may be controlled by these larger scale tectonic processes.

The broad outline of the tectonic history responsible for the formation of HPLT rocks such as those found on Syros is fairly well understood. The initial stages involve the subduction of material to lower crustal depths at convergent plate margins. It is during this phase that the characteristic mineral assemblages develop However, the fact that such rocks now exposed at the surface indicates that at some stage they must be transferred from the down going slab to the accretionary wedge which forms the hanging wall of the subduction zone and subsequently exhumed.

A number of processes have been suggested to account for this transfer. Where rocks contain relatively low pressure assemblages it can be attributed to offscraping at the toe of the accretionary wedge. However, where higher pressure assemblages are present the material must have been transported to significant depths beneath the accretionary wedge before the transfer occurs. Some models have suggested that this deeper level transfer is involves significant tectonic disruption and the formation of melange units on a variety of scales. However, where coherent terranes in which the stratigraphy is preserved on a km scale, such as the Syros section, are exhumed these models are obviously inapplicable and an alternative process must be responsible for the transfer.

Such coherent HPLT terranes must result form the transferring from the downgoing footwall to the relatively static hanging wall of packets of rock which are larger than the observed volume of undisrupted stratigraphy. If this process is subduction driven i.e. there is a dominant inclined shear surface or parallel shear surfaces, as suggested by thrust solution earthquakes at intermediate depths, then progressive downward propagation of the thrust surfaces would seem to be the likely process. This is the upside down equivalent of hanging wall collapse in thrust duplexes. In this case it is footwall collapse i.e. footwall material is transferred to the hanging wall. This process is what is generally termed underplating. For 15 Kb blueschist to appear at the surface during steady state subduction this process must continue to introduce successive packets below each transferred slice to achieve the uplift to drive unroofing. Uplift can also be achieved by the attempted subduction of the edge of continents whereby a buoyant 'lump' induces excess topography in a single (and terminal) event which then drives unroofing. However, a continuous underplating process has to be involved to drive the unroofing of material buried to 45 km since topography of that magnitude cannot be sustained.

The process of underplating will cause a significant change in the strain regime within the accreted packet. During burial when the package is moving downwards while pinned to the slab the deformation will be dominated by shear strain (sub-) parallel to the subduction thrust surface. The intensity of this strain will increase toward the thrust contact. When the package is underplated the detachment will shift to the bottom of the package. The shear strain will then increase in intensity toward the base of the packet. In addition the end of downward transport will be associated with shortening of the package caused by the transfer of stress across the thrust surface from the footwall to the hanging wall. This will probably be evident as folding and possibly by the formation of ductile duplexes.

By definition, the accretionary wedge is less able to flow laterally than the slab itself and there will be a quasi-horizontal resisting force of some magnitude applied to the packet transferring from footwall to hanging wall. The strain history of

the Syros blueschists can be readily interpreted in the context of such a model. The initial phase of the deformation dominated by layer parallel simple shear and synchronous with the development of the blueschist assemblages is clearly the result of the subduction of the sediments as part of the downgoing slab. The underplating process itself is recorded by the onset of ductile thrusting during the second phase of the deformation. This interpretation is supported by observations on the relative timing of the thrusting and critical metamorphic reactions. The initiation thrusting is synchronous with the growth of lawsonite which marks the peak pressure of metamorphism and therefore the maximum burial depth. However, the deformation has ceased before the lawsonite pseudomorphing which occurs in the initial phase of the exhumation path.

The internal fabrics of vein-related lawsonites indicate that they grew during the earliest stage of the folding of the S1 cleavage. This indicates that the fluid infiltration is synchronous with an important transition in deformation style which can be reasonably correlated with the start of the underplating of the metasedimentary packet to which this part of Syros belonged. The coincidence in the timing of the two events strongly suggests that infiltration and possibly the generation of the fluid is a result of the underplating process. A number of mechanisms, could be responsible for the apparent link. Three of which are discussed here. The underplating might perturb the thermal structure of the underplated terrane causing generation of large volumes of fluid. The intense ductile deformation accompanying the underplating might promote fluid generating reactions and / or cause the expulsion of the fluid phase from its source region. The deformation of the metasediments themselves might increase their permeability and allow the fluid to enter them. These are discussed in detail below.

1/. Perturbation of the thermal structure within the underplated units.

Underplating involves the consecutive emplacement / accretion of discrete, coherent packages of material bound by thrust surfaces to form a duplex/ imbricate

stack. If there is a significant difference in temperature between the base of each underplated package and its top, resulting from a thermal gradient in the upper part of the slab, then the there will be large differences in temperature between the bottom of one package and the top of the package emplaced below it (see Figure 8.1). Whether the bottom of the package above is colder than the package below or vice versa is dependent on the nature of the thermal gradient in the upper part of the slab. Overall, thermal gradient through the stack will display a sawtooth profile. Conduction of heat across the thrust surfaces would cause raising of temperatures on cooler side which could cause blueschist to eclogite reactions generating water-rich fluids.

The magnitude of temperature differences within the stack will depend on combination of the magnitude of the temperature gradient in the upper portion of the slab and the scale and geometry of the underplating process. The steeper the gradient in temperature and the greater the thickness of the individual packages the larger the difference in temperature across the package boundaries. However, there does not need to be a large change in temperature to explain the increased fluid production in rocks down section from the Syros rocks as they must be close to / at temperatures required for blueschist to eclogite transition already as incipient eclogite forming reactions are evident in susceptible lithologies on Syros.

The thermal structure of subduction zones is difficult to model accurately. It depends on a multitude of factors including age of subducted slab, speed of subduction, geometry of subduction, magnitude of shear stress along the shear zone and the possibility of forced convection in the mantle wedge. Several studies have tried to model thermal structure (refs. from Peacock 1995) all producing significantly different results. However, the exact nature of the geothermal structure not important for the model. All the model requires is that there is a gradient in temperature perpendicular to the top of the slab. It is generally accepted that such a gradient will exist.

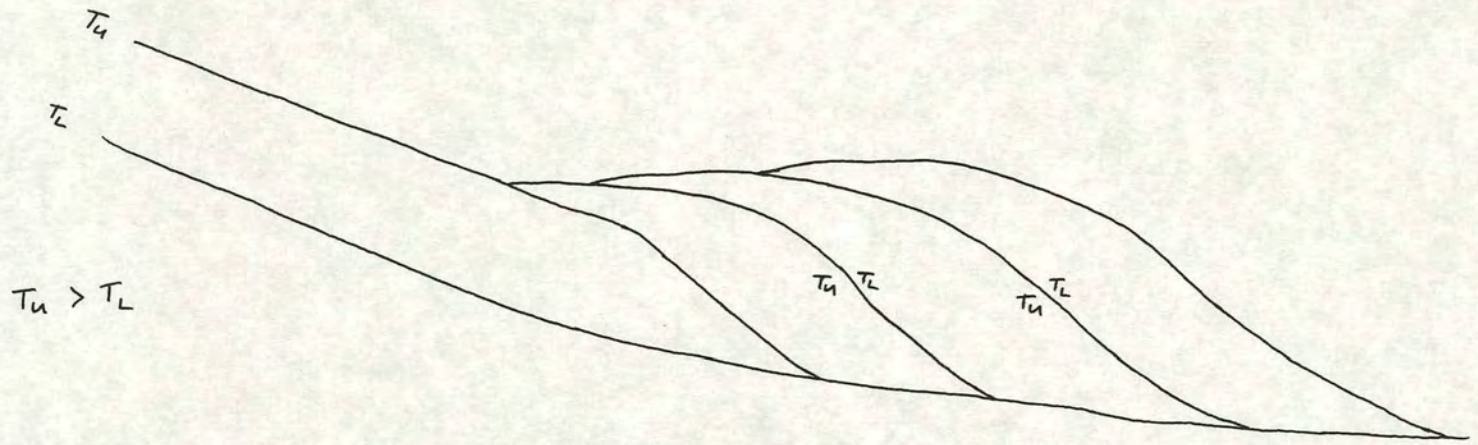

Figure 8.1 Schematic diagram illustrating the temperature difference that may arise between the upper and lower surfaces of adjacent underplated packages.

A limit can be placed on the size of an individual packet. If packets are too large then the temperature will have cooled at the top before the next infiltration event occurs, i.e. it will not appear to be at peak blueschist. A reasonable upper limit packet thickness would seem to be 10 km i.e. one 1/4 of the overlying thickness and 1/4 of the temperature drop to the surface. Most probably it is less and of the order of the thickness of the sedimentary section ~5 km.

2/. Promotion of fluid generating reactions.

It is proposed that the formation of the fluid is the result of the transition from blueschist facies assemblages to eclogite facies assemblages in rocks of the subducting slab. The progress of such reactions is often limited by kinetic factors, particularly in relatively anhydrous meta-igneous lithologies which make up much of the oceanic crust. This results in dis-equilibrium on a small scale and considerable overstepping of eclogite-forming reactions. However, reaction progress is aided by grain-scale deformation (Ridley & Dixon 1984, Koons et al 1987). Typically, rocks that have been strongly deformed, e.g. those in shear zones, are completely reacted to eclogite assemblages while those within undeformed regions display more localised equilibrium and corona textures. Thus, if the change in deformation in the Syros blueschists also affects the source region of the fluid it might accelerate the eclogite forming reactions resulting in a rapid generation of large volumes of fluid.

3/. Deformation enhanced permeability

As noted in the previous section the fluid flow during deformation is typically dominated by channelized flow along fractures. This is clearly the case during the lawsonite-generating infiltration event. The formation of these fractures by hydro-fracture is dependent on the balance between the fluid pressure and the stress field. Expressed simply, a fracture will form when the effective pressure (σ_3 - Pf) exceeds the tensile strength of the rock. However, at high values of deviatoric stress fractures may form when the effective pressure is considerably less than the tensile strength of

the rock (Price & Cosgrove 1990 p29-33). The change in the strain regime must be due to a change in the stress field. This in turn might result in an increase in the deviatoric stress which may increase the permeability of a rock body at a given fluid pressure.

On these grounds it appears possible that the ability of the lawsonite-generating fluid to infiltrate the greyschists is critically dependent on the style of deformation. This in turn raises the possibility that the similarity in the internal fabrics of the lawsonites may not reflect an identical timing for the various vein sets but that they formed at a similar state of strain which may have been achieved at different times in different places within the rock body.

8.5 Comparison of Fluid Flow in Syros Blueschists with that in other HP/LT Terranes and Implications for our understanding of Fluid Flow in subduction zones

The overall quantity of data available on the fluid regime in subduction zones is small relative to that available on fluid regimes in other metamorphic environments. To a large extent this can be explained by the comparatively small number of well preserved high-pressure low temperature terranes. However, with the suggestion that the introduction of a slab-derived fluid component to the overlying mantle wedge is involved in the generation of island arc magmas (e.g. Gill 1981) an understanding of the fluid regime in subduction zones has become critically important. With this in mind a number of recent studies have considered the nature of subduction zone fluids and the extent to which they may be able to leave the slab and enter the mantle wedge though at blueschist depths this would be lithospheric and not directly relevant to arc magma generation.. The vast majority of these investigated two specific regions, the Catalina Schists, California and eclogite bodies in the Alps. These HPLT terranes formed at significantly different depths in subduction zones. Comparison of the results of the studies has lead to the suggestion that the fluid regime in subduction zones varies systematically with depth (Selverstone et al 1992).

The rocks of the Catalina schist preserve a record of metamorphism occurring in relatively shallow levels of a subduction zone from depths of 15 to 45 km. Veining, changes in bulk rock composition and changes in stable isotopic composition provide abundant evidence of syn-metamorphic fluid flow on scales ranging from metres to kilometres. In particular, silicification and homogenisation of stable isotopes in the matrix of melange zones requires that they have been pervasively infiltrated by large volumes of fluid. Fluid flow in more coherent metasedimentary and metabasic units is less pervasive and some primary isotopic heterogeneity may be preserved. However, such units contain abundant veins with attendant wallrock alteration. The calculated $\delta^{18}O$ values for the vein fluids and the associated shift in the rocks from their likely primary values indicate that the metasomatism is the result of infiltration by a remarkably homogeneous fluid with $\delta^{18}O = 12.5 \pm 1$ %. This indicates that the fluid had equilibrated with meta-sedimentary units in the slab and suggests that it is probably derived from them though it is possible that its source lies considerably deeper in the subduction zone. The contents of veins and alteration of adjacent wall rocks provides evidence for the mobility of a wide range of dissolved species including Si, Na, Al, Ca, K and LILE. The mineralogy of the veins and analysis of fluid inclusions indicate that the fluids are very water-rich.

The studies in the Alps concentrate on eclogites resulting which are the products of subduction zone metamorphism at depths of > 40 to 45 km. The fluid regime in such units appear to contrast strongly with that observed in the Catalina schists. While the eclogites typically contain veins and segregations which attest to the presence of a fluid phase containing high concentrations of dissolved species there is no evidence of fluid homogeneity on anything other than the smallest of scales. Selverstone et al 1992 identified fluid heterogeneity on a scale of mm to cm in finely banded eclogites from a coherent sequence of meta-sedimentary and metabasic rocks form the Tauern Window. Segregations of high P minerals within the eclogites are clearly in equilibrium with their wall rocks and are assumed to be locally derived.

No traces of an interconnected vein network are present. These observations are confirmed by analysis of stable isotopic variation and trace element distribution within the same rocks (Getty & Selverstone 1994). Phillipot and Selvertsone (1991) identified similar fine-scale variation in fluid composition by comparing the compositions of different fluid inclusion populations in mafic eclogites and eclogitic veins from the Monviso Massif. They attributed the formation of the majority of the veins to localised redistribution of fluid from early fluid inclusions during ductile deformation and dynamic recrystallization rather than any larger scale fluid transport. However, they suggest that larger, metre-scale shear fractures may record the influx of large volumes of externally derived fluids .possibly derived from more hydrous layers associated with the metagabbros. There is no evidence that the eclogitic wall rocks have equilibrated with this fluid. Barnicoat and Cartwright (1995) showed the eclogitic rocks from the Piemonte ophiolite have retained their original sea floor isotopic signatures with the exception of small, predicable shifts caused by isotopic fractionation during dehydration.

The presence of the assemblage jadeite + quartz in some Syros rocks indicates a minimum depth of subduction of ~45 km. Similarly, the presence of paragonite indicates that the maximum depth of subduction was ~60 km. Unfortunately no other equilibria have been identified which can further refine the pressure of metamorphism. However, geobarometry on an sequence of blueschists and eclogites from the nearby island of Sifnos gives a pressure of 15 ± 2 Kb. This suggests that the maximum depth of metamorphism is toward the shallower end of the range. Thus, the Syros rocks may preserve a record of the fluid regime at depths generally intermediate between the Catalina schists and the majority of the studied Alpine Eclogites.

Observations suggest that the fluid regime in the Syros metasediments shares some characteristics with each of the regions described above. The vein controlled growth of lawsonite described in this study shows fracture controlled transport of fluids over considerable distances and that the vein fluids are able to infiltrate and

metasomatise the wall rocks on a relatively pervasive scale. However, on a large scale there is no evidence for widespread pervasive exchange with a mobile fluid phase and the blueschists preserve evidence of fluid heterogeneity on small scale (Barr 1989). Even where the infiltrating fluid has exchanged with the schists the volume of fluid was not large enough to homogenise the oxygen stable isotopic values in the greyschists. Instead the isotopic composition of the fluid appears to be buffered by the country rocks.

As noted above the difference in the scale of fluid transport in the Catalina Schists and Alpine eclogites has been interpreted as reflecting a change in fluid regime with depth in subduction zones. Getty and Selverstone (1994) suggest that this change may be explained by the incremental decrease in the volume of fluid relative to rock with continuing devolatilisation of the slab during its subduction. Within the upper portions of the subduction zone the generation of large volumes of fluid, initially by the expulsion of pore fluids and later as a result of extensive dehydration and decarbonation reactions, results in large scale transfer of fluids along a fracture network and permeable horizons such as the Catalina Schist melange zones. However, with increasing depth the volume of fluid produced by devolatilisation will wane. This will result in a decrease in the scale of fluid transport until in eclogites localised equilibrium will prevail.

In broad scale the fluid regime in the Syros meta-sediments at the peak of the blueschist metamorphism appears to conform to this simple model. As would be expected the extent of fluid flow is considerably less than that in the Catalina schists but greater than that found in the Alpine eclogites. However, when considered in more detail the relationship between the fluid regime in the Syros blueschists and that in other regions metamorphosed at different depths seems less straight forward.

While large scale pervasive fluid flow clearly occurred in the Catalina schists it is largely confined to the ultramafic-rich melange zones. Within the intervening more coherent meta-sedimentary units, similar to the greyschists, fluid flow was

focused in spaced fractures now evident as veins. While there is some evidence of homogenisation of stable isotopic signatures in the rocks adjacent to the fractures those further away typically preserve small scale heterogeneities. This seems little different to the situation found in the greyschists. A number of laterally persistent ultramafic melange zones are present in the within the upper part of the Syros section which might have acted as conduits for large scale fluid flow. Unfortunately, no attempt has been made to assess the extent of isotopic homogeneity within and between these units so it is not possible to test this hypothesis. However, it appears possible that despite its greater depth of metamorphism the Syros section has a broadly similar fluid regime to the Catalina schists.

Furthermore, it seems unlikely that the volume of fluid produced by devolatilisation of the slab will display a uniform decrease with depth. Instead one might expect pulses of fluid production relating to the crossing of particular devolatilisation reactions. This is supported by the occurrence of multiple generations of cross cutting veins in subduction zone rocks and the evidence of multiple crack seal events within the veins themselves. Thus, one might expect subducted rocks to display episodes of large scale fluid transport between which localised fluid equilibrium will prevail. Such a situation seems evident on Syros. Large volumes of fluid must have been removed from the metasediments at higher levels in the subduction zone during the development of the blueschist assemblages which would require large scale fluid transport. This must have involved layer parallel flow and channelisation, possibly along the melange zones, in order to preserve small scale isotopic heterogeneities. However, by the time the lawsonite generating infiltration event occurs all reactions involved in the generation of the high grade blueschist assemblages appear complete. Thus, little or no fluid would be present and the scale of fluid transport should be small. However, with the initiation of eclogitization in rocks down section producing the lawsonite-generating fluid is produced and the blueschist are once again the site of large scale fluid transport. The question is why this fluid is not seen infiltrating the blueschists continuously as a series of veins of all relative ages since deeper rocks must still be generating fluid

while the greyschists were acquiring their pre-lawsonite-vein glaucophane-chlorite garnet assemblage. The critical observation is that the fracture filling dilation event occurs at the same recognisable point of transition in the fabric history, strongly implying that fluid generation, fluid re-routing and the change in structural style are all linked together.

CHAPTER 9

CONCLUSIONS

9.1 Conclusions

The main conclusions of this study have been discussed in the previous chapter. They are briefly summarised again here.

1. The lawsonite growth in the greyschists is controlled by a syn-deformational fracture-controlled fluid infiltration event. The site of the former fluid pathways is now marked by quartz veins associated with abundant lawsonite growth in adjacent schists

2. Lawsonite growth in the schists is the result of metasomatic reactions between the veins fluids and the wall-rocks they infiltrate. This involves both the generation of lawsonite by reactions between mica and the Ca-rich fluid and, in the zones closest to the veins, the direct precipitation of lawsonite from the fluid. These processes are accompanied by dissolution of quartz. Overall the schists gain Ca, Al, Sr, Pb and lose Si, Na, K, Ba, Rb, Zn.

3. The pattern of fluid infiltration is controlled by the deformation and the fabrics it generates. The focusing of the fluid into discrete fractures reflects the destruction of more pervasive permeability by ductile deformation and the promotion of hydrofracture. Pervasive fluid infiltration in the vein wall rocks is a result of hydrofracture / micro-veining parallel to the S1 cleavage. Thus, on a sub-outcrop scale the permeability of individual horizons to the vein fluid is directly proportional to the strength of their planar fabrics and therefore to their mica content.

4. The channelized nature of the fluid flow accounts for the preservation small scale variation in fluid composition and thus accounts for the apparent paradox between fluid driven lawsonite-growth and the locally buffered fluid regime identified by Barr 1989.

5. The timing of the lawsonite-generating event is synchronous with a major change in the style of the syn-blueschist deformation. Consideration of the nature of the tectonic history required for formation and exhumation of blueschists leads to the conclusion that it is a result of the transfer of the terrane containing the Syros section from the down-going slab to the overlying accretionary wedge by underplating. The synchronous timing suggests that the two events are related i.e. the lawsonite-generating infiltration is a result of the underplating process. Three possible models may explain this link. The underplating process may perturb the local thermal structures and cause fluid-generating reactions to occur. Dynamic recrystallization associated with the deformation might drive fluid generating eclogite forming reactions in another part of the packet. Alternatively, the deformation associated with the underplating may increase the permeability of the greyschists allowing the fluid to enter them.

6. The infiltrating fluid is derived eclogite-forming reactions generated in hotter, probably deeper, parts of the subduction zone. The similarity between the lawsonite-generating event and rodingization suggests that the fluid may have interacted with ultramafic material between its formation and entering the greyschists.

9.2 Future work

Two obvious areas for future study arrive from this thesis.

1. An expansion of the study into the rest of Syros blueschist terrane.

Other Ca-Al-silicate-bearing veins have been observed elsewhere in Syros. However, these contain epidote rather than lawsonite and cross-cut epidote-bearing schists. No attempt has been made to assess the extent to which the epidote in the schists may be related to the veining. However, the stability of epidote relative to lawsonite is critically controlled by bulk rock iron. Thus, these

veins may be Fe-rich analogues of the vein-related lawsonite growth in the magnesian greyschists

2. Comparison of this study with fluid -driven lawsonite growth in the Alps

Pognante (1989) describes distribution on of lawsonite in the southern Sesia zone which is remarkably similar to the observations from Syros. It would be interesting to examine these features in the light of the conclusions from the Syros rocks and find out just how widespread these events are in blueschist rocks.

APPENDIX 1

LIST OF SAMPLES

APPENDIX 1 Catalogue of samples.

This section lists the samples referred to in the text and illustrations of the thesis, recording the location from which they were collected and giving a brief description of the samples themselves.

Key to abbreviations used for locations:-

LGSU	Samples collected from the Lower Greyschist Unit between Marmaris Bay and Gria Spilia.
UGSU	Samples collected from the Upper Greyschist Unit along the Panavlies Ridge.
CTO	Samples from the Cedar Tree Outcrop in the LGSU.
OHO	Samples from the Over Hanging Outcrop in the LGSU.
GSB	Samples from the Gria Spilia Meta-igneous Body.

Sample No	**Location**	**Description**
Samples illustrating structural history		
92/2	LGSU	Greyschist containing decimetre-scale fold.
92/3	LGSU	Weakly deformed greyschist with fine-scale primary layering.
92/4	LGSU	Weakly deformed greyschist with fine-scale primary layering.
92/11B	LGSU	Greyschist with localised syn-S1 crenulation discordant with S2.
92/12	LGSU	Greyschist with strongly developed S2 from core of a fold.
92/30F	CTO	Quartz-rich greyschist with 'classic' S1 fabric.
92/31A	CTO	Greyschist with disharmonic S2 crenulation.
92/44B	LGSU	Mica-poor greyschist with poorly developed S1.

Sample No	Location	Description
92/163	LGSU	Greyschist with well-developed S1 and weak S2 crenulation.
92/166	LGSU	Greyschist with localised syn-S1 crenulation discordant with S2.
93/25	UGSU	Greyschist with well developed S2 fabric.
93/31	UGSU	Greyschist with post S2 extensional crenulation.
93/36	UGSU	Greyschist with well developed S2 fabric.
93/40	UGSU	Greyschist with well developed S2 fabric.
91/ASP6	ASPRO	Intensely deformed talc-rich schist.

Samples illustrating the timing of lawsonite growth

92/4	LGSU	Greyschist with lawsonite overgrowing S2 crenulation.
92/30C	CTO	Greyschist with lawsonite displaying birds-nest fabric.
92/47	LGSU	Greyschist containing lawsonites clearly overgrowing early stages of S2 crenulation.
92/59A	OHO	Greyschist with no apparent S2 crenulation but lawsonites with sigmoidal internal fabrics.
92/74	OHO	Greyschist with lawsonite displaying well developed sigmoidal fabric
92/80	OHO	Greyschist containing lawsonites with parallel fabrics overgrowing S2.
93/34	PSO	Sample containing lawsonites with well developed internal fabrics discordant with S2 transposition fabric.

Samples analysed in geochemical study.

92/20	CTO	Block of lawsonite rich greyschist extending between the two planar veins.

Sample No	Location	Description
92/33A-E	CTO	Samples from single compositional horizon forming a section perpendicular to the larger planar vein.
93/56-63	CTO	Series of core samples along transect perpendicular to the larger planar vein.
93/84A-D	CTO	Subdivided core drilled perpendicular to larger planar vein and parallel to compositional layering.
92/160A-E	GSB	Samples forming section through lawsonite enrichment zone at margin of meta-igneous block.

Samples used in oxygen stable isotopic study.

92/23	CTO	Quartz from planar quartz veins.
92/28AQ	CTO	Quartz from planar quartz veins.
92/24A	CTO	Quartz from planar quartz veins.
92/25A	CTO	Quartz from S1 parallel quartz veinlets.
92/25B	CTO	Quartz from S1 parallel quartz veinlets.
93/73	CTO	Quartz from S1 parallel quartz veinlets.
92/28A-E	CTO	Samples from individual lawsonite-rich horizon forming section perpendicular to the larger of the planar quartz veins.
92/30A-C	CTO	Samples from individual lawsonite-poor horizon forming section perpendicular to the larger of the planar quartz veins.
93/56-63	CTO	Series of core samples along transect perpendicular to the larger planar vein.
93/93A	OHO	Quartz from planar quartz veins.
93/93B	OHO	Quartz from planar quartz veins.

Sample No	Location	Description
92/63	OHO	Greyschist adjacent to planar quartz vein from lower lawsonite-rich horizon.
93/114	OHO	Sample of quartz boudin from lower lawsonite-rich horizon several metres from planar quartz vein.
92/100	OHO	Sample of greyschist from lower lawsonite-rich horizon several metres from planar quartz vein.
92/57	OHO	Greyschist adjacent to planar quartz vein from upper lawsonite-rich horizon.
92/96	OHO	Sample of quartz boudin from upper lawsonite-rich horizon several metres from planar quartz vein.
92/160A-E	GSB	Samples forming section through lawsonite enrichment zone at margin of meta-igneous block.
92/2	LGSU	Greyschist
92/3	LGSU	Greyschist
92/4	LGSU	Greyschist
92/6	LGSU	Greyschist
92/8	LGSU	Greyschist
92/35A	LGSU	Greyschist
92/45	LGSU	Greyschist
92/46	LGSU	Greyschist
92/50	LGSU	Greyschist
92/51A	LGSU	Greyschist
92/74	LGSU	Greyschist
92/131	LGSU	Greyschist
92/132	LGSU	Greyschist
92/133	LGSU	Greyschist
92/134	LGSU	Greyschist
92/135	LGSU	Greyschist

Sample No	Location	Description
93/39	LGSU	Calc silicate horizon
92/40	LGSU	Calc silicate horizon
92/40Q	LGSU	Quartz veinlet from calc silicate horizon
92/41	LGSU	Calc silicate horizon
42/43	LGSU	Calc silicate horizon
93/6	UGSU	Quartz from quartz body associated with lawsonite-rich halo in adjacent schists.
93/12	UGSU	Quartz from quartz body associated with lawsonite-rich halo in adjacent schists.
93/19	UGSU	Quartz from quartz body associated with lawsonite-rich halo in adjacent schists.
93/20	UGSU	Quartz from quartz body associated with lawsonite-rich halo in adjacent schists.
93/52	UGSU	Quartz from quartz body associated with lawsonite-rich halo in adjacent schists.
93/54	UGSU	Quartz from quartz body associated with lawsonite-rich halo in adjacent schists.
93/LD4	UGSU	Quartz from quartz body associated with lawsonite-rich halo in adjacent schists.
93/LD7	UGSU	Quartz from quartz body associated with lawsonite-rich halo in adjacent schists.
93/LDL	UGSU	Quartz from quartz body with no lawsonite-rich halo in adjacent schists.
93/LDU	UGSU	Quartz from quartz body with no lawsonite-rich halo in adjacent schists.
93/43	UGSU	Quartz from quartz body with no lawsonite-rich halo in adjacent schists.
93/LD1	UGSU	Quartz from quartz body with no lawsonite-rich halo in adjacent schists.

Sample No	Location	Description
92/38	UGSU	Graphitic schist
93/51	UGSU	Graphitic schist
92/173	UGSU	Graphitic schist
92/175	UGSU	Graphitic schist
92/176	UGSU	Graphitic schist
92/177	UGSU	Graphitic schist

REFERENCES

Altherr, R., Schliestedt, M, Okrusch, M., Seidel, E. Kreuzer, H. Hame, W., Lenz, H., Wendt, I. & Wagner, G. A., 1979. Geochronology of high-pressure rocks on Sifnos (Cyclades, Greece). *Contrib. Mineral. Petrol.*,**70**, 245-255.

Barker, A. J., 1994. Interpretation of porphyroblast inclusion trails: limitations imposed by growth kinetics and strain rates. *Journal of Metamorphic Geology*, **12**, 681-694.

Barnicoat, A. C. & Cartwright, I., 1995. Focused fluid flow during subduction: Oxygen isotope data from high-pressure ophiolites of the western Alps. *Earth and Planetary Science Letters*, **132**, 53-61.

Barr, H. M., 1989. Fluid-rock interactions during blueschist and greenschist metamorphism in the Aegean area of Greece. PhD Thesis, University of Edinburgh.

Barr, H. M., 1990. Preliminary fluid inclusion studies in a high-grade blueschist terrain, Syros, Greece. *Mineralogical Magazine*, **54**, 159-168.

Bell, T. H., 1981. Foliation development: the contribution, geometry and significance of progressive bulk inhomogeneous shortening. *Tectonophysics*, **75**, 273-296.

Bell, T. H., 1985. Deformation partitioning and porphyroblast rotation in metamorphic rocks: a radical reinterpretation. *Journal of Metamorphic Geology*, **3,** 109- 118.

Bell, T. H., 1986. Foliation development and refraction in metamorphic rocks: reactivation of earlier foliations and decrenulation due to shifting patterns of deformation partitioning. *Journal of Metamorphic Geology*, **4**, 412-444.

Bell, T. H. & Rubenach, M. J., 1983. Sequential porphyroblast growth and crenulation cleavage development during progressive deformation. *Tectonophysics*, **92**, 171-194.

Bell, T. H. & Johnson, S.E., 1989. Porphyroblast inclusion trails: the key to orogenesis. *Journal of Metamorphic Geology*, **7**, 279-310.

Bell, T. H., Fleming, P. D. & Rubenach, M. J., 1986. Porphyroblast nucleation, growth and dissolution in regional metamorphic rocks as a function of deformation partitioning during foliation development. *Journal of Metamorphic Geology*, **4**, 37-67.

Bell, T. H., Johnson, S. E., Davis, B., Forde, A., Hayward, N. & Wilkins, C., 1992. Porphyroblast inclusion-trail orientation data: eppure non son girate! *Journal of Metamorphic Geology*, **10**, 295-307.

Bickle, M., & Baker, J., 1990. Migration of reaction and isotopic fronts in infiltration zones: assessments of fluid flux in metamorphic terrains. *Earth and Planetary Science Letters*, **98**, 1-13.

Brocker, M., Kreuzer, A., Matthews, A. & Okrush, M. (1993). 40Ar / 39Ar and oxygen isotope studies of polymetamorphism from Tinos Island, Cycladic blueschist belt, Greece. *J. Met. Geol.* **11**, 223-240.

Busa, M. D. & Gray, N. H., 1992. Rotated staurolite porphyroblasts in the Littleton Schist at Bolton, Connecticut, USA. *Journal of Metamorphic Geology*, **10**, 627-636.

Cheeney, R. F., 1983. Statistical methods in Geology, George Allen & Unwin Ltd (London), 169pp.

Coward, M. P., 1982. Fold nappes: examples from the Moine and Himalayan thrust zones. *Tectonophysics*.

Coward, M. P. & Kim, J. H., 1981. Strain within thrust sheets. In: K. R. McClay and N. J. Price (Eds), Thrust and Nappe Tectonics. *Spec. Pub. Geol. Soc. London*, **9**, 275-292.

Crawford, M. L., Filer, J & Wood, C, 1979. Saline fluid inclusions associated with retrograde metamorphism. *Bull. Mineral.* **102**, 562-568.

Dixon, J.E., 1969. The metamorphic rocks of Syros, Greece. PhD Thesis, University of Cambridge.

Dixon, J.E. & Ridley, J., 1987. Excursion guide to field trip on Syros. In: H.C. Helgeson (Ed), *Chemical Transport in Metasomatic Processes,* 489-518.

Fry, N., 1979. Random point distribution and strain measurement in rocks. *Tectonophysics*, **60**, 89-105.

Fyson, W. K., 1980. Field fabrics and the emplacement of an Archaen granitoid pluton, Cleft Lake, Northwest Territories. *Canadian journal of Earth Sciences*, **17**, 325-332.

Garlick, G. D., 1966. Oxygen isotope fractionation in igneous rocks. *Earth and Planetary Science Letters*, **1**, 361-368.

Getty, S. R. & Selverstone, J., 1994. Stable isotopic and trace element evidence for restricted fluid migration in 2 Gpa eclogites. *Journal of Metamorphic Geology*, **12**, 747-760.

Gill, J. B., 1981. Orogenic andesites and plate tectonics. Springer-Verlag (New York).

Gomez-Pugnaire, M. T., Visona, D. & Franz, G., 1985. Kyanite, margarite and paragonite in pseudomorphs in amphibolitized eclogites from the betic cordilleras, Spain. *Chemical Geology*, **50**, 129-141.

Grant, J. A., 1986. The isocon diagram - A simple solution to Gresens' equation for metasomatic alteration. *Economic Geology*, **81**, 1976-1982.

Gresens, R. L., 1967. Composition-volume relationships of metasomatism. *Chemical Geology*, **2**, 47-55.

Guiraud, M., Holland, T. & Powell, R., 1990. Calculated mineral equilibria in the greenschist-blueschist-eclogite facies in Na_2O-FeO-MgO-Al_2O_3-SiO_2-H_20, Methods, results and geological applications. *Contrib. Mineral. Petrol.*, **104**, 85-98.

Hansen, E, 1971. Strain facies. Springer-Verlag (New York), 207pp.

Herron, M., 1988. Geochemical classification of terrigenous sands and shales for core and log data. *Journal of Sedimentary Petrology,* **58**, 820-829.

Hey, M. H., 1954.A new review of chlorites. *Minearological Magazine* **30**, 277-292.

Holland, T. J. B., & Powell, R., 1988. An internally consistent dataset with uncertainties and correlations: 2. Data and Results. *Journal of Metamorphic Petrology*, **3**, 343-370.

Holness, M. B. & Graham, C. M., 1991. Equilibrium dihedral angles in the system H_20-CO_2-NaCl-calcite, and implications for fluid flow during metamorphism. *Contrib. Mineral. Petrol.,***108**, 368-383.

Hunt, J. A., & Kerrick, D. M., 1977. The stability of sphene: experimental redetermination and geologic implications. *Geochim. Cosmochim. Acta.* **41**, 279-288.

Keenan, P. S., 1971 Porphyroblast rotation and the kinematic analysis of a small fold. *Geological Magazine*, **108** (3), 221-228.

Koons, P. O., Rubie, D. C. & Frueh-Green, G., 1987. The effect of disequilibrium and deformation on the mineralogical evolution of quartz diorite during metamorphism in the eclogite facies. *Journal of Petrology*, **28**, 679-700.

Korzhinskii, D. S., 1959. Physico-chemical basis of the analysis of the paragenesis of minerals. Consultants bureau Inc. (New York), 142pp.

Matthews, A. & Schliestedt, M. (1984). Evolution of the blueschist and greenschist facies rocks of Sifnos, Cyclades, Greece. *Contrib. Mineral. Petrol.* **88**, 150-163.

Mittewede, S. K. & Schandl, E. S., 1992. Rodingites from the southern Appalachian Piedmont, South Carolina, USA. *Eur. J. Mineral*, **4**, 7-16.

Nitsch, K. H., 1972. Das P-T-XCO_2 - Stabilitätsfeld von Lawsonit. *Contrib. Min. et Pet.*, **34**, 116-134.

Nitsch, K. H., 1974. Neue Erkentnisse zur Stabilität von Lawsonit. *Fortschr. Miner.*, **51**, 34-35.

Olesen, N. O., 1982. Heterogeneous strain of a phyllite as revealed by porphyroblast-matrix relationships. *Journal of Structural Geology* **4**, 481-490.

Oliver, N. H. S., 1996. Review and classification of structural controls on fluid flow during regional metamorphism. *Journal of Metamorphic Geology*, **14**, 477-492.

Olsen, S. N. & Grant, J. A., 1991. Isocon analysis of migmatization in the Front Range, Colorado, USA. *Journal of Metamorphic Geology*, **9**, 151-164.

Patrick, B. E., 1988. Synmetamorphic structural evolution of the Seward Peninsula blueschist terrane, Alaska. *Journal of Structural Geology*, **10**, 555-565.

Peacock, S. M., 1993. The importance of blueschist→eclogite dehydration reactions in subducting oceanic crust. *Geological Society of America Bulletin*, **105**, 684-694.

Perkins, E. H., Brown, T. H. & Berman, R. G., 1986. PT-system, T-X-system, PX-system: three programs which calculate pressure-temperature-composition phase diagrams. *Computers & Geosciences*, **6**, 749-755.

Philippot, P. & Selverstone, J., 1991. Trace-element-rich brines in eclogite veins: implications for fluid composition and transport during subduction. *Contrib. Mineral. Petrol.* **106**, 417-430.

Phillips, E. R. & Key R. M., 1992. Porphyroblast-fabric relationships: an example from the Appin Group in the Glen Roy area. *Scottish Journal of Geology*, **28**, 89-101.

Pognante, U., 1989. Lawsonite, blueschist and eclogite formation in the southern Sesia zone (western Alps, Italy). *Eur. J. Mineral*, **1**, 89-104.

Pognante, U., 1991. Petrological constraints on the eclogite- and blueschist-facies metamorphism and P-T-t paths in the Western Alps. *Journal of Metamorphic Geology*, **9**, 5-17.

Powell, R. & Holland, T. J. B., 1988. An internally consistent dataset with uncertainties and correlations: 3. Applications to geobarometry, worked examples and a computer program. *Journal of Metamorphic Geology*, **6**, 173-204.

Price, N. J. & Cosgrove, J. W., 1990. Analysis of Geological Structures. Cambridge University Press, Cambridge.

Prior, D.J., 1987. Syntectonic porphyroblast growth in phyllites: textures and processes. *Journal of Metamorphic Geology*, **5**, 27-39.

Ramsay, J. G., 1962. the geometry and mechanics of formation of 'similar' type folds. *Journal of Geology*, **70**, 309-327.

Ramsay, D. M. & Stuart, B. A., 1973. An analysis of non-cylindrical and incongruous fold patterns from the Eo-Cambrian rocks of Soroy, northern Norway; II, The significance of synfold stretching lineation in the evolution of noncylindrical folds. *Tectonophysics*, **18**, 109-122.

Rattey, R. P. & Sanderson, D. J., 1982. Deformation in thrust sheets in SW England. *Tectonophysics* **88**, 247-267.

Reinsch, D., 1979. Glaucophanites and Eclogites from Val Chiusella, Sesia-Lanzo Zone (Italian Alps). *Contrib. Min. et Pet.*, **70**, 257-266.

Rosenfeld, J. L., 1970. Rotated garnets in metamorphic rocks. *Geological Society of America Special Paper*, **129**.

Ridley, J. R., 1982. Tectonic style, strain history, and fabric development in a blueschist terrain, Syros, Greece. PhD Thesis, University of Edinburgh.

Ridley, J., 1984. The significance of deformation associated with blueschist facies metamorphism on the Aegean island of Syros: In: *The Geological evolution of the eastern Mediterranean*, (Geol. Soc. Lond. Spec. Publ. No. 17 (Dixon, J. E. and Robertson, A. H. F., eds), 545-551.

Ridley, J. & Dixon, J. E., 1984. Reaction pathways during the progressive deformation of a blueschist metabasite: the role of chemical disequilibrium and restricted range equilibrium. *Journal of Metamorphic Geology*, **2**, 115-128.

Sanderson, D. J., 1982. Models of strain variation in nappes and thrust sheets: a review. *Tectonophysics* **88**, 201-233.

Schliestedt, M. & Matthews, A. (1987). Transformation of blueschist to greenschist facies rocks as a consequence of fluid infiltration, Sifnos (Cyclades), Greece. *Contrib. Mineral. Petrol.* **97**, 237-250

Schliestedt, M., Altherr, R. & Matthews, A. (1987). Evolution of the cycladic crystalline complex: petrology, isotope geochemistry and geochronology. In: *Chemical Transport in Metasomatic Processes* (ed. Helgeson, H. C.), pp. 389-428. Reidel Publishing Company.

Schoneveld, C., 1977. A study of typical inclusion patterns in strongly paracrystalline-rotated garnets. *Tectonophysics*, **39**, 453-471.

Schoneveld, C., 1979. The geometry and the significance of inclusion patterns in syntectonic porphyroblasts. *Published PhD Thesis, University of Leiden.*

Schwerdtner, W. M., 1970. Hornblende lineations in Trout Lake area, Lac La Rouge map sheet, Saskatchewan, *Canadian Journal of Earth Sciences*, **7**, 884-899.

Selverstone, J., Franz, G., Thomas, S. & Getty, S. R., 1992. Fluid variability in 2 GPa eclogites as an indicator of fluid behaviour during subduction. *Contributions to Mineralogy and Petrology*, **112**, 341-357.

Spry, A., 1963. The origin and significance of snowball structure in garnet. *Journal of Petrology*, **4**, 211-222.

Ulmer, P., Trommsdorff, V & Reusser, E, 1994. Experimental investigation of antigorite stability to 80 kbar. *Mineralogical Magazine*, **58A**, 918-919.

Vernon, R. H., Paterson, S. R. & Foster, D., 1993. Growth and deformation of porphyroblasts in the Foothills terrane, central Sierra Nevada, California: negotiating a microstructural minefield. *Journal of Metamorphic Geology*, **11**, 203-222.

Visser, P. & Mancktelow, N. S., 1992. The rotation of garnet porphyroblasts around a single fold, Lukmanier Pass, Central Alps, *Journal of Structural Geology*.

Williams, P. F., & Compagnoni, R., 1983. Deformation and metamorphism in the Bard area of the Sesia Lanzo Zone, Western Alps, during subduction and uplift. *Journal of Metamorphic Geology*, **1**, 117-140.

Wilson, R. W., 1971. On syntectonic porphyroblast growth. *Tectonophysics*, **11**, 239-260.

Yardley, B. W. D., & Baltatzis, E., 1985. Retrogression of staurolite schists and the sources of infiltrating fluids during metamorphism. *Contrib. Mineral. Petrol.*, **89**, 59-68.